

POLITECNICO DI TORINO

Master's Degree in
Mechatronic Engineering

Master's degree thesis

**Analysis and control of an inverse pendulum on cart
either pneumatically or electrically actuated**



Advisor:
Prof. Luigi Mazza

Candidate:
Lazzaro Morretta

Co-advisors:
Dr. Giuseppe Pepe
Dr. Luigi Lentini

Academic Year 2020/2021

Abstract

This thesis project, developed in the Dimeas department of the Politecnico of Turin, has as primary objective the design and control of an inverse pendulum on cart. Such a control is realized through a configuration of cascade PIDs, implemented in a PLC s7-1500. The system uses an electric actuation, by means of a brushless servomotor, that receives the control signals by the drive S210.

After a short review of the scientific literature, where it is described the state of the art of this argument, it is reported the project of the test bench, realized through the software Solidworks. Moreover, all the adopted components are described. This section concludes with the realization phases of the test bench.

Next, the technological objects, used for the movimentation of the axis of the cart, are handled in the details. Moreover, it is analyzed, step by step, their setting operations in the TIA Portal environment, in reference to the used PLC.

The next three sections describe the modellization of the mechanical system cart-pendulum, the electric motor and the pneumatic motor. There is the presentation of the PID controllers, in their configuration on cascade and parallel, applied to both the linearized models and the non-liner ones, and the Model Predictive Control (MPC). For each of them, the simulations, performed in Matlab/Simulink, are reported.

Successively, it is described Simscape and Simscape Multibody, by reporting their main features and blocks. In particular, the physical model of the pneumatic actuator and electric motor are deepened. Then, cascade and parallel PIDs are designed for both of them.

The main part of the thesis is concentrated in the final part, where it is reported the experimental phase that led to the stabilization of the real physical system. The obtained results are highlighted, by imposing as setpoint firstly a step signal, then a square wave signal and a sinusoidal signal too. Some of these tests are conducted by varying the concentrated mass of the pendulum and length of the rod.

Contents

1	Introduction	11
1.1	Scientific references	13
2	Test bench	17
2.1	Components	17
2.1.1	Pendulum	17
2.1.2	Cart group	19
2.1.3	Motor	20
2.1.4	PLC	21
2.1.5	Drive	23
2.1.6	Angular sensor	24
2.1.7	Linear guide and runner	24
2.1.8	Joint	25
2.1.9	Anti vibration puffers	26
2.1.10	Screw-nut-supports	26
2.1.11	Supports BK15-BF15	28
2.2	Construction of the test bench	28
2.2.1	Basic structure and foreplay operations	29
2.3	Assembly of the cart group and screw-nut	29
2.3.1	Assembling of the pendulum group	30
2.3.2	Connection of the motor	31
2.4	Assembly of the vertical panel and the control system	32
2.5	Electrical circuit	33
3	Overview of technological objects	35
3.1	PLC	35
3.2	Drive	36
3.3	Motion control	37
3.4	Technological object	38
3.4.1	SpeedAxis	40
3.4.2	Positioning Axis	42
3.4.3	Synchronous Axis	44
4	Guide for the setting configuration	46
4.1	Technological axis and its configuration	48
4.2	PID compact	54
5	Pendulum-cart model	59
5.1	Nonlinear model of the inverse pendulum with cart	59
5.2	Linearized model of the inverse pendulum with the cart	64
5.3	Cascade PID control	67
5.4	Parallel PID	76
5.5	Model Predictive Control	84

6	Electromechanical model	90
6.1	Simulink model	92
6.2	Linearized model	94
6.3	Cascade PID controller	97
6.4	Parallel PID controller	104
6.5	MPC	110
7	Pneumatic model	113
7.1	Cascade PID	115
7.2	Parallel PID	122
7.3	MPC	124
8	Simscape	127
8.1	Pneumatic actuator model in Simscape	129
8.2	Electric motor in Simscape	132
8.3	Simscape Multibody and model of the pendulum and cart	133
8.4	Simulations	139
9	Experimental experience	147
9.1	Control strategy in the s7-1200	147
9.2	Control strategy in the s7-1500	148
9.3	PIDs calibration and encountered problems	149
9.3.1	Influence of the PID parameters	150
9.4	Experimental results	152
9.4.1	Step response and impulsive disturbances	153
9.4.2	Square wave signal	162
9.4.3	Sinusoidal signal	163
10	Future developments	168
11	Appendix A: Technical drawings	168
12	Appendix B: s7-1500	175
13	Appendix C: s7-1200	185

List of Figures

1	Simplified model of the system pendulum-cart	12
2	Control scheme	14
3	PID in parallelo	15
4	PID in parallelo ed LQR	15
5	PID ed LQR	16
6	Complete representation of the test bench	17
7	Structure of the pendulum	18
8	Structure of the cart group	19
9	Brushless motor	20
10	PLC s7-1200	21
11	PLC s7-1500	22
12	Drive	23
13	Angular sensor	24
14	Linear guide and runner	25
15	Bellows joint	26
16	Anti vibration puffer	26
17	Screw and nut	27
18	Manufacturing of the screw from the support BK15	27
19	Manufacturing of the screw from the support BF15	28
20	System of the supports	28
21	Complete Test bench	29
22	Assemeling of the cart group and screw-nut	30
23	Assembly pendulum group	31
24	Link with the motor	32
25	Complete test bench	32
26	Synthetic scheme of the connection among all the devices	33
27	Circuitual scheme for the generation of 5V	34
28	Feedback structure of the drive	36
29	Selection of telegrams	37
30	Example of time distribution	39
31	Matrioska model	40
32	MC_power block	40
33	MC_Reset block	41
34	MC_MoveVelocity	41
35	MC_Halt block	42
36	MC_MoveJog block	42
37	MC_Home block	43
38	MC_MoveAbsolute block	43
39	MC_MoveRelative block	44
40	Example of relative and absolute gearing	45
41	Blank PLC in TIA PORTAL	46
42	Identification of the drive	46
43	Drive representation in TIA PORTAL	47
44	Selection of the motor	47
45	Link between drive and PLC	48

46	Topological view	48
47	Insert new axis	49
48	Basic parameters of the technological axis	49
49	Configuration of the drive	50
50	Configuration of the encoder	50
51	Choice of the telegram	51
52	Choice of the telegram of the encoder	51
53	Mechanical configuration of the drive	52
54	Emergency stop	53
55	Configuration of end strokes	53
56	Dynamic configuration of the drive	54
57	PID selection	55
58	Mode of regulation	55
59	Input and output of PID	55
60	Limits of the instantaneous value	56
61	Setting of analog inputs	56
62	Limits of the output	57
63	Setting of PID parameters	57
64	Output formula for the PID	58
65	Model of the system cart-pendulum and reference systems	60
66	Free body diagram of the pendulum	61
67	Free body diagram of the cart	62
68	Symbolic tool of Matlab	62
69	Model of the cart-pendulum in Simulink environment	63
70	Cart behaviour in (a), pendulum behaviour in (b)	64
71	Bode diagrams of G_{xF}	65
72	Bode diagrams of $G_{\theta F}$	66
73	Bode diagrams of $G_{x\theta}$	66
74	Scheme of the Cascade PID	67
75	Scheme of the inner loop	67
76	Nyquist plot of $G_{\theta F}$	68
77	PID auto tuning	69
78	Nyquist plot of $G_{ol\theta}$	70
79	Gain and phase margins of $G_{ol\theta}$	70
80	Bode diagrams of $G_{cl\theta}$	71
81	Nyquist plot of G_{olx}	72
82	Nyquist plot of the new G_{olx}	73
83	Gain and phase margins of G_{olx}	73
84	Bode diagrams of the final G_{clx}	74
85	Step response of the linear position of the cart in the cascade architecture	75
86	Behaviour of the angle of the pendulum in the cascade architecture	75
87	Parallel PID scheme	76
88	Nyquist plot of G_{olx}	78
89	Scheme for the application of the Ziegler-Nichols method	78
90	Limit of stability with Ziegler-Nichols method	79
91	Ziegler-Nichols table	79
92	x and θ behaviour with the values given by Ziegler-Nichols method	80

93	Nyquist plot of $G_{ol}(s)$ with the final PID parameters	80
94	Gain and phase margins of $G_{ol}(s)$ with the final PID parameters	81
95	Bode diagrams of $G_{cl}(s)$	82
96	Step response of the linear position of the cart in the parallel architecture .	83
97	Behaviour of the angle of the pendulum in the parallel architecture	83
98	Saturation phenomenon	84
99	Basic principles of MPC	85
100	Discrete time system production and saving in other variables	86
101	Function generating the MPC controller	87
102	MPC block scheme in Simulink	88
103	Step response of the linear position of the cart in the MPC architecture . .	88
104	Behaviour of the angle of the pendulum in the MPC architecture	89
105	Electric circuit of the motor	90
106	Overall electromechanical system	91
107	Electromechanical system in Simulink	92
108	Model of the motor	93
109	Model of the transmission	93
110	Model of the pendulum	94
111	Linearization manager for the evaluation of G_{xV_a}	94
112	Bode diagram of G_{xV_a}	96
113	Bode diagram of $G_{\theta V_a}$	96
114	Bode diagram of $G_{x\theta}$	97
115	Cascade scheme	97
116	Nyquist diagram of $G_{\theta V_a}$	98
117	Nyquist diagram of $G_{ol\theta}$	99
118	Magnitude and phase margins of $G_{ol\theta}$	99
119	Nyquist diagram of G_{olx}	100
120	Nyquist diagram of the definitive G_{olx}	101
121	Magnitude and phase margins of G_{olx}	101
122	Bode diagrams of the definitive G_{clx}	102
123	Cascade scheme with the non linear system	102
124	Step response of the linear position of the cart in the cascade architecture and electromechanical system	103
125	Behaviour of the angle of the pendulum in the cascade architecture and electromechanical system	104
126	Parallel scheme with the linear system	105
127	Nyquist plot of G_{olx}	106
128	Nyquist plot of the final G_{olx}	107
129	Magnitude and phase margins of G_{olx}	107
130	Bode diagrams of G_{clx}	108
131	Non linear parallel scheme	108
132	Step response of the linear position of the cart in the parallel architecture and electromechanical system	109
133	Behaviour of the angle of the pendulum in the parallel architecture and electromechanical system	110
134	BMPC scheme of the electromechanical system	112
135	Linear model of the pneumatic actuator	113

136	Bode diagram of G_{xu}	114
137	Bode diagram of $G_{\theta u}$	114
138	Bode diagram of $G_{x\theta}$	115
139	Linear cascade scheme of the pneumatic system	115
140	Nyquist plot of $G_{\theta u}$	116
141	Nyquist plot of $G_{ol\theta}$	117
142	Nyquist plot of G_{olx}	118
143	Nyquist plot of the final G_{olx}	119
144	Gain and phase margins of G_{clx}	120
145	Linear pneumatic motor and nonlinear mechanical system	120
146	Step response of the linear position of the cart in the cascade architecture and pneumatic system	121
147	Behaviour of the angle of the pendulum in the cascade architecture and pneumatic system	121
148	Step response of the linear position of the cart in the parallel architecture and pneumatic system	123
149	Behaviour of the angle of the pendulum in the parallel architecture and pneumatic system	123
150	Step response of the linear position of the cart in the MPC architecture and pneumatic system	125
151	Behaviour of the angle of the pendulum in the MPC and pneumatic system	125
152	Simscape logo	127
153	RLC equation	127
154	RLC model in Simulink	127
155	RLC model in Simscape	128
156	Scheme of HIL and PIL	128
157	Complete Simscape model of the pneumatic actuator	129
158	2-way directional valve in Simscape	129
159	Pressure source-reservoir-solver configuration-gas properties blocks	130
160	Check valve and orifice	130
161	Double-acting actuator model in Simscape	131
162	Complete pneumatic actuator model	131
163	Ideal force sensor	131
164	Complete model of the electric motor in Simscape	132
165	Model of the motor and screw	133
166	From CAD to Multibody	134
167	Example of identification of DOF	134
168	Example of identification of joints and constraints	135
169	Example of identification of initial condition on a model	135
170	Solver configuration block	136
171	World frame block	136
172	Mechanism configuration block	136
173	Solid block	137
174	Rigid transform block	137
175	Weld joint block	137
176	Prismatic joint block	137
177	Revolute joint block	138

178	Model of pendulum on cart in Simscape Multibody	138
179	Wrap angle subsystem	139
180	Pendulum-cart representation in Simscape Multibody	139
181	Step response of the linear position of the cart in the cascade architecture and electromechanical Simscape system	140
182	Behaviour of the angle of the pendulum in the cascade and electromechanical Simscape system	141
183	Step response of the linear position of the cart in the parallel architecture and electromechanical Simscape system	142
184	Behaviour of the angle of the pendulum in the parallel and electromechanical Simscape system	142
185	Step response of the linear position of the cart in the cascade architecture and pneumatic Simscape system	143
186	Behaviour of the angle of the pendulum in the cascade and pneumatic Simscape system	144
187	Step response of the linear position of the cart in the parallel architecture and electromechanical Simscape system	145
188	Behaviour of the angle of the pendulum in the parallel and electromechanical Simscape system	145
189	Parameters of PID_x	148
190	Parameters of PID_θ	149
191	Effect of K_{px} on the steady-state oscillations of the cart	150
192	Effect of $K_{p\theta}$ on the steady-state oscillations of the cart	151
193	Effect of $T_{d\theta}$ on the steady-state oscillations of the cart and of the angle . .	152
194	Step response with $l = 550mm$ and $m = 180g$	153
195	Behaviour of θ to the step response with $l = 550mm$ e $m = 180g$	154
196	Response to impulsive disturbances with $l = 550mm$ and $m = 180g$	155
197	Angular response to the impulsive disturbances with $l = 550mm$ and $m = 180g$	156
198	Step response and impulsive disturbances response with $l = 550mm$ and $m = 560g$	157
199	Behaviour of θ to the step response and impulsive disturbances with $l =$ $550mm$ e $m = 560g$	158
200	Step response and impulsive disturbances response with $l = 550mm$ and $m = 800g$	159
201	Behaviour of θ to the step response and impulsive disturbances with $l =$ $550mm$ and $m = 800g$	160
202	Step response with $l = 400mm$ and $m = 180g$	161
203	Behaviour of θ to the step response with $l = 400mm$ e $m = 180g$	161
204	Square wave response	162
205	Behaviour of the angle	163
206	Sinusoidal wave response with $T=10s$ and $A=100mm$	164
207	Sinusoidal wave response with $T=7.5s$ and $A=100mm$	165
208	Sinusoidal wave response with $T=6s$ and $A=100mm$	166
209	Sinusoidal wave response with $T=6s$ and $A=50mm$	167

List of Tables

1	Motor characteristics	20
2	Characteristics of the PLC s7-1200	21
3	Characteristics of the PLC s7-1500	22
4	Characteristics of the drive	23
5	Characteristics of the angular sensor	24
6	Gammas of drives	36

1 Introduction

The problem of the inverse pendulum is considered by IFAC (International Federation of Automatic Control Theory Committee) as one of the basic control problems, due to its huge number of applications in the engineering world. Some practical feedback can be identified in the following application:

- stabilization of the SEGWAY, a typology of smart scooter able to start moving, to stop, to reverse with easy movements of the body, as shown in Figure 1a;
- maintenance of the vertical position of humanoid robots, in both static and dynamic conditions (such as walking, running, show jumping), as shown in Figure 1c;
- control of the correct orientation of aerospace devices, as it can be seen in Figure 1b.



(a)



(b)



(c)

The system to be analyzed is made up of a rigid rod, linked by means of an hinge to a cart. This one moves along a linear guide, that allows it to shift of a unidirectional motion. The hinge, without any mass, allows the pendulum to rotate freely in the plane that is identified by the direction of the motion of the cart. The pendulum is modeled with a point-like mass posed on the top of the rod.

From the control point of view, such a system presents the following characteristics:

- It is non linear, because of the presence in the equations of the model of the trigonometric functions sine and cosine and of state variables with the power operation;
- it is under-implemented, because the two state variables, recognized into the linear position of the cart and the angle of the pendulum with respect to the vertical axis, must be controlled through a unique input;
- ideally it has an infinite number of equilibrium points. By taking in consideration the simplified model in Figure 1, for values of

$$\theta = 0 + 2k\pi \quad (1)$$

the system is in unstable equilibrium points, so small disturbances will cause the departure of the pendulum from its vertical position. for values, instead, of

$$\theta = \pi + 2k\pi \quad (2)$$

the system is in stable equilibrium points.

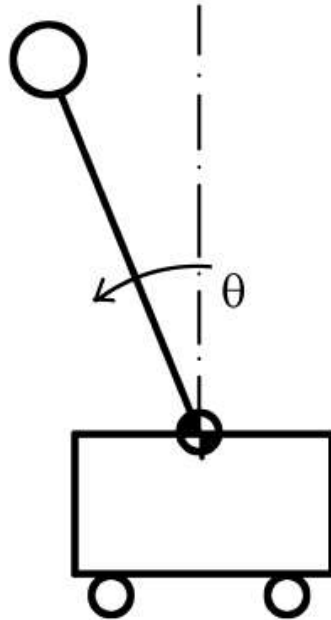


Figure 1: Simplified model of the system pendulum-cart

The first step of the thesis project has been the modelling of the system pendulum-cart by taking into account the friction inside the hinge, linked to the angular velocity, and the friction acting on the cart, that is provoked by its linear velocity.

The objective of the thesis is to apply on it several control techniques. All the controllers are designed such that a duplex control action is applied:

- to keep the pendulum in the vertical position ($\theta = 0$), its unstable position point;
- to limit the position of the cart, due to its limited stroke.

Among the several control algorithms, the chosen ones are:

- PIDs, in their configuration in cascade and parallel;
- model predictive control.

The thesis work also includes an experimental part where some PIDs are implemented by means of a PLC controller. This part has been developed by considering the system pendulum-cart connected to a brushless motor and it has been carried out along with the student of mechanical engineering Calogero Lo Curto, as long as the drafting of the CAD drawings of such a system. The remaining part of the thesis has been carried on by myself and it is about the control study of the pneumatic system. Moreover, both the electromechanical system and the pneumatic ones have been implemented in the Simscape environment, in order to take into account all non linearities, that are generally hard to handle.

1.1 Scientific references

The problem of the inverse pendulum is a fundamental reference point for control theory. An exhaustive discussion is provided in [1]. The strong non-linearities of the system, along with an easy realization of a test bench for its study, made it, in its possible variants, the most spread benchmark system of the various control techniques. The studies are about, above all, the single inverted pendulum, double inverted pendulum and Furuta pendulum [2]. The control problem is made up of two main aims: the first one consists of letting the pendulum oscillate from its stable position towards its position of unstable equilibrium, with the rod in the vertical position. The second objective is the stabilization of the pendulum itself in this position. There are several applications in reality of the inverted pendulum; in fact, this mechanical system is representative of a class of problems whose aim is the stabilization in the vertical position. The considered control algorithms to solve such a problem are different:

- PID
- Fuzzy logic
- Pole placement
- LQR
- MPC

Several actuation systems are handled, like:

- Pneumatic actuation
- Electric actuation

In [3], for instance, it is reported the stabilization of an inverted pendulum through static feedback based on "Pole Placement". The first step consists of choosing where to locate the poles of the closed-loop system, as the open-loop function is unstable. Starting from the position of the poles it is possible to determine, through the Ackermann formula, the gain matrix K. The four poles are chosen by starting from the equation of the closed-loop system:

$$q(\lambda) = (s^2 + 2\zeta\omega_n s + \omega_n^2)(s^2 + as + b) \quad (3)$$

Where, by means of (ζ, ω_n) , the dominant poles are chosen with respect to the desired performances, and the couple (a,b) is posed far from the left half plane through the separation of the factors, where s is a parameter to vary:

$$(a, b) = (s\zeta, (s\omega_n)^2) \quad (4)$$

By imposing ζ e ω_n as a function of the desired response in terms of overshoot and settling time, and by simulating in several conditions the separating factor, it is possible to obtain the gain matrix K that stabilizes the overall system. In [4], it is described the control of an inverse pendulum that is actuated by electric motor and controlled in three diferent stages by a PV controller and an LQR one. The first phase consists of the swing-up of the pendulum; the second phase foresees the maintenance of the pendulum in its unstable position, even with the application of disturbances caused by wind; the third phase is represented by the capacity to track a certain trajectory imposed to the cart. The control system is reported in Figure 2:

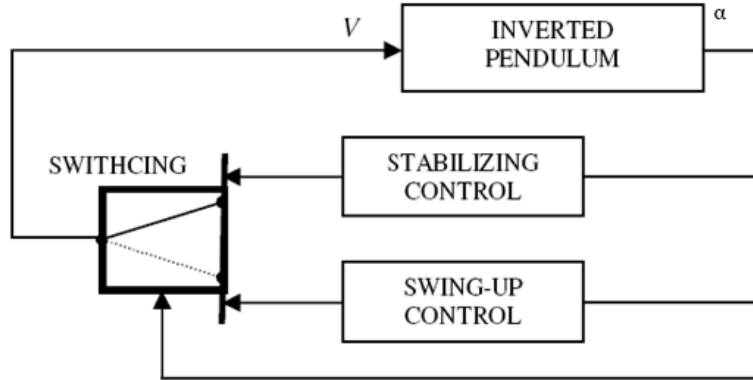


Figure 2: Control scheme

The swing-up is handled through the PV controller, made up of a proportional term associated to the position of the cart and one associated to its velocity according to the following relation:

$$V_{motor}(t) = K_d e_c(t) + K_v \frac{d}{dt} x_c(t) \quad (5)$$

The swing-up needs 12 oscillations before the pendulum to be in the vertical position. From now on, the LQR controller acts by stabilizing the system. The energy required for

the swing-up appears to be significantly higher than that relating to stabilization. Then a noise is introduced that changes the angle and angular velocity of the pendulum, but the control system manages to cancel the oscillations in less than two seconds. The tracking of a trajectory established by a square wave allows, finally, to compare the results through the LQR controller with those that could be obtained through the static feedback from the state with pole placement. From these results it is shown that the LQR controller has an advantage in terms of rise time, settling time and overshoot. Various combinations of control architectures are presented in [5]. This article compares three techniques for controlling the reverse pendulum. The first uses two PID controllers, one for the angular position and one for the carriage position, in order to generate the u command:

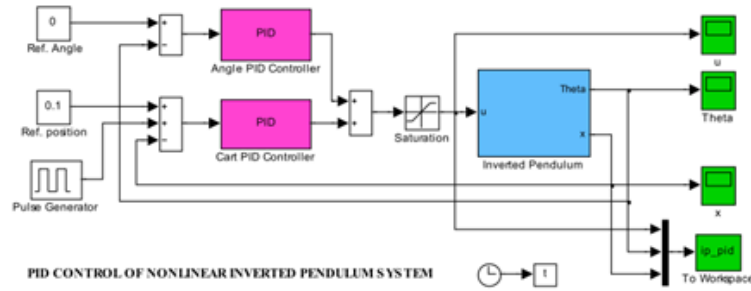


Figure 3: PID in parallel

The second technique adds a state feedback to the control process of the two PIDs, where the feedback matrix is obtained through LQR.

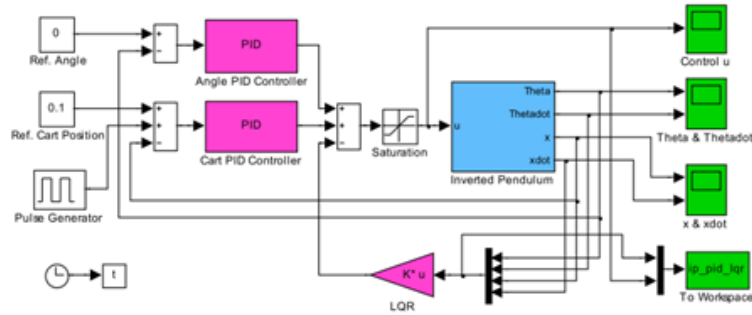


Figure 4: PID in parallel ed LQR

The third technique uses a single PID controller to move the carriage to which is added an additional control term imposed by the LQR.

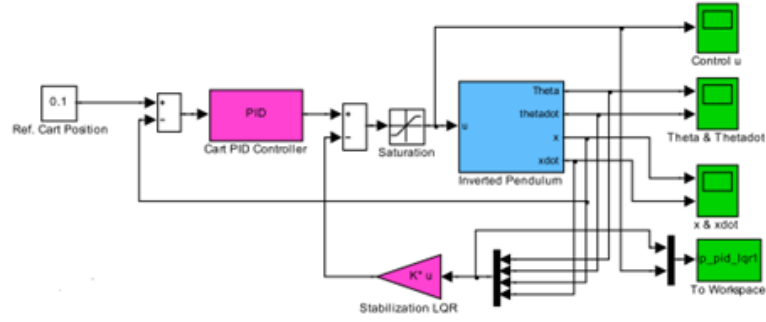


Figure 5: PID ed LQR

From the experimental results, the presence of a control through LQR improves the performance of the control in terms of speed and overshoot. The performance of the configuration with two PID's in parallel and LQR and that consisting of a single PID and LQR are comparable, but the addition of this second PID complicates system design. The presence of the second PID controller for the angular position is justified by an improvement in the response in the presence of disturbances.

Fuzzy logic is covered in [6], where it is used to control a pneumatically actuated reverse pendulum. The authors modeled the mechanical and pneumatic system considering also the friction. The non-linear model was studied to define a fuzzy type predictive controller. The article describes the experimental phase for determining the parameters of viscous friction at the pendulum hinge and those that characterize the pneumatic cylinder. Finally, reference is made to the texts [7], [8], [9], [10] and [11] for everything concerning system modeling and control theory, used for the project of controllers.

2 Test bench

The design of the test bench has been performed by means of the CAD software SOLIDWORKS 2020. In this chapter, all the electrical and mechanical components, adopted in the overall test bench, are highlighted, by trying to privilege the simplicity of the assembly, the maintenance and the economical aspect. In fact, the choice of some components as the angular sensor, the linking joint between the crankshaft and the screw-nut group and the anti-vibration mounts has been done by considering the performances of each elements with respect to its cost. The realization of the designed pieces has taken place in collaboration with the external mechanical workshop OCMAS-CERVAI. The complete representation of the test bench is reported in Figure 6.

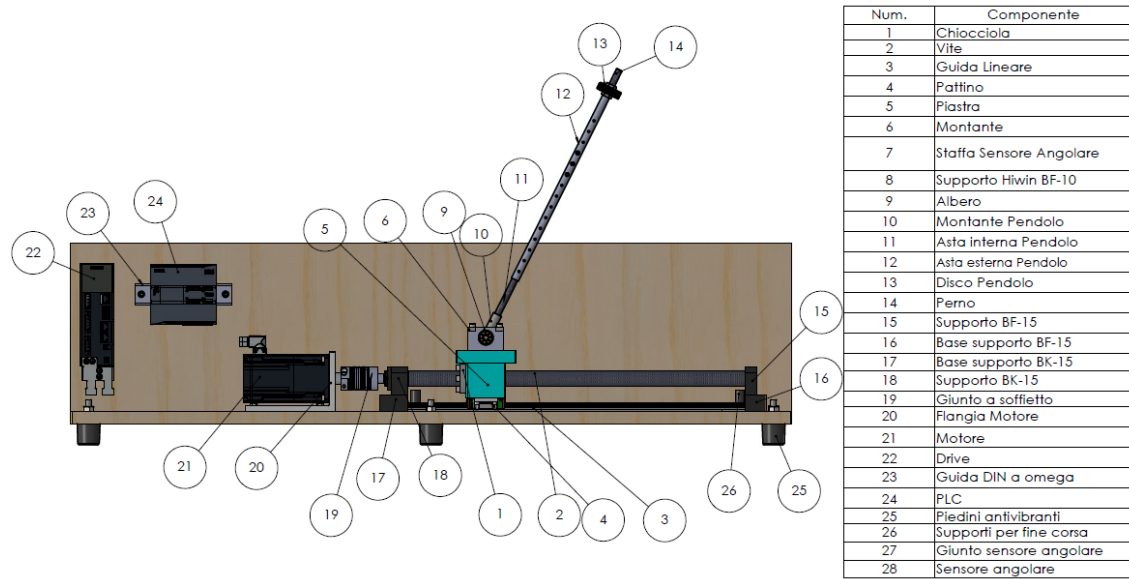


Figure 6: Complete representation of the test bench

2.1 Components

In this section, the relevant components inside the CAD and, so, the test bench are analyzed.

2.1.1 Pendulum

The design of the pendulum, shown in Figure 7, has been developed by the student Marco Pontin. Its realization has taken place by arranging the necessity to vary the length of the rod and the value of the concentrated mass, and by configuring a mounting that guaranteed the possibility to detach the pendulum group from the remaining part of the bench.

The length of the rod can vary from a minimum value of $400mm$ to a maximum value of $700mm$, by considering incremental steps of $20mm$. This is made possible by means of a telescopic rod made up of the elements 11 and 12. Once the requested height has been selected, the blocking happens through the bolts.

The concentrated load can be modified by inserting some steel elements of various dimension. In order to simplify the assembly, the link with the element 10 is realized by means of

a thread; that is why it is needed to screw or unscrew to allow the assembly and the disassembly of the rod.

In order to guarantee the hypothesis of concentrated mass, all the elements of the pendulum, apart from the disks, have been created in aluminium.

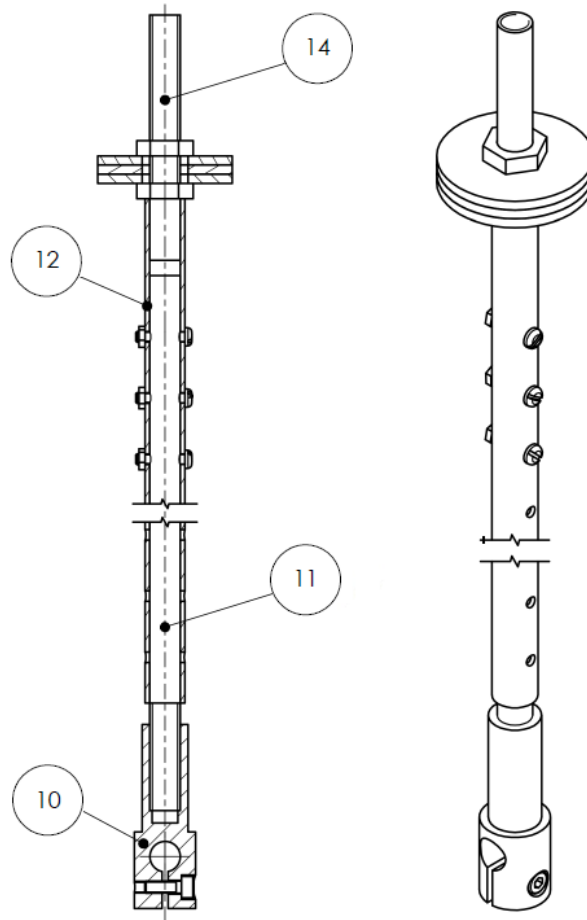


Figure 7: Structure of the pendulum

2.1.2 Cart group

The cart group, represented in Figure 8, allows the pendulum to be linked to the remaining parts of the test bench. The transformation of the motion from rotational to translational happens by means of the screw(2)-nut(1) group. The nut, during the translational motion, drags the element slab (5). This is connected from the top to all the elements the pendulum is hooked to. In particular, the supports for the bearings (8) and the crankshaft (9) constitutes the hinge around which the pendulum can rotate. The purpose of the elements marked with the number 6 is to limit the maximum angle the pendulum can assume with respect to the vertical axis (that is $\pm 25^\circ$), so that it can be avoided its fall on the test bench. In order to measure the angle that, time by time, the pendulum assumes, an angular sensor, fixed to the bracket identified by the number 7, is adopted.

The slab (5) is then linked, through threaded holes located in the lower part, to the runner (4).

It has a section where there are some rollers that permit the positioning of the runner itself in the linear guide (3). Such a configuration leads to a reduction of the friction between the two components.

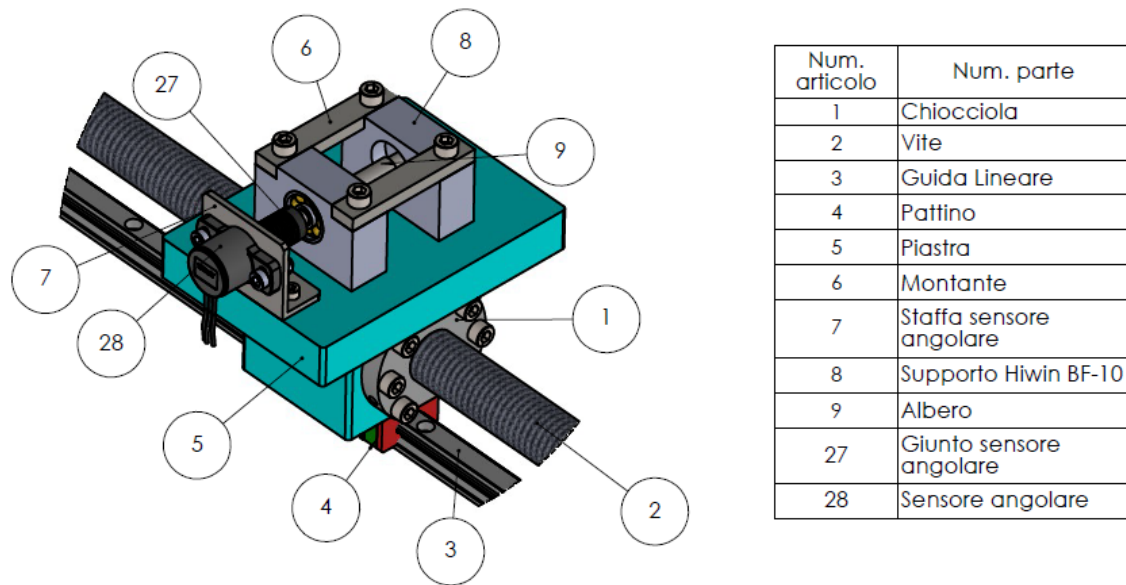


Figure 8: Structure of the cart group

2.1.3 Motor

The actuation system is made up of a brushless motor that is connected, through a steel bellows coupling to the screw. The motor generates a driving force that provokes the rotation of the screw, followed by the linear motion of the cart. The actuator has inside a 22 bit absolute encoder thanks to which it is possible to determine the angular position assumed by the crankshaft and, consequently, by considering the pitch of the screw, to estimate the linear position of the cart. One of the objectives of the used control strategies is to regular the position of the cart and, in this way, there is no need to install a further linear sensor.

The motor SIMOTICS-1FK2104-4AK10-1MA0 is provided by the company Siemens and has the characteristics shown in the table 1:

Static torque	1.27 Nm
Static current	2.4 A
Maximum torque	3.85 Nm
Maximum current	8.7 A
Maximum number of laps	8000 rpm
Nominal torque	0.95 Nm
Nominal current	1.9 A
Nominal number of laps	6000 rpm
Nominal power	0.6 kW
Armature resistance	1.7 Ω
Torque constant	0.53 $\frac{Nm}{A}$
Moment of inertia of the rotor	0.430 $Kgcm^2$

Table 1: Motor characteristics

The motor is shown in Figure 9. In order to favor the thermal dissipation, it has a cantilever connection through a steal flange by means of four screws M6. The flange presents further four holes that allow the blocking at the base of the wood.

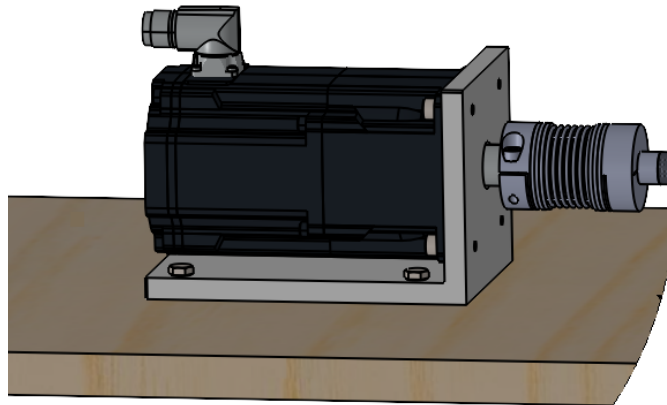


Figure 9: Brushless motor

2.1.4 PLC

The first PLC that has been adopted in the experimental test bench is provided by the company Siemens and it is part of the family S7-1200 with CPU 1214C DC/DC/DC. It is shown in the Figure 10, and its characteristics are shown in the Table 2.



Figure 10: PLC s7-1200

Digital inputs	14
Fast digital inputs	6
Analogue inputs	2(0 – 10V)
Analogue outputs	0
Digital outputs	10
Supply	24 V_{cc}

Table 2: Characteristics of the PLC s7-1200

The PLC that is used for stabilizing the pendulum belongs to the family "S7-1500" with CPU 1512C-1 PN. It is shown in Figure 11 and its main features are reported in Table 3:



Figure 11: PLC s7-1500

Digital inputs	32
Fast digital inputs	6
Analogue inputs	5
Analogue outputs	2
Digital outputs	32
Display	1.35"
Supply	24 V_{cc}

Table 3: Characteristics of the PLC s7-1500

2.1.5 Drive

The servo drive SIEMENS SINAMICS S210 is a device that is mandatory for the communication between the PLC and the motor. It is shown in Figure 12



Figure 12: Drive

The system made up of the PLC, servo drive and the motor defines the whole electric circuit of the actuation. The servo drive allows, by using telegrams, to impose all the commands to the motor that are required by the PLC. Its main characteristics are shown in Table 4.

Mains voltage	1AC 200 – 240V
Power	0.4kW
Bus system	PROFINET
Digital inputs	two fast and one for the temperature control
Braking resistance external	optional
Protection grade	IP20

Table 4: Characteristics of the drive

2.1.6 Angular sensor

The angular sensor allows the measurement of the angle the pendulum assumes with respect to the vertical axis. It is a fundamental element for the control of the pendulum itself as, time by time, it provides the value of the angle. The considered model is the sensor VISHAY 981HE0B4WA1F16. This sensor uses the Hall effect to take the angular feedback and presents the characteristics reported in Table 5:

Measurement interval	$0^{\circ} - 360^{\circ}$
Supply	$5 V_{DC}$
Linearity	$\pm 1\%$
Output	$10 - 90\% V_{SUPPLY}$; PWM 1 kHz 10 – 90% duty cycle
Shaft diameter	$6.35mm$

Table 5: Characteristics of the angular sensor

The image of the sensor is shown in Figure 13:



Figure 13: Angular sensor

2.1.7 Linear guide and runner

The linear guide HGR 15R-0600 and the runner HGW 15 CC Z0C used for this test bench are provided by the company HIWIN. They are shown in Figure 14, where it is possible to visualize the detail of the ball recirculation in the runner.

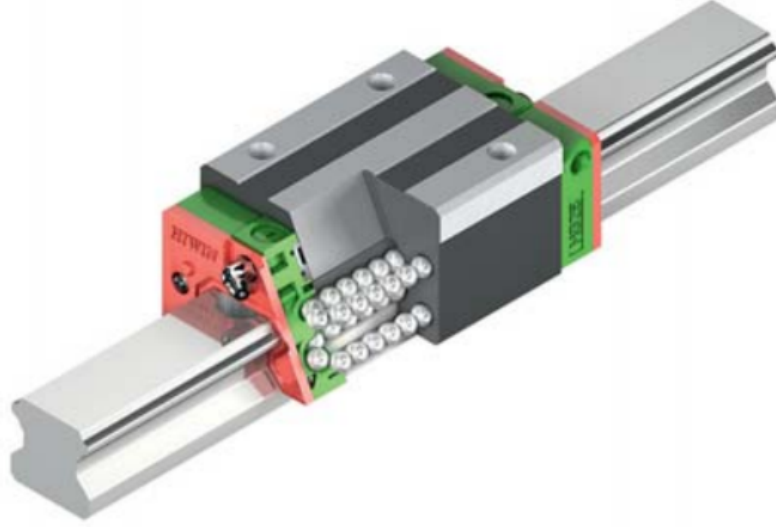


Figure 14: Linear guide and runner

The two components belong to the family HG that presents a big capacity of load and quite good stiffness. They are characterized by four ball recirculations arranged at 45° that allow a capacity of equivalent load in all directions. The main aspect is the elevated efficiency due to the reduced friction forces. The runner is positioned on the linear guide and slides on it through a system of ball recirculation.

2.1.8 Joint

The adopted joint to be able to connect the screw to the crankshaft is the bellows joint GSF GR2 with holes 13/19 from the firm CominTec.

This joint has been selected for several reasons:

- ease and modularity in the coupling; this allows the connection of the crankshaft with the screw one, despite different diameters;
- reduced moment of inertia;
- high torsional stiffness;
- wear resistance;
- it is ideal for couplings with servo motor thanks to its excellent dynamic characteristics, that permit fast reverses. The sizing has been effectuated starting from the maximum transmissible torque from the servo motor and determining the nominal torque guaranteed by the joint according to such a relation:

$$C_{NOM\ JOINT} = \frac{C_{MAX} \cdot K \cdot J_{UTI}}{J_{UTI} + J_{MOT}} \quad (6)$$

Where K is the load factor, whose value is function of the considered application. Due the usage of the servo motor, its value is equal to $K = 1.5$ It is represented in Figure 15.



Figure 15: Bellows joint

2.1.9 Anti vibration puffers

The anti vibration puffers are devices able to cut vibrations, bumps and the noise generated by all the parts in rotation and in movement.

The used puffers are produced by the firm ELESa with code DVB.6-38-35-M10-40-40 and each of them can bear a load of $840N$.

In the case under exam, six puffers have been considered that are connected to the wooden base through some holes M4 made on the base itself.



Figure 16: Anti vibration puffer

2.1.10 Screw-nut-supports

The screw FSC R25-10-0650-0650-0.05 and the nut R25-10K4-FSCEW-E are provided by the firm HIWIN. Together they form the screw-nut group whose aim is to convert the rotational motion to a translational one.

The group uses a system of rolled recirculating balls that, unlike the classic models with

sliding screws, reduce remarkably the dissipations due to friction and noise. They are shown in Figure 17.

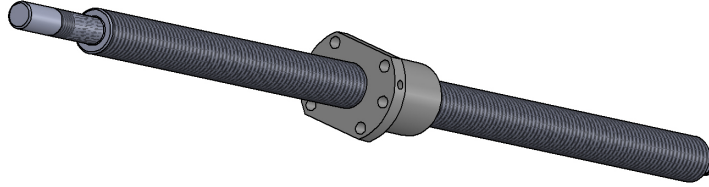


Figure 17: Screw and nut

The screw has then been manufactured by allowing in this way the coupling with the supports. From the side of the fixed support (BK15) the configuration on Figure 18 has been considered:

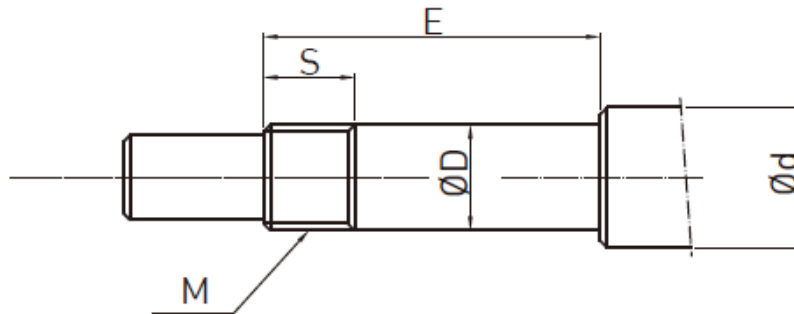


Figure 18: Manufacturing of the screw from the support BK15

This foresees a former reduction of the diameter until $\Phi D = 15mm$ to insert the support and a thread M15x1 of $S = 12m$ long to allow the blocking through the lock nut.

At the end, the left ending has been worked until a diameter of $\Phi D = 13mm$ to permit the insert of the lock nut, given its crest diameter $\Phi \approx 13.7mm$.

The side of the free support (BF15) has the configuration shown in Figure 19.

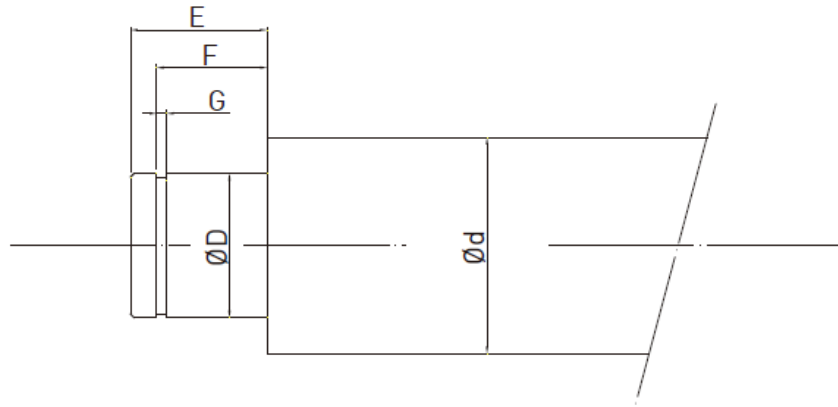


Figure 19: Manufacturing of the screw from the support BF15

In this case a manufacturing operation has been performed too to adapt the diameter to the one of the support, with $\Phi D = 15mm$.

Finally, a throat has been inserted to a Seeger ring. It creates a constraint, not of force, between the bearing the the screw itself.

2.1.11 Supports BK15-BF15

The screw-nut group is sustained by the supports BK15 e BF15 from the company HIWIN.

The configuration expects the insert of both a fixed and a mobile supports.

The fixed one (BK15) binds the screw both radially and axially.

All the loads in the axial direction discharge on the fixed support by means of a lock nut inserted through a thread generated on the rod of the screw.

The mobile support (BF15) reacts only to radial loads. Its purpose is to allow small axial movements that could be present because of thermal dilations. The system of the supports is shown in Figure 20

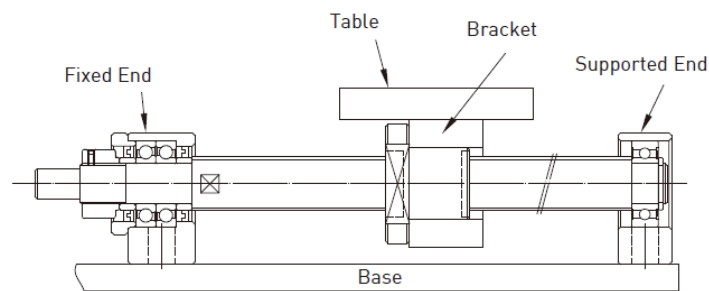


Figure 20: System of the supports

2.2 Construction of the test bench

This section analyzes the several operations that have brought to the completion of the test bench, shown in Figure 21. The enumeration of the adopted components in this

chapter refers to what is seen in the Figures 6 and 8. For this phase of realization, the co-rapporteurs Lentini and Pepe's help was indispensable.

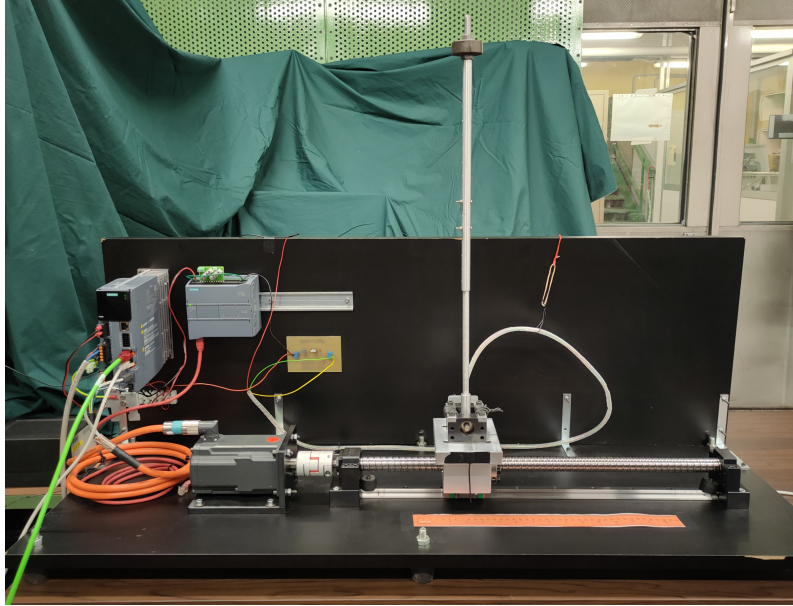


Figure 21: Complete Test bench

2.2.1 Basic structure and foreplay operations

The assembly of the test bench has been realized starting from a wooden piece that has been divided into two parts in such a way to create the base to support the actuation system and all mechanical components, and a support panel for the control elements.

The two structures have a thickness of $20mm$, a width of $400mm$ and a length of $1.15m$. The base has then been holed in several points, to allow the linear guide (3), the supports for the screw-nut group (15-18) and the motor flange (20) to be positioned.

The linear guide (3) has been blocked on the wooden base, by drilling it in five points. The more external holes allow the insert of two blocking elements (26) through two screws M4 $70mm$ long that are fixed through some nuts; these elements are used to avoid, in case of a software malfunction, the collision between the cart and the supports BK15 (17) and BF15 (15). The aim of the three intermediate holes is the blocking of the guide by means of some screws M6. In order to permit the fixing of all the support components, four through holes are realized, that consent to lock them by means of screws M6 and some clumping nuts. By proceeding in the same way, the support flange has been anchored to the motor.

The vertical panel is, instead, utilized to fix the drive (22) and a DIN omega guide (23), where the PLC (23) is mounted. The adoption of the DIN guide allows to insert eventual expansion modules of the PLC, if needed.

2.3 Assembly of the cart group and screw-nut

The first assembling operation was based on the inserting of the nut (1) in the bore on the slab (5). The nut (1), then, is blocked by positioning six biting screws M6, disposed at 45° relative to each other. Once this operation has been completed, the ball screw is inserted.

To avoid them falling, this screw is inserted by using the appropriate mounting tube in the nut (1).

A ball slide (4) is then attached on the surface below the slab (5) through four biting screws M4. It is then let flow on the linear guide (3), arranged on the basis. At the end, the fixed support Bk15 (18) and the mobile support Bf15 (15) are mounted, with corresponding bases (16-17), that are necessary to obtain the coaxiality of the screw with the crankshaft. The result of this first assembling phase is visible in Figure 22:

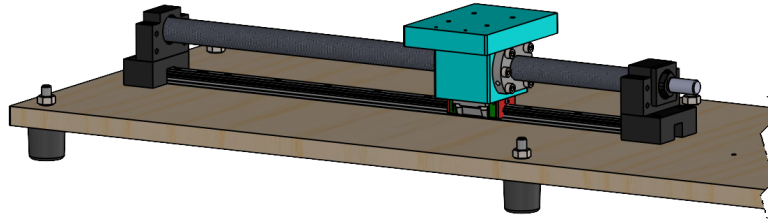


Figure 22: Assembling of the cart group and screw-nut

2.3.1 Assembling of the pendulum group

Next phase is the assembling of the pendulum group. This is made up of a threaded pin (14) that is linked, through a spine, to the external rod of the pendulum (12). Here, the internal rod (11) has been inserted, that has been constrained with three screws M3 and blocking nuts. Successively, everything has been fixed in the element strut of the pendulum (10) and fits on a shaft (9). The shaft is supported by some bearings that are inside the support elements HIWIN BF10 (8). The overall pendulum group and corresponding supports are mounted, through four screws M6, to the element slab (5). To monitor the angular quote, an angular sensor (28) is connected, that is made solidarity to the shaft (9) of the pendulum through an elastic joint (27), that allows to compensate even small misalignments. The angular sensor (28) is supported by an L bracket (7), fixed on the slab (5), through some biting screws M4. Lastly, some risers (6) are added, components that limit the angular shift of the pendulum in a range between $(-26.5^\circ, 26.5^\circ)$.

In Figure 22, it is possible to visualize the final result of such a phase.

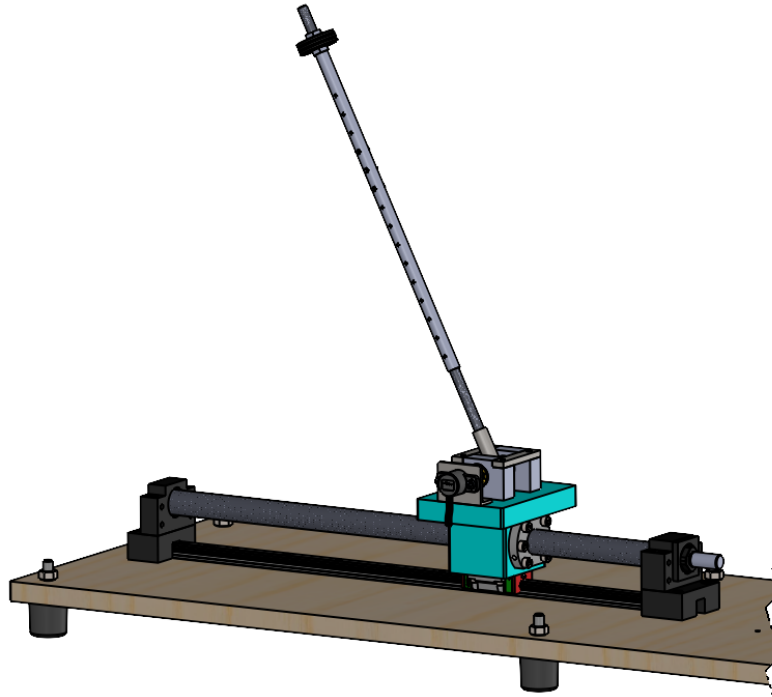


Figure 23: Assembly pendulum group

2.3.2 Connection of the motor

In order to optimize the management of the connecting cable OCC MOTION-CONNECT, the rotation of 180° of the round linking connector has been prepared, by acting on the screws that fix the connector to the carcass of the motor.

The motor (21) is hooked to the flange (20) through four screws M6 and concerning blocking nuts. The link between the crankshaft and the one of the screw is finalized by inserting a bellows joint (19). This is characterized by two different diameters by allowing an easy inserting and linking of the two shafts. The assembly operation is completed by tightening the blocking clamp screws, by using a dynamometric key such that the tightening torque reported on the catalogue is met. The joint enables the compensation of eventual misalignments due to the assembly or generated during the exercise.

The transmission of the torque is realized through the friction on the surfaces of the shafts and the joint.

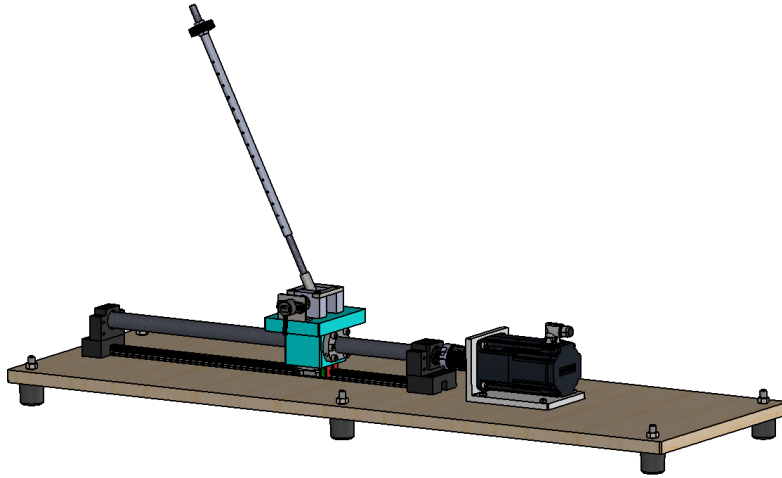


Figure 24: Link with the motor

2.4 Assembly of the vertical panel and the control system

The terminal phase of the assembly operation foresees the insertion of the vertical panel where to collocate the needed control devices. The wooden vertical panel is linked to the base through four L supports, that are very stiff. The blocking is realized by means of some screws M4 and relative tightening nuts. Then, it is realized all the bores that permit the Drive (22) and the DIN omega guide (23) to be fixed, where to thread the PLC (24) and some eventual expansion modules.

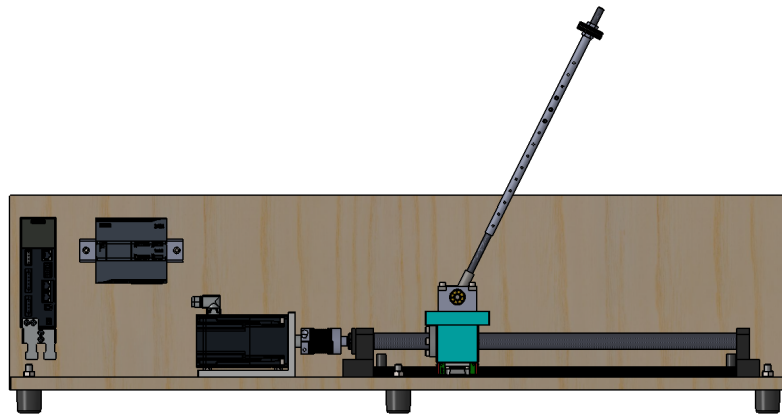


Figure 25: Complete test bench

The electrical plant comprehends all the connections and wirings, that are necessary to the correct functioning of all the electrical and electronic devices present on the bench. The general connection scheme among all the devices is shown in Figure 26.

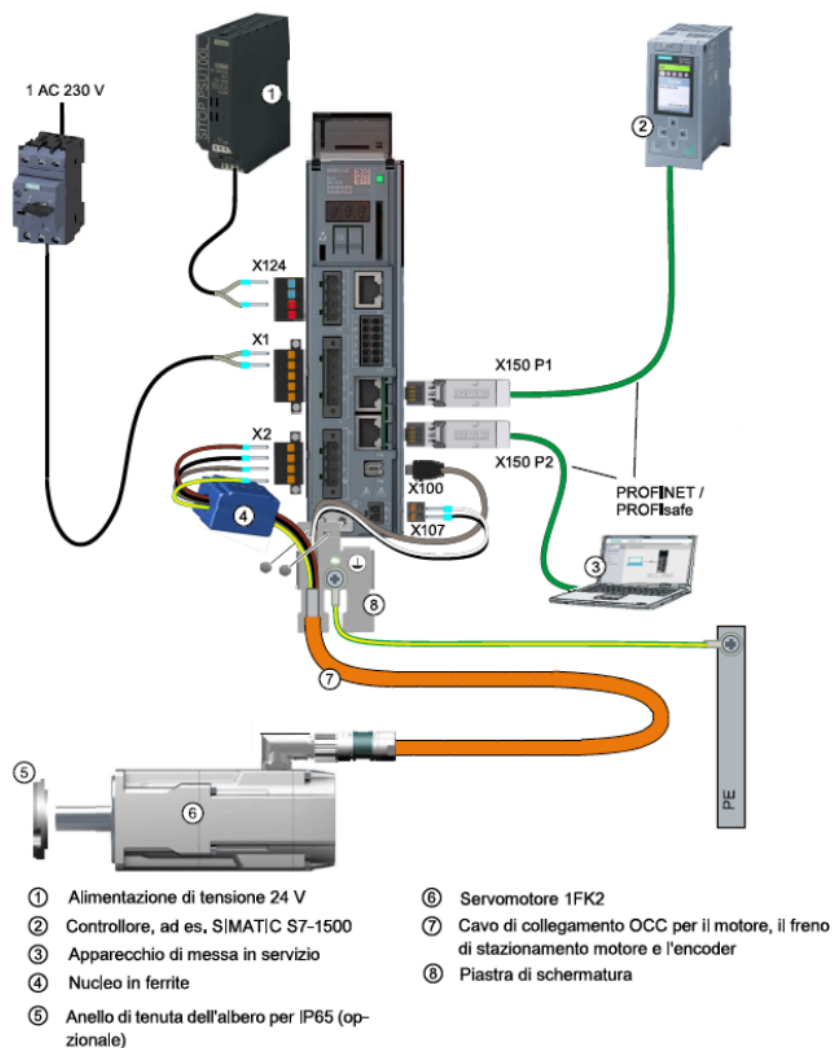


Figure 26: Synthetic scheme of the connection among all the devices

Each device, to work properly, requires a specific level of supply voltage; that is why, it is possible to identify three different DC voltage lines:

- 220 V, that is the maximum voltage on the bench. This is withdrawn by connecting a mobile quick wiring socket, specially sized, to the network sub-panel, that is present in the lab. It permits to supply the part of the drive whose purpose is the transmission of power to the motor. The connection with the drive happens through the connector X1, while the connection of the motor to the drive exploits the connector X2. The transmission of both power and data with the motor is realized by means of a cable OCC MOTION-CONNECT that starts from the connector X2 and is linked to the motor through a round connector with ten pins;

- 24 V, supply voltage of both the PLC and Drive. It is provided by a stabilized power supply from the "GRUPPO K.E.R.T";
- 5 V, voltage required by the angular sensor. It is generated by means of an electronic device L7805 and two capacitors, one of $0.33\mu F$, the other of $0.1\mu F$, located on a PCB. The used circuit for the generation of such a level of voltage is shown in Figure 27. The input voltage V_I is the same as the one of the Drive and the PLC, the output voltage V_O is about 5V. The presence of the capacitors allows to filter and improve all transients.

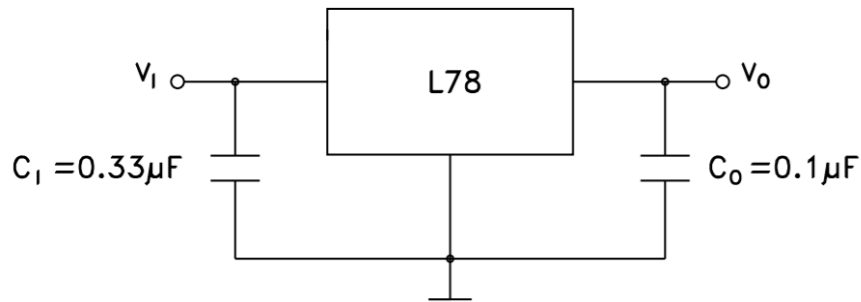


Figure 27: Circuital scheme for the generation of 5V

3 Overview of technological objects

This section handles some aspects. First of all, it is considered PLC with its main features; then it is put attention on drives, that allow the control of the brushless motor; all the technologies that can be used for the control and the management of the axis are considered. At the end, a guide is provided, where there are some basic notions of programming of TO in Tia Portal.

3.1 PLC

PLC (Programmable logic controller) is an electronic device for industry that is specialized in the management and control of industrial processes.

It is constituted by two fundamental parts, one software and one hardware.

The main hardware elements of a PLC are:

- The supply, that is used to feed all the cards of the PLC with electrical energy and it is normally a voltage of 24V;
- CPU, that interprets and manages the succession of instructions of the program. Moreover, CPU handles the communication with all buses of the PLC, transferring data and commands from and to the external world;
- digital and analog input cards, that are used for the management and control of digital and analogue quantities;
- digital and analog output cards, that are mainly adopted to command digital and analog actuators;
- communication cards.

The software part is made up of an operating system that is realized by manufacturer of the PLC itself, in the case in exam Siemens.

The drafting of the software happens through some programming languages the operator can use so that the PLC behaves in the proper manner. Among these, it is possible to remember graphical and textual languages.

About graphical languages:

- contact languages (LD, Ladder diagrams);
- sequential functional diagram (SFC, Sequential Functional Chart);
- block functional diagram (FBD, Functional Block Diagram).

About textual languages:

- instruction list (IL, Instruction List);
- structured text (ST, Structured Text);

The realization of the programs, in PLC Siemens, happens through the software TIA PORTAL v16, that is necessary to communicate with the PLC and execute the upload of programs in memory.

3.2 Drive

Drives can be distinguished mainly into two categories:

- continuous motion;
- discontinuous motion.

The former are linked to all motors whose velocity does not vary but in a very limited range; the latter is used, instead, for all axis that need continuous changes of velocity and that are characterized by important variations in their dynamic.

Several gammas of drives exist and are shown in Table 6:

	Continuous	Discontinuous
Basic	SINAMICS V20	SINAMICS V90
MEDIUM	SINAMICS G120	SINAMICS S210
HIGH	SINAMICS S120	SINAMICS S120

Table 6: Gammas of drives

Drive foresees a feedback system that is distributed in three levels, as shown in Figure 28. The inner one consists of a current loop the drive performs a current control with, that feeds the motor.

The setpoint of current is produced by the controller that is located in the second feedback level, that is a velocity loop. The setpoint of velocity can be imposed either manually by the programmer or it is provided by the outer feedback level (optional) that is a position/pressure feedback.

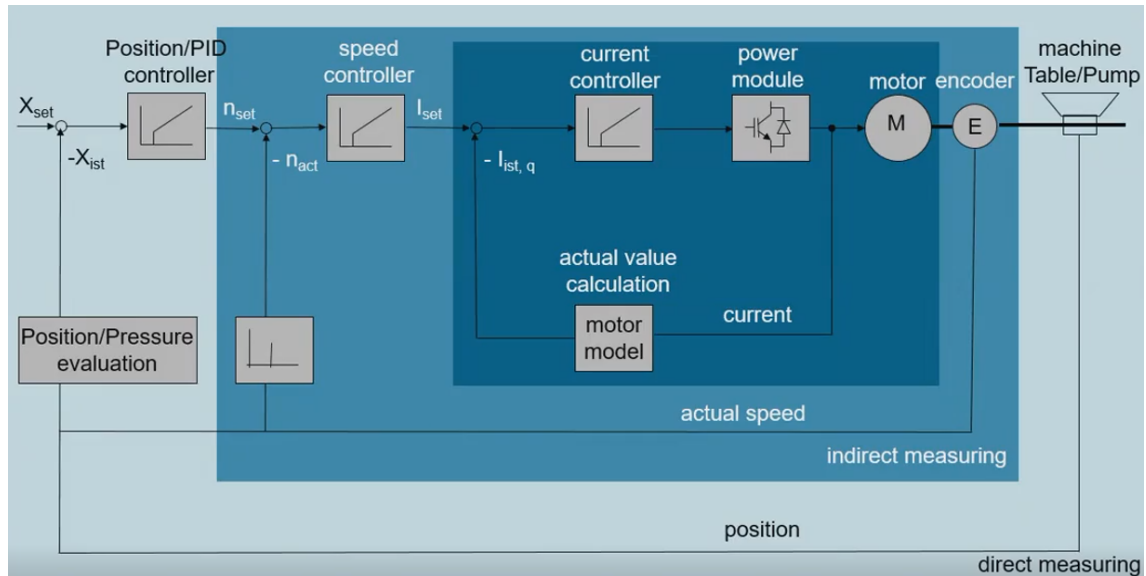


Figure 28: Feedback structure of the drive

By considering, for instance, the control in velocity, the setpoint can be provided in three ways:

- through a panel for the manual command;
- by means of a terminal block, that organizes analog and digital inputs and outputs;
- through a field bus that is a physical mean with a standard communication protocol where some info can travel. In the case under exam the PROFINET protocol is used, that is adapt to the exchange of data packets.

The programming of the drive is closed, that is to say it is not possible to produce some editable code. Control logics are given by the manufacturer of the drive, only small changes are admitted, by acting on a list of parameters.

3.3 Motion control

Motion controller is the mind of every control system of movement. In feedback systems, it sends a command toward the drive, it compares it with the feedback signal and introduces a corrective action that is needed to align the output signal (desider position) to the input one (real position), ideally with the minimun error possible.

Moreover, motion controller defines all trajectories the motor must follow to achieve the imposed commands. In other words, motion control works on the movements of all the axis linked to mechanical parts. The exchange of data repeats in a cyclical way through the telegrams PROFIdrive. PLC uses such telegrams to write on drive and, at the same time, it can read information from the drive itself. Telegrams are subdivided into words and each of them is made up of 16 bits and represents an informative content. The most popular ones are:

- standard telegram 3;
- standard telegram 5;
- standard telegram 102;
- standard telegram 105.

Telegrams allow the execution of the control of an axis in position or velocity. In TIA PORTAL, they can be selected in the section "Configuration devices", in the subsection "Regulation drive-telegrams", as shown in Figure 29:

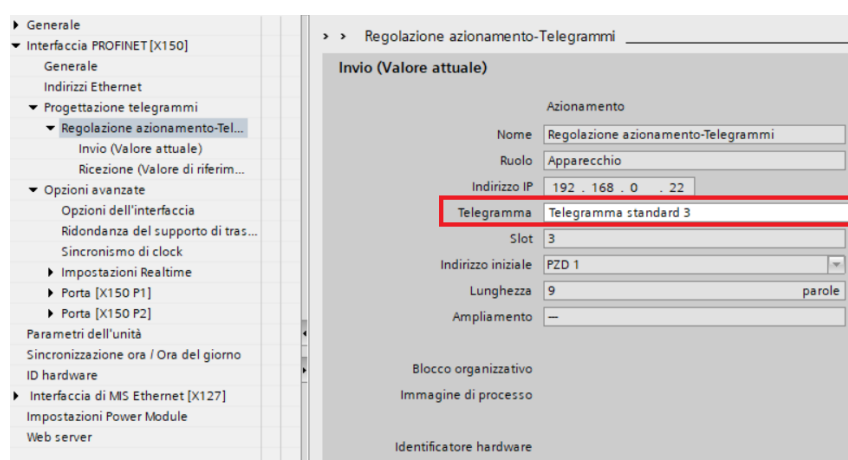


Figure 29: Selection of telegrams

In an industrial environment, it is possible to consider two kinds of motion control:

- EPOS;
- TO.

TO (technological object) can simplify the configuration of an axis with the respective associated drive. TO implies PLC to take on the responsibility of the closure of the position ring while the ones of velocity and current are managed by the drive. This implies PLC has a higher computational load because it has to sort out the position ring, but it reduces the complexity of the parameters of the drive.

EPOS, instead, shuts all the three rings inside the drive. This is adopted only if the aim is to lighten the computational load of the PLC, generally when more axis are to be controlled.

Once the process has been started, by booting the execute command of the OT, all info (position, velocity and acceleration) are sent to the interpolator that is something physical inside the PLC. It produces the setpoint of position that derives from the ramps of acceleration and deceleration imposed by the PLC. Once the setpoint has been generated, it is compared with data coming from the encoder and the resulting error is fed to the positioner that, in turn, produces a setpoint of velocity which is delivered to the drive. As regards EPOS, the solution is decentralized for the position control; in this case, the position control is managed by the drive too, without the data from the encoder reaching PLC. In fact, it provides only the setpoint of position deriving from the program block.

3.4 Technological object

The technological object is a simplified user interface toward real objects, such as drives and inverters. It is up to the OT to generate the commands to send to the drive for the parameterization and communicate the setpoint of velocity in real time. It needs also to receive information and introduce it in a legible way to a user. Configuration data are memorized in a DB technological block.

The most important TO are:

- SpeedAxis, technological object velocity axis;
- PositioningAxis, technological object positioning axis;
- SynchronousAxis, technological object synchronous axis;
- ExternalEncoder, technological object for the usage of an external encoder.

In PLC several blocks can be identified:

- MC-PreServo (OB67);
- MC-Servo (OB91);
- MC-PostServo (OB95);
- MC-Interpolator (OB92);
- OB1

The blocks MC-PreServo and MC-PostServo are not mandatory, and they are useful for the conversion of the data of telegrams in input and output, before them to be computed by PLC.

The block MC-Servo calculates the algorithms of regulation of all OTs that are designed in the CPU.

The block MC-Interpolator handles the production of the setpoint for all OTs designed in the CPU.

Computational times that are linked to the operation of such blocks are strictly correlated to the number of axis that are to be controlled. That is why the needed time between a motion cycle and the next one must be such to guarantee the resolution of all the tasks not to cause overflow.

This may happen when the main block (OB1), continuously interrupted by the blocks with higher priority, cannot be elaborated completely in $150ms$; this causes the stop of the CPU. An example of this concept is shown in Figure 30.

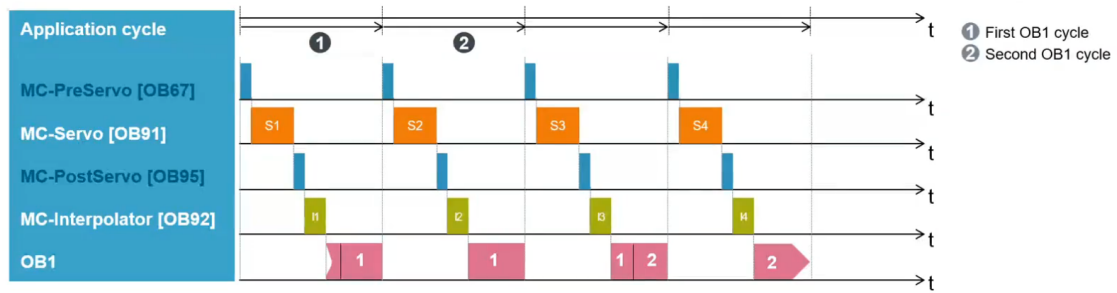


Figure 30: Example of time distribution

Generally, the blocks MC-Servo and MC-Interpolator take $4ms$ to be computed by PLC (when just an axis is managed) to which the time of OB1 should be added, that varies according to the quantity of present instructions.

Technological objects follow a matrioska model (shown in Figure 31) that comprehends three levels. The inner one is occupied by SpeedAxis; the intermediate one by PositioningAxis; the outer one by SynchronousAxis. This implies the more external level can also carry out operations that are connected to the inner levels, but not the contrary.

For example, PositioningAxis has the SpeedAxis inside too, but not the contrary.

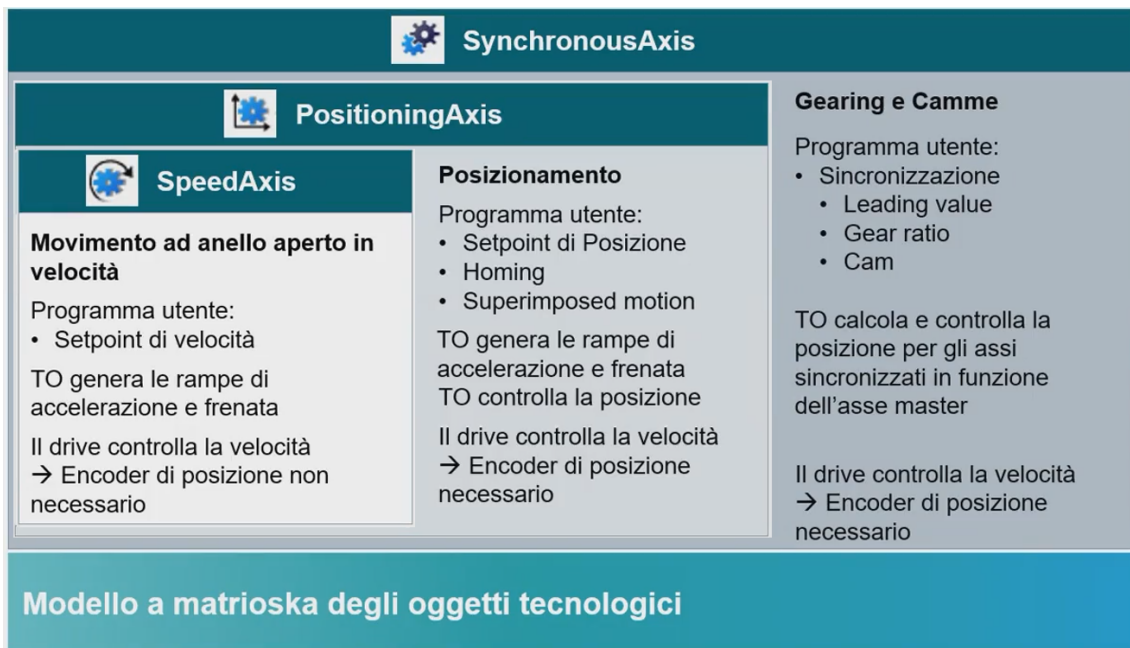


Figure 31: Matrioska model

3.4.1 SpeedAxis

A speed axis goes back to the open loop model, it is not needed an encoder for the regulation of the position for.

Such an axis handles the generation of ramps of acceleration and deceleration as function of the setpoint of speed.

In order to control such a technological object, several blocks are used through TIA PORTAL:

- **MC_Power**, shown in Figure 32, that allows the dwelling of the technological object through the activation of the "enable";

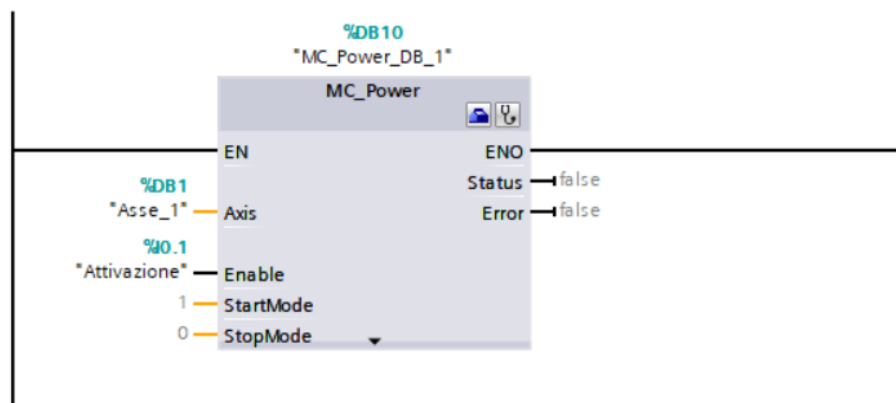


Figure 32: MC_power block

- **MC_Reset**, in Figure 33, whose aim is to reset the technological object if any errors

occur;

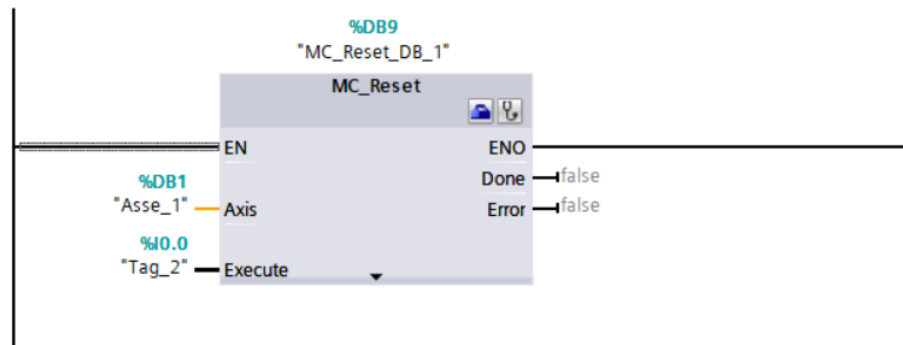


Figure 33: MC_Reset block

- **MC_MoveVelocity**, shown in Figure 34, that is an actuation block of velocity. Once activated, the axis is forced to the inserted velocity value in the parameter "Velocity";

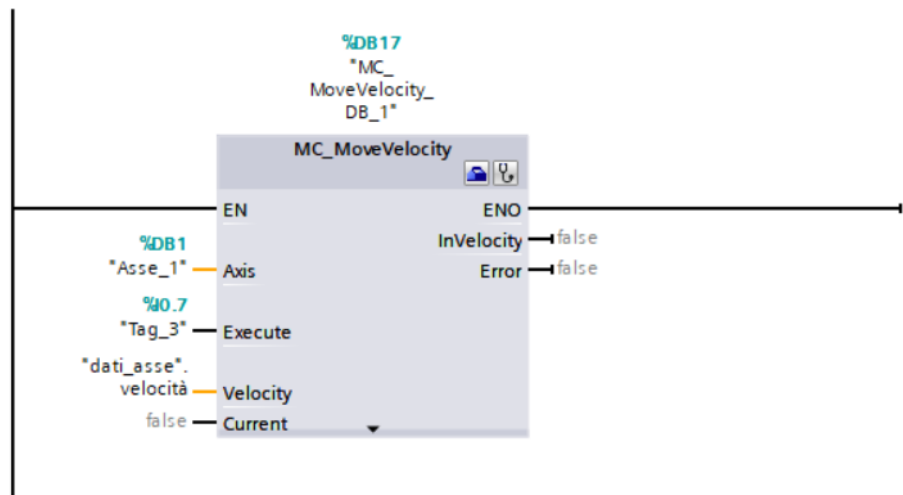


Figure 34: MC_MoveVelocity

- **MC_Halt**, Figure 35, that is used to stop the movement of the technological axis. In particular, it is adopted in association with MC MoveVelocity, as it can be disabled only through such a block;

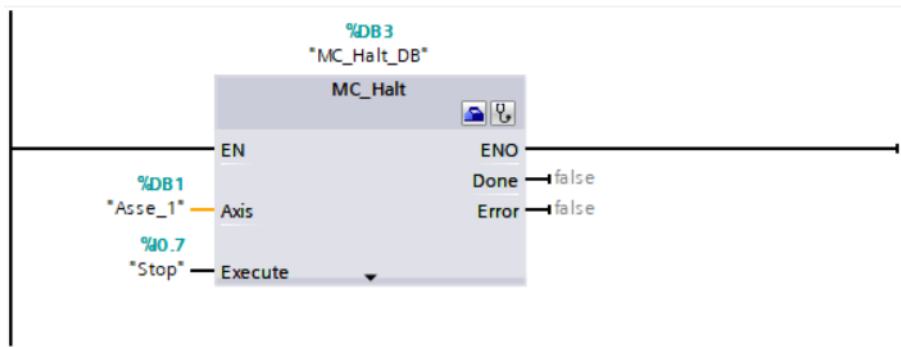


Figure 35: MC_Halt block

- **MC_MoveJog**, in Figure 36, that acts on the bit state of the sections "JogForward" and "JogBackward". When the logic value of the bit is 1, the axis starts moving, with the speed selected in the parameter "Velocity", in the positive direction in case of JogForward, negative if JogBackward is activated. Once the bit is moved back to 0, the motion stops.

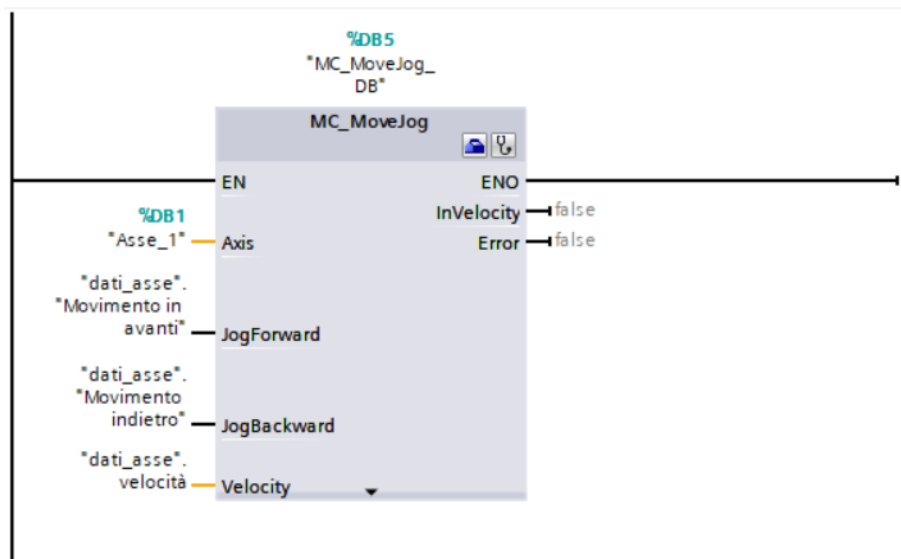


Figure 36: MC_MoveJog block

3.4.2 Positioning Axis

The main difference between the positioning axis and the speed axis is the presence of an encoder. Now, the OT generates the ramps of acceleration and deceleration and it controls its position.

The same control blocks as the SpeedAxis are implemented inside the PositioningAxis, three further control blocks for the control of position are added to:

- **MC_Home**, in Figure 37, used to take back the axis to the origin of the reference frame;

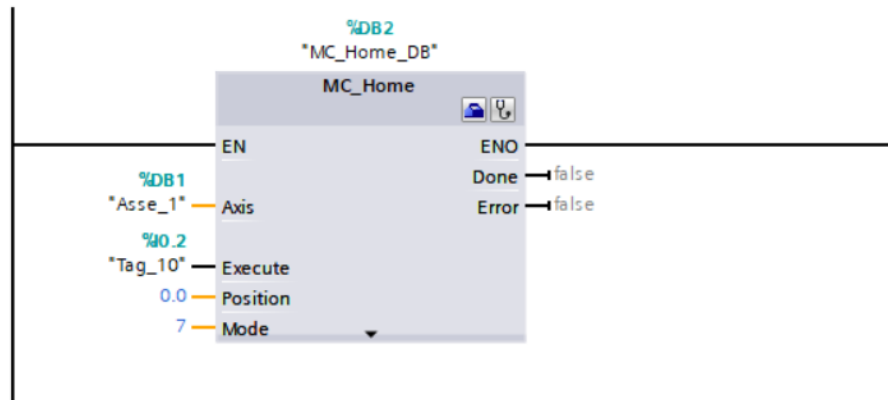


Figure 37: MC_Home block

The research of the reference point can be performed both in an passive and a active way. The former foresees the user has to move the axis until to cross the zero mark with a quite low speed, but not equal to 0. The latter is characterized by the axis itself that fulfills a routine of movements to reach the zero mark with an almost zero velocity. The active research is more accurate than the passive one.

- **MC_MoveAbsolute**, in Figure 38, that permits the axis to move in an absolute manner, that is with respect the origin of the reference frame, defined by homing:

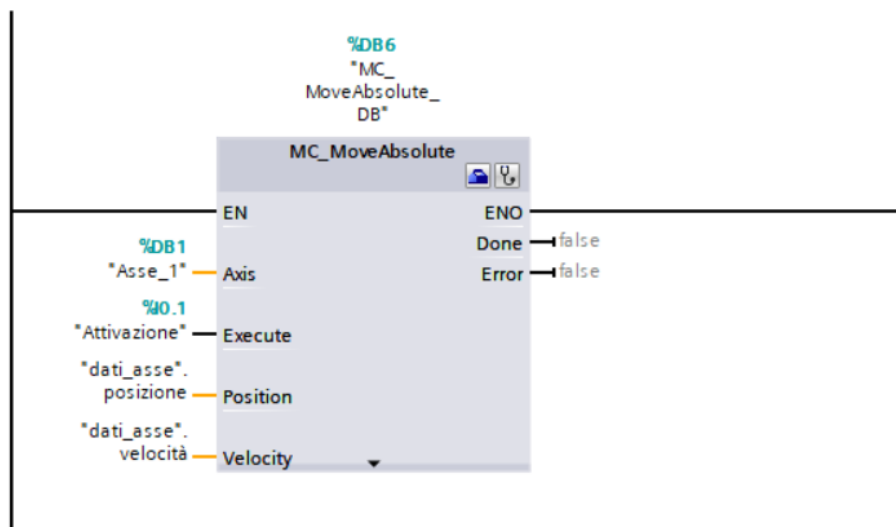


Figure 38: MC_MoveAbsolute block

- **MC_MoveRelative**, Figure 39, thanks to which the axis can translate (or rotate) in a relative manner with respect to the actual position of the axis itself;

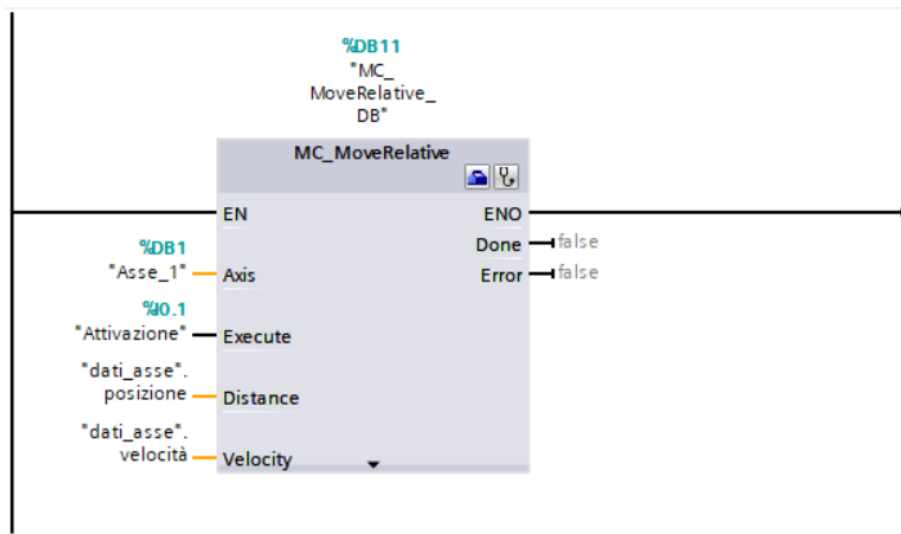


Figure 39: MC_MoveRelative block

3.4.3 Synchronous Axis

Its aim is to keep a synchronization between the axis to be commanded and a master axis. Two kinds of synchronization are possible:

- Relative synchronization (or relative gearing) is used to hook a slave axis to a master one with respect to its setpoint of velocity, without communicating a position of synchronization. Once driven, the slave axis starts moving till to synchronize its speed to the one of the master axis.
- Absolute synchronization (or absolute gearing) allows the slave axis to be hooked to the master one, not only in velocity but also in position so that a faithful one by one coupling between the two axis is obtained.

It is shown in Figure 40.

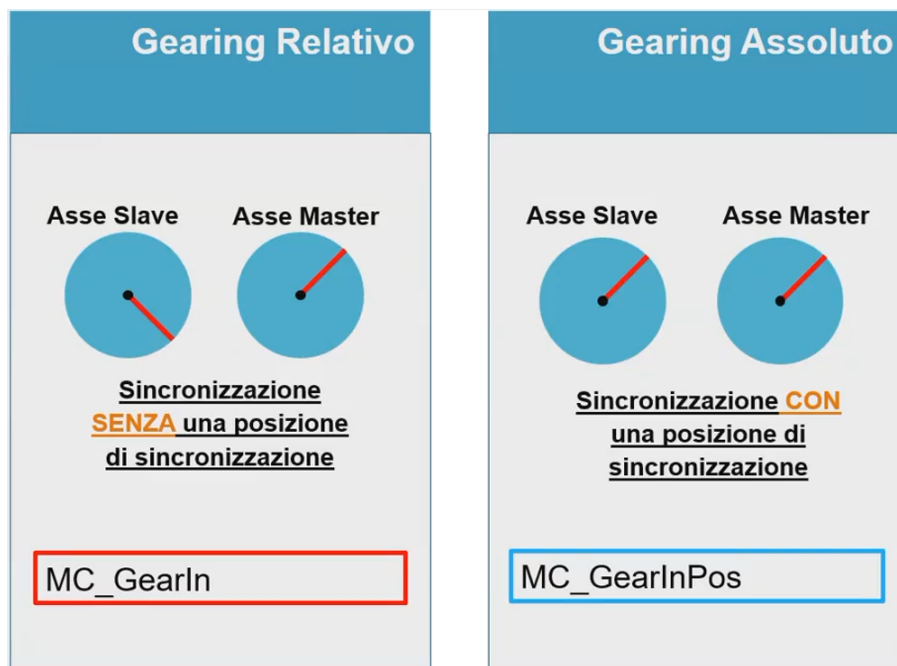


Figure 40: Example of relative and absolute gearing

4 Guide for the setting configuration

The realization of the project in TIA PORTAL environment has been performed by following several steps.

Firstly, it needs to define PLC to use among the ones reported in list; the best way to meet this requirement, in order to avoid problems of recognition, is to consider a blank PLC (in the case in interest one from the family s7-1500), Figure 41, and effectuate then the operation of detection.

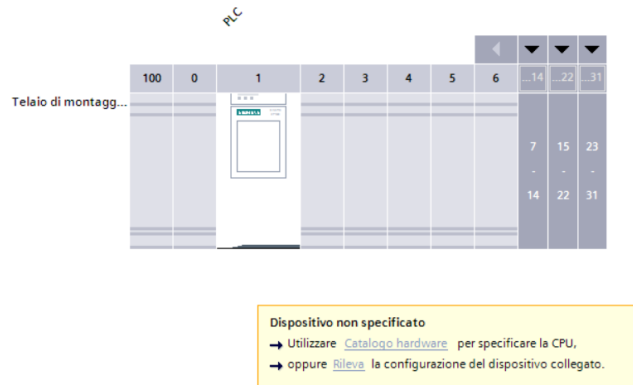


Figure 41: Blank PLC in TIA PORTAL

Once the PLC has been identified, there is the possibility to visualize, in the section properties, some information as the manage of all analog and digital inputs and outputs, the possibility to define a fast counter HSC in case of an external encoder or sensor, and all options about the communication Profinet.

Next step consists of the recognition of the drive, that can be inserted manually or through a hardware identification, as shown in Figure 42.

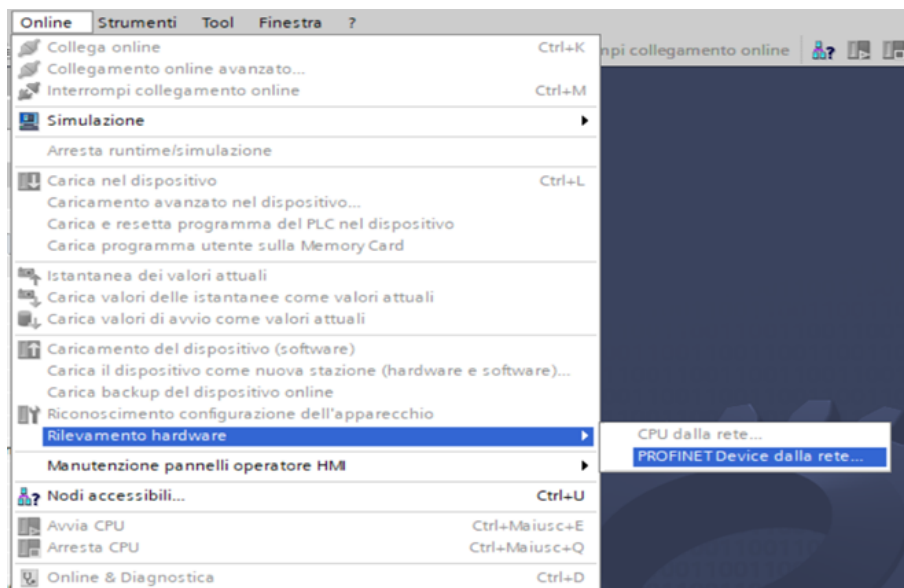


Figure 42: Identification of the drive

In the project the drive has been inserted manually, from the section in TIA PORTAL "Aggiungi nuovo dispositivo", "Azionamento" and, finally, by choosing the device to use. In the considered case, a drive SINAMICS S210 1 AC,200 – 240V, 0.4kW (Figure 43) has been adopted.

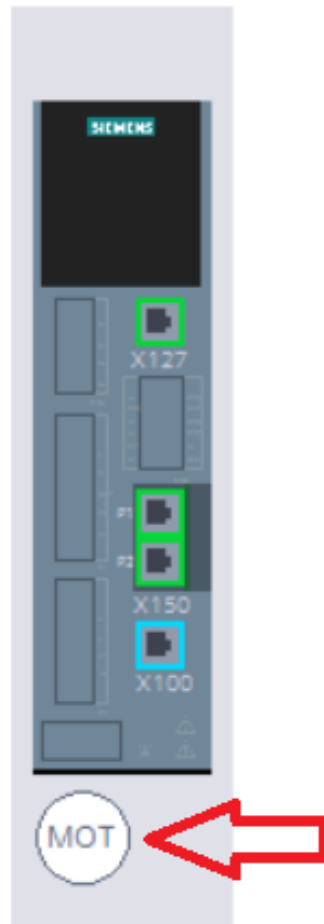


Figure 43: Drive representation in TIA PORTAL

From this point, it is possible to select the motor from a catalogue that is present inside the subsection "Selezione del motore", in the section "Generale", shown in Figure 44.

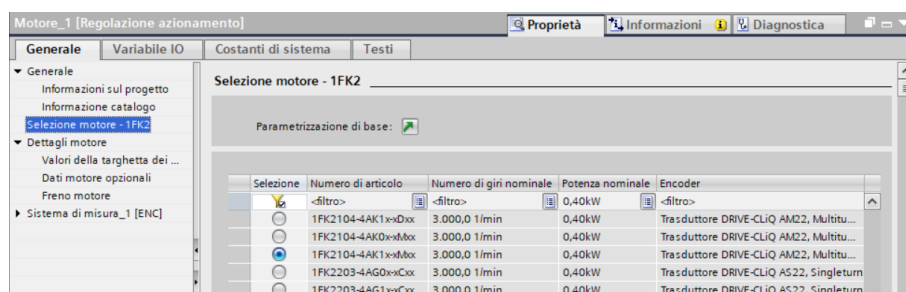


Figure 44: Selection of the motor

Once both the PLC and the drive with respective motor have been defined, the link between the two devices need to be done, so that they can communicate correctly, by means of a Profinet cable. This is to guarantee the iteration through PROFIBUS protocol. This can be performed in the section "Vista di rete", by linking the two devices and forcing, by double clicking on the junction wire, the Profinet configuration (Figure 45).



Figure 45: Link between drive and PLC

Once this first connection has been effectuated, it is necessary to link the CPU and the Drive in the topological view too (Figure 46). In particular, it is mandatory to connect the physical used ports of both the devices, not to fall in error.



Figure 46: Topological view

4.1 Technological axis and its configuration

Next step consists of configuring the technological object "PositioningAxis". The first step foresees the consideration of the section "Oggetti tecnologici", to open a new object and, from the resulting window, to select the positioning axis (Figure 47).

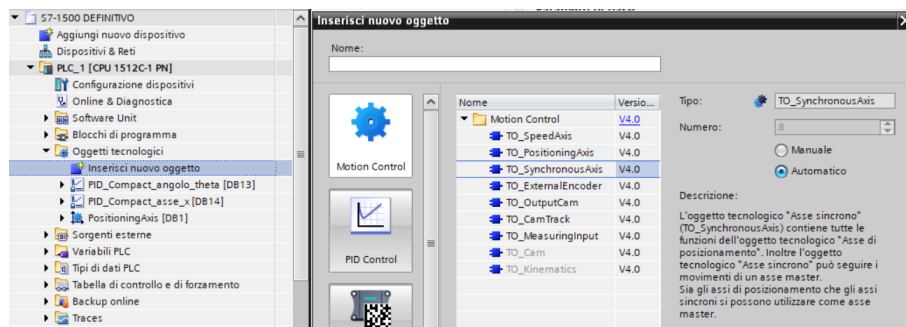


Figure 47: Insert new axis

Once the new technological axis has been created, it must be configured so that it works properly with the chosen system. As follows, the main steps to consider for its correct configuration are listed. First, it needs to set the basic parameters and the hardware interface:

- "Parametri di base", where it is possible to give a name to the axis and the considered unit of measurement for the axis. The chosen unit of measurement is millimeters, as it is going to control a linear motion of the cart along the guide. As a real axis is available, no simulation has been considered. This is shown in Figure 48;

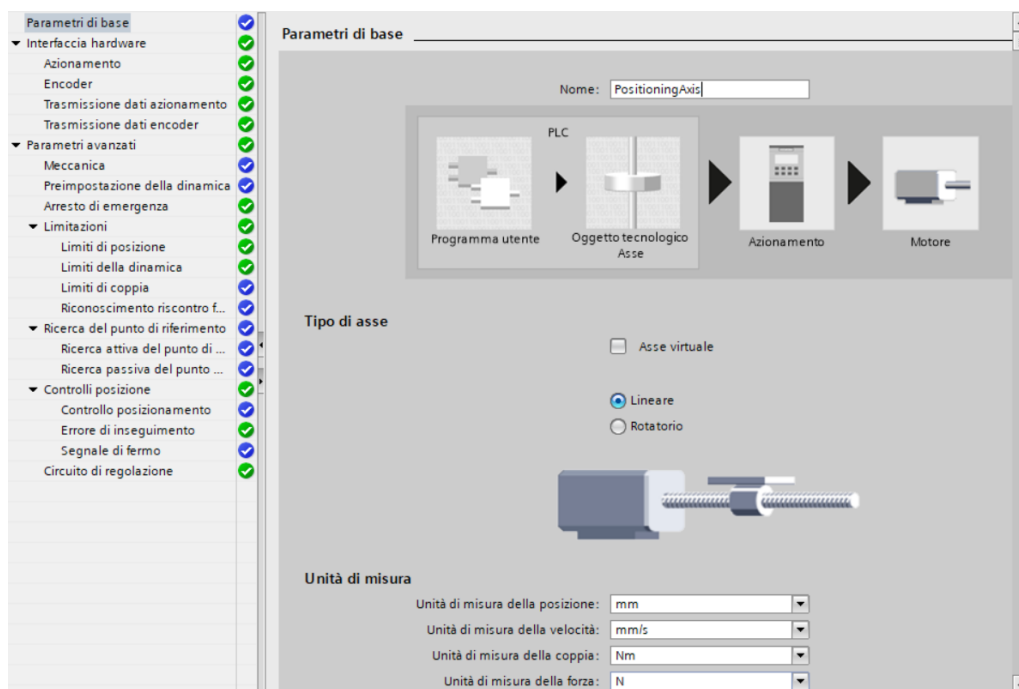


Figure 48: Basic parameters of the technological axis

- "Azionamento", where there is the need to select the kind of communication the drive is to be controlled. and which of them is connected to the PositioningAxis to control. In this case, the selection of the protocol of communication is Profidrive. PTO, in fact, establishes the usage of a pulse train, applicable, for example, to step motors.

By clicking in the subsection "azionamento", the complete list of all available drives is reported. In this case, the defined drive at the previous step has been chosen.

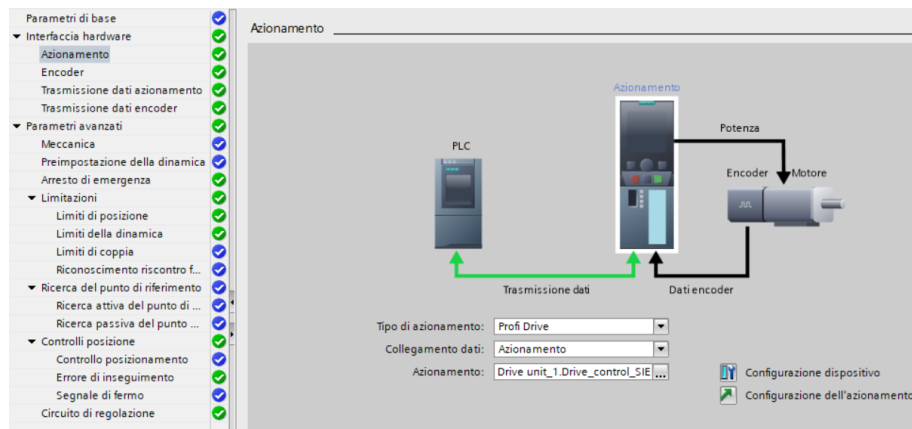


Figure 49: Configuration of the drive

- "Encoder", where it is possible to choose either an encoder on Profibus or one on fast counter HSC. As it is present an internal encoder in the motor that is being used, the first option is considered (Figure 50). From the data sheet of the motor, it infers the encoder is rotational absolute.

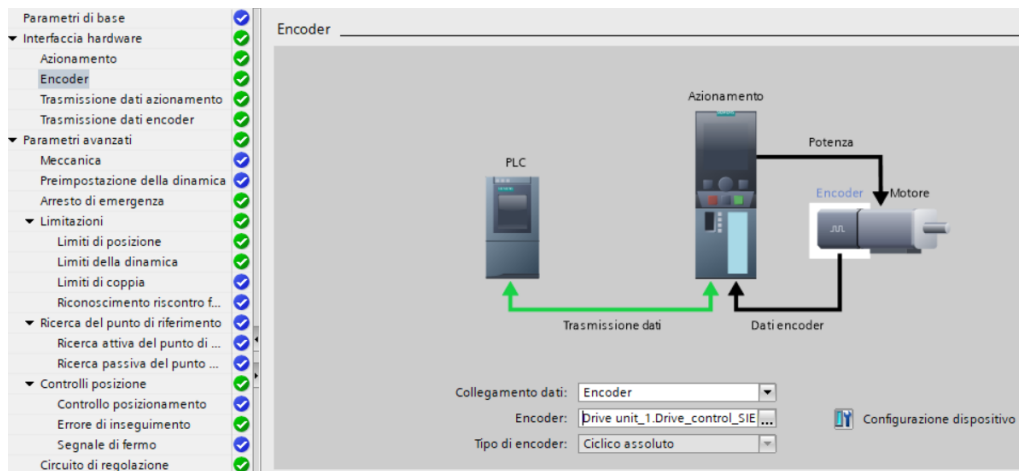


Figure 50: Configuration of the encoder

- "Trasmissione dati azionamento"; an important parameter is the selection of the telegram of communication as, if a not compatible setting with the CPU is considered, all the devices do not work in the proper way. As the CPU S7-1500 has any clock available for the synchronism with the drive, which is activated with the telegram 105, it is possible to maintain it. It transmits command and state words, the reference value and the present value of the number of turns, the state of the encoder and its real position. At the end, it is possible to impose the automatic acquisition of the values of the drive that, in some cases, may cause errors relative to the acquisition of the parameter p1082 corresponding to the maximum number of turns. Therefore, the

manual acquisition has been adopted, by imposing as number of turns of reference 8000rpm and maximum number of turns 8000rpm. It is shown in Figure 51;

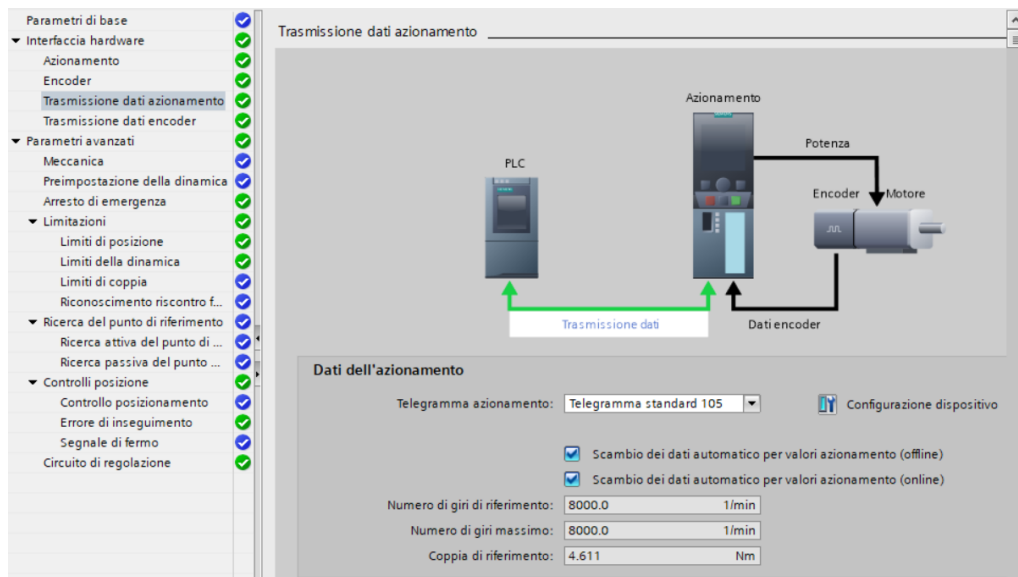


Figure 51: Choice of the telegram

- "Trasmissione dati encoder", where it has to select the same telegram as the one used for the transmission of the data between Drive and PLC (Telegram 105). It is shown in Figure 52:

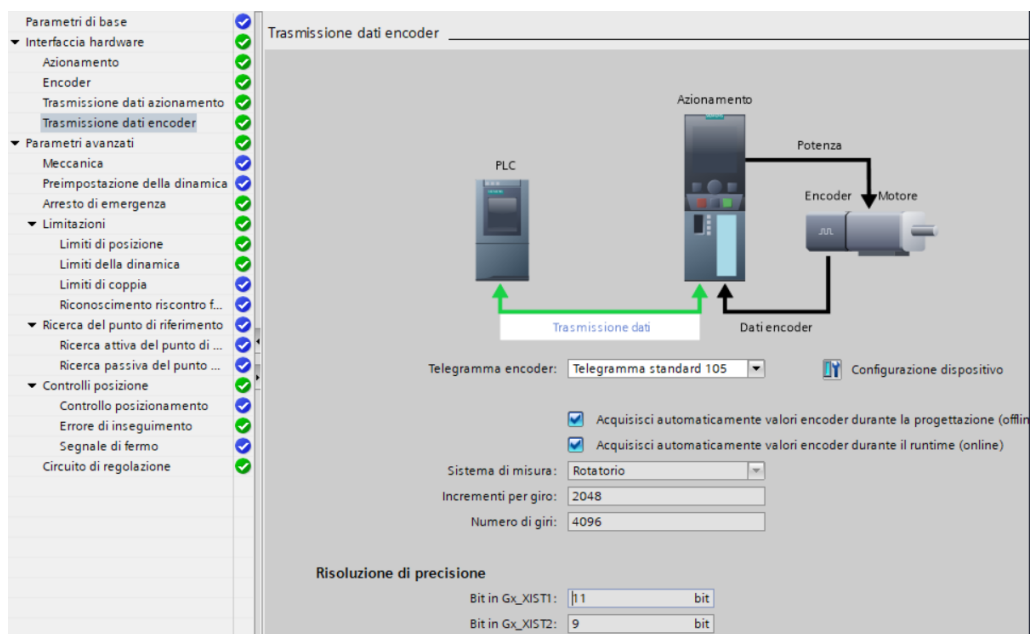


Figure 52: Choice of the telegram of the encoder

Next step consists of considering the section "parametri avanzati", where, mainly, two subsections need to be set:

- "Meccanica", where it is possible to identify the assembly of the encoder on the crankshaft or externally from it. In this case, it is mounted on the crankshaft. Moreover, it needs to insert the pitch of the screw, that highlights the linear translation of the screw-nut group for every turn of the motor. This allows the reading of the present position coming from the encoder and written directly in linear position. In this case, the pitch is 10mm . This is shown in Figure 53;

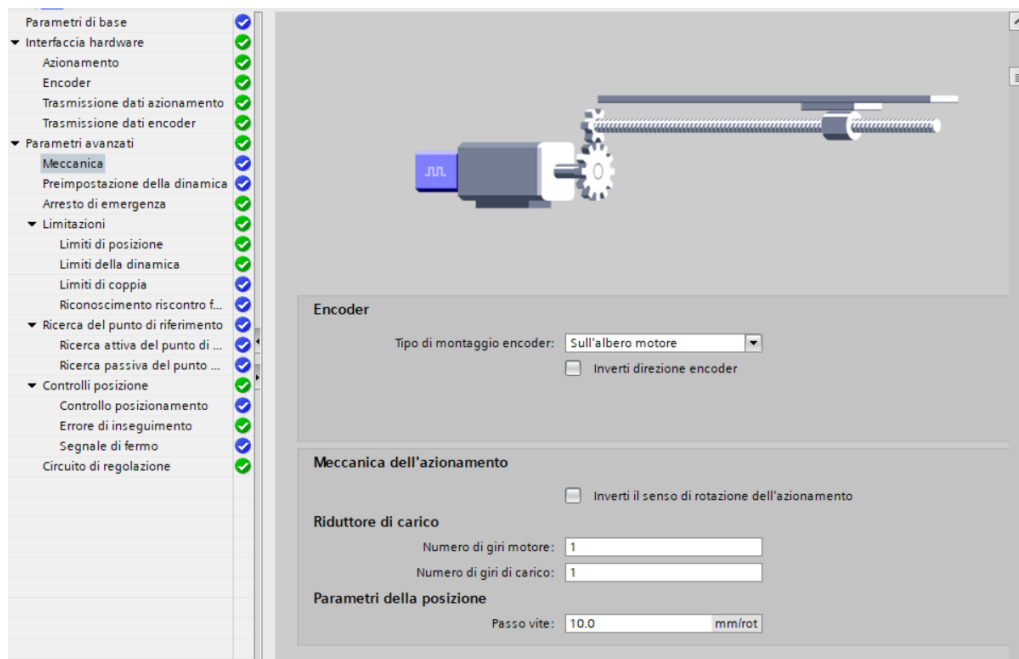


Figure 53: Mechanical configuration of the drive

- "Arresto di emergenza", where it is possible to define the needed time for a complete stop in case of emergency. This can be set either by acting on deceleration time or directly on its maximum value. The former is linked to the stopping time by considering the axis at its maximum speed. It is shown in Figure 54:

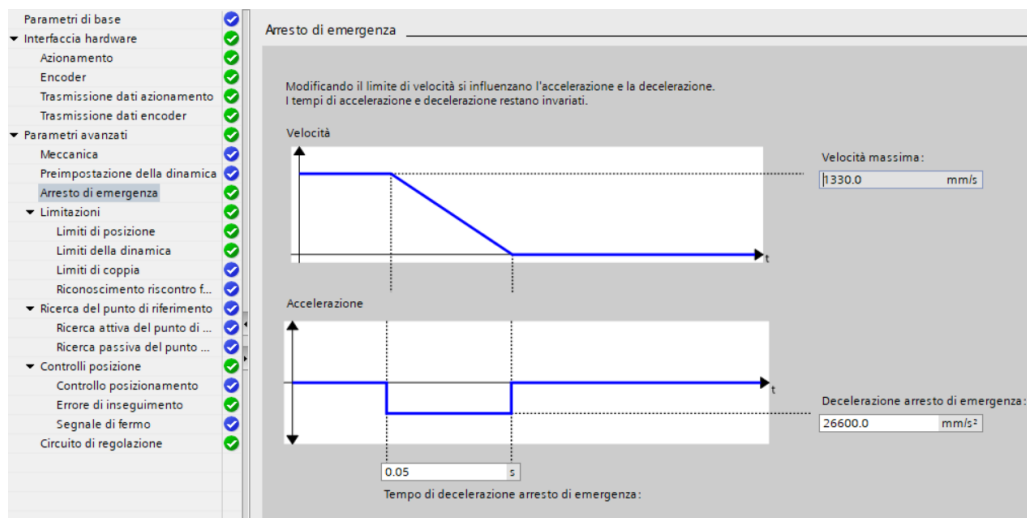


Figure 54: Emergency stop

At the end, the section "Limitazioni" needs to be set, that is made up of the following subsections:

- "Limiti di posizione", where it can be imposed some hardware or software end stroke. The former are possible only if some sensors of position, that identify the end strokes linked directly to the PLC, are physically present. Then, all associated inputs must be inserted in the sections "ingresso finecorsa hardware inferiore" and "ingresso finecorsa hardware superiore". As such sensors are not available, the second option is considered, that is feasible only after establishing the reference point (homing). After choosing as reference the centre of the linear guide, the two virtual end strokes are located at a distance in absolute value equal to 230mm. In this way, if the cart should get to the determined limits, the system stops according to a dynamic that is configured in the previous step. This is demonstrated in Figure 55.

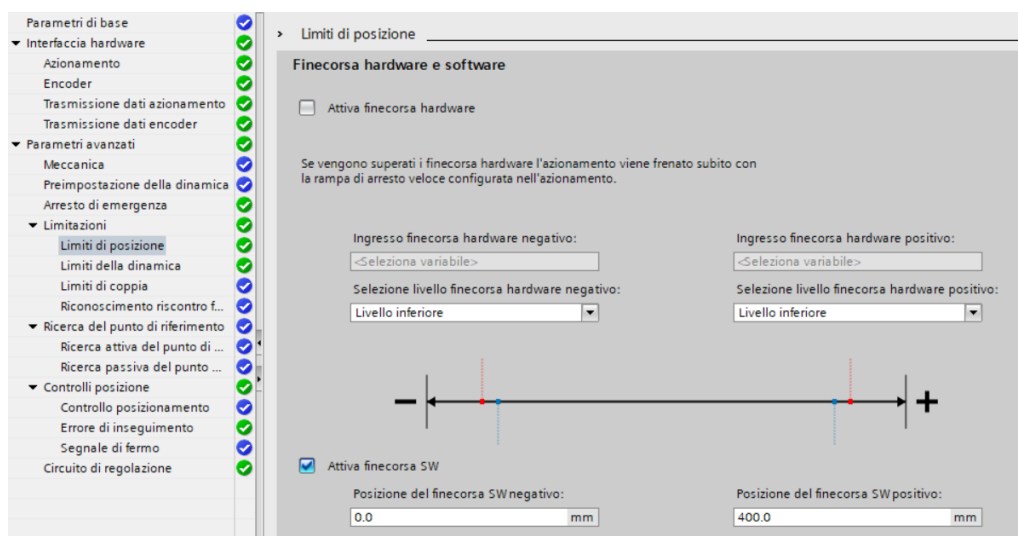


Figure 55: Configuration of end strokes

- "Limiti della dinamica", where it is possible to select the maximum speed, in terms of rpm or $\frac{mm}{s}$, of the axis. It can either set directly the parameters of "Accelerazione massima" and "Decelerazione massima" or indirectly modify them by means of the "Tempo di accelerazione" and "Tempo di decelerazione". The former is the time needed to reach the maximum velocity by starting from a rest condition; the latter is the time needed to stop the axis, starting from the maximum velocity. Moreover, there is the possibility to impose a maximum value for the jerk too, in the section "Strappo". It is shown in Figure 56

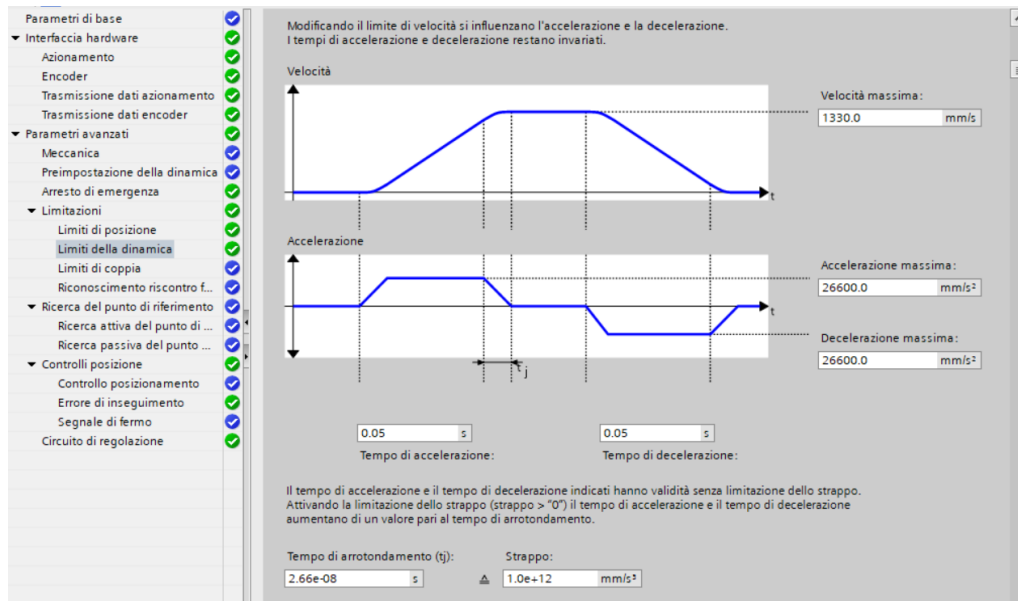


Figure 56: Dynamic configuration of the drive

The remaining sections have not been dealt with because out of the scope of this project.

4.2 PID compact

PID controller, in the TIA PORTAL environment, is presented in form of technological object. In order to define it, it is necessary, like for the technological object, to create a new OT. Once "inserisci un nuovo oggetto" has been clicked, it needs to consider the section "PID control" and select the section "PID_compact", as reported in Figure 57.

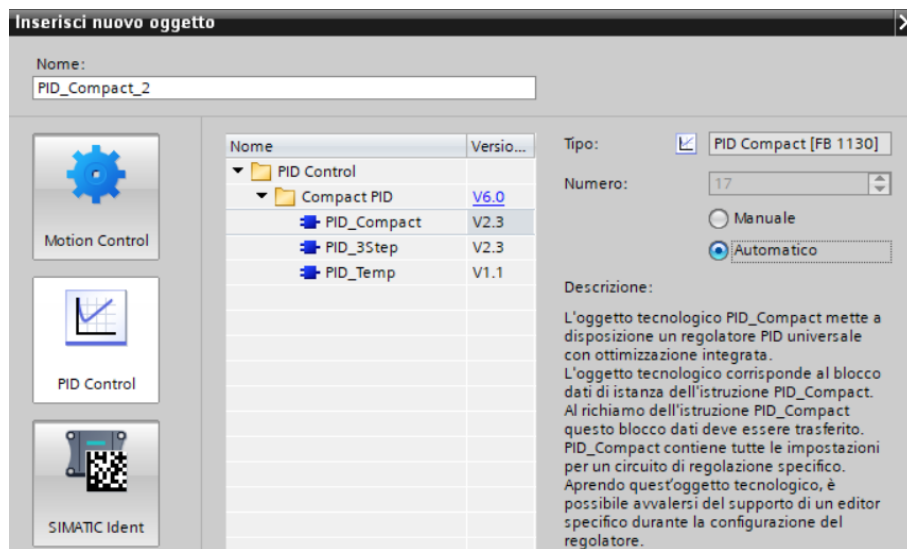


Figure 57: PID selection

The configuration of the controller is done, as for the axis, in several steps. First of all, basic settings have to be handled, section that is subdivided into two parts:

- "Modo di regolazione", Figure 58, where to insert the physical quantity that is going to be controlled, its unit of measurement and setting up the functioning of the controller in an automatic way; in this way, the controller is effectively on;

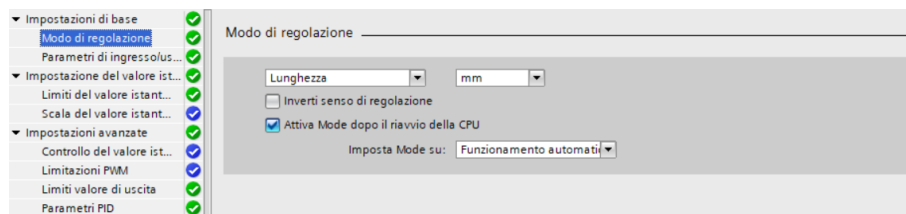


Figure 58: Mode of regulation

- "Parametri ingresso/uscita", Figure 59, where it is possible to choose between two typologies of inputs and among three kinds of outputs. The PER version indicates a signal fed in input to the controller or, similarly, leaves it as an output, through analog channels of the CPU. The other version, instead, considers signals directly signals coming from the program. The PWM output, finally, produces a pulse modulated signal.

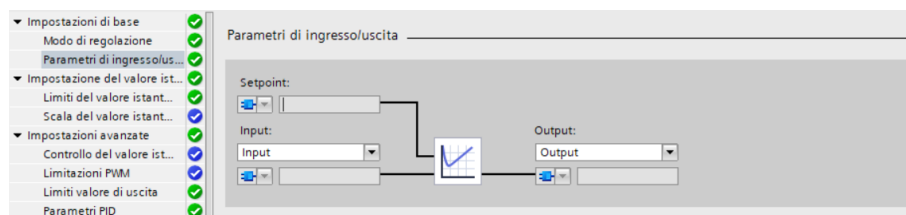


Figure 59: Input and output of PID

Afterwards, the category "impostazione del valore istantaneo" is configured. It is made up of two parts:

- "limiti del valore istantaneo", Figure 60, that establishes the limits of the input scaled variable. On the basis of these values, the OT scales the input by attributing to 0% the lower limit, 100% the upper limit;

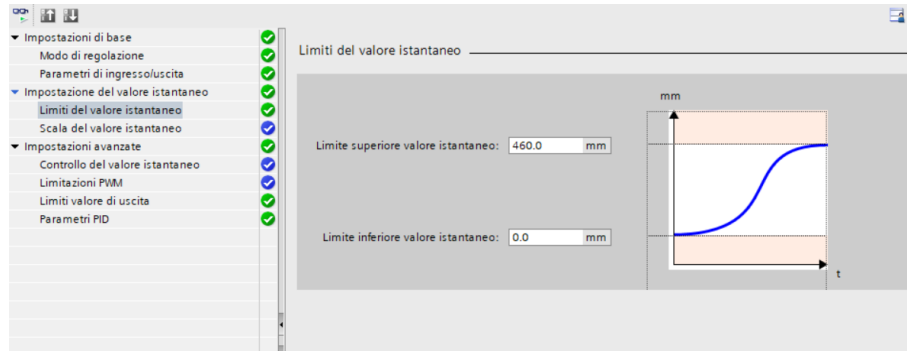


Figure 60: Limits of the instantaneous value

- "scala del valore istantaneo", Figure 61, used to scale all analog inputs handled in a standard way in a interval $0 - 27648$.

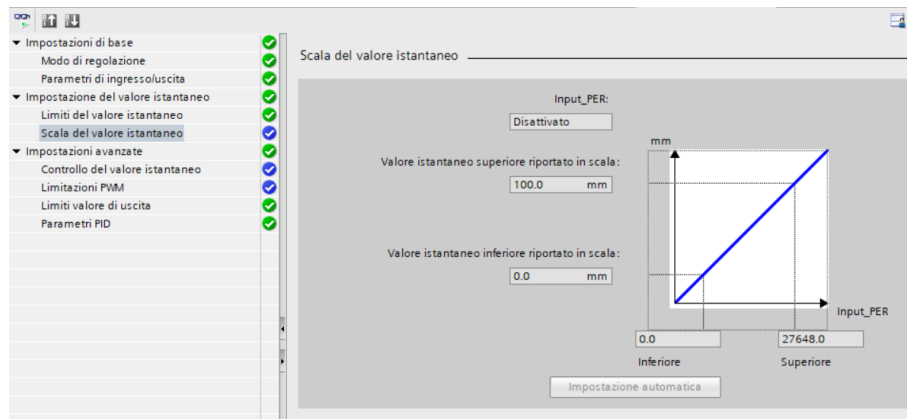


Figure 61: Setting of analog inputs

The final step consists of dealing with "impostazioni avanzate". The first two setting options have not been taken into account in this project, but in principle the "controllo del valore istantaneo" allows to impose some limits of input that activate an error bit if reached; the "limitazioni PWM" are used only in case of output PWM.

The accounted settings are the following:

- "limiti valori di uscita", Figure 62, where it establishes in which percentage scale the output is generated. If only positive values are required, the default scale ($0 - 100\%$) can be used; if, how in this case, also negative values are needed, the scale can be set in a range ($-100\%, 100\%$);

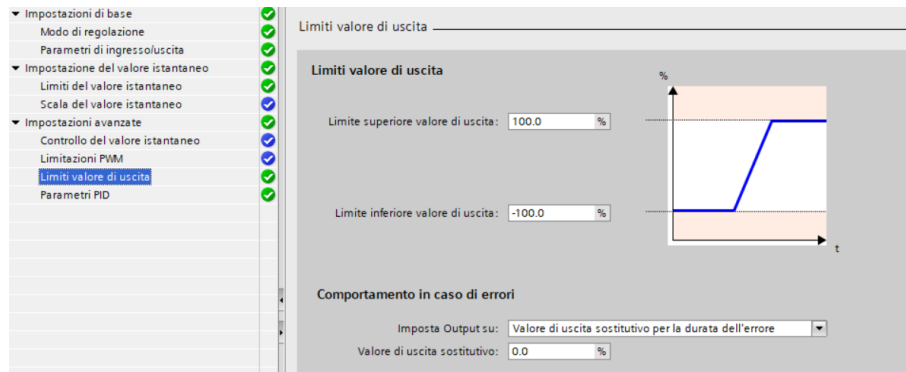


Figure 62: Limits of the output

- "parametri PID", Figure 63, where PID parameters can be set.

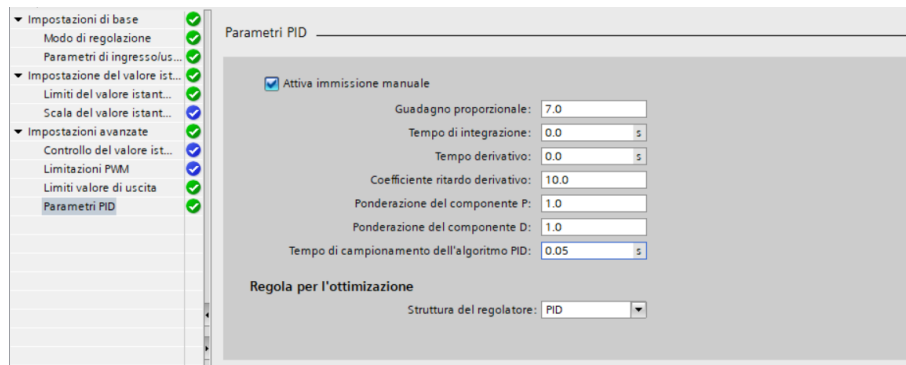


Figure 63: Setting of PID parameters

By analyzing all the terms that constitute the PID controller, it is possible to distinguish three contributes:

- **Proportional action**, function of the instantaneous error. A big K_p generates an incisive control action even if small errors occur, while a small K_p will make the present value of the error less relevant;
- **integral action** acts on the past behaviour of the error. The integrative constant K_i is defined as the ratio between the proportional coefficient K_p and the integrative time T_i , by resulting in the equation

$$K_i = \frac{K_p}{T_i} \quad (7)$$

A tiny value of T_i , with the same K_p , will make the control action more relevant in case of a higher past error, while a lofty value of T_i will tend to reduce the ratio; this make the control signal $u(t)$ less sensible to the past values of the error, by giving more importance to the proportional action and, eventually, to the future behaviour of the error;

- **derivative action** acts instead on future dynamics of the error. The derivative constant K_D is defined as the product of the proportional coefficient K_p and the

integrative time T_D , by resulting in the equation

$$K_D = T_D \times K_p \quad (8)$$

The more T_D increases, the more the control action in case of variations of the error intensifies; smaller T_D becomes, instead, more insensitive the control action will be to the variations of the error, by considering more and more the past and present values of the same. A strong derivative action determines a superior readiness of the control system, above all it needs to pursue a desired value for the variable output, and not a fixed setpoint.

To compute the output of the PID _Compact, the controller uses the formula shown in Figure 64:

$$y = K_p \left[(b \cdot w - x) + \frac{1}{T_i \cdot s} (w - x) + \frac{T_d \cdot s}{a \cdot T_d \cdot s + 1} (c \cdot w - x) \right]$$

y	Valore di uscita	x	Valore istantaneo
w	Setpoint	s	Operatore di Laplace
K _p	Guadagno proporzionale (componente P)	a	Coefficiente del ritardo derivativo (componente D)
T _i	Tempo dell'azione integrativa (componente I)	b	Ponderazione dell'azione proporzionale (componente P)
T _d	Tempo dell'azione derivativa (componente D)	c	Ponderazione dell'azione derivativa (componente D)

Figure 64: Output formula for the PID

5 Pendulum-cart model

This chapter reports the non linear model of the system cart-pendulum, by putting particular attention to the equations constituting the system. Then, the linearized system is handled, by showing the resulting linear system and the transfer functions in interest. Finally, parallel and cascade PIDs are considered, first applied to the linear functions and then to the non linear model. The MPC technique is considered for the only linear model.

5.1 Nonlinear model of the inverse pendulum with cart

The system that is going to be analyzed is an inverse pendulum that is mounted, by means of an hinge, on a mobile cart that moves along a prismatic guide. The pendulum consists of a rod that is $400mm$ long and whose mass is negligible. On the top of the rod a concentrated mass is located, representing the real mass of the pendulum that is $0.2Kg$. This analysis takes in consideration of the friction linked to the rotational speed of the pendulum, and the viscous friction, function of the linear velocity of the cart, in order to get to a more realistic model. As reference systems, the fixed one has been chosen in the middle of the maximum stroke of the cart while, the mobile one has been selected in the center of the hinge. The final system that is obtained in this way is characterized by the cart, that can only move frontwards and backwards along the x axis of the fixed reference system and the pendulum that can only rotate thanks to the hinge. The rotation is considered positive in the counterclockwise sense. The model all the equations are drawn from, is shown in Figure 65:

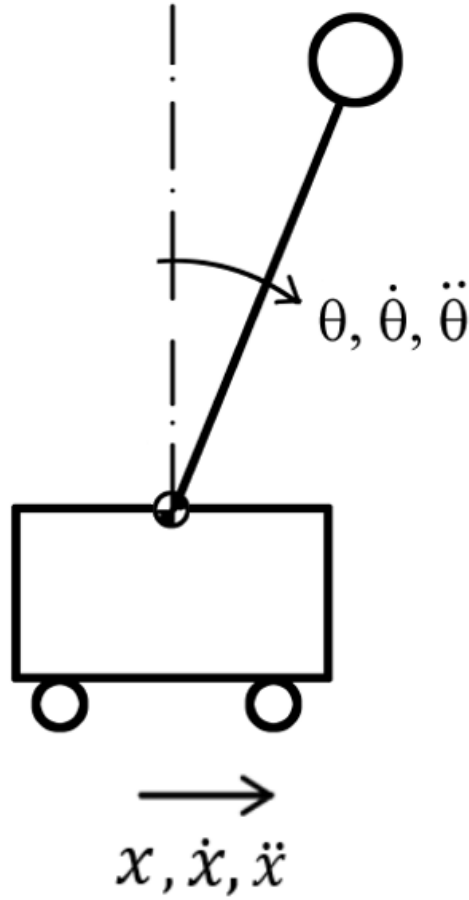


Figure 65: Model of the system cart-pendulum and reference systems

In order to obtain the final model of the system pendulum-cart, forces and torques are studied by means of the classical laws of dynamic:

$$\begin{cases} \sum F_i = 0 \\ \sum M_i = 0 \end{cases} \quad (9)$$

In particular, in order to achieve this goal, the system is decomposed into two subsystems, by considering the equilibrium equation of the hinge. As it allows the pendulum only to rotate, it develops both a horizontal and a vertical reaction that blocks all kinds of translation for the pendulum. The first part of the model that is taken into account is the pendulum one (Figure 66):

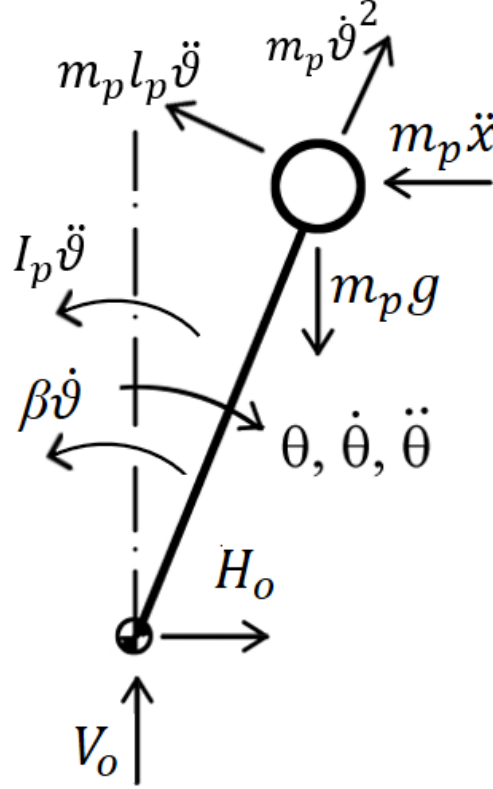


Figure 66: Free body diagram of the pendulum

Equilibrium along the x axis:

$$H_0 = M_p \ddot{x} - m_p l_p \dot{\theta}^2 \sin(\theta) + m_p l_p \ddot{\theta} \cos(\theta) \quad (10)$$

Equilibrium along the y axis:

$$V_0 = m_p g - m_p l_p \dot{\theta}^2 \cos(\theta) - m_p l_p \ddot{\theta} \sin(\theta) \quad (11)$$

Moment equilibrium by choosing the inch as reference:

$$\beta \dot{\theta} + I_p \ddot{\theta} - m_p g l_p \sin(\theta) + m_p l_p^2 \ddot{\theta} + m_p l_p \ddot{x} \cos(\theta) = 0 \quad (12)$$

Next step is to consider the lower part of the system, that is the cart model (Figure 67), by considering also the reactions of the hinge with inverted signs. The only equilibrium that is exploited is along the x axis, as the cart can only move along such an axis and neither a static nor a sliding friction is added to the model.

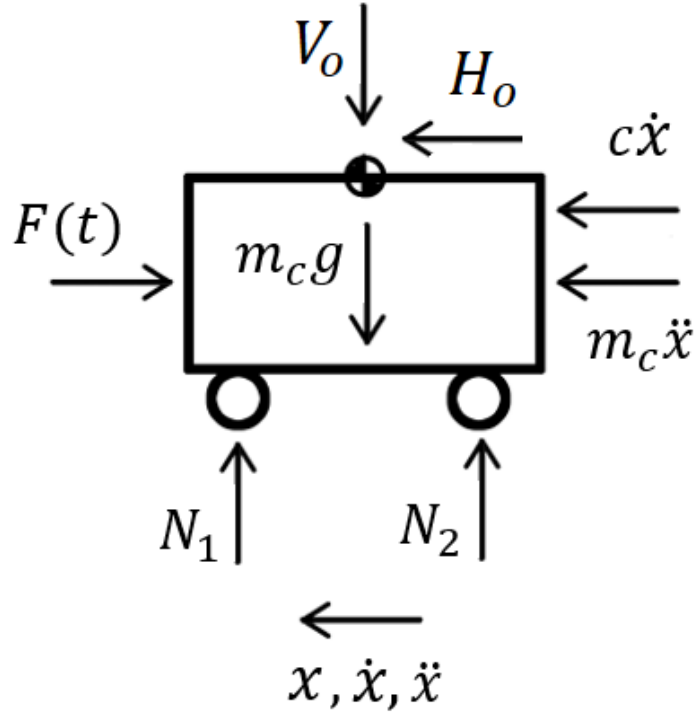


Figure 67: Free body diagram of the cart

By considering the only equilibrium along the x axis:

$$-F(t) + c\dot{x} + m_c\ddot{x} + H_0 = 0 \quad (13)$$

By combining all the equations, it is possible to get:

$$\begin{cases} \ddot{\theta}(t) = \frac{1}{I_p + m_p l_p^2} (m_p g l_p \sin(\theta(t)) - \beta \dot{\theta}(t) - m_p l_p \ddot{x} \cos(\theta(t))) \\ \ddot{x}(t) = \frac{1}{m_p + m_c} (F(t) - c\dot{x}(t) + m_p l_p \dot{\theta}^2 \sin(\theta(t)) - m_p l_p \ddot{\theta}(t) \cos(\theta(t))) \end{cases} \quad (14)$$

In order to solve this system and obtain as solutions $\ddot{\theta}(t)$ and $\ddot{x}(t)$, the symbolic tool of Matlab has been used (Figure 68):

```
%% non linear symbolic system
syms F mp mc lp g x_2 teta teta_2 teta_1 x_1 jp beta c
S=solve([teta_2==(mp*g*lp*sin(teta)-beta*teta_1-mp*lp*x_2*cos(teta))/(jp+mp*lp^2),
        x_2==(F-c*x_1+mp*lp*teta_1^2*sin(teta)-mp*lp*teta_2*cos(teta))/(mc+mp)], [x_2, teta_2]);
S.x_2
S.teta_2
```

Figure 68: Symbolic tool of Matlab

Once all the terms are set in Matlab in a symbolic way by means of “syms”, the system of the two equations is solved through “solve” and the two solutions saved in the vector “S”:

$$\begin{cases} \ddot{x}(t) = \frac{(I_p + l_p^2 m_p)(F(t) - c\dot{x} + m_p l_p \dot{\theta}^2(t) \sin(\theta(t)) - \frac{1}{2} g l_p^2 m_p^2 \sin(2\theta(t)) + \beta m_p l_p \dot{\theta}(t) \cos(\theta(t)))}{l_p^2 m_p^2 (\sin(\theta(t)))^2 + m_c m_p l_p^2 + I_p (m_c + m_p)} \\ \ddot{\theta}(t) = \frac{-\beta \dot{\theta}(t)(m_c + m_p) - F(t) m_p l_p \cos(\theta(t)) + g l_p m_p^2 \sin(\theta(t)) - l_p^2 m_p^2 \dot{\theta}^2(t) \sin(\theta(t)) \cos(\theta(t)) + c m_p l_p \cos(\theta(t)) \dot{x} - g l_p m_p m_c \sin(\theta(t))}{l_p^2 m_p^2 (\sin(\theta(t)))^2 + m_c m_p l_p^2 + I_p (m_c + m_p)} \end{cases} \quad (15)$$

These equations represent the system pendulum-cart in a nonlinear fashion. In order verify them, they are reported in the Simulink environment, in Figure 69:

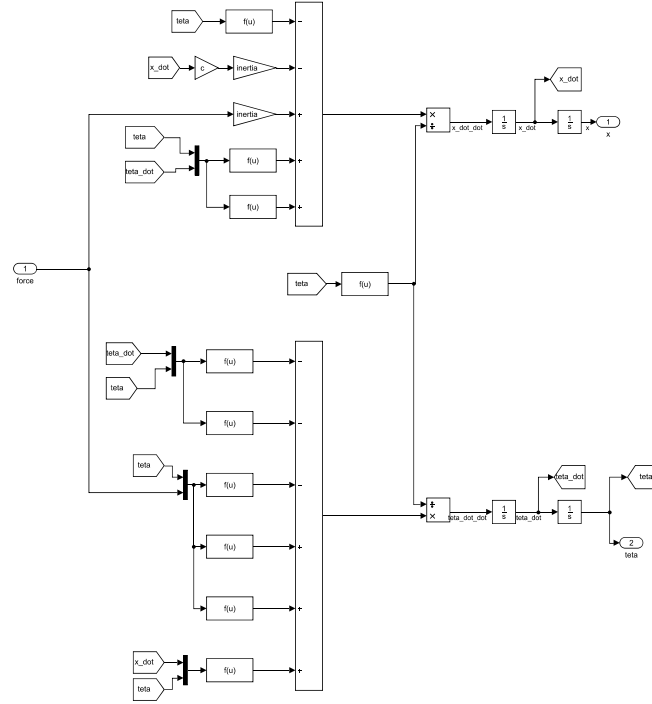


Figure 69: Model of the cart-pendulum in Simulink environment

The exact behaviour of the model can be checked by showing that, with no force applied and an initial condition on theta equal to zero, the system does not fulfill any movements. By applying, for instance, an initial condition on θ of 2° , it can be noticed that the pendulum starts oscillating until it reaches the rest position at 180° . The cart instead is characterized by small movements caused by the pendulum rotating:

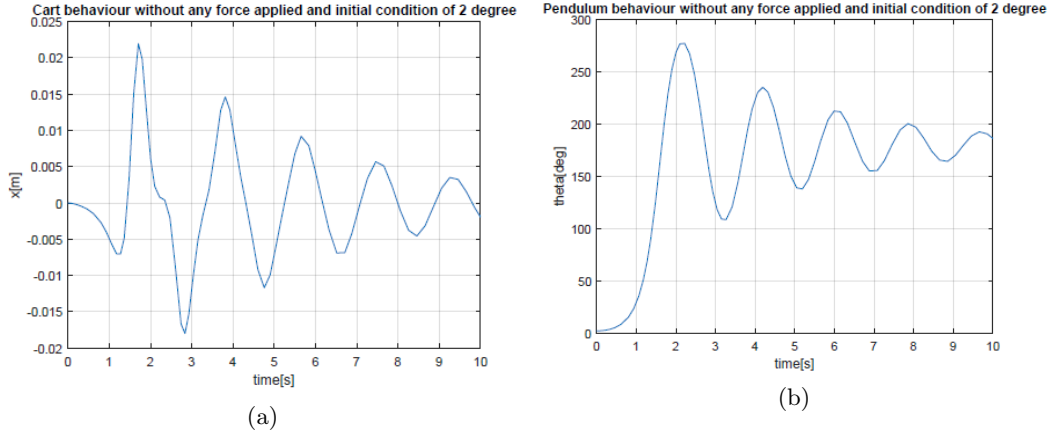


Figure 70: Cart behaviour in (a), pendulum behaviour in (b)

Suitable results are obtained in case an external force is applied, by resulting in a good model of the inverse pendulum with cart.

5.2 Linearized model of the inverse pendulum with the cart

The first step to approach PID control is to get a linearized model of the system such that transfer functions can be evaluated. In order to do so, it is convenient to suppose small angles. This assumption leads to some simplifications that elide nonlinearities:

- $\cos(\theta) \approx 1$
- $\sin(\theta) \approx \theta$
- $\dot{\theta} = 0$

By applying the Laplace transform, by supposing null initial condition, the equations become:

$$\begin{cases} \theta(s)s^2 = \frac{1}{I_p + m_p l_p^2} (m_p g l_p \theta(s) - \beta s \theta(s) - m_p l_p X(s)s^2) \\ X(s)s^2 = \frac{1}{m_p + m_c} (F(s) - c s X(s) - m_p l_p s^2 \theta(s)) \end{cases} \quad (16)$$

In particular, there are three transfer functions that need to be calculated:

- $\frac{\theta(s)}{F(s)}$
- $\frac{X(s)}{F(s)}$
- $\frac{X(s)}{\theta(s)}$

As before, they are calculated by means of the symbolic tool in Matlab, by obtaining:

$$\begin{cases} G_{xF}(s) = \frac{m_p l_p^2 s^2 - g l_p m_p + I_p s^2 + \beta s}{s(A s^3 + B s^2 + C s + D)} \\ G_{\theta F}(s) = \frac{-l_p m_p s}{s(A s^3 + B s^2 + C s + D)} \\ G_{X\theta}(s) = \frac{-m_p l_p^2 s^2 + g m_p l_p - I_p s^2 - \beta s}{l_p m_p s^2} \end{cases} \quad (17)$$

Where, for the sake of simplicity in the exposition of the equations:

$$\begin{cases} A = l_p^2 m_c m_p + I_p(m_c + m_p) \\ B = \beta(m_c + m_p) + c(I_p + l_p^2 m_p) \\ C = \beta c - gl_p m_p^2 - gl_p m_c m_p \\ D = -cgl_p m_p \end{cases} \quad (18)$$

By expressing these equations numerically, with all the data considered so far, the final results are:

$$\begin{cases} G_{xF}(s) = \frac{0.52632(s+3.742)(s-3.273)}{s(s+9.586)(s+3.675)(s-3.294)} \\ G_{\theta F}(s) = \frac{-0.65789s}{(s+9.586)(s+3.675)(s-3.294)} \\ G_{x\theta}(s) = \frac{-0.8(s+3.742)(s-3.273)}{s^2} \end{cases} \quad (19)$$

As follows, the Bode diagrams of the three transfer functions respectively:

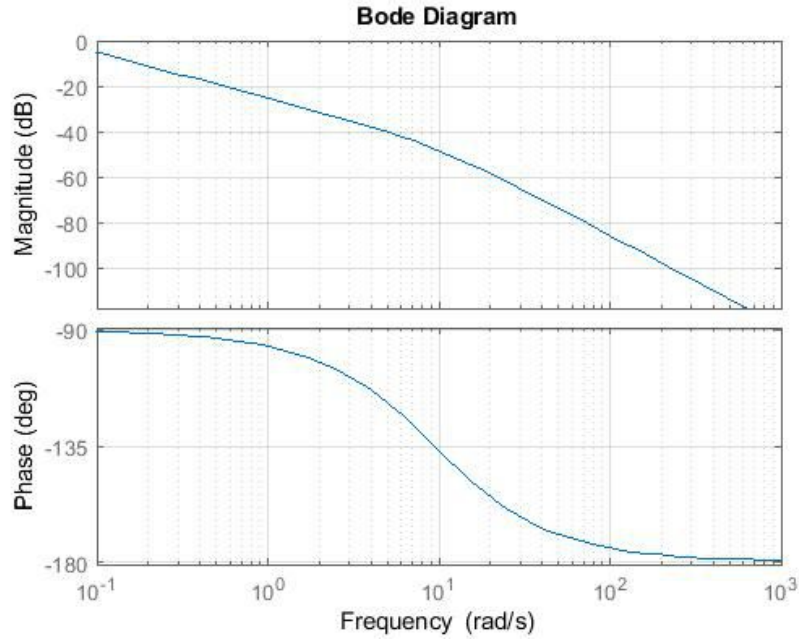


Figure 71: Bode diagrams of G_{xF}

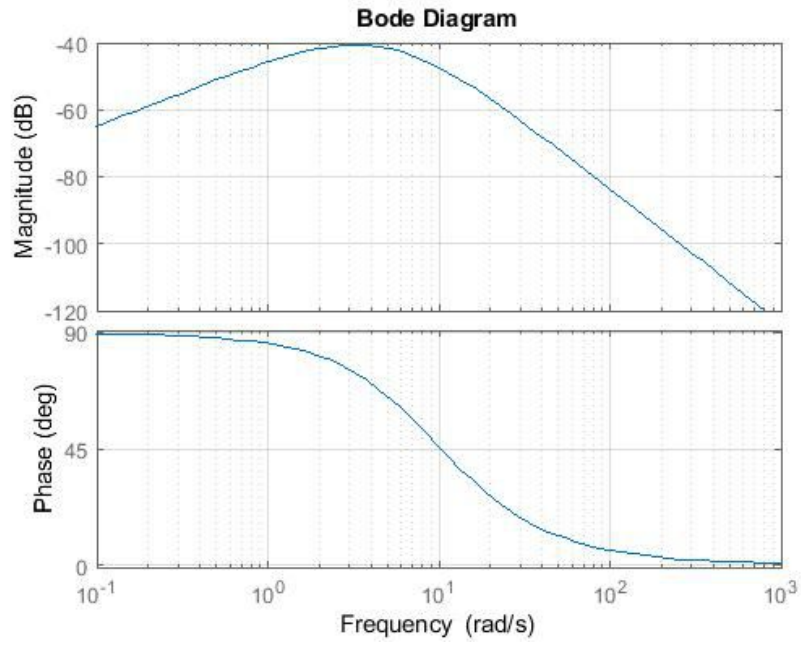


Figure 72: Bode diagrams of $G_{\theta F}$

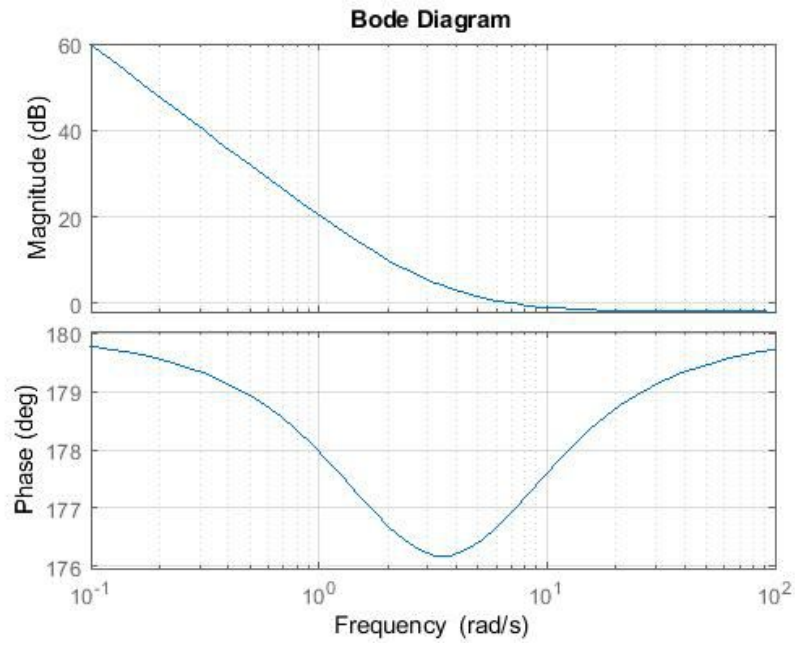


Figure 73: Bode diagrams of $G_{x\theta}$

5.3 Cascade PID control

The first kind of control system that is analyzed is made up of two PID controllers that are posed in cascade and whose aim is to keep the pendulum in the vertical position, by limiting the cart in the linear guide. In particular, the external loop is aimed to stabilize the position of the cart while the inner loop acts on the angle of the pendulum (Figure 74). The studied system is SIMO, standing for Single Input Multiple Outputs, as there is a single input, that is the force applied to the cart but two outputs, that are the angle of the pendulum and the position of the cart. All the constant values referred to transducers can be neglected, by supposing they have a faster dynamic than the one of the considered system.

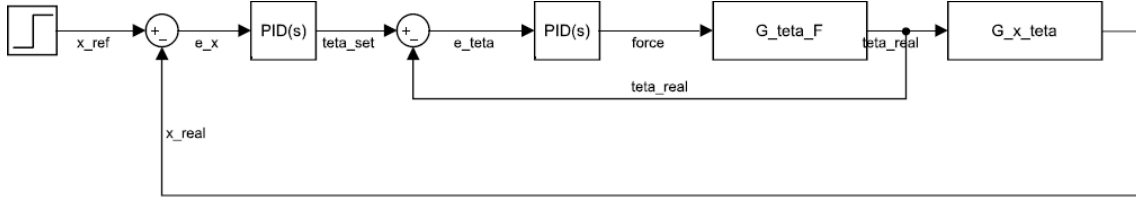


Figure 74: Scheme of the Cascade PID

The transfer function $G_{x\theta}$ provides the real position of the cart, by receiving in input the real angle of the pendulum with respect to the vertical axis. On the basis of the tracking error relative to the position of the cart, the first PID generates a θ set, that is the reference signal entering the inner loop. The tracking error that is here generated is the input of the second inner PID that produces the force acting on the cart, by letting the pendulum be in a vertical position. The transfer function $G_{\theta F}$ provides the angle of the pendulum. As it is possible to notice from the scheme reported above, the first step is to tune the PID linked to the inner loop (Figure 75).

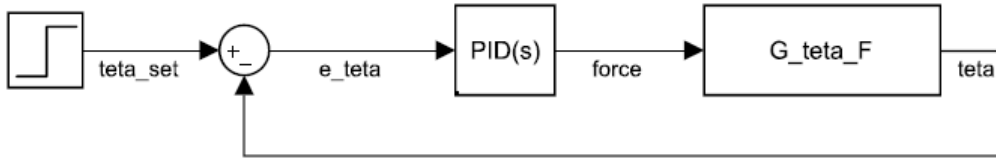


Figure 75: Scheme of the inner loop

In order to perform a complete analysis, before tuning the PID it is possible to show that the closed-loop function is not stable, by taking into account the open-loop transfer function, by imposing the controller equal to 1.

$$G_{ol\theta}(s) = C_{\theta}(s)G_{\theta F}(s) = G_{\theta F}(s) \quad (20)$$

The Nyquist criterion establishes that, by naming with Z the number of the poles of the closed-loop system in the right half plane (i.e with real part greater or equal to zero), and P is the number of unstable poles of the open-loop transfer function, the resultant contour will encircle in a clockwise way the critical point $(-1+j0)$ N times, with $N=Z-P$.

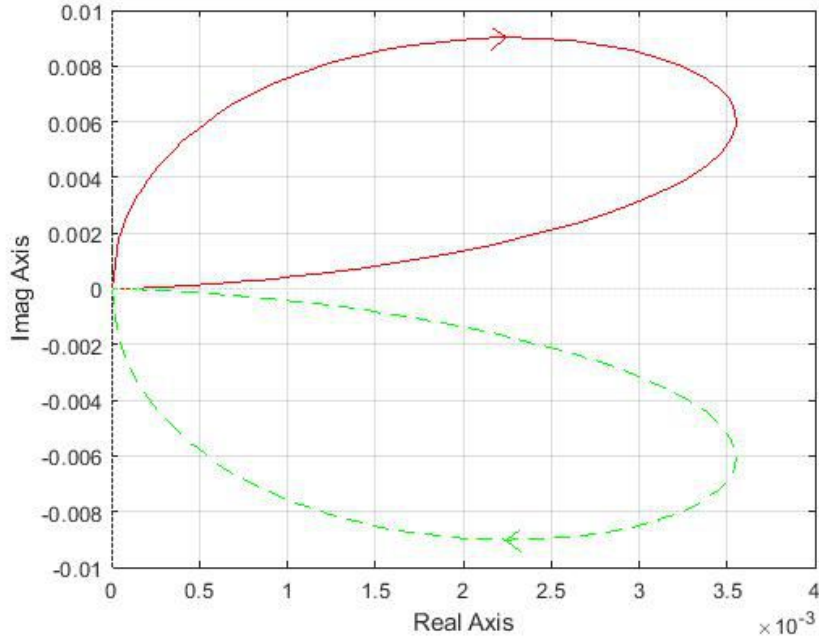


Figure 76: Nyquist plot of $G_{\theta F}$

As expected, because of the presence of a pole with positive real part, the closed-loop system is unstable. In fact $N = Z - P \Rightarrow 0 = Z - 1 \Rightarrow Z = 1$. The inner PID controller can be tuned automatically by means of the auto tuning function that is present in the PID block in Simulink. It is possible to perform two kinds of auto tuning (Figure 77): one based on the transfer function and one based on the frequency response. The former has a more intuitive approach, as it acts directly on the transfer function and tunes the PID by providing the behaviour of the system in the time domain, with certain PID parameters. The latter acts, instead, on the Bode diagram of the system and the PID is tuned on the basis of frequency requirements that should be known a priori. This analysis considers the first approach.

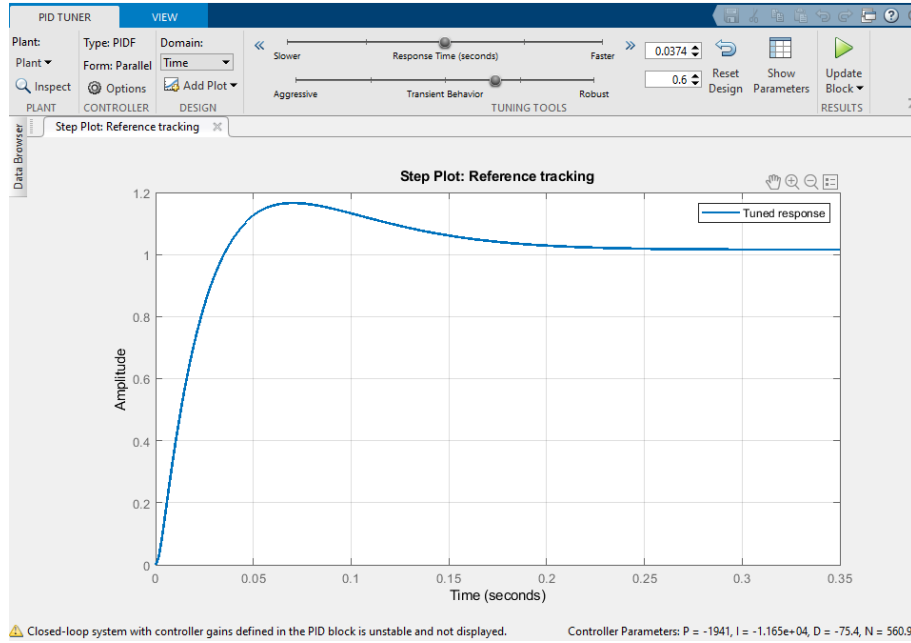


Figure 77: PID auto tuning

If possible, the auto tuning provides a first controller that stabilizes the loop where it is located by considering a unitary step as reference signal. This function allows also to search for a controller that can be either more robust, in presence of disturbances, or faster in terms of rise time. Rise time is generally identified as the time the output of the system takes to vary from 10% to 90% of its steady state value, without oscillating. Generally these two parameters are inversely proportional in the sense that, if a really fast controller is considered, surely it can't be strongly robust and vice versa. In this case, a good performance can be got with a controller that ensures a rise time $t_r = 0.032s$. The transfer function of the inner controller is:

$$C_{\theta}(s) = \frac{-1.049 * 10^5 (s + 32.68)(s + 12.74)}{s(s + 1250)} \quad (21)$$

The new open-loop transfer function of the inner loop becomes:

$$G_{ol\theta}(s) = \frac{69016(s + 32.68)(s + 12.74)}{(s + 9.586)(s + 3.675)(s - 3.294)(s + 1250)} \quad (22)$$

The Nyquist plot of such a transfer function is provided in Figure 78:

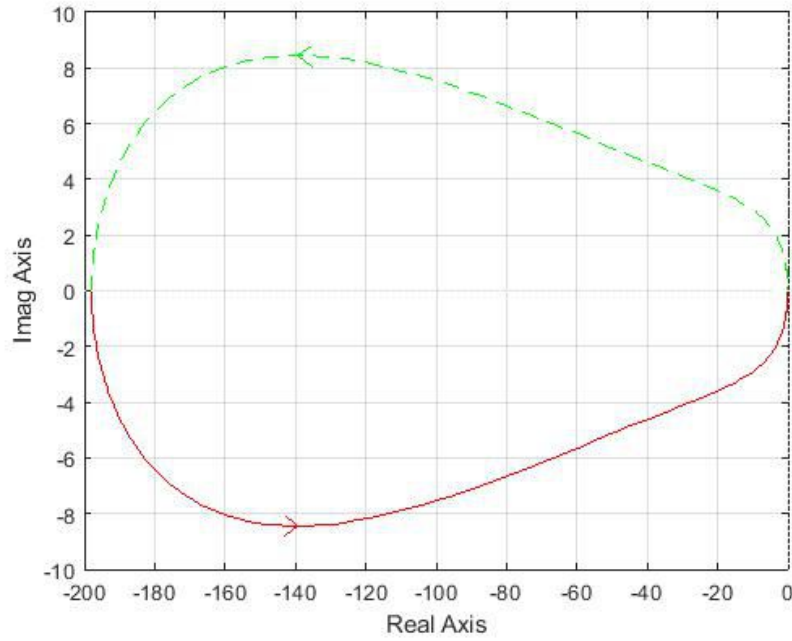


Figure 78: Nyquist plot of $G_{ol\theta}$

As shown by the Nyquist diagram, now the open-loop function encircles counterclockwise the critical point $(-1+j0)$, by resulting $Z = 0$. By means of the Bode diagram, it is possible to visualize also the gain margin and the phase margin, in Figure 79:

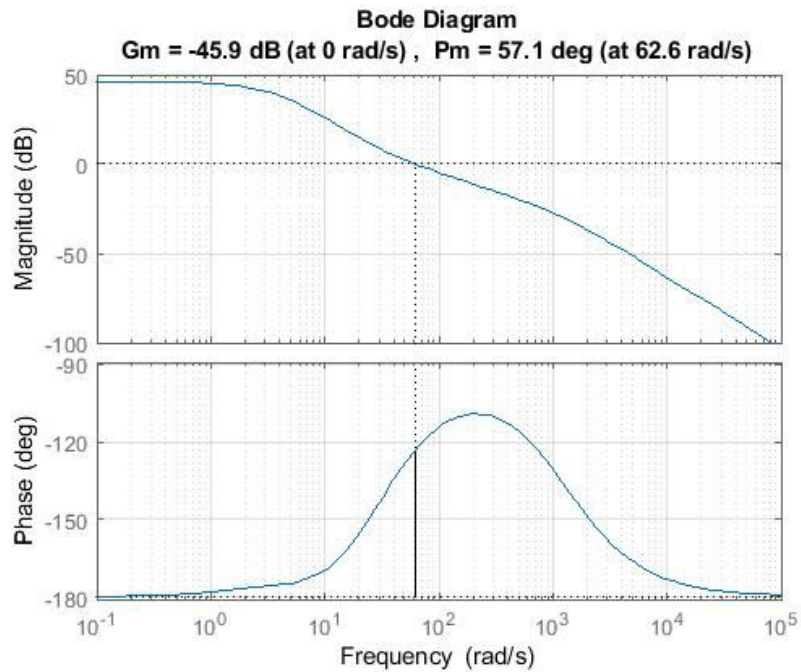


Figure 79: Gain and phase margins of $G_{ol\theta}$

The final closed-loop transfer function can be written as:

$$G_{cl\theta}(s) = \frac{C_\theta(s)G_{\theta F}(s)}{1 + C_\theta(s)G_{\theta F}(s)} = \frac{69016(s + 32.68)(s + 12.74)}{(s + 1194)(s + 12.4)(s^2 + 53.65s + 1931)} \quad (23)$$

Its Bode diagrams are shown in Figure 80:

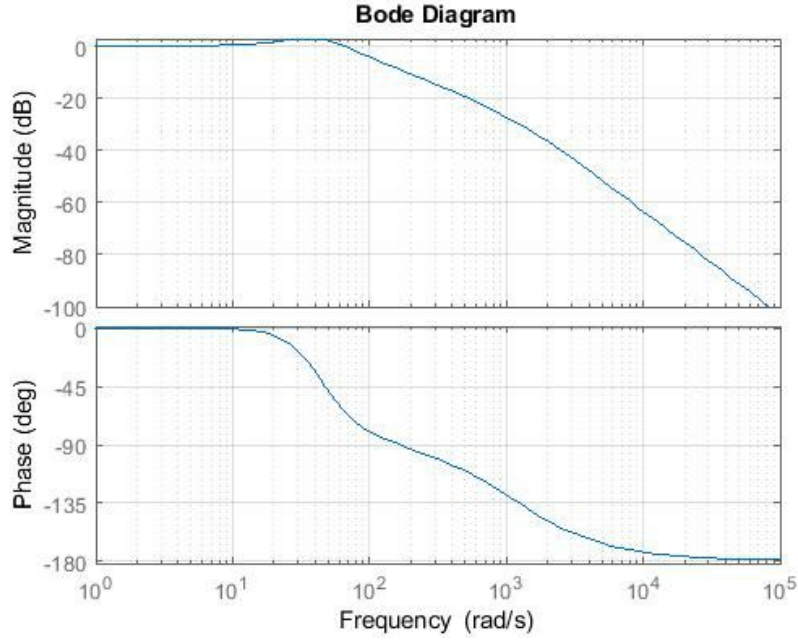


Figure 80: Bode diagrams of $G_{cl\theta}$

Once the inner loop has been stabilized, the last step is to look for a controller that makes the whole closed-loop system stable. As performed in the previous step, let's consider the open-loop function by starting with a unitary controller:

$$G_{olx}(s) = G_{cl\theta}(s)G_{x\theta}(s) = \frac{-55213(s + 32.68)(s + 12.74)(s + 3.742)(s - 3.273)}{s^2(s + 1194)(s + 12.4)(s^2 + 53.65s + 1931)} \quad (24)$$

Whose Nyquist plot is given in Figure 81:

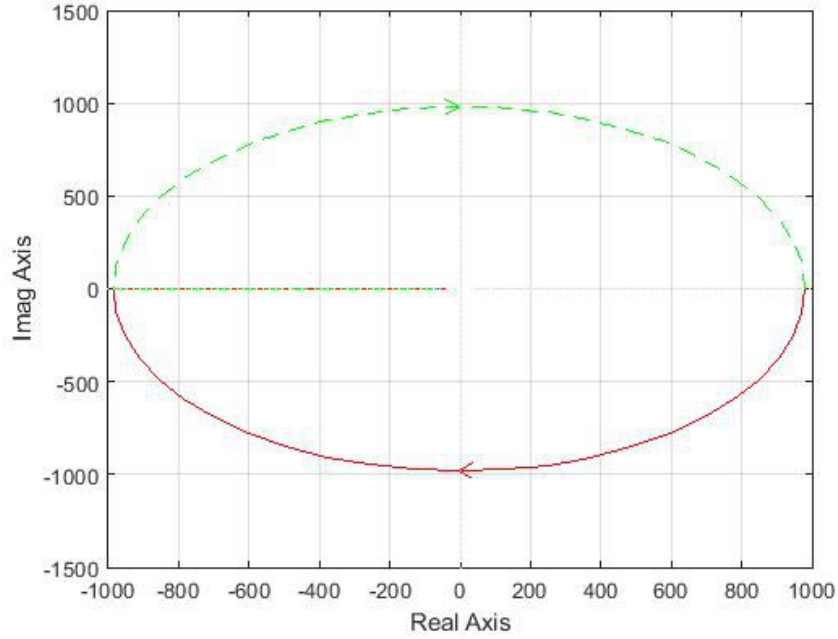


Figure 81: Nyquist plot of G_{olx}

It is possible to notice that the Nyquist plot of the open-loop function encircles clockwise the critical point. This leads to an unstable closed-loop system, as $Z = 1$. As the case of the inner loop, the outer PID has been tuned by means of the auto tuning function, by getting the final transfer function of the controller:

$$C_x(s) = \frac{0.29389(s + 0.155)(s + 0.1126)}{s(s + 2.5036)} \quad (25)$$

The system reacts quickly and in a quite robust way with these parameters. This controller can stabilize the whole closed loop system, and this can be seen by showing the Nyquist plot (Figure 82) and Bode diagrams (Figure 83) of the new open-loop transfer function:

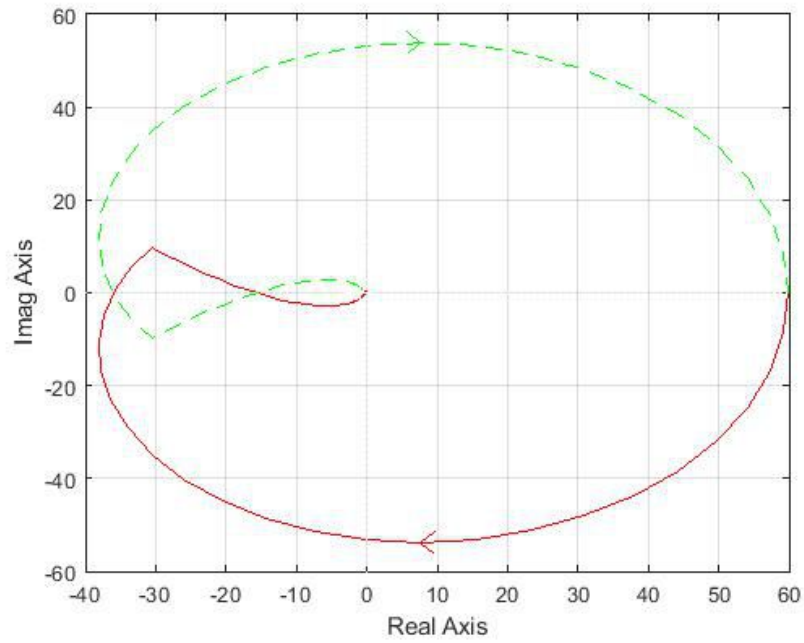


Figure 82: Nyquist plot of the new G_{olx}

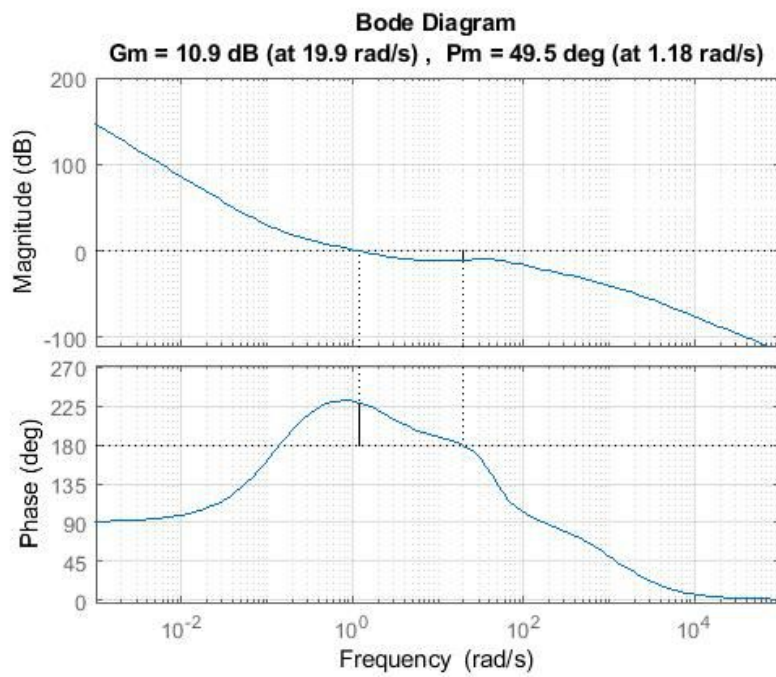


Figure 83: Gain and phase margins of G_{olx}

The final closed-loop transfer function is given by:

$$G_{clx}(s) = \frac{-16227(s + 0.155)(s + 0.1126)(s - 3.273)(s + 3.742)(s + 12.74)(s + 32.68)}{(s + 1208)(s + 12.3)(s + 0.2393)(s + 0.09852)(s^2 + 2.719s + 2.81)(s^2 + 39.52s + 1467)} \quad (26)$$

Whose Bode diagram is reported in Figure 84:

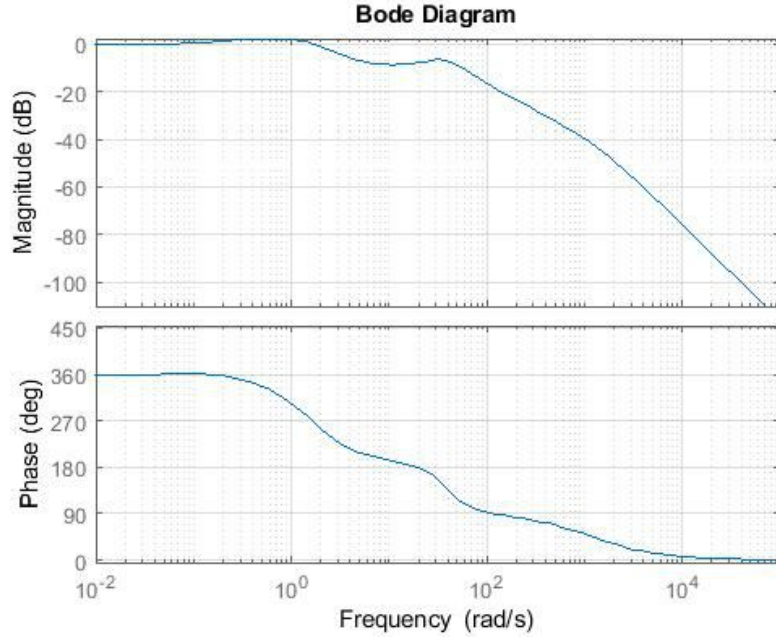


Figure 84: Bode diagrams of the final G_{clx}

There is no need, in this case, to perform an analysis of the non-linear case as the PIDs designed for the linearized model works properly for the non-linear case too.

Next step consists of showing the behaviour of the overall non-linear system, by putting particular attention to the behaviour of the linear position of the cart and the angle of the pendulum with respect to the vertical axis. This simulation is performed by considering three different initial conditions on the angle, that is to say $\theta_0 = 0^\circ$, $\theta_0 = 6^\circ$ and $\theta_0 = 12^\circ$.

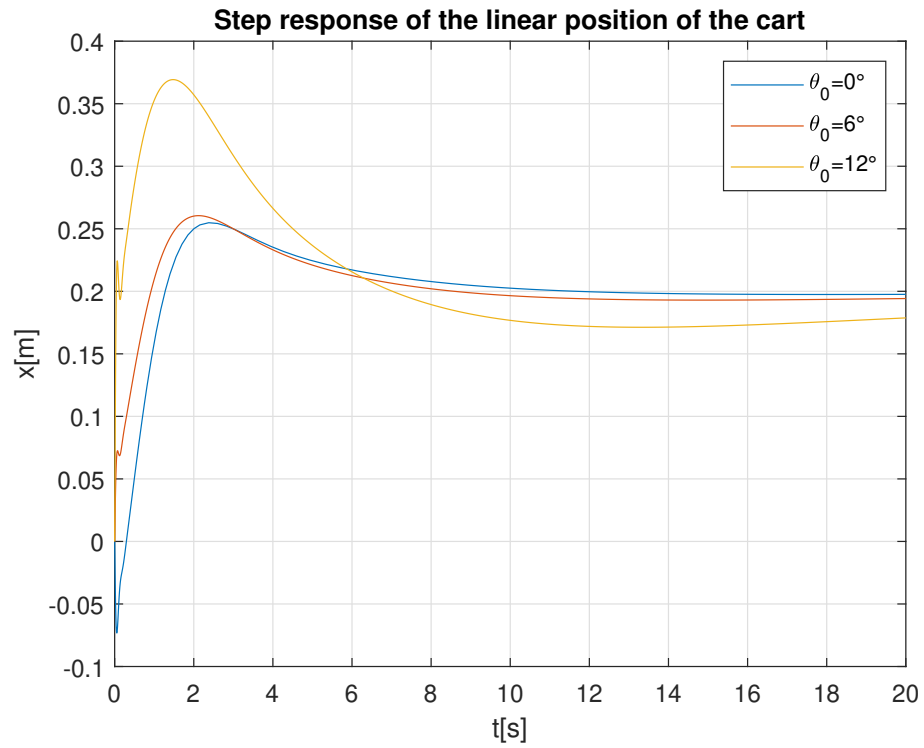


Figure 85: Step response of the linear position of the cart in the cascade architecture

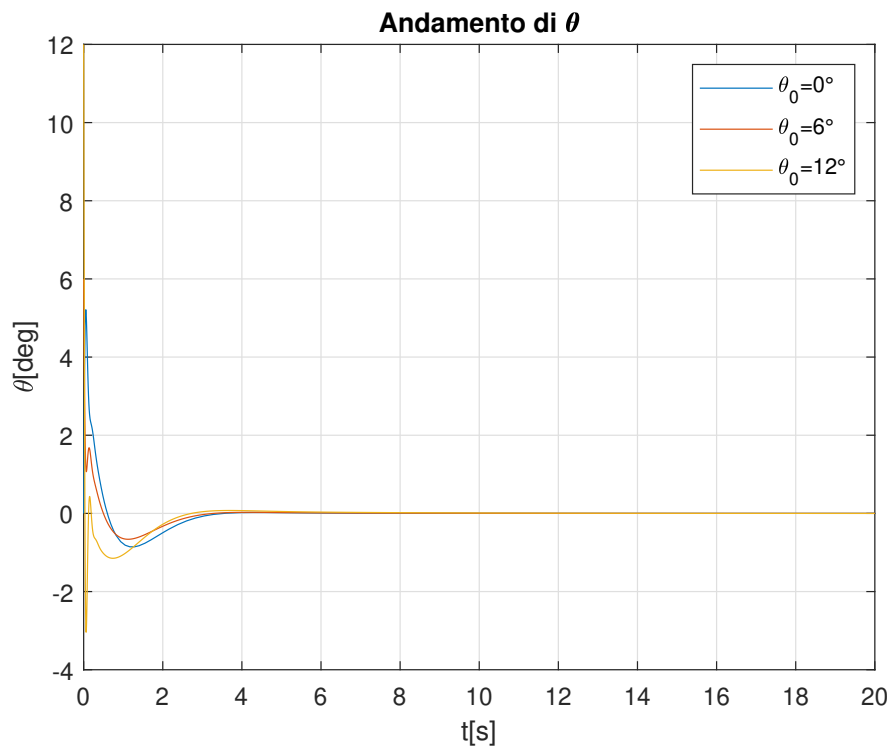


Figure 86: Behaviour of the angle of the pendulum in the cascade architecture

By considering the Figure 85, it is possible to notice that, starting from a null initial condition on the angle and imposing a step of $200mm$ as reference signal, the rising time is about $1.3s$ and the overshoot is 25% . This means that the cart, firstly, goes far from the defined setpoint of about $25mm$, then it extinguishes its motion, practically, in about $6.5s$, by getting to the established point. The bigger the initial condition on the angle is, the higher the overshoot becomes, along with the rising time. This means that the performances are getting worse and the cart takes much more time to conclude its motion. If the starting angle increases more, the designed PID no longer guarantee stability and the step response would present a divergent behaviour.

The Figure 86, instead, reports the behaviour of the angle of the pendulum with the considered initial conditions. It is possible to notice that the angle response is faster than the one of the cart, for all the three initial conditions. After a small undershoot, that increases slightly with the initial condition, the pendulum reaches the desired position of 0° in about $2.7s$.

5.4 Parallel PID

Another kind of control system that is implemented by considering PIDs controllers consists of two PIDs regulator located in a parallel form, in Figure 87:

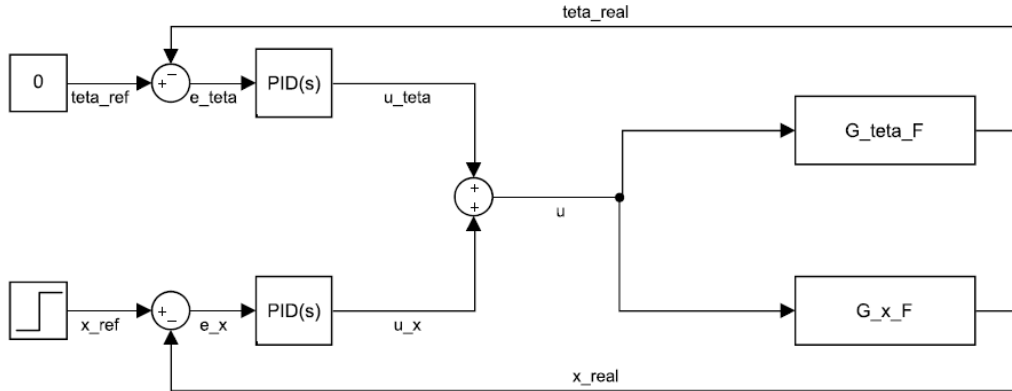


Figure 87: Parallel PID scheme

This type of control system is characterized by an input that is the sum of two contributes: one coming from the PID controlling the angle of the pendulum u_θ and one coming from the PID regulating the position of the cart u_x .

$$\begin{cases} u(s) = u_\theta(s) + u_x(s) \\ u_\theta(s) = C_\theta(s)e_\theta(s) \\ u_x(s) = C_x(s)e_x(s) \end{cases} \quad (27)$$

Where C_θ and C_x are, respectively, the transfer functions of the controllers on the pendulum angle and on the linear position of the cart. By considering the general case, there are two references in this scheme and this leads to write the tracking errors:

$$\begin{cases} e_\theta(s) = \theta_{ref}(s) - \theta_{real}(s) \\ e_x(s) = x_{ref}(s) - x_{real}(s) \end{cases} \quad (28)$$

By substituting the tracking error equations in the previous system and by remembering that:

$$\begin{cases} \theta_{real}(s) = \frac{G_{\theta F}(s)}{u(s)} \\ x_{real}(s) = \frac{G_{xF}(s)}{u(s)} \end{cases} \quad (29)$$

It is possible to obtain the final expression of the input that feeds both the transfer function between x and the input and the one between θ and the input.

$$u(s) = \frac{C_{\theta}(s)\theta_{ref}(s) + C_x(s)x_{ref}(s)}{1 + C_{\theta}(s)G_{\theta F}(s) + C_x(s)G_{xF}(s)} \quad (30)$$

As it can be deduced from such an equation, in the general case the problem becomes complex to handle with typical control methods because of the presence of two reference signals and two outputs. As a matter of facts, the system is MIMO, that stands for Multiple Inputs Multiple Outputs. In order to simplify the treatment, without losing the objective of this analysis, the reference signal feeding the PID on θ can be chosen equal to 0. In fact the purpose is to maintain the pendulum in the vertical position, that means an reference angle equal to 0. In this way, the problem is simplified and the new input becomes:

$$u(s) = \frac{C_x(s)x_{ref}(s)}{1 + C_{\theta}(s)G_{\theta F}(s) + C_x(s)G_{xF}(s)} \quad (31)$$

The first step, as the case of cascade PID, is to look for a controller that stabilizes the closed-loop system containing $G_{\theta F}(s)$. As this is the same case the cascade PID, a smart choice of the PID can be the same as the previous one:

$$C_{\theta}(s) = \frac{-29981(s + 29.47)(s + 9.38)}{s(s + 656.1)} \quad (32)$$

Before starting with the analysis of the PID on the x branch, it is useful to show that, by imposing a unitary control on x , the resulting open-loop function is not stable, by means of the Nyquist plot (Figure 88):

$$G_{olx}(s) = \frac{G_{xF}(s)}{1 + C_{\theta}(s)G_{\theta F}(s)} = \frac{0.52632(s + 3.742)(s - 3.273)(s + 1250)}{s(s + 1194)(s + 12.4)(s^2 + 53.65s + 1931)} \quad (33)$$

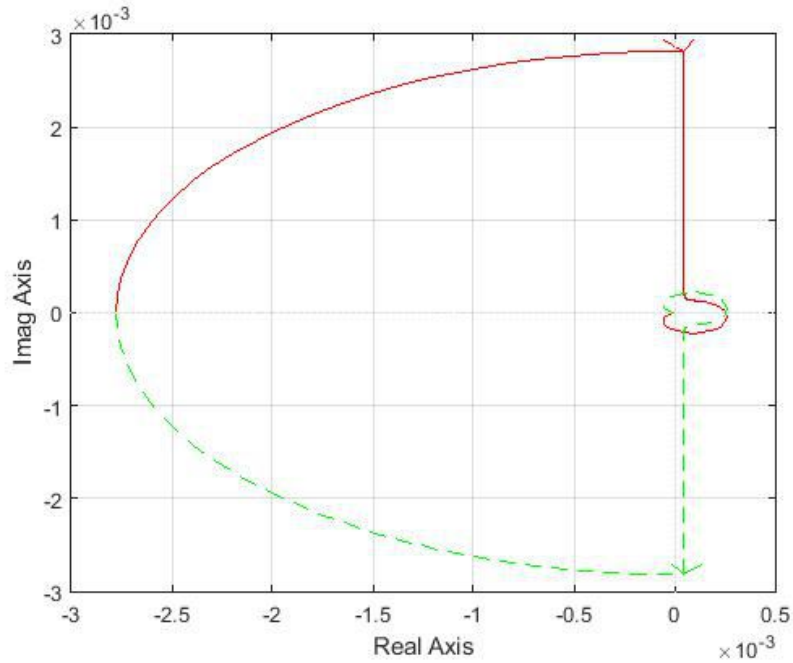


Figure 88: Nyquist plot of G_{olx}

As it can be seen by the Nyquist plot, there is the encirclement of the critical point $(-1, j0)$ in a clockwise fashion, that means the closed-loop function is not stable. Next step is to find a PID controller that stabilizes the overall closed-loop function. A way to find it is to apply the Ziegler-Nichols method, that now can be applied because it can be noticed that the system can be stabilized through a constant negative value. It was developed in 1942 and its purpose is to search for the critical gain, from which the other parameters of the PID can be evaluated. The first step is to increase (or decrease) the constant gain of the controller until the output of the control loop reaches the the limit of stability, as shown in Figure 89.

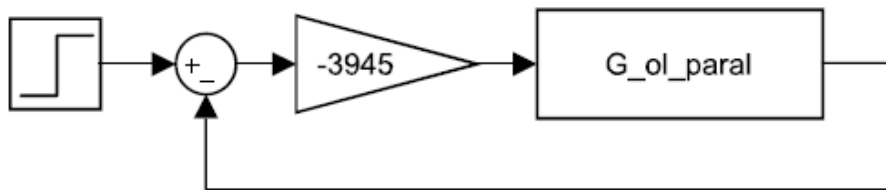


Figure 89: Scheme for the application of the Ziegler-Nichols method

By trial and error, it has been possible to reach the value of -3945 , thanks to which the system reaches its limits of stability by showing a behaviour that is completely oscillating (Figure 90):

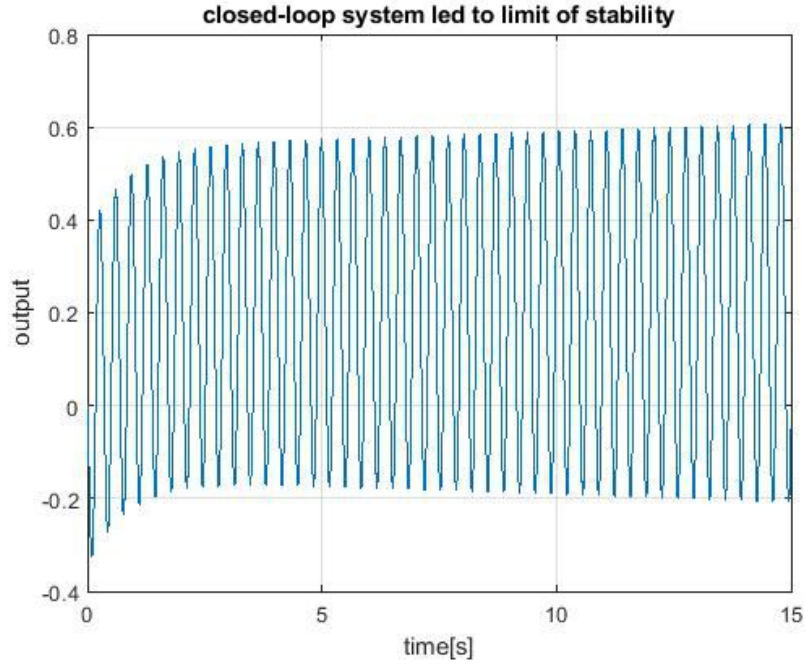


Figure 90: Limit of stability with Ziegler-Nichols method

From this graph, it is possible to get, by calculating the time that passes between a peak and the next one, the critical period $T_c = 0.34s$, that is used to set the parameters of the overall PID, by using the following table:

Controller type	K_p	T_i	T_d	K_i	K_d
P	$0.5K_c$	-	-	-	-
PI	$0.45K_c$	$T_c/1.2$	-	K_p/T_i	-
PD	$0.8K_c$	-	$T_c/8$	-	$K_d T_d$
PID	$0.6K_c$	$T_c/2$	$T_c/8$	K_p/T_i	$K_d T_d$

Figure 91: Ziegler-Nichols table

As the aim is to tune a PID controller, the last row of the table is considered. The calculated parameters are:

$$\begin{cases} K_p = -2574 \\ T_i = 0.17 \\ T_d = 0.0425 \\ K_i = -1.5141 * 10^4 \\ K_d = 109.395 \end{cases} \quad (34)$$

With these parameters, the overall system becomes stable but the performances are not satisfactory at all, as there are still some oscillations in both the outputs, as shown in Figure 92:

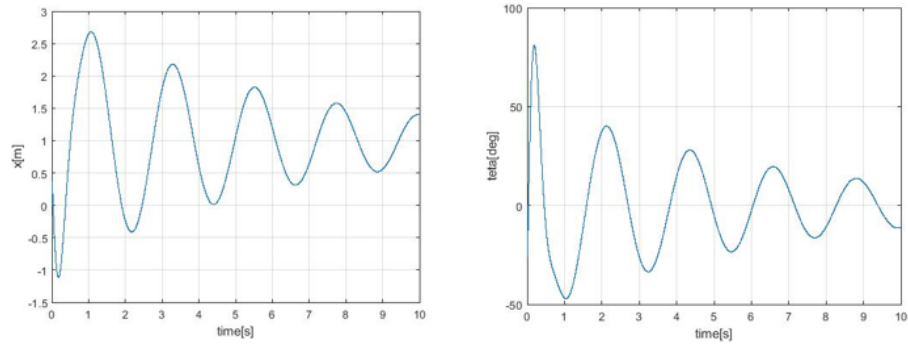


Figure 92: x and θ behaviour with the values given by Ziegler-Nichols method

Despite the system is stable, from simulation it is possible to notice that the system is still at the limits of stability and even if the presence of small disturbances could make the system unstable, as it is not so robust. Starting from these parameters, it has been possible to effectuate an auto tuning thanks to which a really good controller could be found. By considering the parameters of the PID written in terms of K_p , K_i , K_d and N , they become:

$$\begin{cases} K_p = -3402.9 \\ K_i = -700.8 \\ K_d = 574.9 \\ N = 5.9 \end{cases} \quad (35)$$

It is possible to see that now the system is stable, by considering the Nyquist plot and the Bode diagram, where the gain margin and phase margin of the open-loop transfer function are shown.

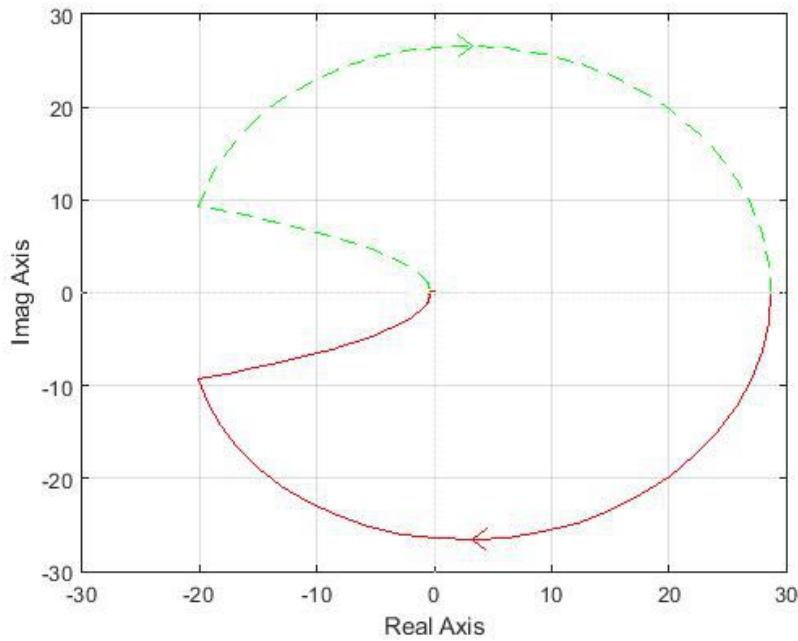


Figure 93: Nyquist plot of $G_{ol}(s)$ with the final PID parameters

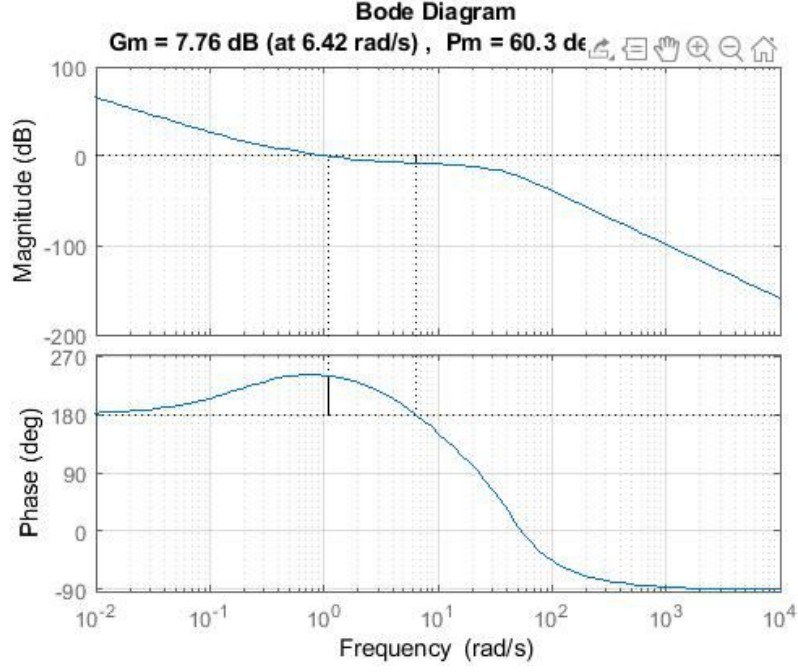


Figure 94: Gain and phase margins of $G_{ol}(s)$ with the final PID parameters

The final closed-loop transfer function becomes:

$$G_{cl}(s) = \frac{-1.1967 * 10^{-12}(s + 3.742)(s - 3.273)(s + 0.199)(s + 1250)(s + 9.167 * 10^{15})}{(s + 1194)(s + 1.043)(s + 0.2637)(s^2 + 9.341s + 44.75)(s^2 + 61.32s + 2277)} \quad (36)$$

Whose Bode diagrams are shown in Figure 95:

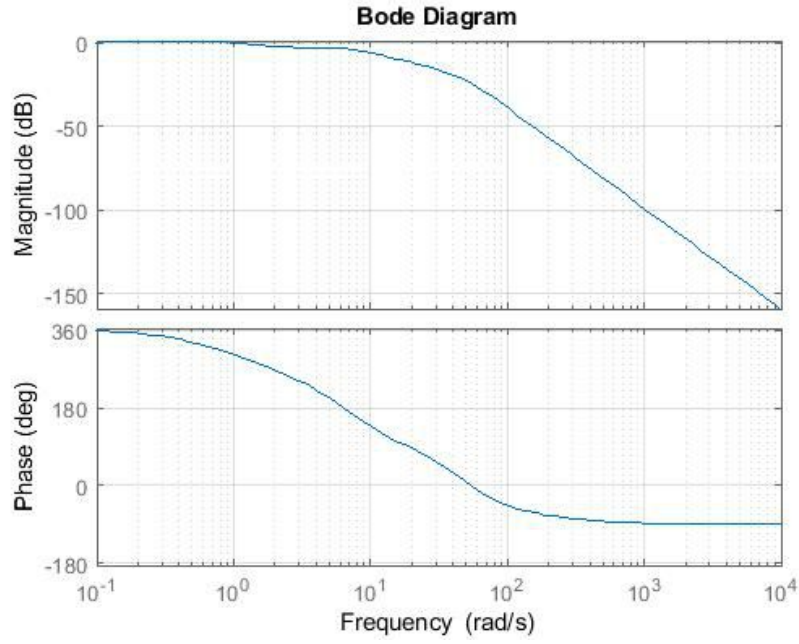


Figure 95: Bode diagrams of $G_{cl}(s)$

As the cascade case, the designed parallel architecture for the linear case works properly for the non-linear mechanical system too, as it still has few nonlinearities.

In order to check the behaviour of the non-linear system, next step is to report the step response of the linear position of the cart and the behaviour of the angle of the pendulum, by considering as initial conditions on the angle 0° , 6° and 12° .

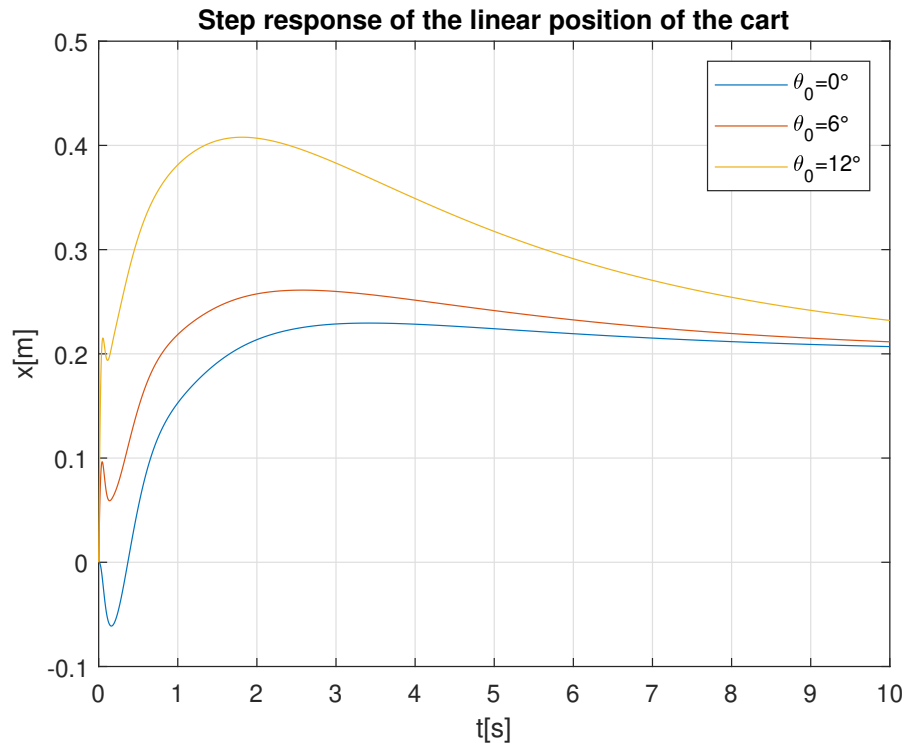


Figure 96: Step response of the linear position of the cart in the parallel architecture

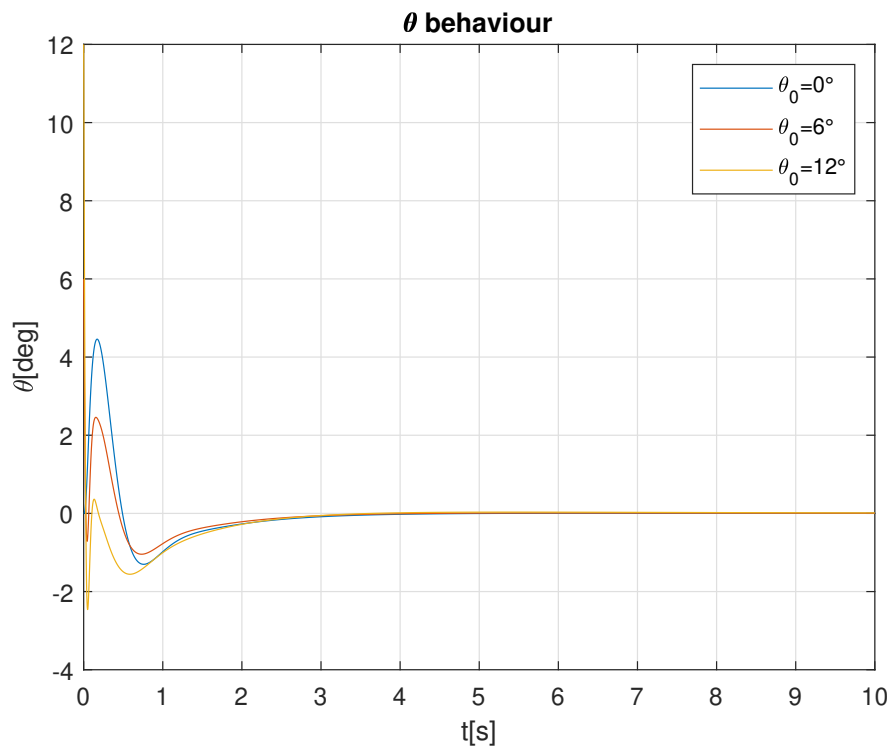


Figure 97: Behaviour of the angle of the pendulum in the parallel architecture

The Figure 96 shows the step response of the linear position of the cart, with a setpoint of $200mm$ and varying the initial condition on the angle. By considering a null initial condition, it can be seen that the cart, after a small undershoot, presents a rising time of about $1.8s$, an overshoot of about 12% and it concludes its motion, practically, in about $7s$. The higher the initial condition is, the more the overshoot increases and the step response of the cart slows down. The time it takes to extinguish its motion and reach the setpoint becomes higher and higher with the growth of the initial condition. The two designed PIDs cannot stabilize the system anymore if the starting angle of the pendulum is chosen even bigger, by resulting in an unstable system.

The Figure 97 shows, instead, the behaviour of the angle of the pendulum by varying its initial condition. As the cascade case, the angle response is much faster than the cart one and it goes to 0 in about $2s$, for all the considered initial condition. The only effect that can be noticed is the slight increase of the undershoot.

5.5 Model Predictive Control

From a practical point of view, when a controller is designed, generally, it is not possible to take into account constraints on the generated signal $u(t)$, feeding the plant, and on the controlled output $y(t)$. A trial-and-error approach is needed, that, sometimes, can be hard to apply. Physical limitations of actuator devices impose hard constraints on the control input. For instance, by considering the cart-pendulum system pneumatically actuated, the maximum force that cylinders can impose is about $124N$, that cannot increase due to physical limitations of the system, in particular the selected pressure and the areas of the pistons. When the inferior or superior limits are reached by the input signal $u(t)$, a saturation phenomenon appears (Figure 98), by turning the initial linear problem into a non linear one. Generally, whether this saturation zone lasts little, the behaviour of the overall system could not change. Problems arises above all in presence of long saturation zones, such as a worsening in performances (e.g overshoot, rise time) and, in the most dangerous case, a lost of stability.

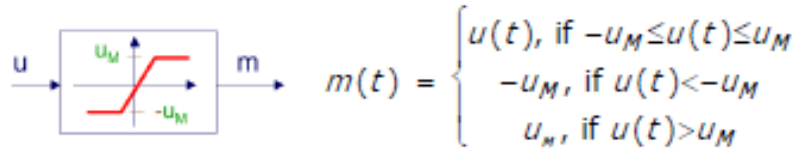


Figure 98: Saturation phenomenon

In order to solve the saturation problem, a possible and strong approach is the Model Predictive Control, whose aim is to predictive future behaviour of the considered state variables to develop an optimal control action. Such a method generates a control action by minimizing a cost function to which some input and output constraints may be applied, as shown in Figure 99:

$$\begin{aligned}
& \min_{\Delta u(k|k)} \sum_{i=0}^{H_p} (y(k+i|k) - r(i))^T Q_y (y(k+i|k) - r(i)) + \\
& \quad + \Delta u^T(k+i|k) R \Delta u(k+i|k) \\
& \Delta u(k|k) = [\Delta u(k|k) \quad \Delta u(k+1|k) \quad \dots \quad \Delta u(k+H_p-1|k)]^T \\
& \text{s.t.} \begin{cases} \begin{bmatrix} x(k+1) \\ u(k) \end{bmatrix} = \begin{bmatrix} A & B \\ 0 & I \end{bmatrix} \begin{bmatrix} x(k) \\ u(k-1) \end{bmatrix} + \begin{bmatrix} B \\ I \end{bmatrix} \Delta u(k) \\ u_{\min} \leq u(k+i|k) \leq u_{\max}, i = 0, \dots, H_p-1 \\ \Delta u_{\min} \leq \Delta u(k+i|k) \leq \Delta u_{\max}, i = 0, \dots, H_p-1 \\ y_{\min} \leq y(k+i|k) \leq y_{\max}, i = 1, \dots, H_p \end{cases}
\end{aligned}$$

Figure 99: Basic principles of MPC

In few words, the cost function embraces two quantities; the first is tracking error, the second is the input variation, controlled by means of the two weighting matrices Q and R. The cost function is applied until a certain prediction horizon H_p , that increases the quality of the control the higher it is chosen. The drawback is linked to computational complexity that can become enormous if H_p is too big. The constraints on input, variation of input and controlled output are imposed through linear inequalities. In particular, the ones on the input are hard constraints, as they will never be outcome. So, if a feasible controller exists, it is sure the saturation is avoided. Constraints on the output, on the other hand, are soft in the sense that, if necessary, they can be surpassed of small quantities.

In order to proceed with the design of the controller, some parameters and quantities need to be set in the Matlab environment. First of all, as this involves a discrete time control, the starting continuous time plant must be discretized. So, the first step, consists of considering the linear time-invariant plant written in the matrix form:

$$\begin{cases} \dot{x}(t) = Ax(t) + Bu(t) \\ y(t) = Cx(t) + Du(t) \end{cases} \quad (37)$$

In the case in exam, that is the system with the only cart and pendulum, by considering as states:

$$\begin{cases} x_1 = x \\ x_2 = \dot{x} \\ x_3 = \theta \\ x_4 = \dot{\theta} \end{cases} \quad (38)$$

And as outputs the linear position of the cart and the angle of the pendulum with respect to the vertical axis, the continuous time matrices become:

$$A = \begin{bmatrix} 0 & 1 & 0 & 0 \\ 0 & -9.4737 & -0.5158 & 0.0197 \\ 0 & 0 & 0 & 1 \\ 0 & 11.8421 & -10.3158 & -0.4939 \end{bmatrix} \quad (39)$$

$$B = \begin{bmatrix} 0 \\ 0.5263 \\ 0 \\ -0.6579 \end{bmatrix} \quad (40)$$

$$C = \begin{bmatrix} 1 & 0 & 0 & 0 \\ 0 & 0 & 1 & 0 \end{bmatrix} \quad (41)$$

$$D = 0 \quad (42)$$

A fundamental step is the selection of the sampling frequency (or sampling period), that should be great enough (small enough) to avoid the superimposition of the periodic replicas, known as aliasing, according to the Nyquist-Shannon criterion. But it cannot be too high (too small) in order to avoid computational issues. In the case in exam, a good behaviour of the system is obtained with a sampling period of $T_s = 0.03s$.

Once the system has been defined, it must be made discrete by using the chosen sampling period, by means of the command `c2d`, and considering as reconstruction method the zero order hold one. The discrete matrices are then saved into further variables, as show in Figure 100:

```
%now I create the discrete time system
sys_dt=c2d(sys,Ts,'zoh');
%now I define the discrete matrixes
Ad=sys_dt.a;
Bd=sys_dt.b;
Cd=sys_dt.c;
Dd=sys_dt.d;
```

Figure 100: Discrete time system production and saving in other variables

The resulting discrete matrices in the case in example are:

$$A_d = \begin{bmatrix} 1 & 0.0261 & -0.0002 & 0 \\ 0 & 0.7527 & -0.0135 & 0.0003 \\ 0 & 0.0048 & 0.9954 & 0.0297 \\ 0 & 0.3064 & -0.3092 & 0.9808 \end{bmatrix} \quad (43)$$

$$B_d = \begin{bmatrix} 0.02 \\ 0.0137 \\ -0.0003 \\ -0.017 \end{bmatrix} \quad (44)$$

$$C_d = \begin{bmatrix} 1 & 0 & 0 & 0 \\ 0 & 0 & 1 & 0 \end{bmatrix} \quad (45)$$

$$D_d = 0 \quad (46)$$

Next, a list of several parameters need to be set:

- $C_y = \text{eye}(4)$, that represents the measured output, corresponding always to the measured states;

- $C_z=C_d$, $D_z = [0;0]$ linked to the controlled outputs;
- $C_c=C_d$, $D_c = 0$, linked to the constrained outputs;
- Q is a square matrix, where on the diagonal the weights for the tracking errors referred to the considered states are posed; in this case, good performances are given with

$$Q = \begin{bmatrix} 10 & 0 \\ 0 & 18 \end{bmatrix} \quad (47)$$

- R is referred to inputs, and now it is chosen as $R = 0.1$;
- z_{max} and z_{min} determine the presence of constraints on the output; in this case the former goes from 0 to 0.5, referred to the limited linear guide where the cart moves; the latter has no limit;
- u_{max} and u_{min} refers to constraints on the input and, in this case the former is imposed to 4000, the latter to -4000;
- du_{max} and du_{min} are linked to rate constraints and now they are imposed equal to infinite;
- h is equal to the sampling time;
- $cmode$ selects the mode with which the system works; if it is 0, there is the state feedback mode that works on a fake system that has as outputs all the considered states; if it is 2, a Kalman filter is considered and the system works with the normal discrete system. Now it is 0;
- H_p and H_u are, respectively, the prediction horizon and the control horizon. Initially, they are chose equal to 50 but, once the controller is designed, they can be reduced until performances start declining. The former, in any case, must always be greater or equal than the latter. H_w is instead the first penalty sample and is, generally, considered as 1;
- z_{blk} and u_{blk} are linked to blocking signals and are chosen as 1, by indicating their absence;
- W and V are covariance matrices that are taken into account only for the Kalman filter case.

Once all the parameters have been set, the final controller is computed by means of the following function:

```
md=MPCInit(Ad,Bd,Cy,Cz,Dz,Cz,Dz,Hp,Hw,zblk,Hu,ublk, ...
           du_max,du_min,u_max,u_min,z_max, ...
           z_min,Q,R,[],[],h,cmode,solver);
```

Figure 101: Function generating the MPC controller

The study of the performances of the controller has been performed by means of the Simulink model, that is reported in Figure 102:

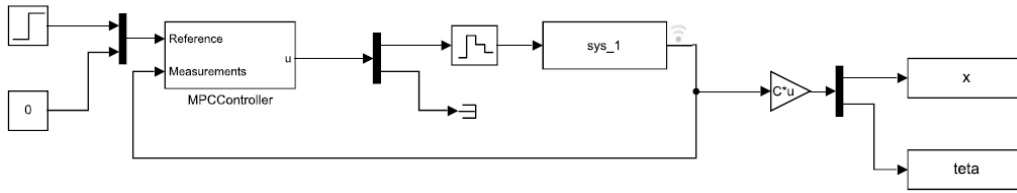


Figure 102: MPC block scheme in Simulink

Where *sys_1* is the fake system whose outputs are all the states, and as reference signals a step signal for the position of the cart and 0 for the angle of the pendulum have been selected. In order to visualize the overall behaviour of the system, next step is to show the step response of the linear position of the cart, by imposing a step reference signal of $200mm$, and the angle of the pendulum. This analysis considers only the initial condition on the angle equal to 0° .

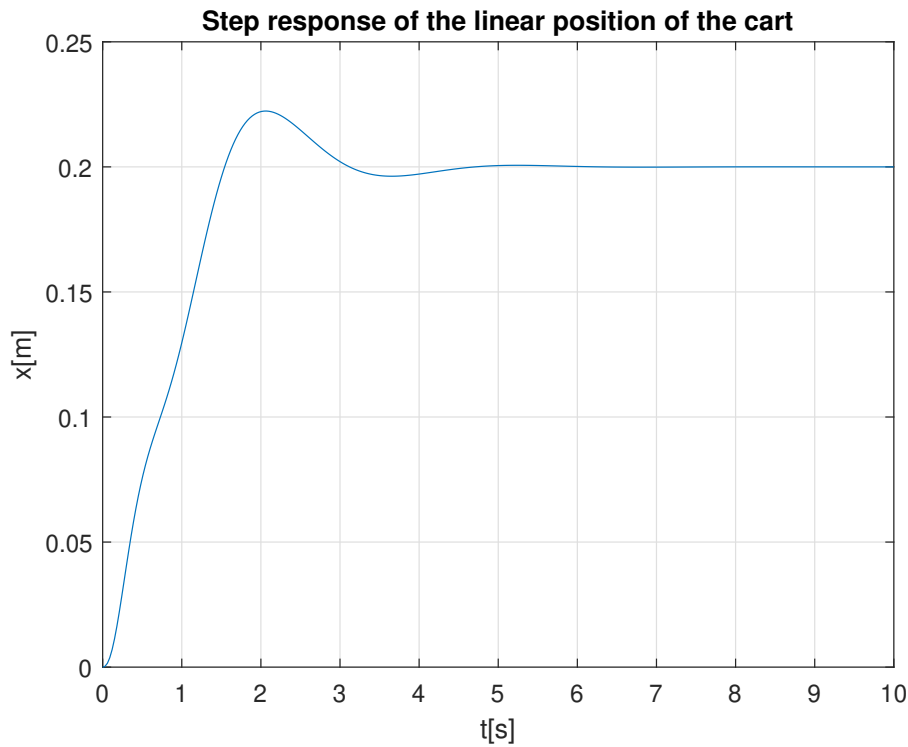


Figure 103: Step response of the linear position of the cart in the MPC architecture

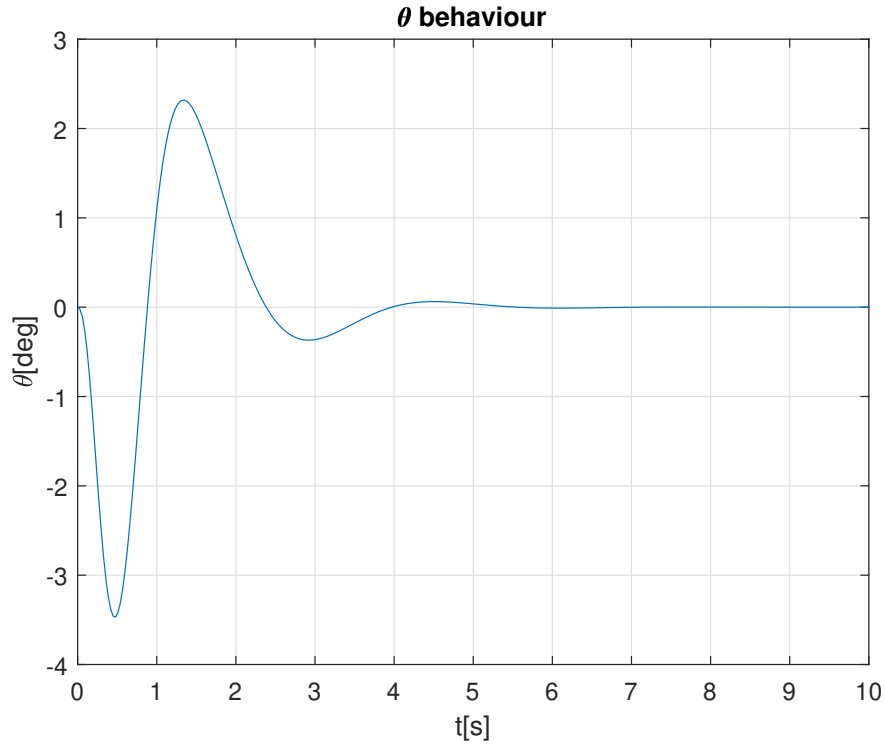


Figure 104: Behaviour of the angle of the pendulum in the MPC architecture

The Figure 103 shows the step response of the cart. It presents a rising time of about 1.56s, an overshoot of about 11%, and the setpoint can be considered reached after about 3s. The Figure 104 reports, instead, the behaviour of the angle of the pendulum. After an undershoot of about 3.4° the angle reaches an overshoot of 2.3°. Finally, after a new small undershoot of about 0.2°, the angle gets to zero in about 4s.

6 Electromechanical model

The electromechanical system consists of an electrical brushless motor and a transmission system, linked to the model of the pendulum and cart analyzed previously. The equations of the pendulum and cart are the same as the ones written in the chapter 5.

The transmission system allows to transmit the power coming from the motor to the pendulum-cart system, by creating a kinematic constraint between the rotation of the crankshaft and the linear position of the cart. This kinematic property can be obtained from the pitch of the screw, defined as follows:

$$i_v = \frac{2\pi}{p_v} \quad (48)$$

This permits to connect not only the position, but also the velocity and the acceleration of the cart to the ones of the screw:

$$i_v = \frac{\alpha}{x} = \frac{\dot{\alpha}}{\dot{x}} = \frac{\ddot{\alpha}}{\ddot{x}} \quad (49)$$

Where x, \dot{x} and \ddot{x} are respectively the position, the velocity and the acceleration of the cart while $\alpha, \dot{\alpha}$ and $\ddot{\alpha}$ are the angular position, the angular velocity and the angular acceleration of the screw/motor.

The adopted electric motor is a brushless permanent magnets motor, whose circuit is shown in Figure 105:

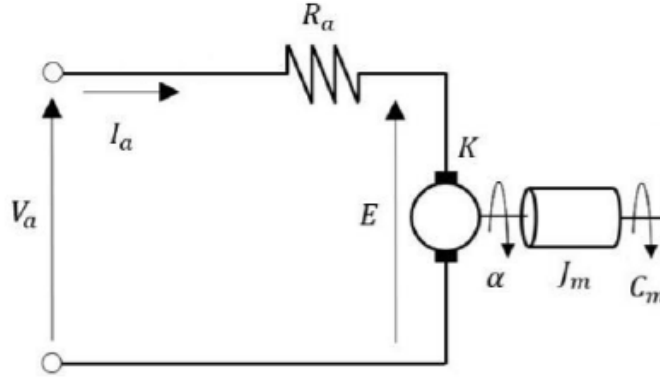


Figure 105: Electric circuit of the motor

Such a model considers some assumptions that simplify the treatment:

- the magnetic circuit is linear;
- mechanical friction is negligible;
- the armature inductance L_a is neglected.

By adopting the Kirchoff's laws, it is possible to obtain:

$$V_a(t) = R_a I_a(t) + E(t) \quad (50)$$

Where $E(t)$ is the electromotive force that can be linked to the angular velocity of the motor:

$$E(t) = K \dot{\alpha}_{motor} \quad (51)$$

Starting from the voltage applied to the motor, it is possible to calculate its torque by means of the following relation:

$$C_m(t) = K I_a(t) \quad (52)$$

Typically, the motor is connected to a system to move, that produces a resistant torque C_r , opposing the motion torque C_m . By considering the overall system, it is possible to write a relation of dynamic equilibrium to the rotation of the crankshaft:

$$C_m(t) - C_r(t) = J_{tot} \ddot{\alpha} \quad (53)$$

where J_{tot} represents the overall moment of inertia of the system, given by the contribute of the inertia of the motor and the one of the system to move, considered with respect the motion axis. The overall system is made up of the mechanical system connected to the electric one. It is shown in Figure 106:

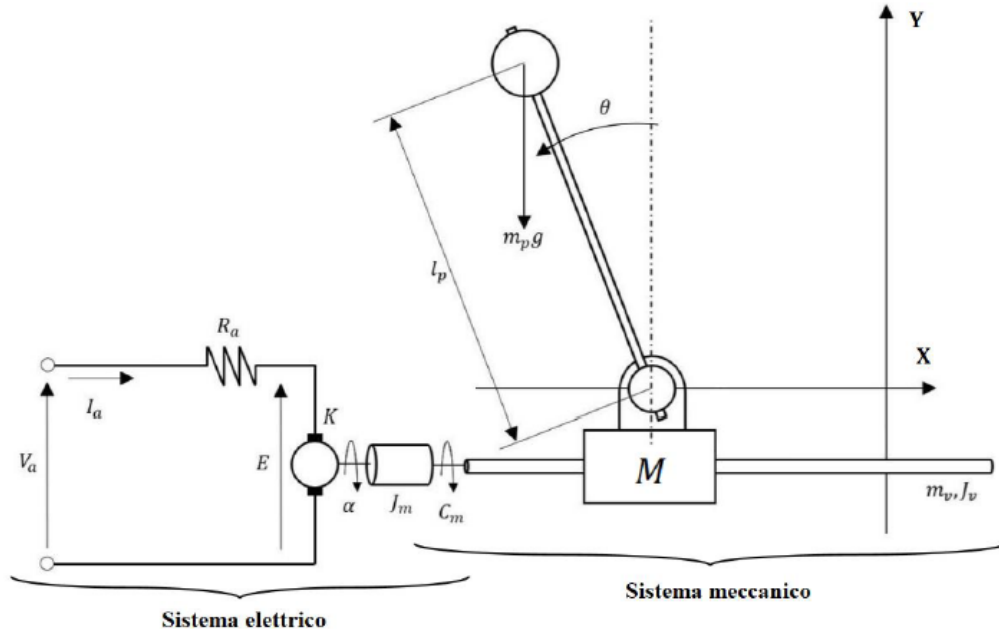


Figure 106: Overall electromechanical system

By coupling the two systems, the screw is constrained to the crankshaft. The kinematic constraints analyzed before allow to write down the following relations:

$$\begin{cases} \alpha = \alpha_{motor} = \alpha_{screw} = x_{cart} i_v \\ \dot{\alpha} = \dot{\alpha}_{motor} = \dot{\alpha}_{screw} = \dot{x}_{cart} i_v \\ \ddot{\alpha} = \ddot{\alpha}_{motor} = \ddot{\alpha}_{screw} = \ddot{x}_{cart} i_v \end{cases} \quad (54)$$

The equations of the motor are the same as the ones expressed previously, the only modification needs to be done in the equation (50), where it establishes the resistant torque C_r is equal to the one imposed by the screw.

This one derives from the transmission system and it is related to the horizontal force F

applied to the cart. The resulting equations become:

$$\begin{cases} C_m(t) - C_r(t) = J_{tot}\ddot{\alpha} \\ C_r(t) = \frac{F(t)}{\eta i_v} \\ J_{tot} = J_{motor} + J_{screw} \end{cases} \quad (55)$$

By combining the equation (11) with the equation (46), it is possible to express the component of the force F applied to the cart by taking into account the kinematic constraints. This leads to:

$$F(t) = (M + m)\frac{\ddot{\alpha}}{i_v} + m_p l_p \dot{\theta}(t)^2 \sin(\theta(t)) - m_p l_p \ddot{\theta} \cos(\theta(t)) + c \frac{\dot{\alpha}}{i_v} \quad (56)$$

By combining the relation of $C_r(t)$ with the equation (53), it can be obtained:

$$C_r(t) = \frac{(M + m)\frac{\ddot{\alpha}}{i_v} + m_p l_p \dot{\theta}(t)^2 \sin(\theta(t)) - m_p l_p \ddot{\theta} \cos(\theta(t)) + c \frac{\dot{\alpha}}{i_v}}{\eta i_v} \quad (57)$$

This leads to the final dynamic equation that allows to evaluate $\ddot{\alpha}$:

$$\ddot{\alpha}(t) = \frac{1}{J_{eq}}(K I_a(t) - \frac{m_p l_p \dot{\theta}(t)^2 \sin(\theta(t)) - m_p l_p \ddot{\theta} \cos(\theta(t)) + c \frac{\dot{\alpha}}{i_v}}{\eta i_v}) \quad (58)$$

where J_{eq} is given by:

$$J_{eq} = J_{tot} + \frac{M + m}{\eta i_v^2} \quad (59)$$

6.1 Simulink model

The numeric simulations have been performed by developing the Simulink model of the overall system. The construction of the model is based on the non linear equations (11) for the cart-pendulum group, that are integrated with the equations relative to the transmission and the motor.

In order to simplify the writing of some schemes, it is created some subsystems containing the overall equations. The overall electromechanical system in the Simulink environment is reported in Figure 107:

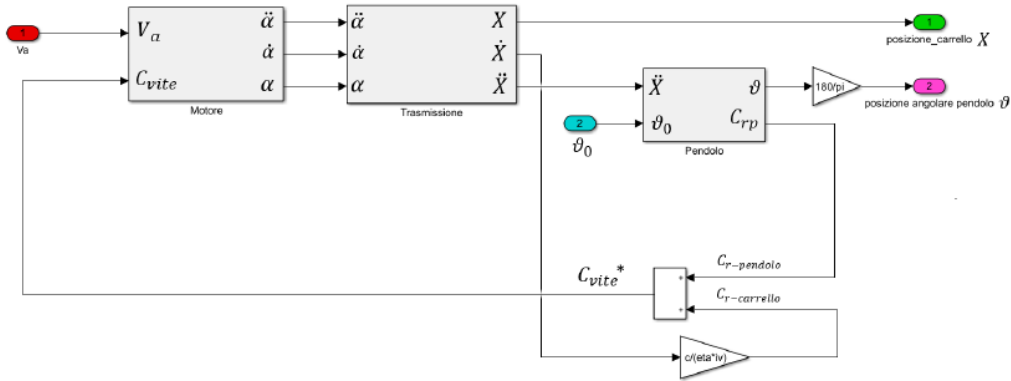


Figure 107: Electromechanical system in Simulink

The model is made up of three main subsystems relative to the motor, the transmission and the pendulum.

It seems the cart is not present but, actually, it is included in the output of the transmission block.

The inputs of the system are the voltage V_a and the initial angle of the pendulum θ_0 . Each subsystem can be exploited in order to visualize the equations reported before.

The model of the motor is shown in Figure 108:

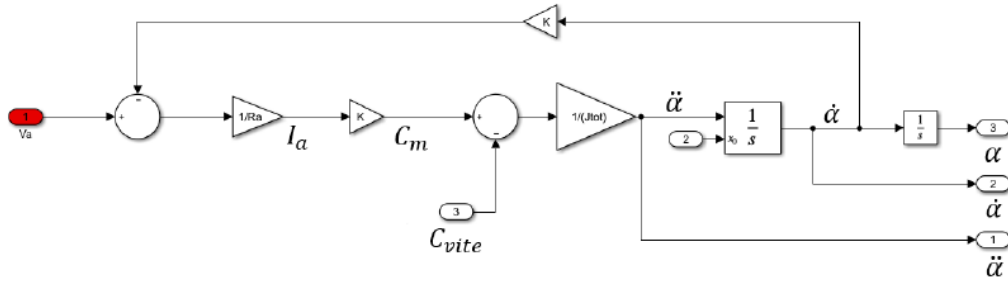


Figure 108: Model of the motor

The Figure 109 reports the model of the transmission:

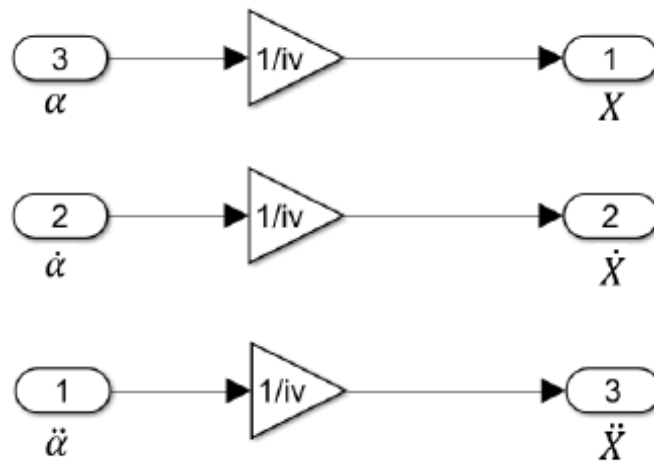


Figure 109: Model of the transmission

The pendulum model is represented in Figure 110:

Once imposed input and output, the "App model linearizer" tool provides the matrices A, B, C and D of the SISO linearized system:

$$A = \begin{bmatrix} -0.1798 & 0 & 3612 & -0.4761 & 22.14 \\ 1 & 0 & 0 & 0 & 0 \\ -196.3 & 0 & -629.6 & 0 & 0 \\ -0.0004088 & 0 & 8.212 & -0.3021 & 14.05 \\ 0 & 0 & 0 & 1 & 0 \end{bmatrix} \quad (60)$$

$$B = \begin{bmatrix} 0 \\ 0 \\ 370.4 \\ 0 \\ 0 \end{bmatrix} \quad (61)$$

$$C = [0 \quad 0.00159200 \quad 0 \quad 0 \quad 0] \quad (62)$$

$$D = 0 \quad (63)$$

from which it is possible to get:

$$G_{xV_a}(s) = \frac{2129.9}{s(s^2 + 629.8s + 7.091 * 10^5)} \quad (64)$$

By following the same steps, this approach permits the calculation of $G_{\theta V_a}$, by imposing the output on the θ branch. The new matrices become:

$$A = \begin{bmatrix} -0.1798 & 3612 & -0.4761 & 22.14 \\ -196.3 & -629.6 & 0 & 0 \\ -0.0004088 & 8.212 & -0.3021 & 14.05 \\ 0 & 0 & 1 & 0 \end{bmatrix} \quad (65)$$

$$B = \begin{bmatrix} 0 \\ 370.4 \\ 0 \\ 0 \end{bmatrix} \quad (66)$$

$$C = [0 \quad 0 \quad 0 \quad 1] \quad (67)$$

$$D = 0 \quad (68)$$

$G_{\theta V_a}$ results:

$$G_{\theta V_a} = \frac{3041.7(s - 8.28 * 10^{-6})}{(s + 3.895)(s - 3.594)(s^2 + 629.8s + 7.091 * 10^5)} \quad (69)$$

Finally, the last transfer function can be obtained as ratio of G_{xV_a} and $G_{\theta V_a}$:

$$G_{x\theta} = \frac{0.70023(s + 3.895)(s - 3.594)}{s(s - 8.28 * 10^{-6})} \quad (70)$$

As follows, the Bode diagrams of the three transfer functions:

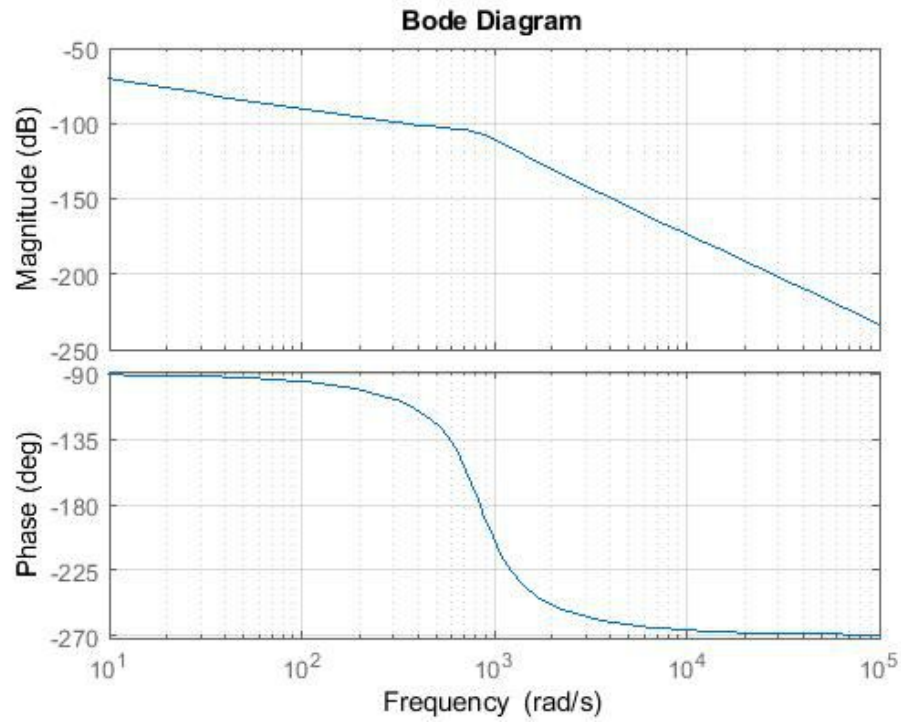


Figure 112: Bode diagram of G_{xV_a}

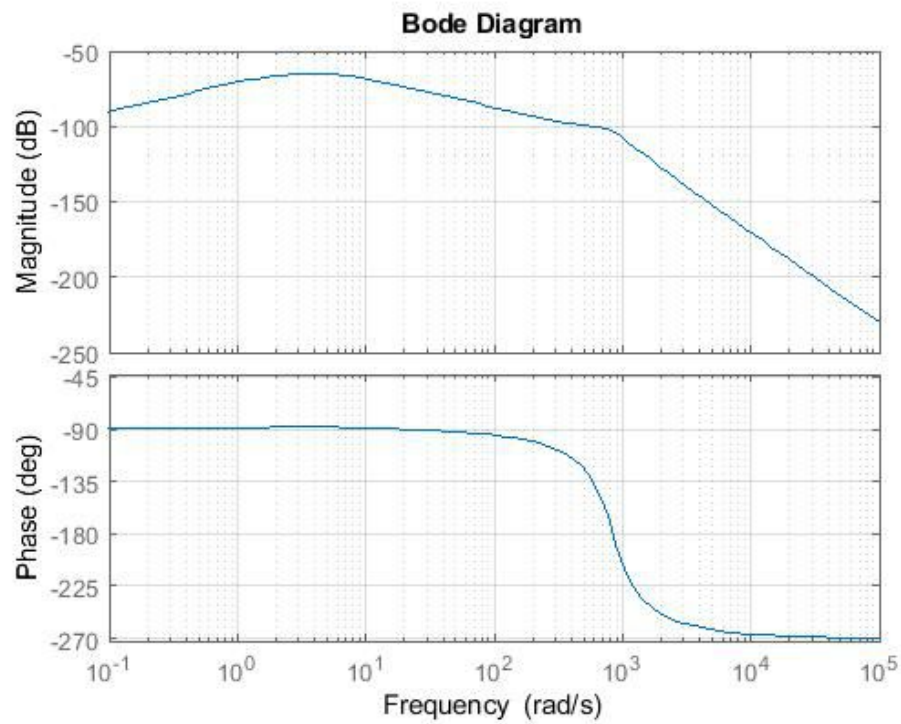


Figure 113: Bode diagram of $G_{\theta V_a}$

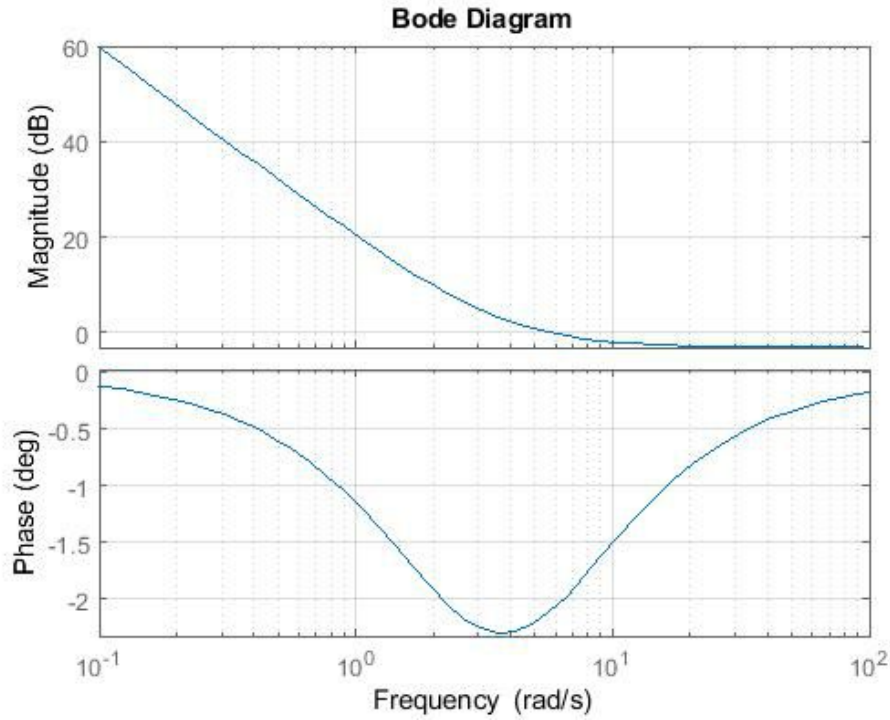


Figure 114: Bode diagram of $G_{x\theta}$

6.3 Cascade PID controller

The design of the cascade PID controllers is realized by following the same steps reported in the section 5.3. The scheme it refers to is shown in Figure 115:

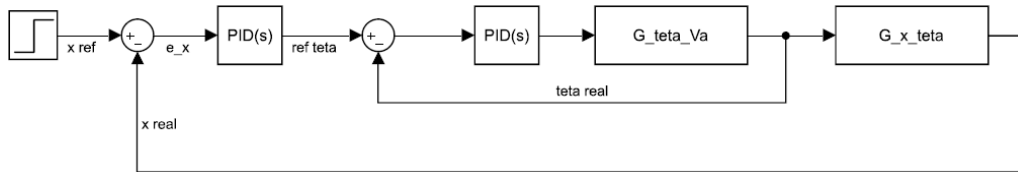


Figure 115: Cascade scheme

The first step consists of designing the inner PID controller, in order to stabilize the transfer function $G_{\theta V_a}$ in closed-loop. In fact, its Nyquist diagrams demonstrates its instability, by supposing a unitary inner PID controller (Figure 116):

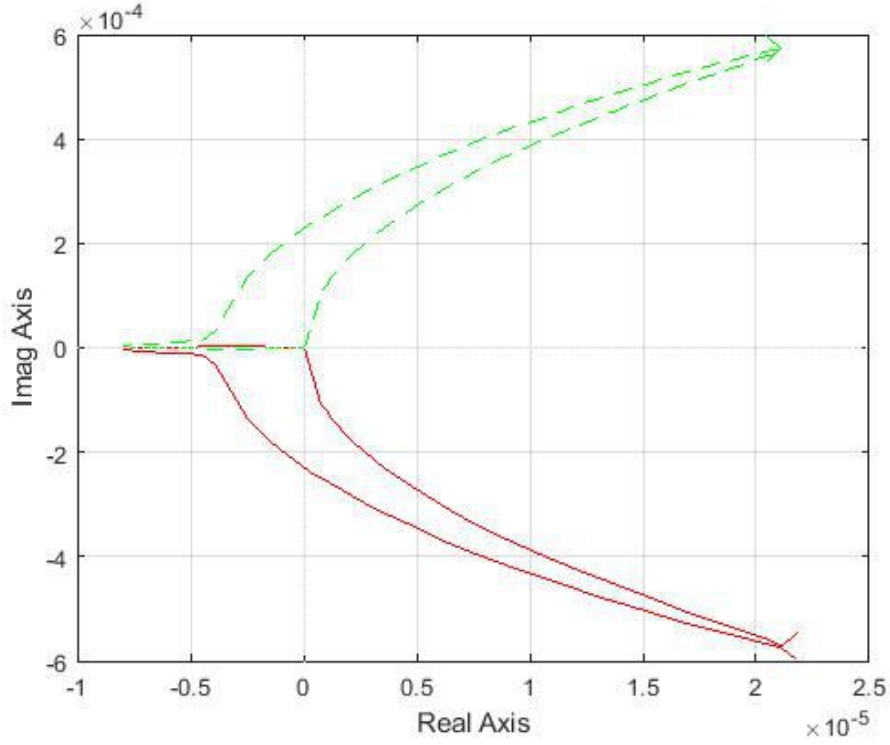


Figure 116: Nyquist diagram of $G_{\theta V_a}$

The inner PID controller is designed through the help of the autotuning tool in Simulink, as the previous cases. Due to the complexity of the system and, so, of the transfer functions in interest, this tool cannot find a stabilizing controller immediately. It is necessary to act on the rising time, one of the two parameters characterizing the autotuning tool. By choosing a time that is too small (e.g. $10ms$), the resulting PID parameters are too high, above all the integrative coefficient whose value wanders around 10^5 . By trial and error, it has been possible to find a good trade-off in terms of time and PID parameters. By imposing a rise time of about $2s$, the resulting PID transfer function is:

$$PID_{\theta}(s) = \frac{32789(s + 16.78)(s + 4)}{s(s + 457.1)} \quad (71)$$

The new open-loop inner transfer function becomes:

$$G_{ol\theta}(s) = \frac{9.9736 * 10^6 (s + 16.78)(s + 4)}{(s + 457.1)(s + 3.895)(s - 3.594)(s^2 + 629.8s + 7.091 * 10^5)} \quad (72)$$

whose Nyquist diagram and margins are plotted in Figure 117 and Figure 118:

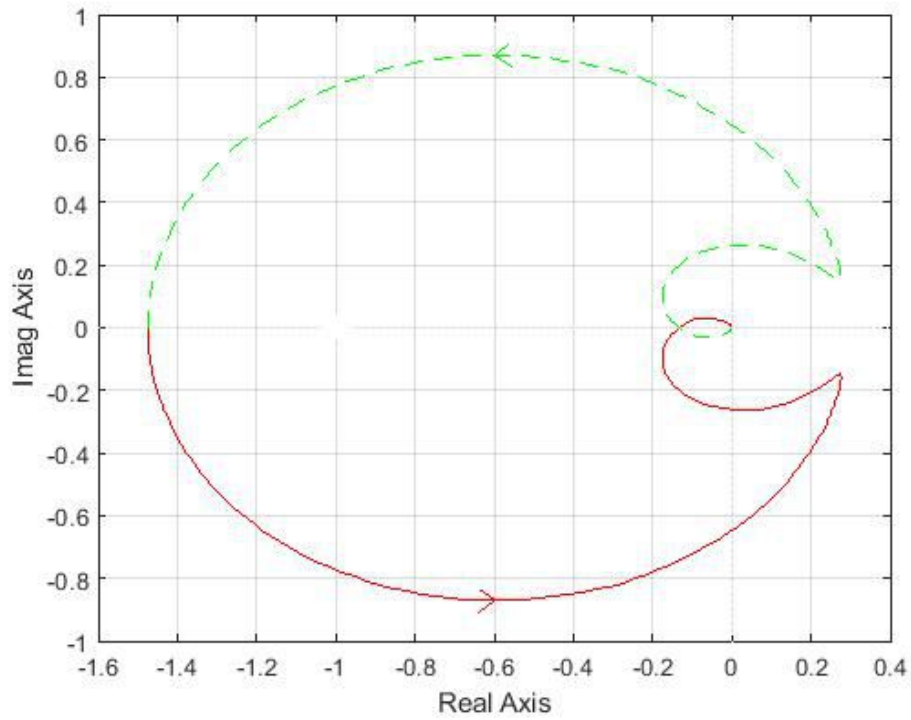


Figure 117: Nyquist diagram of $G_{ol\theta}$

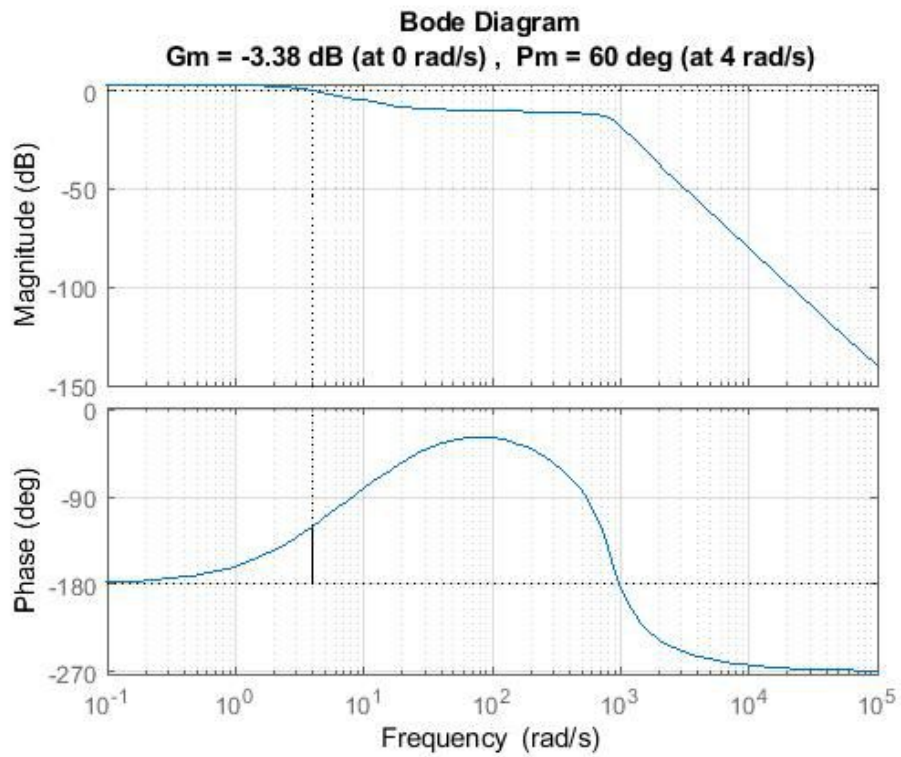


Figure 118: Magnitude and phase margins of $G_{ol\theta}$

The encirclement of the unstable point $(-1, j0)$ compensates the unstable pole present in the open-loop transfer function, by resulting in a stable closed-loop transfer function. Last step consists of finding the external PID controller, acting on the linear position of the cart. The inner closed-loop function becomes:

$$G_{cl\theta}(s) = \frac{G_{ol\theta}(s)}{1 + G_{ol\theta}(s)} = \frac{9.9736 * 10^7 (s + 16.78)(s + 4)}{(s + 596.8)(s + 3.767)(s + 1.366)(s^2 + 485.2s + 7.022 * 10^5)} \quad (73)$$

The outer PID controller is necessary to obtain an overall stable system. In fact, by supposing a unitary PID, the overall closed-loop transfer function is unstable, as shown in the Nyquist diagram in Figure 119:

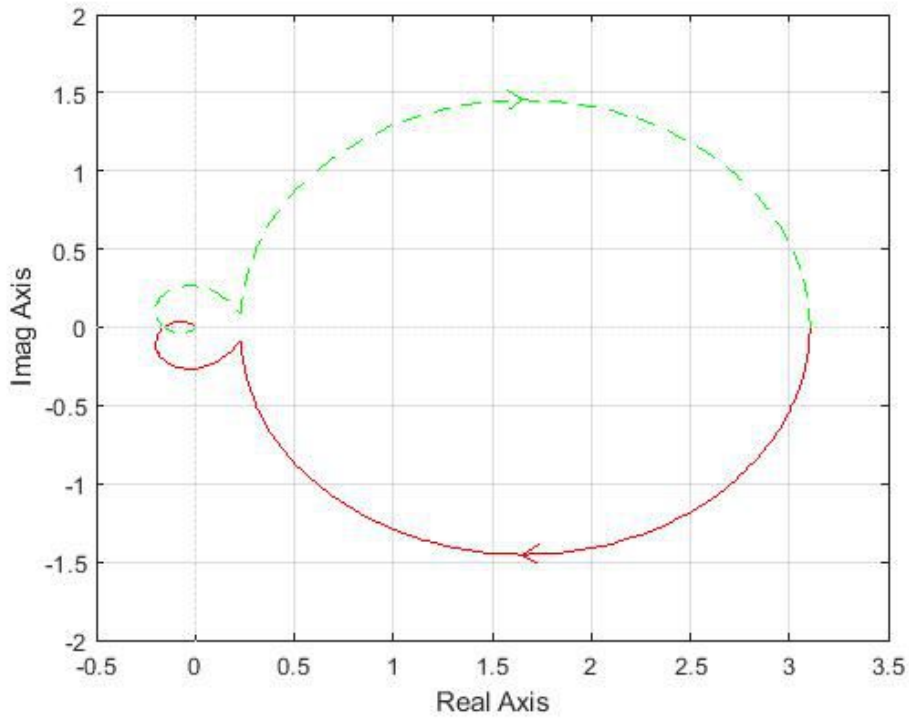


Figure 119: Nyquist diagram of G_{olx}

As the previous case, the outer PID controller is designed through the autotuning tool in Simulink, by acting on the rise time. By considering a rise time of about $4s$, the final outer PID transfer function becomes:

$$PID_x(s) = \frac{-0.056742(s + 0.03813)(s + 0.02279)}{s(s + 4.196)} \quad (74)$$

The final overall open-loop transfer function is the following:

$$G_{olx}(s) = \frac{-5.6562 * 10^6 (s + 0.03813)(s + 0.02279)(s + 4)(s + 16.78)}{s(s + 4.196)(s + 3.767)(s + 1.366)(s + 596.8)(s^2 + 485.2s + 7.022 * 10^5)} \quad (75)$$

whose Nyquist diagram and margins are shown in Figure 120 and Figure 121:

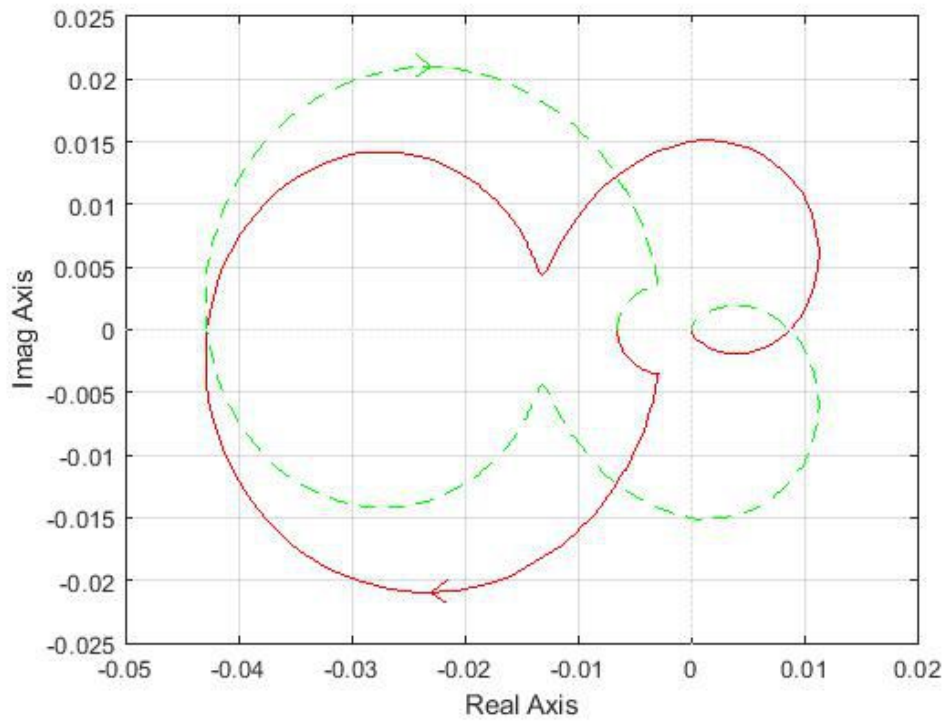


Figure 120: Nyquist diagram of the definitive G_{olx}

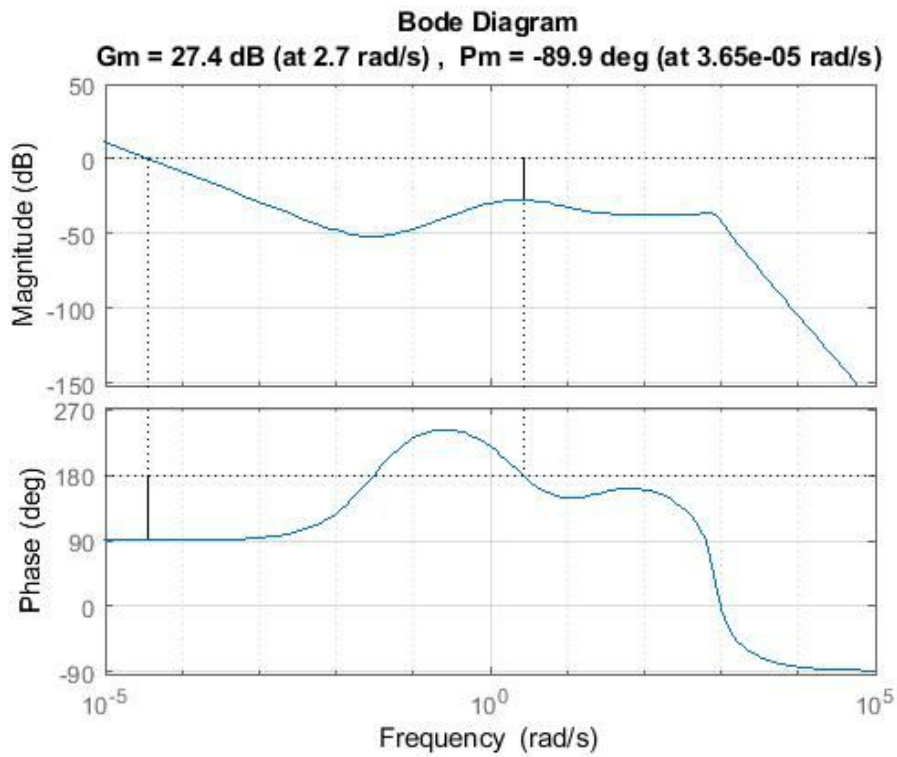


Figure 121: Magnitude and phase margins of G_{olx}

The resulting overall closed-loop transfer function is equal to:

$$G_{clx}(s) = \frac{-5.6592 * 10^6 (s + 0.03813)(s + 0.02279)(s + 4)(s + 16.78)}{(s + 589.6)(s + 4.133)(s + 3.57)(s + 1.486)(s - 3.658 * 10^{-5})(s^2 + 492.7s + 7.015 * 10^5)} \quad (76)$$

Its Bode diagrams are reported in Figure 122:

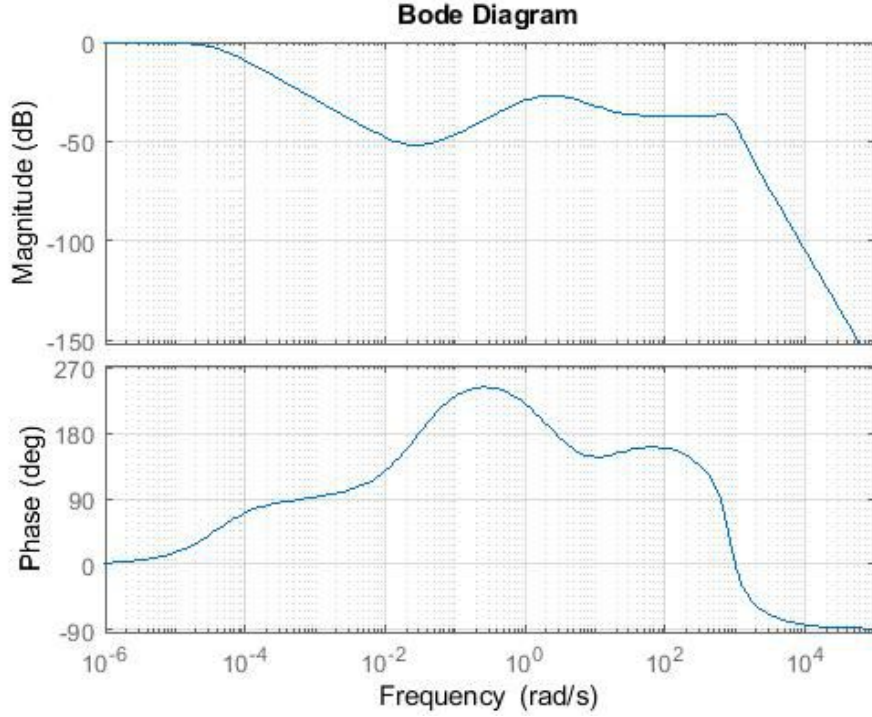


Figure 122: Bode diagrams of the definitive G_{clx}

Unlike the simple mechanical system, the PID stabilizing the linear system do not work properly for the non linear one. In order to find controllers that stabilize the overall non linear system, it is considered a cascade scheme where the linear transfer functions are substituted with the complete non linear model (Figure 111), as represented in Figure 123:

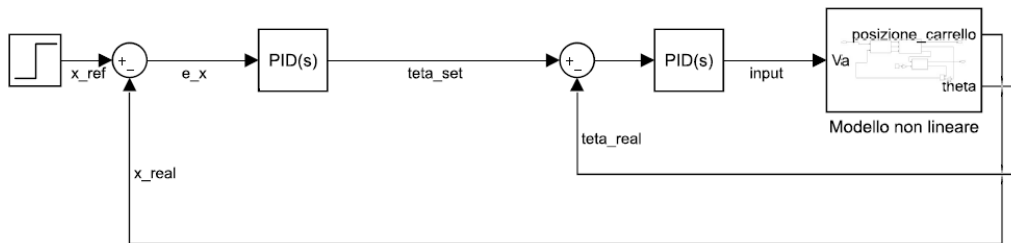


Figure 123: Cascade scheme with the non linear system

As performed in the previous case, the autotuning tool helps finding both the inner and the outer PID controllers. As regard the inner one, proper performances are reached with

such a controller:

$$PID_{\theta nl}(s) = \frac{4291.7(s + 359)(s + 28.57)}{s(s + 268.1)} \quad (77)$$

Once the inner PID controller has been found, the same procedure leads to the design of the outer PID, whose transfer function is:

$$PID_{xnl}(s) = \frac{-0.28031(s + 0.06933)(s + 0.05415)}{s(s + 3.966)} \quad (78)$$

A further more complete analysis is shown in another chapter by using the Simscape environment in Simulink. As performed previously, in order to visualize the behaviour of the non linear system by adopting the designed cascade architecture, it is useful to report the step response of the linear position of the cart, with an amplitude of $200mm$, and the angle of the pendulum.

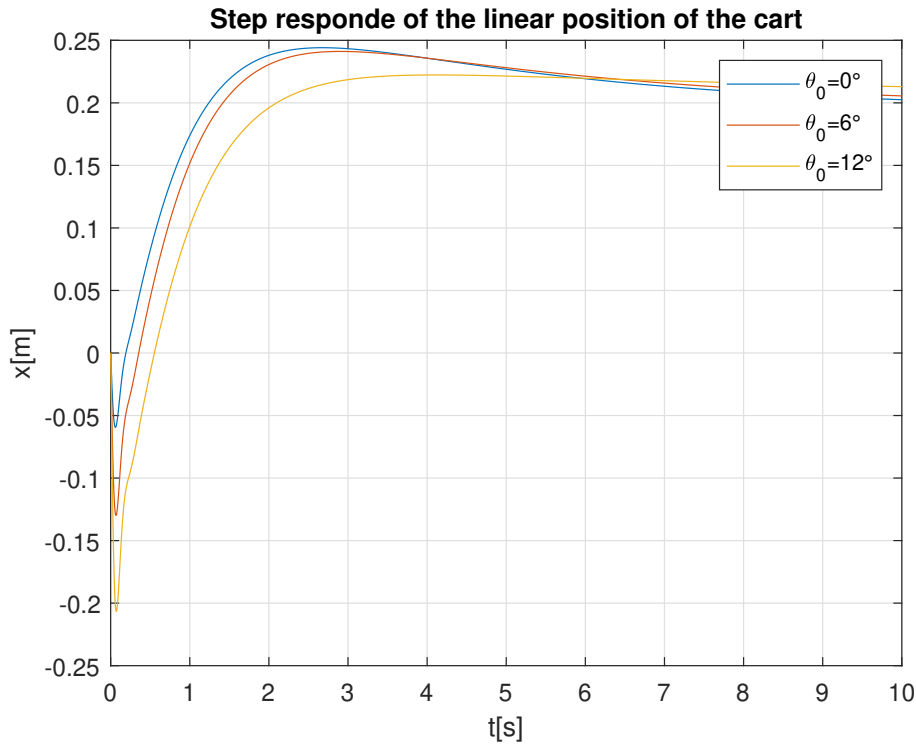


Figure 124: Step response of the linear position of the cart in the cascade architecture and electromechanical system

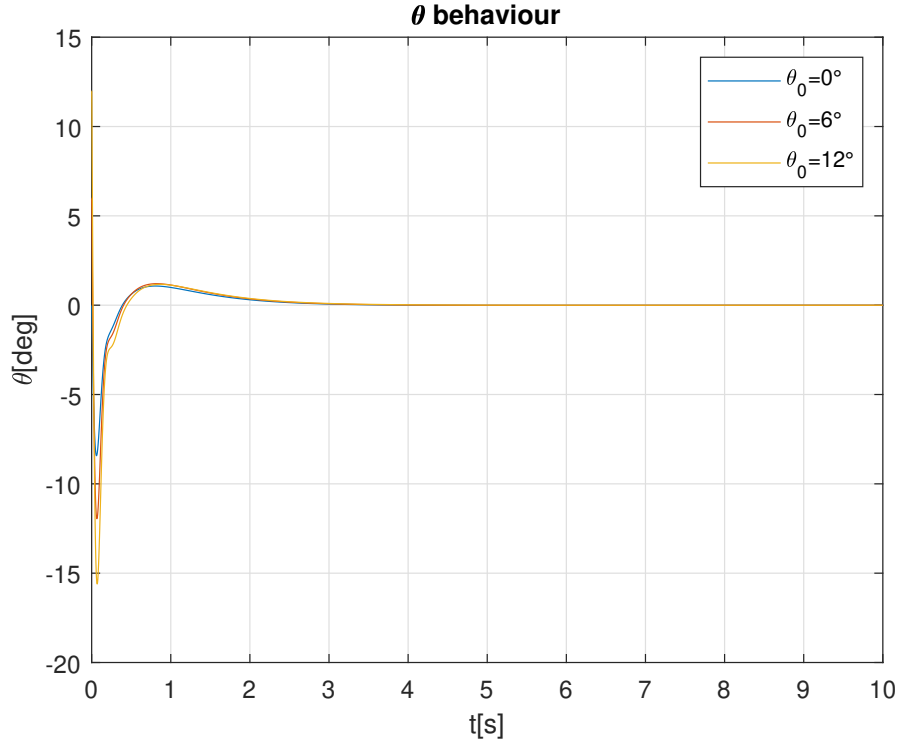


Figure 125: Behaviour of the angle of the pendulum in the cascade architecture and electromechanical system

The simulations are performed by considering the same three initial conditions as before. The Figure 124 shows the step response of the linear position of the cart and it can be noticed that, by considering a null initial condition, the response presents an higher overshoot, about 24.3%, but it is faster; in fact, the rising time is about 1.35s and the setpoint can be considered reached in about 8s. Moreover, the initial undershoot is very small but it increases by considering higher initial angles. Such conditions reduce the overshoot of the step response, but they slow down it as the rising time and the settling time increase too. The Figure 125 shows, instead, the behaviour of the angle of the pendulum. It can be seen that the pendulum gets to its vertical position in about 2s, whatever initial condition is considered.

6.4 Parallel PID controller

The second kind of the considered control technique is the parallel PID scheme, as shown in Figure 126:

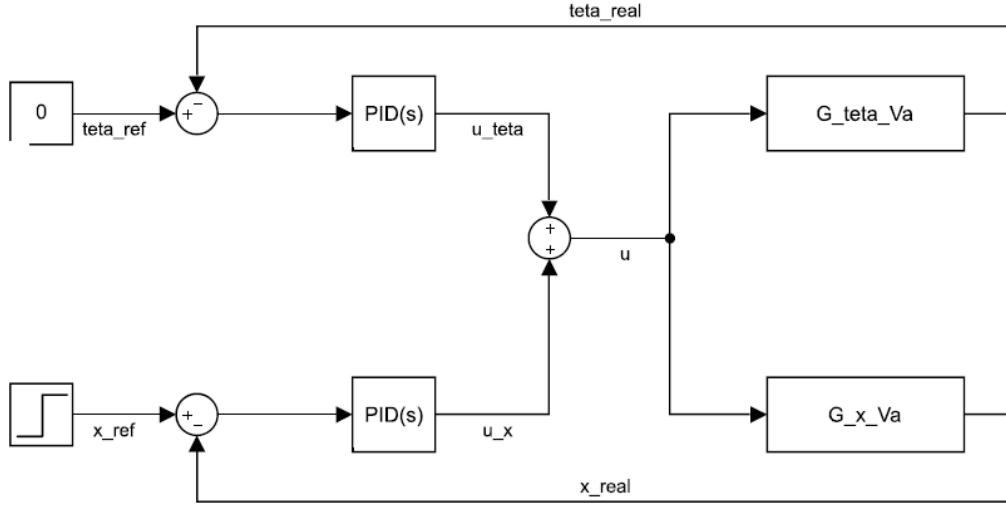


Figure 126: Parallel scheme with the linear system

The logic on which this technique is based, is reported in the details in the section 5.4. The considered transfer functions are $G_{\theta Va}$, providing the angle of the pendulum in output, and $G_{x Va}$, providing the position of the cart. The complete input feeding both the transfer functions is the sum of two contributes, u_θ coming from the PID acting on the angle and u_x from the PID acting on the position of the cart.

The first step is to stabilize $G_{\theta Va}$ and, for the sake of simplicity, it is taken into account the same PID_θ as the cascade case.

Before starting with the analysis of the PID on the x branch, it is useful to show that, by imposing a unitary control on x, the resulting open-loop function is not stable, by means of the Nyquist plot (Figure 127):

$$G_{olx}(s) = \frac{G_{xVa}(s)}{1 + C_\theta(s)G_{\theta Va}(s)} = \frac{2129.9(s + 457.1)(s + 3.895)(s - 3.594)}{s(s + 596.8)(s + 3.767)(s + 1.366)(s^2 + 485.2s + 7.022 * 10^5)} \quad (79)$$

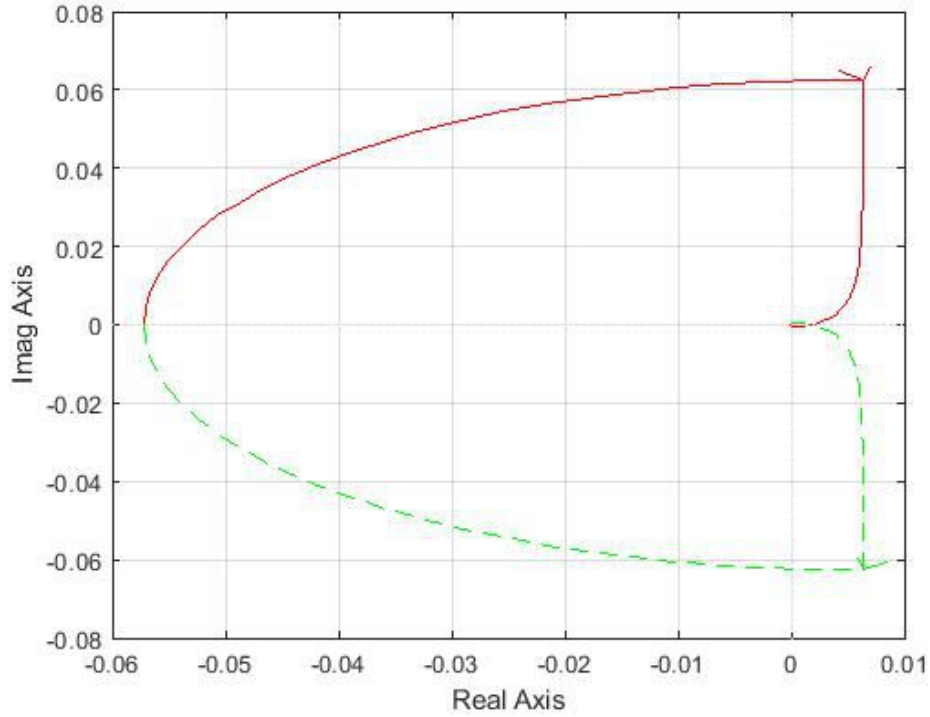


Figure 127: Nyquist plot of G_{olx}

The autotuning allows the evaluation of the PID acting on the linear position of the cart too. The resulting transfer function of this PID is the following:

$$PID_x(s) = \frac{-1191.6(s + 1.076)(s + 0.1271)}{s(s + 7.272)} \quad (80)$$

The resulting stable open-loop overall function is the following one:

$$G_{olx}(s) = \frac{-2.538 * 10^6 (s + 457.1)(s + 3.895)(s - 3.594)(s + 1.076)(s + 0.1271)}{s^2(s + 596.8)(s + 7.272)(s + 3.767)(s + 1.366)(s^2 + 485.2s + 7.022 * 10^5)} \quad (81)$$

whose Nyquist diagram and margins are reported in Figure 128 and Figure 129:

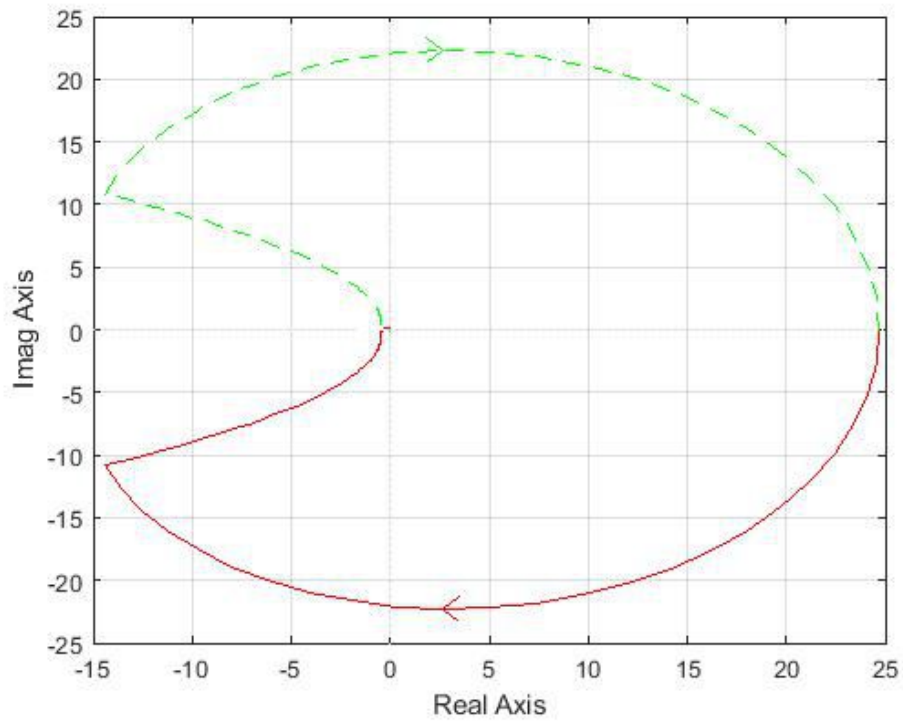


Figure 128: Nyquist plot of the final G_{olx}

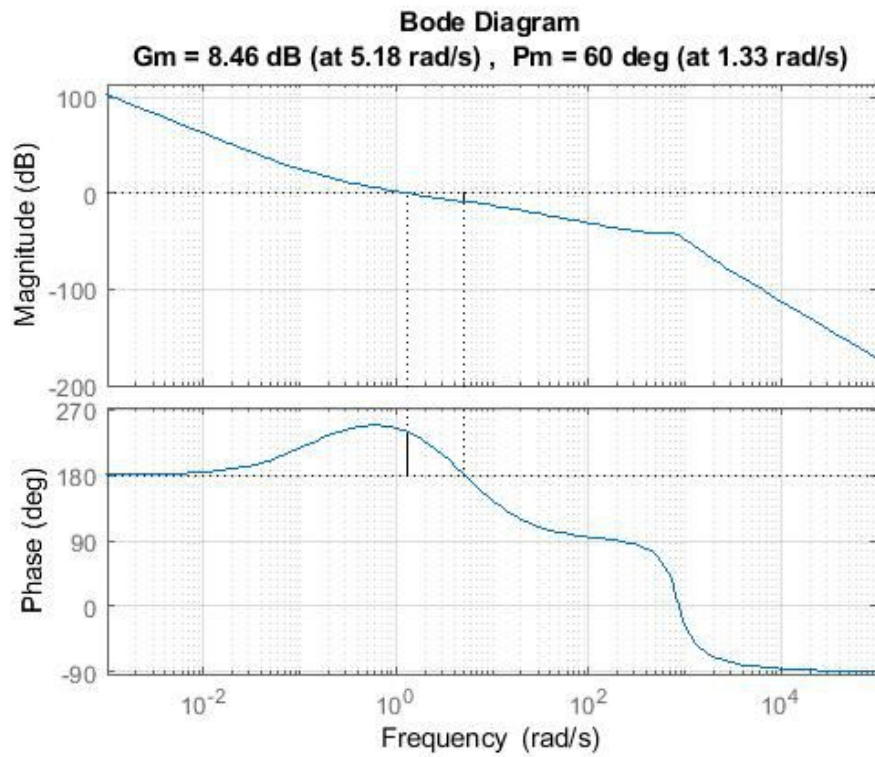


Figure 129: Magnitude and phase margins of G_{olx}

The final closed-loop function of the overall parallel scheme is:

$$G_{clx}(s) = \frac{-2.538 * 10^6 (s + 457.1)(s + 3.895)(s - 3.594)(s + 1.076)(s + 0.1271)}{(s + 596.1)(s + 4.067)(s + 0.8017)(s + 0.1456)(s^2 + 4.618s + 11.16)(s^2 + 488.8s + 7.034 * 10^5)} \quad (82)$$

whose Bode diagrams are shown in Figure 130:

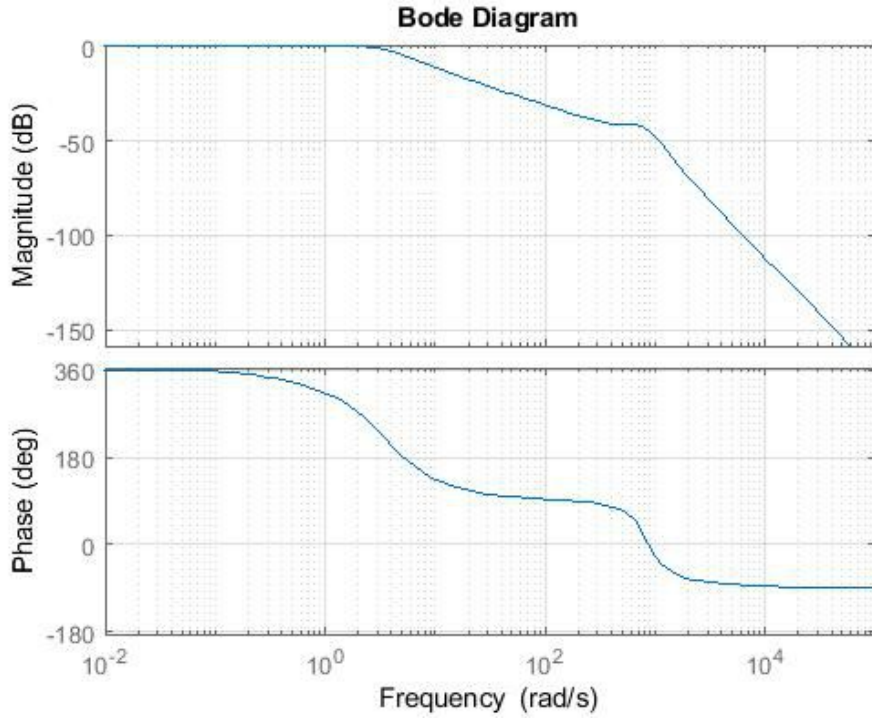


Figure 130: Bode diagrams of G_{clx}

As the cascade case, the non linear system is not stabilized through the PID controllers acting on the linear transfer functions, due to the complexity of the overall system. Therefore, it is necessary to design both the PID acting on the angle and the one acting on the linear position of the cart again.

The complete non linear parallel scheme is shown in Figure 131:

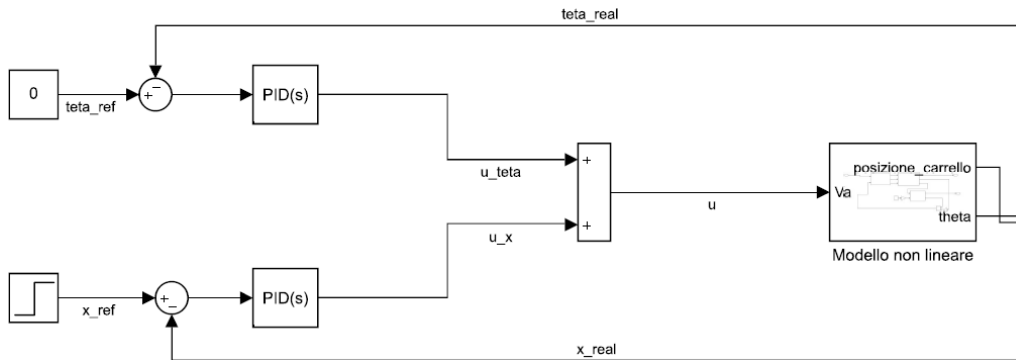


Figure 131: Non linear parallel scheme

The PID acting on the angle is designed by imposing a rise time of about $0.3s$. The resulting transfer function, provided by the autotuning tool is the following:

$$PID_{\theta}(s) = \frac{1.2194 * 10^5 (s + 530.8)(s + 24.96)}{s(s + 7721)} \quad (83)$$

Once define such a PID, the final step is to find a PID acting on the linear position of the cart that can stabilize the overall non linear system. The autotuning tool cannot find a performing controller immediately; as the other cases it is necessary to impose a proper rise time. By choosing as rise time $1s$, the final PID is given by:

$$PID_x(s) = \frac{-2.09(s + 9.039 * 10^4)(s + 0.2438)}{s(s + 7.253)} \quad (84)$$

A further more complete analysis is shown in another chapter through the Simscape tool. In order to visualize the overall behaviour of the non-linear system, next step consists of showing the step response of the linear position of the cart and the behaviour of the angle of the pendulum with respect its vertical axis.

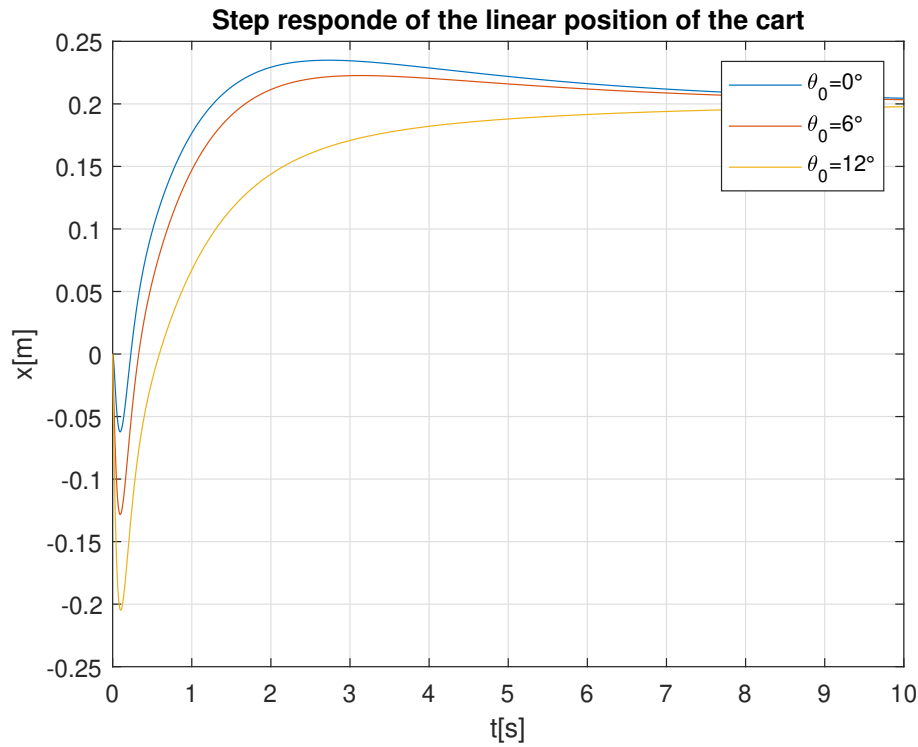


Figure 132: Step response of the linear position of the cart in the parallel architecture and electromechanical system

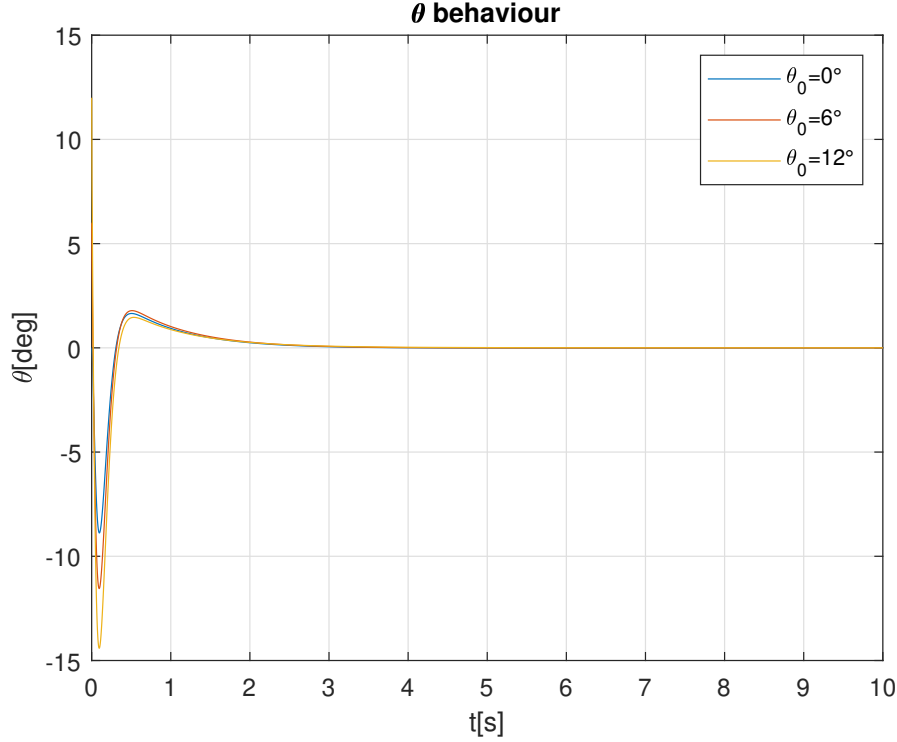


Figure 133: Behaviour of the angle of the pendulum in the parallel architecture and electromechanical system

The Figure 132 demonstrates a similar behaviour of the step response of the cart as the one provided by the cascade architecture. A null initial condition on the angle of the pendulum does that the response presents an higher overshoot, about 23.8%, but it is faster in terms of rising time and settling time. The latter is now intended as the time the cart takes to reach practically the setpoint. The rising time is about 1.2s and it increases along with the initial condition. The settling time is about 7.5s, but it increases along with the initial condition too. The last simulation, with $\theta_0 = 12^\circ$, does not present an overshoot anymore, by causing such a low kind of response.

The Figure 133, instead, shows the angle can meet the null value in about 2s, whatever the considered initial condition is. The only different resides in in initial undershoot that is bigger and bigger.

6.5 MPC

The Model Predictive Control approach is applied to the only linearized discrete model, by following the same rules described in the section 5.5. The first step is to consider the discretized system, by imposing a certain sampling time and a zero order hold technique.

Good performances are met with a time of $T_s = 3ms$. The resulting discrete system is:

$$A_d = \begin{bmatrix} 1 & 1.589 * 10^{-5} & 3.941 * 10^{-5} & 0 & 0 & 0 \\ 0 & -1.034 * 10^{-5} & -7.827 * 10^{-5} & 0 & 0 & 0 \\ 0 & 7.827 * 10^{-5} & -1.034 * 10^{-5} & 0 & 0 & 0 \\ 0 & 0 & 0 & 0.9727 & 1.542 * 10^{-5} & 3.837 * 10^{-5} \\ 0 & 0 & 0 & 0 & -1.034 * 10^{-5} & -7.827 * 10^{-5} \\ 0 & 0 & 0 & 0 & 7.827 * 10^{-5} & -1.034 * 10^{-5} \end{bmatrix} \quad (85)$$

$$B_d = \begin{bmatrix} 1.051 * 10^{-5} \\ 0.01009 \\ 0.004067 \\ 2.074 * 10^{-5} \\ 0.02018 \\ 0.008134 \end{bmatrix} \quad (86)$$

$$C_d = \begin{bmatrix} 8.32 & 0 & 0 & 0 & 0 & 0 \\ 0 & 0 & 0 & 10.4 & 0 & 0 \end{bmatrix} \quad (87)$$

Unlike the approach adopted for the mechanical system, it is decided to apply the Kalman filter version of the MPC, due to the fact the system under exam is more complex than the previous case. In order to do so, it is necessary to introduce two covariance matrices:

- $W = eye(n)$, that means W is a square identity matrix whose size is equal to the number of states of the considered system;
- $V = [1 \ 0; 0 \ 1]$, that means V is a square matrix where, on the diagonal, it considers the covariance weights applied to the considered outputs.

As described in the section 5.5, MPC allows to impose hard constraints on the input. That means the designed controller, if feasible, is such that the input always respects this constraint, even falling in a saturation zone.

In order to impose an output limited in the range $[-24V, 24V]$, two parameters are set:

- $u_{max} = 24$;
- $u_{min} = -24$

As this case adopts the Kalman filter version, it is mandatory to impose the parameter $C_{mode} = 2$. Finally, a trial and error approach is considered to choose the weighting matrices R , acting on the inputs, and Q , acting on the states.

Good performances are reached by means of these matrices:

$$Q = \begin{bmatrix} 40 & 0 \\ 0 & 2 \end{bmatrix} \quad (88)$$

$$R = 0.3 \quad (89)$$

The other parameters are the same as the ones reported in the chapter 5.5. The considered MPC scheme in the Simulink environment is reported in Figure 134:

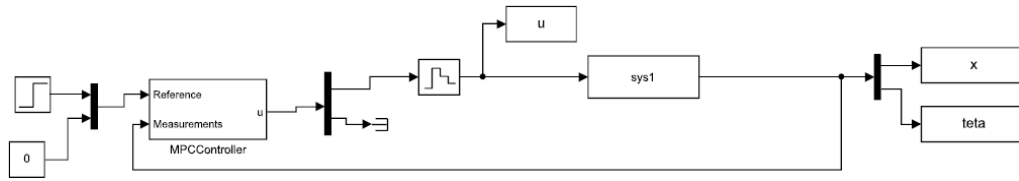


Figure 134: BMPC scheme of the electromechanical system

7 Pneumatic model

The pneumatic circuit in exam is modelled by considering the air as perfect gas and only isotherm transformation. The cylinder is controlled by means of four 2/2 valves; two of them needed for the extension of the cylinder, the remaining ones for the retraction. The complete linear model is studied in the details in [10].

The linear Simulink model of the pneumatic actuator is reported in Figure 135:

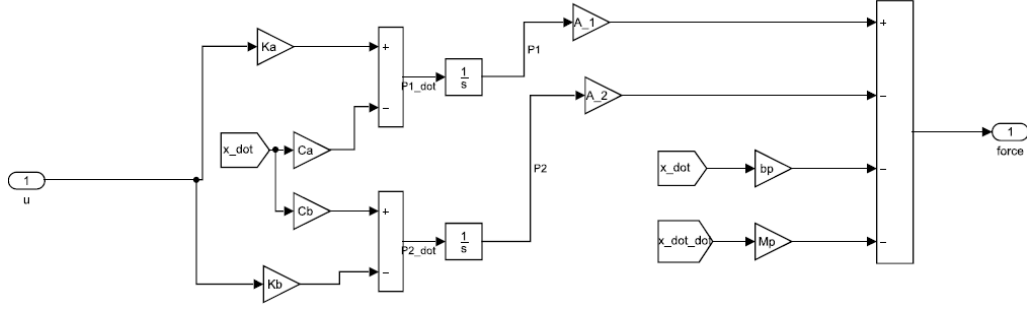


Figure 135: Linear model of the pneumatic actuator

By connecting this model to the one of the pendulum and cart reported in Figure 69, it is possible to obtain the complete model of the system in exam.

As for the electro-mechanical case, the transfer functions needed for the design of the cascade and parallel PIDs are found through the "Model linearizer" tool in Simulink.

The resulting transfer functions are:

$$\begin{cases} G_{xu}(s) = \frac{257.52}{s(s^2 + 11.19s + 131.9)} \\ G_{\theta u}(s) = \frac{-321.9}{(s + 0.4688)(s^2 + 11.19s + 131.9)} \\ G_{x\theta}(s) = \frac{-0.8(s + 0.4688)}{s} \end{cases} \quad (90)$$

whose Bode diagrams are reported, respectively, in Figures 136, 137 and 138:

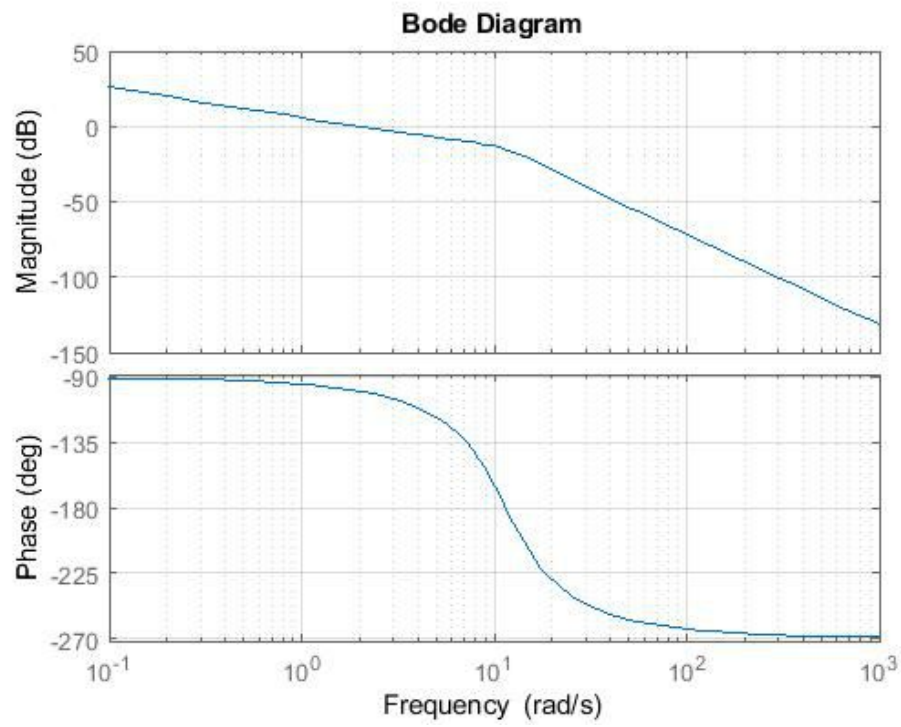


Figure 136: Bode diagram of G_{xu}

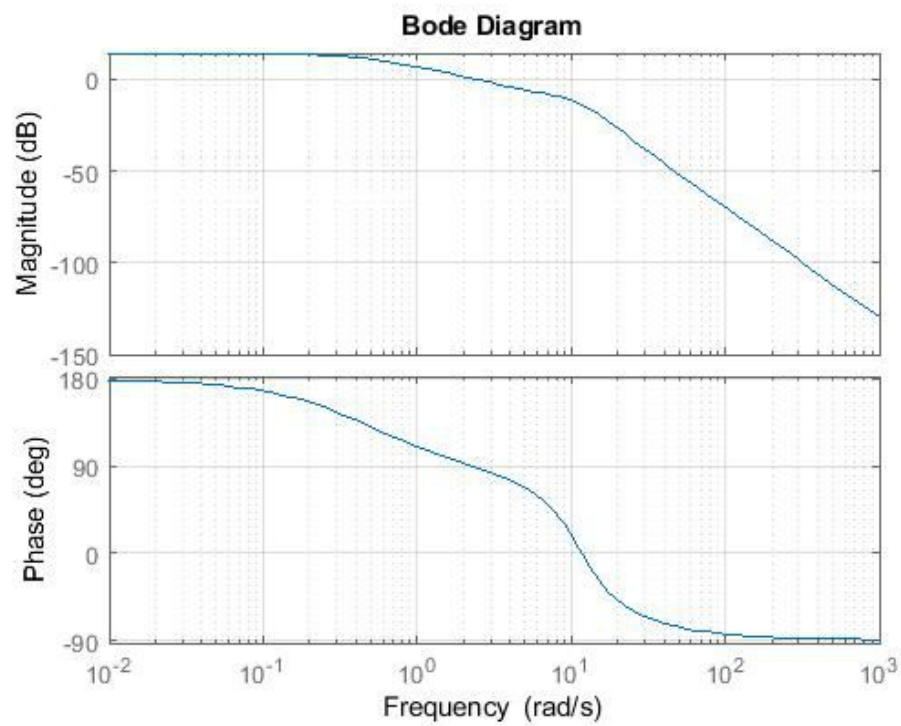


Figure 137: Bode diagram of $G_{\theta u}$

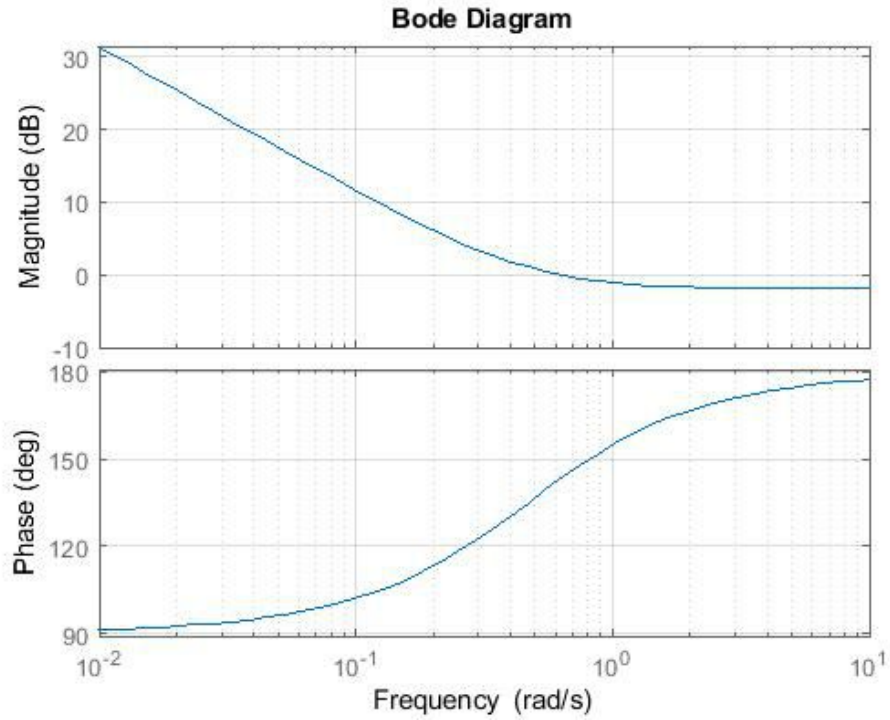


Figure 138: Bode diagram of $G_{x\theta}$

7.1 Cascade PID

The complete cascade linear scheme is shown in Figure 139:

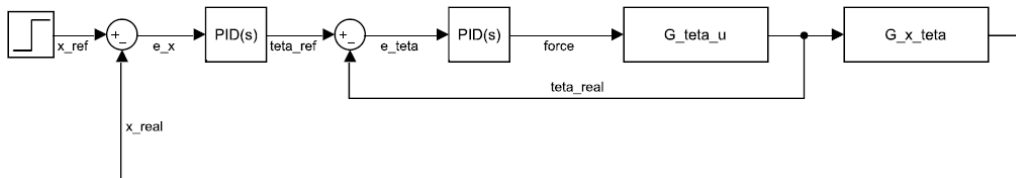


Figure 139: Linear cascade scheme of the pneumatic system

The logic behind this scheme is the same as the one described in all the other cases. The first step, in fact, is to design the inner-loop controller. If it is imposed equal to 1, it can be noticed the open-loop function of the inner loop, defined by $G_{\theta u}$, does not stabilize the inner closed-loop function, as demonstrated in its Nyquist plot in Figure 140:

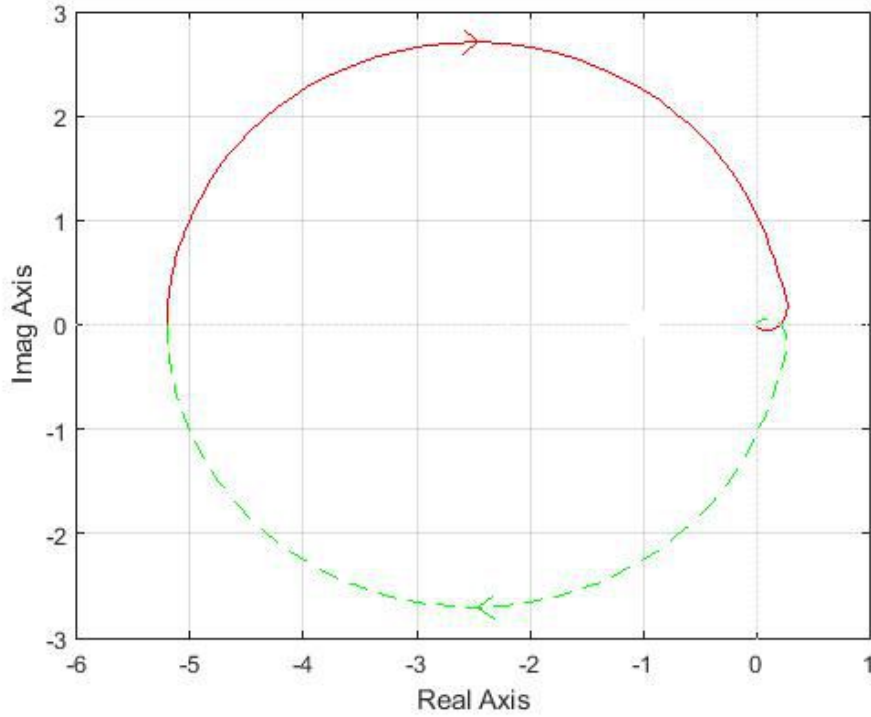


Figure 140: Nyquist plot of $G_{\theta}u$

By using the autotuning function in Simulink, it is found a stabilizing PID, whose transfer function is:

$$C_{\theta}(s) = \frac{-2.5275(s + 1.573 * 10^4)(s + 0.2569)}{s(s + 748.9)} \quad (91)$$

The new open-loop transfer function becomes:

$$Gol_{\theta}(s) = \frac{813.59(s + 1.573 * 10^4)(s + 0.2569)}{s(s + 748.9)(s + 0.4688)(s^2 + 11.19s + 131.9)} \quad (92)$$

This new transfer function can now stabilize the closed-loop system, as shown in its Nyquist plot in Figure 141:

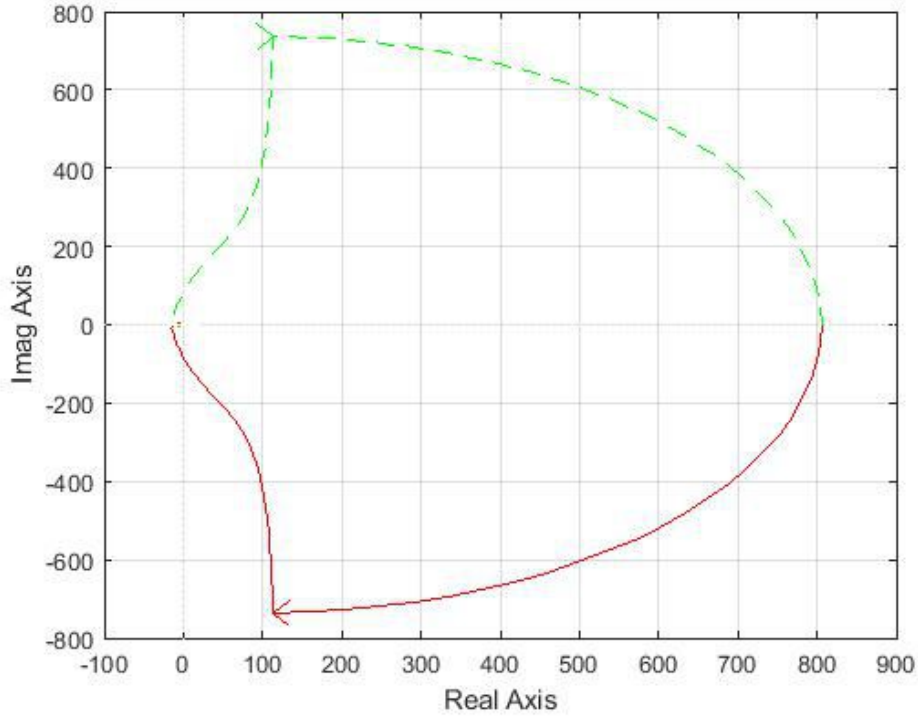


Figure 141: Nyquist plot of $G_{ol\theta}$

Stability is reached as there is no encirclement of the unstable point $(-1,j0)$ anymore. Next step is to stabilize the outer loop. By considering the simple case of unitary outer PID, the open-loop transfer function is given by:

$$G_{olx}(s) = \frac{-650.87(s + 1.573 * 10^4)(s + 0.4688)}{s(s + 748.6)(s + 28.52)(s^2 - 17.09s + 600.1)} \quad (93)$$

whose Nyquist plot is reported in Figure 142:

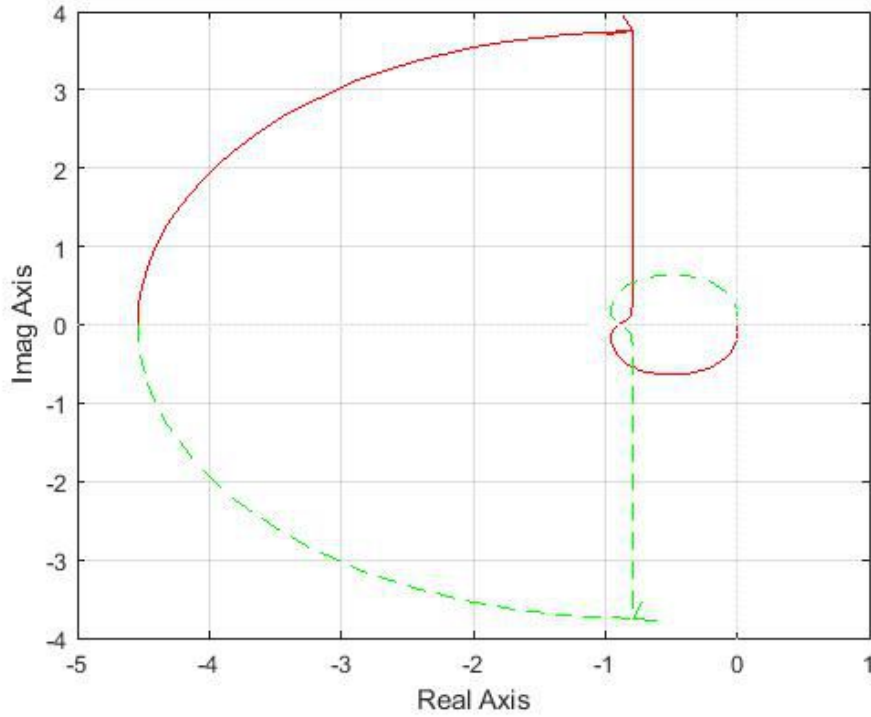


Figure 142: Nyquist plot of G_{olx}

The open-loop function presents two unstable poles to neutralize which, two encirclements around the unstable points are needed. By adopting the usual autotuning function, it is possible to get a stabilizing PID, whose transfer function is:

$$C_x(s) = \frac{-3.5527 * 10^{-15} * (s + 1.695 * 10^{14})(s + 0.08893)}{s(s + 0.485)} \quad (94)$$

The new open-loop transfer function becomes:

$$G_{olx}(s) = \frac{2.3124 * 10^{-12}(s + 1.695 * 10^{14})(s + 1.573 * 10^4)(s + 0.4688)(s + 0.08893)}{s^2(s + 0.485)(s + 28.52)(s + 748.9)(s^2 - 17.09s + 600.1)} \quad (95)$$

This new open-loop transfer function now can stabilize the overall closed-loop system, as shown in its Nyquist diagram in Figure 143:

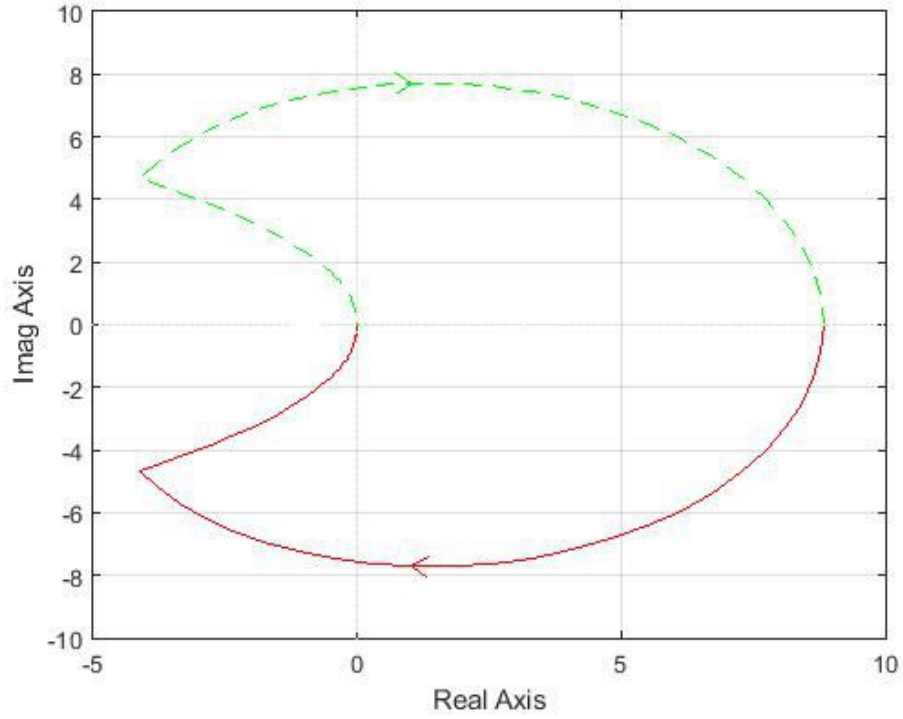


Figure 143: Nyquist plot of the final $G_o l x$

The final closed-loop transfer function is given by:

$$G_{clx}(s) = \frac{2.3124 * 10^{-12}(s + 1.695 * 10^{14})(s + 1.573 * 10^4)(s + 0.4688)(s + 0.08893)}{(s + 748.9)(s + 28.36)(s + 0.5345)(s + 0.3126)(s + 0.1205)(s^2 - 17.42s + 601.2)} \quad (96)$$

whose gain and phase margins are shown in the Figure 144:

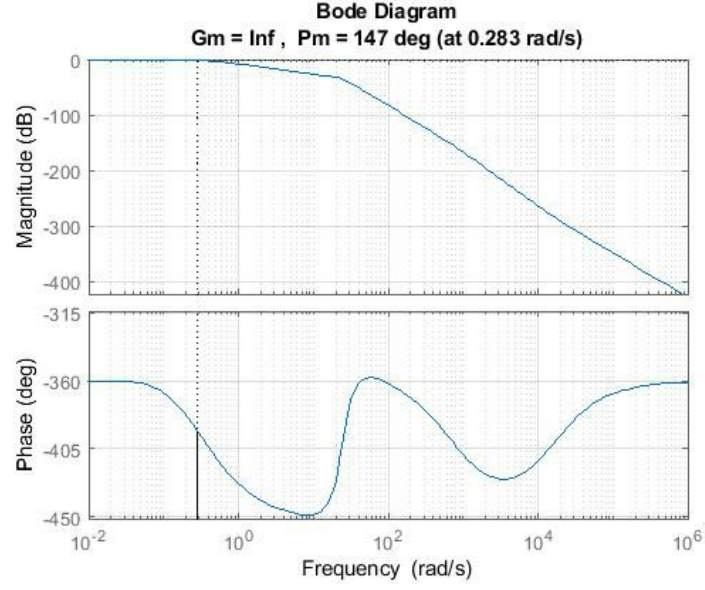


Figure 144: Gain and phase margins of G_{clx}

Next step consists of considering the linear model of the pneumatic motor connected to the non linear model of the pendulum-cart system (Figure 145).

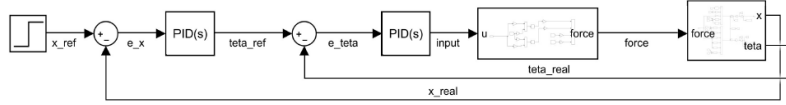


Figure 145: Linear pneumatic motor and nonlinear mechanical system

The PIDs previously designed are no longer able to stabilize such a system, as it is now much more complex. New stabilizing PIDs are found through the autotuning approach:

$$PID_{\theta}(s) = \frac{-53.067(s + 29.37)(s + 6.553)}{s(s + 748.9)} \quad (97)$$

$$PID_x(s) = \frac{0.19876(s + 0.07372)(s + 0.05869)}{s(s + 748.9)} \quad (98)$$

The complete nonlinear system, included the nonlinear model of the pneumatic motor, is considered in the Simscape environment, in the section 8. Next step is to show the simulation of the non-linear overall system, by considering the usual three initial conditions.

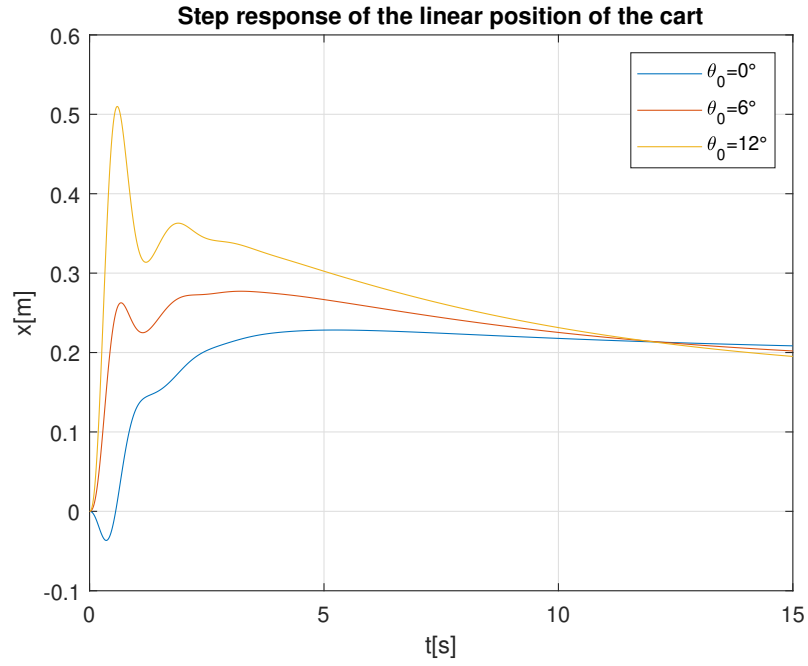


Figure 146: Step response of the linear position of the cart in the cascade architecture and pneumatic system

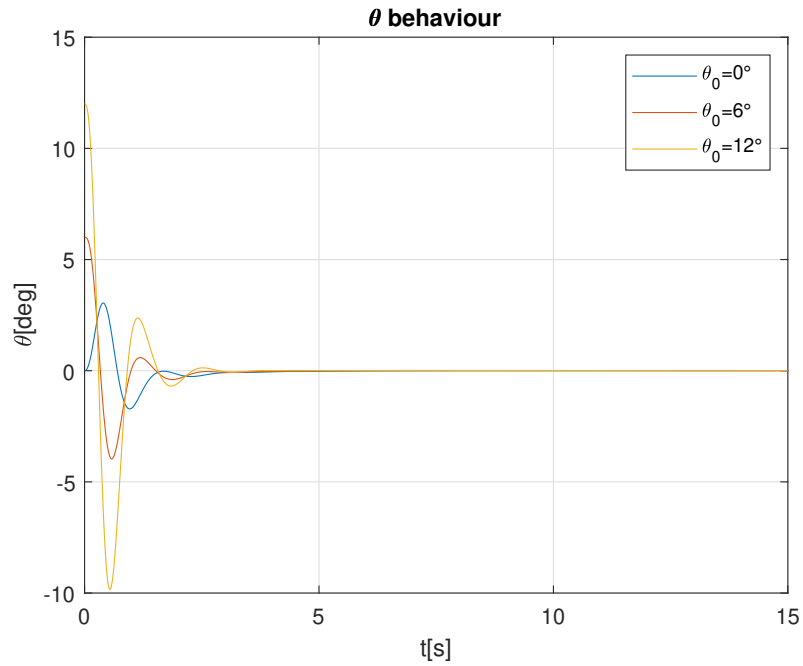


Figure 147: Behaviour of the angle of the pendulum in the cascade architecture and pneumatic system

The Figure 146 shows the step response of the linear position of the cart. After a small undershoot, by considering the null initial condition, the cart touches the setpoint for the

first time in 2.5s, it presents an overshoot of about 25% and it extinguishes slowly, by taking about 12s. By increasing the initial condition, the rise time reduces drastically, but the overshoot becomes bigger and bigger.

The Figure 147, instead, shows that the angle of the pendulum always goes to zero very quickly, in about 3s. A growth of the initial condition simply increases the value of the starting undershoot.

7.2 Parallel PID

As performed previously, next step consists of designing the PID controller in a parallel fashion, first applied to the complete linear model. The complete treatment of the design of Parallel PID is now avoided as it is the same as the one explained previously. The first step consists of designing both the inner and the outer PIDs in the linearized case. As regard the PID acting on the angle, it is the same as the one designed in the cascade scheme. The final outer PID, instead, is obtained through the usage of the autotuning tool in Simulink, by getting:

$$PID_x(s) = \frac{-3.5527 * 10^{-15}(s + 1.695 * 10^{14})(s + 0.08893)}{s(s + 0.485)} \quad (99)$$

The same approach is followed for the non-linear system. First of all, it is designed the PID acting on theta, by using the autotuning approach. The final result is given by:

$$PID_\theta(s) = \frac{-14.557(s + 84.27)(s + 2.556)}{s(s + 472.5)} \quad (100)$$

Once this controlled is obtained, the final step is to design the one acting on the linear position of the cart:

$$PID_x(s) = \frac{-0.658(s + 0.3718)(s + 0.1685)}{s(s + 2.723)} \quad (101)$$

Next step is to provide the simulation of the non-linear system in the parallel architecture, by taking into account the step response of the linear position of the cart and the behaviour of the angle of the pendulum.

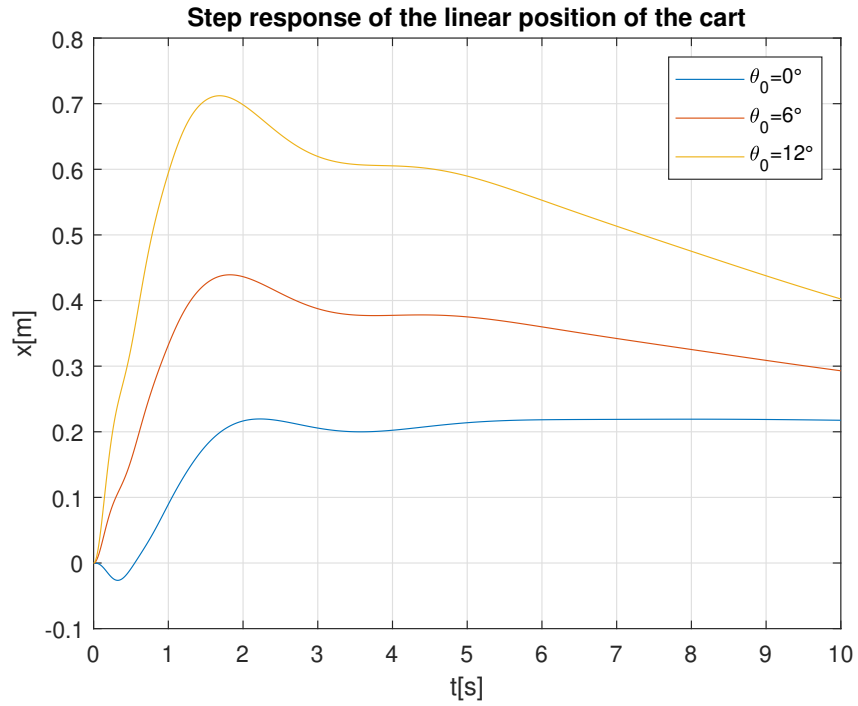


Figure 148: Step response of the linear position of the cart in the parallel architecture and pneumatic system

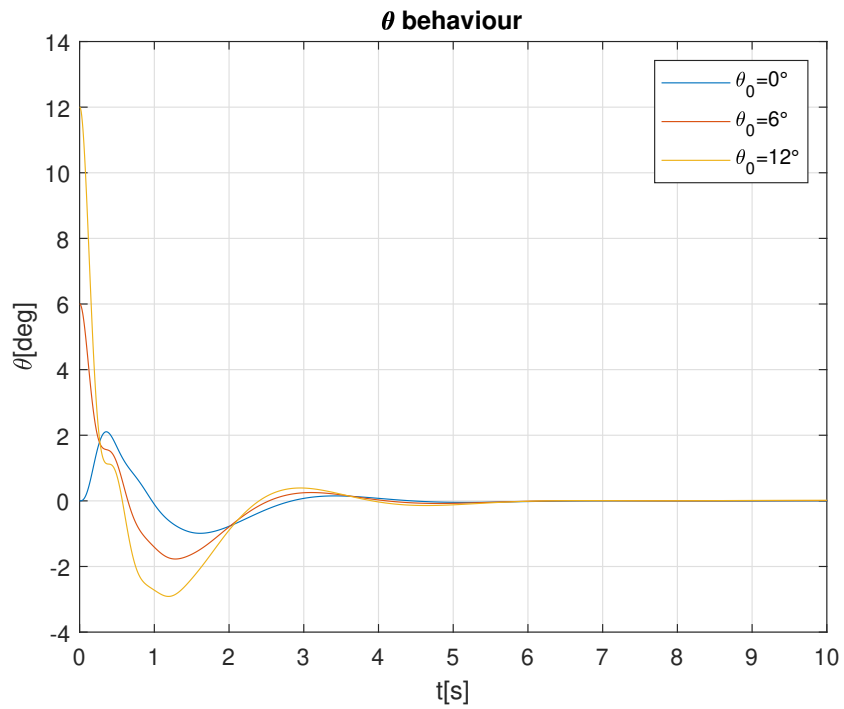


Figure 149: Behaviour of the angle of the pendulum in the parallel architecture and pneumatic system

The Figure 148 shows that, by considering a null initial condition, the response presents a rising time of about $1.83s$, a small overshoot of about 10% and it extinguishes practically in about $4s$. The behaviour of the position of the cart get worse by considering higher initial conditions. In particular, the rising time reduces drastically, but the overshoot becomes bigger and bigger. The time it takes to reach definitely the setpoint grows a lot too. The Figure 149, instead, demonstrates the angulum of the pendulum is brought to zero quite quickly, in about $3s$. The increase of the initial condition only cause a growth of the undershoot.

7.3 MPC

As the treatment of the MPC approach is already handled previously, it is now avoided. By considering a sampling time of $T_s = 0.01s$, the obtained discrete time system is given by:

$$A_d = \begin{bmatrix} 1 & 0.003066 & 0.0001525 & 0 & 0 & 0 \\ 0 & 0.9408 & 0.0947 & 0 & 0 & 0 \\ 0 & -0.0947 & 0.9408 & 0 & 0 & 0 \\ 0 & 0 & 0 & 0.9953 & 0.003058 & 0.0001522 \\ 0 & 0 & 0 & 0 & 0.9408 & 0.0947 \\ 0 & 0 & 0 & 0 & -0.0947 & 0.9408 \end{bmatrix} \quad (102)$$

$$B_d = \begin{bmatrix} 5.184 * 10^{-6} \\ 0.004878 \\ 0.0981 \\ 5.178 * 10^{-6} \\ 0.004878 \\ 0.0981 \end{bmatrix} \quad (103)$$

$$C_d = \begin{bmatrix} 8.047 & 0 & 0 & 0 & 0 & 0 \\ 0 & 0 & 0 & -10.06 & 0 & 0 \end{bmatrix} \quad (104)$$

$$D_d = 0 \quad (105)$$

The crucial point consists of choosing in the proper way the Q and R matrices. By giving more importance to the angle, it is not possible to get a stabilized system that allows the pendulum to stay in the vertical position and the cart in a precise point. It is necessary to act more on the linear position. In particular, a good result is obtained by choosing:

$$Q = \begin{bmatrix} 120 & 0 \\ 0 & 2 \end{bmatrix} \quad (106)$$

$$R = 0.1 \quad (107)$$

This choice is very powerful for the position of the cart, while it is not so good as regard the angle of the pendulum, but at least the desired requirements are met.

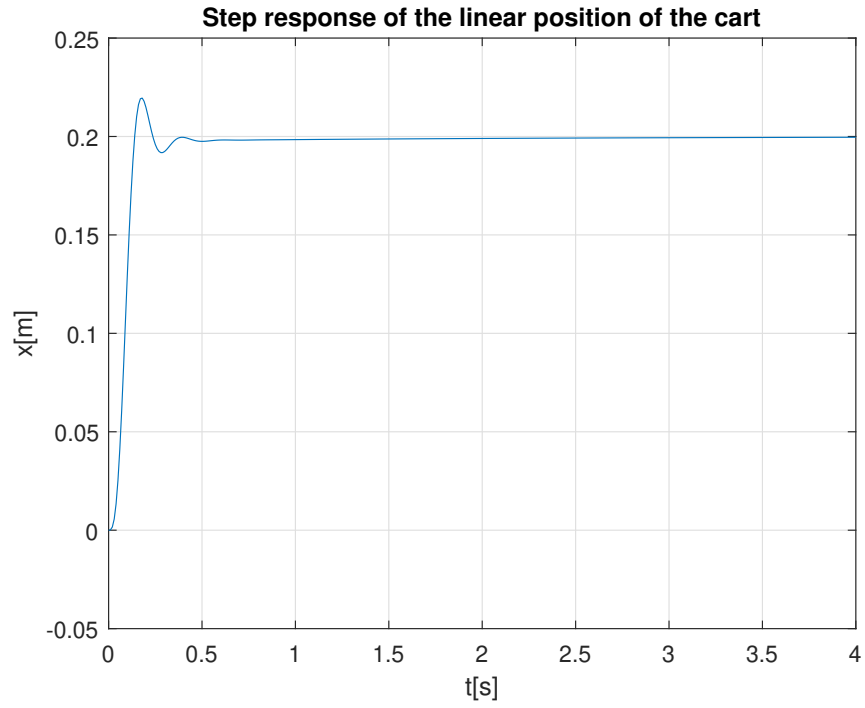


Figure 150: Step response of the linear position of the cart in the MPC architecture and pneumatic system

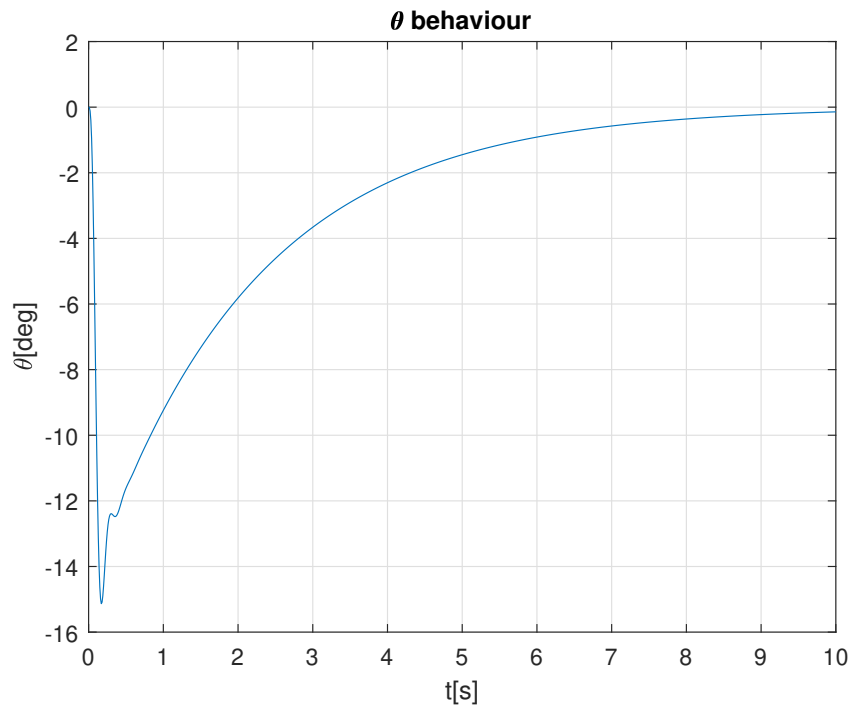


Figure 151: Behaviour of the angle of the pendulum in the MPC and pneumatic system

The Figure 150 shows that the cart reaches the setpoint very quickly, in about $0.2s$, it presents an overshoot of about 20% and it extinguishes in less then $0.5s$. The Figure 151, instead, reports the angle behaviour and it is evident that it presents a strong undershoot, by reaching almost -16° , and it goes to zero slowly, in about $10s$.

8 Simscape

Simscape (Figure 152) is an extension of the Simulink environment that allows to model physical systems. Several systems can be modeled such as DC motors, bridge rectifiers, hydraulic and gas actuators.

The main characteristic of Simscape is linked to the possibility of building models by assembling fundamental components into schematics. So, they are based on physical connections.



Figure 152: Simscape logo

Once the model has been created, Simscape determines automatically the equation that characterizes that system. It is easier than representing it on Simulink directly, because it obliges the usage of the equations of the system in order to create a model. An example is given by the differential equation of a RLC series circuit:

$$\frac{d^2V}{dt^2} = \frac{E_0 - RC \frac{dV}{dt} - V}{LC}$$

Figure 153: RLC equation

By using Simulink, the system must be modelled by means of mathematical blocks as sum, integrators, gains and step signal. The complete model is shown in Figure 154:

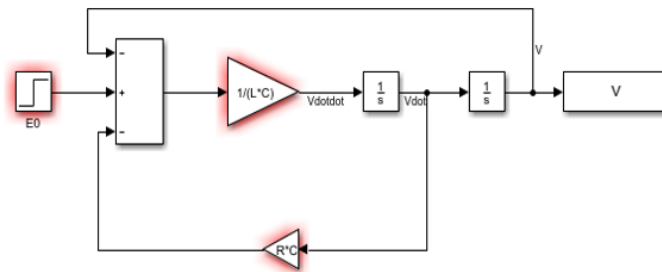


Figure 154: RLC model in Simulink

By using Simscape, the circuit is modelled through physical components like resistor, inductor, capacitor, voltage supply. The voltage on the inductor is then evaluated by means of a voltage sensor. The complete model is shown in Figure 155:

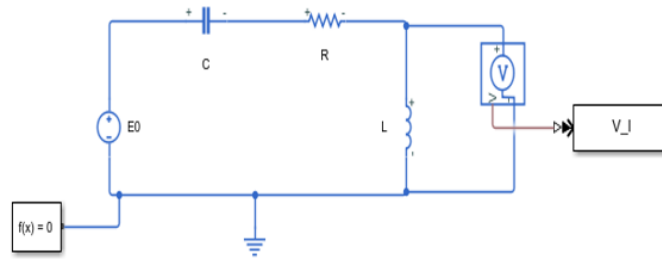


Figure 155: RLC model in Simscape

The advantage of using Simscape is particularly evident when the equations representing a system are hard to implement with Simulink and when an extension of the model is needed. In Simulink, the equation should be repeated and this may lead to a complex approach. In Simscape, the model can be extended by easily copying and pasting the components associated to the single piece.

Simscape offers a set of fundamental components in several physical domains:

- Electrical
- Mechanical
- Hydraulic
- Thermal
- Thermal liquid
- Two-phase gas
- Gas
- Moist air

Finally, all the models can be integrated with 3D mechanical systems in order to analyze their behaviour with an animation resulting from simulation. Such models can be also converted into C-code (by means of «Build model»). This is useful for testing softwares and configurations such as Processor-in-the-loop (PIL) and Hardware-in-the-loop (HIL) (Figure 156).

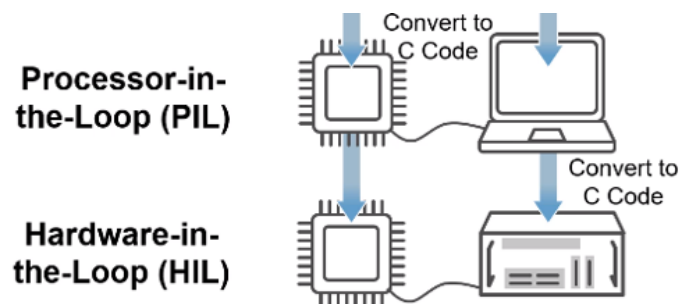


Figure 156: Scheme of HIL and PIL

8.1 Pneumatic actuator model in Simscape

As reported in the chapter 7, the pneumatic actuator is made up of double acting cylinder, regulated by means of four 2/2 valves. The complete Simscape model is reported in Figure 157:

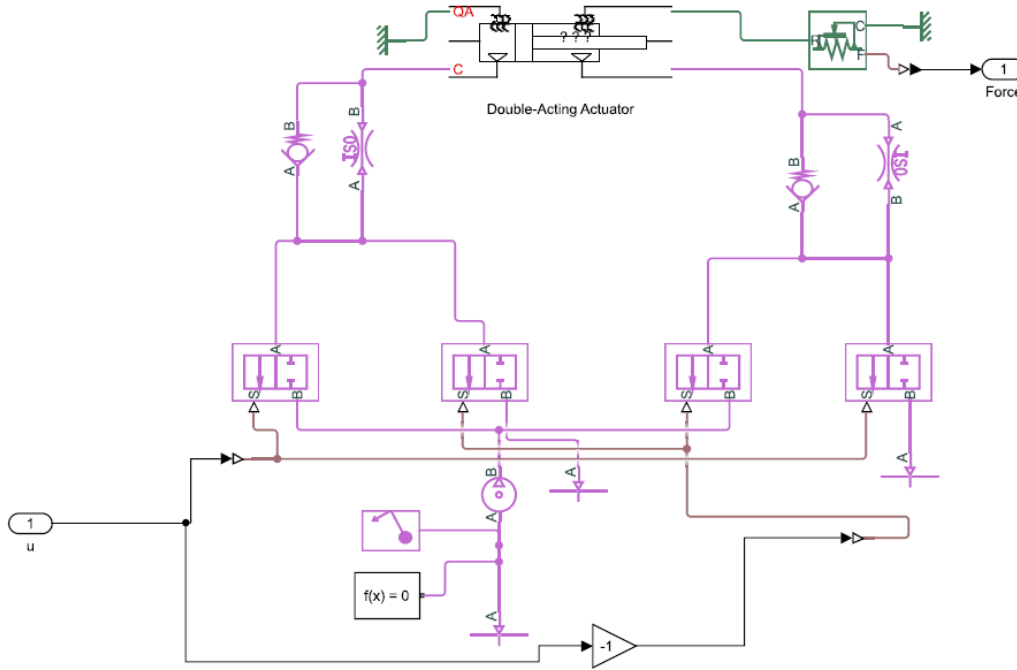


Figure 157: Complete Simscape model of the pneumatic actuator

By analyzing the elements constituting the overall model, it is possible to highlight the single the main features of the single components. First of all, the image of a 2/2 pneumatic valve is shown in Figure 158:

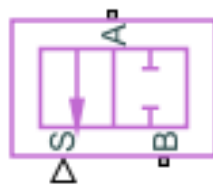


Figure 158: 2-way directional valve in Simscape

S is the control port. When the signal entering S is positive, the port A is connected to the port B, otherwise they are disconnected. As shown in Figure 157, when the signal is positive the valve on the left and the one on the right are activated, by causing the extension of the cylinder. The former is fed by a pressure supply, the latter is connected directly to a reservoir, for the discharge of the air. When the signal is negative, the two central valves are switched on, by causing the retraction of the cylinder. Their working mode is the same as the before.

The Figure 159 reports the pressure supply, the reservoir and the solver configuration blocks:

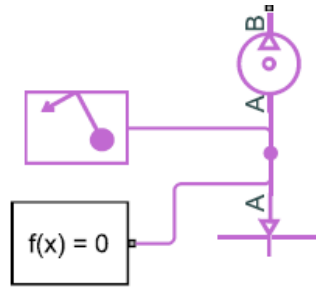


Figure 159: Pressure source-reservoir-solver configuration-gas properties blocks

In particular, the "pressure source" block can maintain a constant pressure; a positive pressure differential leads to a pressure at port B greater than the one at port A.

The "reservoir", instead, sets constant boundary conditions in a gas network.

The "solver configuration" block is necessary for Simscape models. It is not a physical part in the whole system but it requires solver setting information for simulation. Each independent system needs such a block. The "Gas properties" block provides gas properties to the connected gas network. The gas is modeled as perfect, semiperfect, or real. The ideal gas law applies to perfect and semiperfect gas. For semiperfect gas, caloric and transport properties are functions to temperature.

The signal coming from Simulink and feeding the S port of the valves, cannot act directly on them, as it is not a physical signal. It is so mandatory to use a "Simulink-PS converter" in order to turn such a signal into a physical one.

The port A, corresponding to the output of the valves, is connected to a "check valve" and a "Orifice ISO 6358", that are shown in Figure 160:

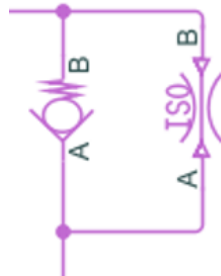


Figure 160: Check valve and orifice

The former allows the gas to move from A to B, while it is blocked from B to A. The latter can be used as C_v coefficient, K_v coefficient, sonic conductance and, like in this case, as restriction area. When the cylinder extends, the gas leaving the left 2/2 valve passes through the check valve, without finding resistance. While the cylinder is moving, the air coming from the right chamber is discharged, moving through the right valve, and passing the restriction that slows it down. The same happens with the retraction of the cylinder. The model of a real "double-acting actuator" is provided by Mathworks itself, by writing in the command window of Matlab "*ssc-pneumatic.actuator*". It is shown in Figure 161:

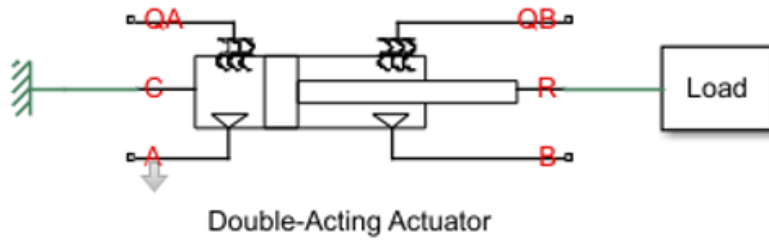


Figure 161: Double-acting actuator model in Simscape

Ports A and B receive pressure from the left and the right 2/2 valves respectively. Ports QA and QB model heat exchanges inside the two chambers. In this case the thermal part is neglected. Ports C and R are mechanical ports. C is connected to a “mechanical translational reference”, while port R to a “Load” subsystem. In this case, the load represents the force that is applied to the cart in order to move it.

By looking inside the cylinder mask (CTRL+U), the expanded model of the pneumatic actuator is shown (Figure 162):

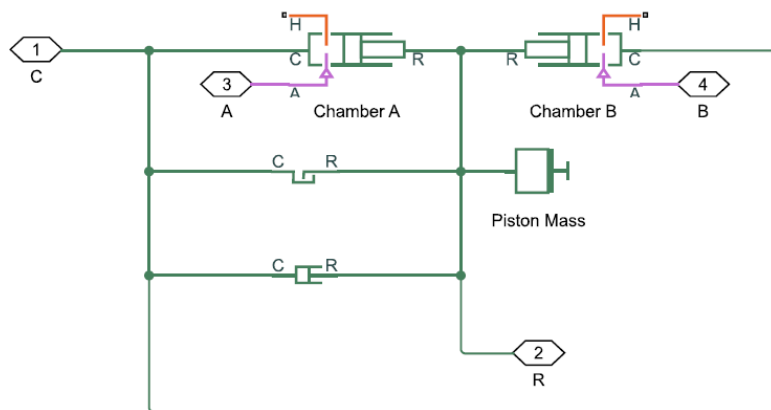


Figure 162: Complete pneumatic actuator model

The two chambers are modelled by means of two “Translational mechanical converters” that represent an interface between a gas network and a mechanical translational network. The left one is oriented positive, the right one negative standing for extension and retraction. A real piston is modelled by mean of a “Mass”, a “Translational Damper” and a “Translational Hard Stop” that limits the motion of a body between upper and lower bounds. thermal part is neglected.

Finally, the force the cylinder develops and that is applied to the cart, has to be taken by means of a force sensor (Figure 163), as it is a physical quantity.

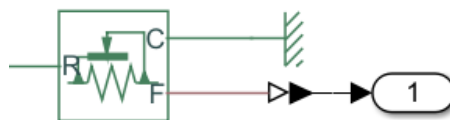


Figure 163: Ideal force sensor

Connections R and C are mechanical translational conserving ports that connect the sensor to the line whose force is being monitored. Connection F is a physical signal port that outputs the measurement result. The sensor positive direction is from port R to port C. The signal coming from the F port is physical and so it cannot be applied directly in Simulink. It needs to be converted by means of a "PS-Simulink converter", by imposing as unit of measure N, corresponding to Newton.

8.2 Electric motor in Simscape

The considered electric motor is brushless DC. The overall model of such a motor in the Simscape environment is reported in Figure 164:

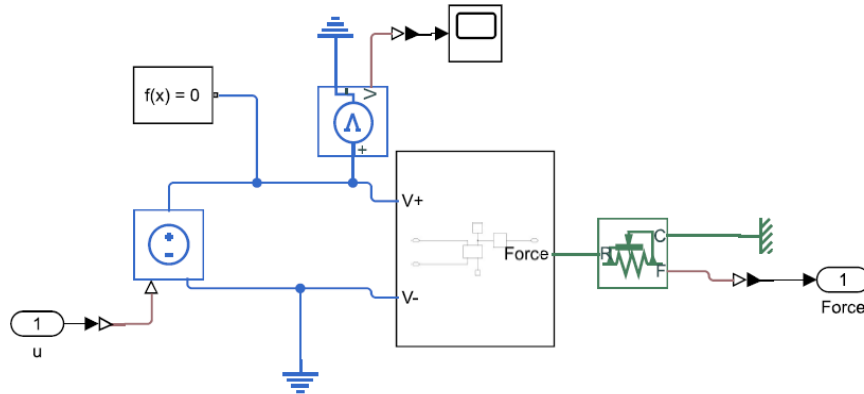


Figure 164: Complete model of the electric motor in Simscape

As the pneumatic case, the "solver configuration" block is mandatory, as the model embraces physical quantities. The electric motor is fed by a "controlled voltage source", that produces a voltage depending on the control signal coming from the controllers designed in the Simulink environment. It is referred to ground by means of an "electrical reference block". As all physical quantities, the voltage can be measured through a sensor, that is the "Voltage sensor" block. The positive voltage enters the subsystem in the $V+$ point, while the $V-$ is connected to ground. The output of the subsystem is the force that is applied to the cart, in order to keep the pendulum in equilibrium in its vertical position. It is measured by means of an "Ideal force sensor".

The subsystem contains the model of the motor and the screw block that converts the rotational motion into a translational one, as shown in Figure 165:

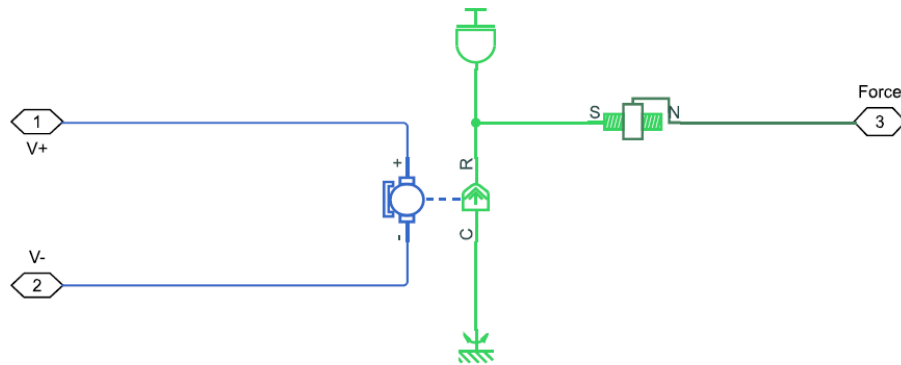


Figure 165: Model of the motor and screw

The motor can be modelled by means of the "DC motor" block. The positive pin is connected to the positive voltage produced by the "controlled voltage source", the negative pin is linked instead to ground. It is possible to set all the parameters of the motor, as the armature resistance, by double clicking the motor block.

It is made up of two parts, an electrical one (in blue) and a rotational one (in green). By considering the rotational part, the C port is referred to ground through a "Mechanical rotational reference" block, the R port is connected to both an "Inertia" block, that represents the inertia of the motor, and to a "Leadscrew" block. It represents a leadscrew that converts rotational motion into translational motion and vice versa. Connection S is the mechanical rotational conserving port corresponding to the screw. Connection N is the mechanical translational conserving port corresponding to the nut. The nut moves in positive direction if a right-hand screw is rotated in positive direction.

8.3 Simscape Multibody and model of the pendulum and cart

Simscape multibody provides a multibody simulation environment for 3D mechanical systems such as robots, vehicle suspensions and construction equipment. These systems can be modelled by assembling blocks representing bodies, joints and force elements into schematics.

The shape of the model can be created by fundamental solid shapes as cylinders, spheres, bricks, ellipsoids and so on.

The main feature of Multibody is its capability to communicate with CAD softwares, such as Solidworks (Figure 166). In fact, it is possible to export a CAD model into the Matlab environment first. Successively, if the model is not too complex and made up of too many pieces, it is converted into a Simscape Multibody model in a proper way, by using the elements present in library.

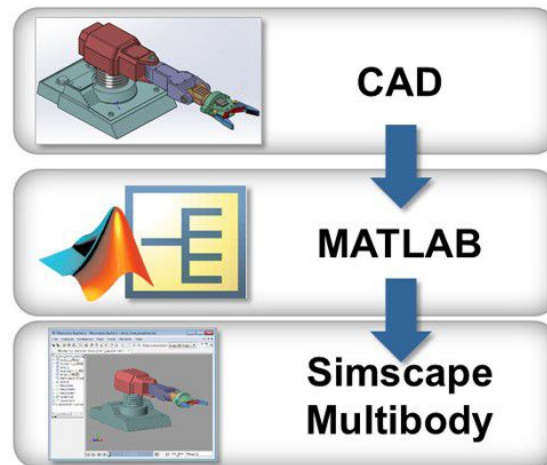


Figure 166: From CAD to Multibody

In order to design a model in the Multibody environment it needs to follow some crucial points.

- Identify degrees of freedom. The aim of this initial part is to analyze the system and how its parts move each other. An example is shown in Figure 167:

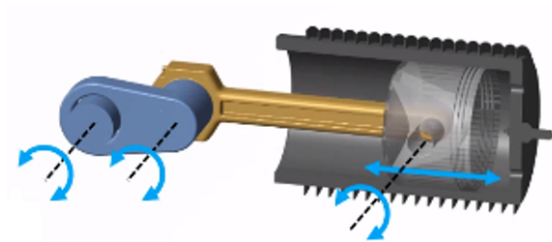


Figure 167: Example of identification of DOF

In this case the system is made up of three rotating parts and a translating one. This info is important in order to collect joints and constraints to model the system.

- Connect ports with joints and constraints. It is possible to use revolute joints for rotational degrees of freedom and prismatic joints for translational degrees of freedom. An example is shown in Figure 168:

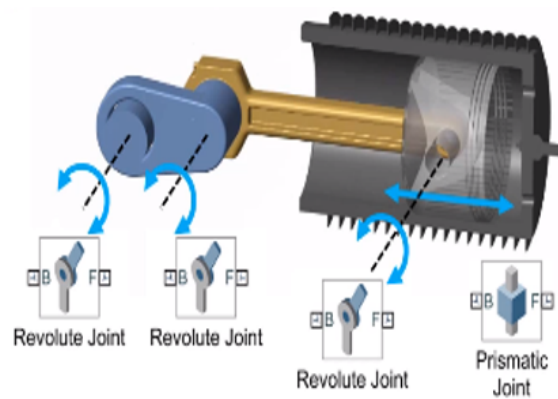


Figure 168: Example of identification of joints and constraints

- Specify initial conditions and velocities with joint targets. In complex mechanisms, sometimes, the exact position of components in the system is known; others it may be difficult to identify.

The initial extension of the actuator in Figure 169, for instance, depends on a lot of design factors. Multibody helps finding initial conditions. Generally, for known values, we can set priority to high otherwise priority can be set to low.

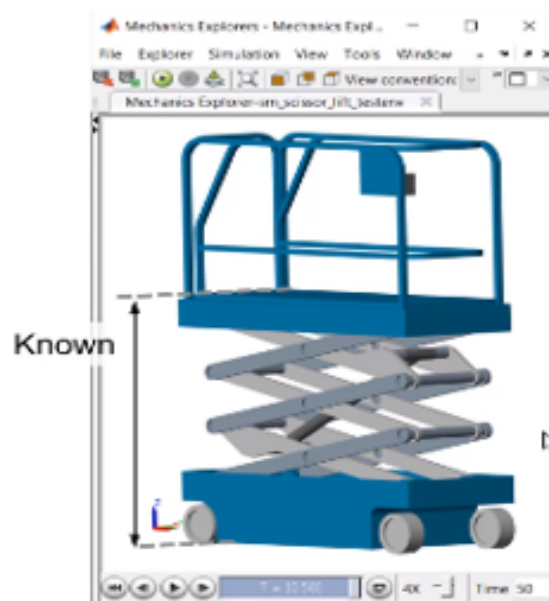


Figure 169: Example of identification of initial condition on a model

- Actuate joints. It is possible either to specify forces and torques to be applied to the actuator or describe the motion. Actuation systems can be also modelled with hydraulic mechanisms, electric actuation or other physical domain.

The most important blocks that can be adopted to crate a Multibody model are reported in the following list:

- Solver configuration (Figure 170)

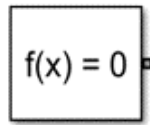


Figure 170: Solver configuration block

Each physical network represented by a connected Simscape block diagram requires solver settings information for simulation. The Solver Configuration block specifies the solver parameters that your model needs before beginning simulation.

- World frame (Figure 171)



Figure 171: World frame block

This block represents the global reference frame in a model. This frame is inertial and at absolute rest. Rigidly connecting a frame to the World frame makes that frame inertial. Frame axes are orthogonal and arranged according to the right-hand rule.

- Mechanism configuration (Figure 172)



Figure 172: Mechanism configuration block

This block provides mechanical and simulation parameters to a mechanism. Parameters include gravity and a linearization delta for computing numerical partial derivatives during linearization. These parameters apply only to the target mechanism, i.e., the mechanism that the block connects to.

- Solid (Figure 173)



Figure 173: Solid block

The Solid block adds to the attached frame a solid element with geometry, inertia, and color. The solid element can be a simple rigid body or part of a compound rigid body, a group of rigidly connected solids, often separated in space through rigid transformations.

- Rigid transform (Figure 174)

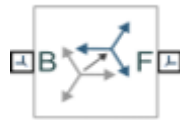


Figure 174: Rigid transform block

This block applies a time-invariant transformation between two frames. The transformation rotates and translates the follower port frame (F) with respect to the base port frame (B). Connecting the frame ports in reverse causes the transformation itself to reverse. The frames remain fixed with respect to each other during simulation, moving only as a single unit.

- Weld joint (Figure 175)



Figure 175: Weld joint block

This block represents a joint with zero degrees of freedom. It contains no joint primitives. Base and follower frames, both connected to a separate rigid body, are coincident for all time. The block dialog box provides sensing options for constraint and total forces and torques.

- Prismatic joint (Figure 176)



Figure 176: Prismatic joint block

This block represents a joint with one translational degree of freedom. One prismatic primitive provides the translational degree of freedom. The base and follower frames remain parallel during simulation.

- Revolute joint (Figure 177)



Figure 177: Revolute joint block

It represents a revolute joint acting between two frames. This joint has one rotational degree of freedom represented by one revolute primitive. The joint constrains the origins of the two frames to be coincident and the z-axes of the base and follower frames to be coincident, while the follower x-axis and y-axis can rotate around the z-axis.

By using some of these blocks, it is possible to design an easy model of the pendulum on cart. Firstly, it has tried to import the CAD model from Solidworks, but it was so complex and constituted by so many pieces, the resulting model in Simscape presented some errors, very difficult to solve. It is important, in fact, that all possible errors or dysfunctions are solved before creating the Multibody model, as it becomes hard to detect them in such an environment.

The Multibody model of the pendulum on cart is shown in Figure 178:

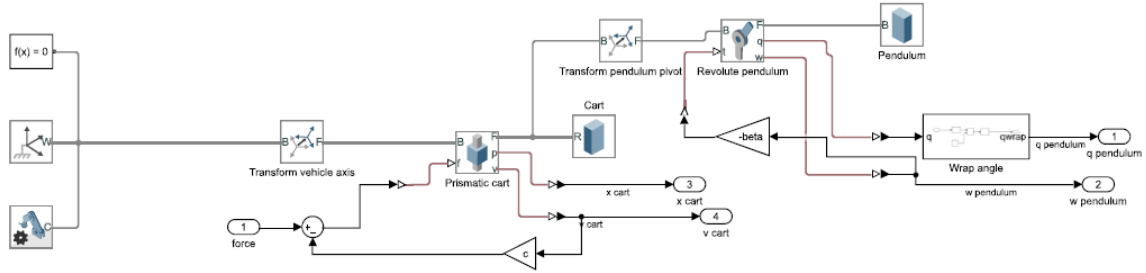


Figure 178: Model of pendulum on cart in Simscape Multibody

As reported previously, the first three elements needed in a Multibody environment are the "Solver configuration" block, the "World frame" block and the "Mechanism configuration" block. The first defines solver settings to use for simulation; the second one provides access to the world or ground frame; the last one is used to impose the value, the direction and the sense of the gravity acceleration. In this case, it is equal to $-9.80665 \frac{m}{s^2}$, by indicating it is orientated downward, along the z-axis.

Then, a "Rigid transform" block is taken into account, in order to make a rotation of 90° in the positive sense around the y-axis. This is necessary to consider the translational motion of the cart along the x-axis. This kind of motion is modelled by means of a "Prismatic joint", attached to a "Solid" block, representing the cart. The joint exploits, apart from

its main ports B and F, three further ports. The "f" port receives as input the force that allows the cart to move and the friction force. The "v" port provides the linear velocity of the cart that is needed to consider the friction force acting on the cart itself. The "p" port is useful for detecting the linear position of the cart, required for the developed control strategies.

Next block is another "Rigid transform" block, that imposes a positive rotation of 90° around the x-axis. In this way it is possible to consider the vertical position of the pendulum in the positive direction of the z-axis. As the pendulum can only rotate around the y-axis, this motion is modelled through a "Revolute joint" block, a "Solid" block representing the pendulum is attached to. The revolute joint presents, like the prismatic joint, besides the usual ports B and F, three further ports. The "t" port receives in input the resistant torque linked to the angular velocity of the pendulum, provided by the port "w", multiplied by the coefficient "beta". The "q" port gives information about the actual angular position of the the pendulum, mandatory for all the considered control strategies.

In order to consider the angle of the pendulum in the vertical unstable position equal to 0° and the angle in its stable position equal to 180° , the "Wrap angle" subsystem has been implemented. Its content is shown in Figure 179:

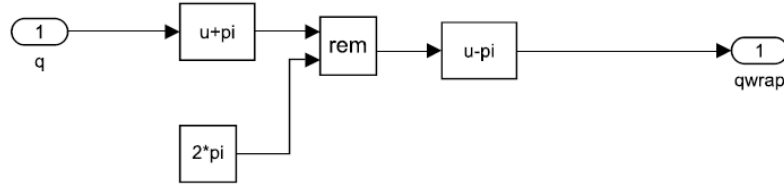


Figure 179: Wrap angle subsystem

The final result of the system pendulum-cart in Simscape Multibody is reported in Figure 180:

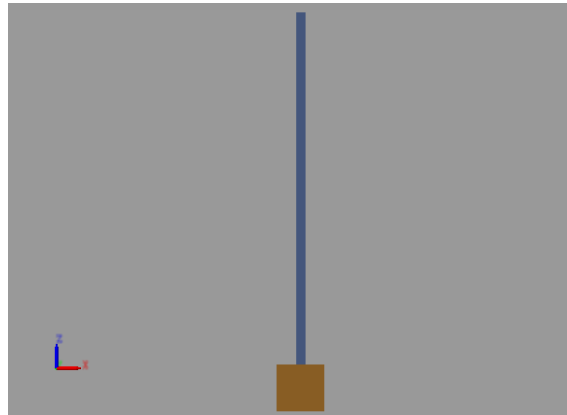


Figure 180: Pendulum-cart representation in Simscape Multibody

8.4 Simulations

This section reports some simulations of the cascade and parallel controller architectures, applied to the Simscape complete non-linear models.

First of all, the electromechanical model is considered. Both the inner and outer PIDs are designed through the autotuning section, as the model is not so complex. The two resulting PIDs, in the cascade architecture, are:

$$PID_{\theta}(S) = \frac{159.74(s + 25.04)(s + 15.88)}{s(s + 9895)} \quad (108)$$

$$PID_x(s) = \frac{-0.54295(s + 0.1433)(s + 0.1189)}{s(s + 4.535)} \quad (109)$$

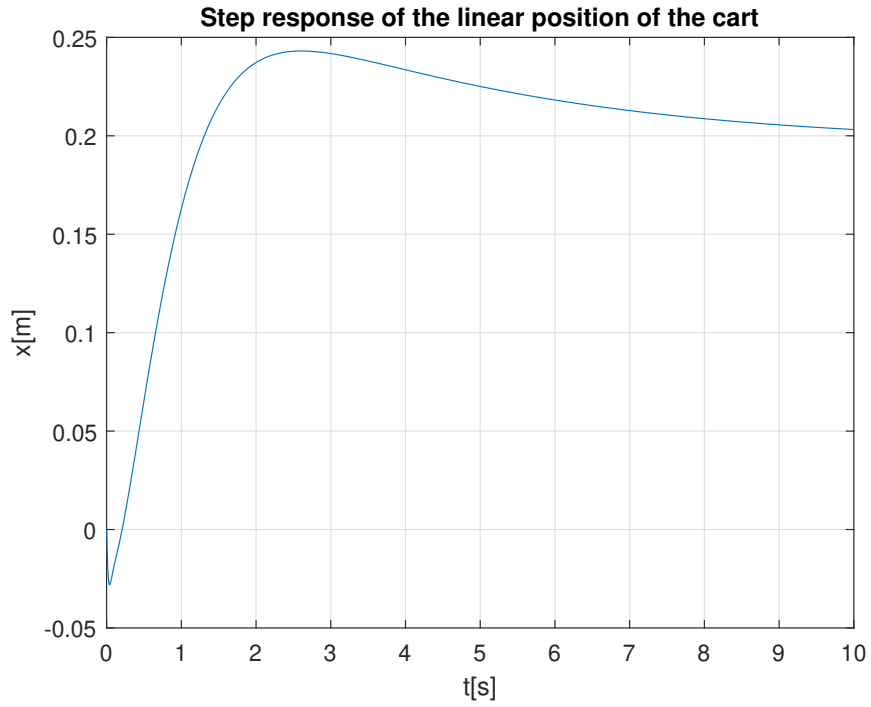


Figure 181: Step response of the linear position of the cart in the cascade architecture and electromechanical Simscape system

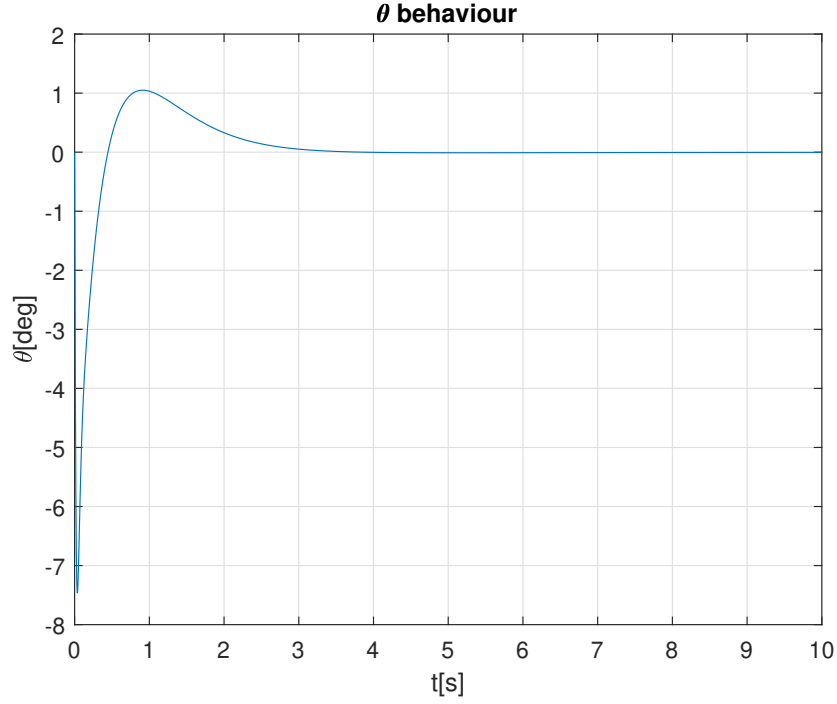


Figure 182: Behaviour of the angle of the pendulum in the cascade and electromechanical Simscape system

The Figure 181 shows that, by considering the only case of null initial condition on the angle, the response presents a rising time of about $1.28s$, an overshoot of about 24.6% and the setpoint can be considered met after about $8s$.

The Figure 182, instead, shows that, after a strating undershoot of about -7.4° , followed by an overshoot of 1° , the pendulum reaches its vertical position in about $3s$.

The inner parallel PID is the same as the cascade one. The only designed PID, in this case, is the outer one acting on the linear position of the cart:

$$PID_x(s) = \frac{-0.08029(s + 167.3)(s + 0.2655)}{s(s + 15.19)} \quad (110)$$

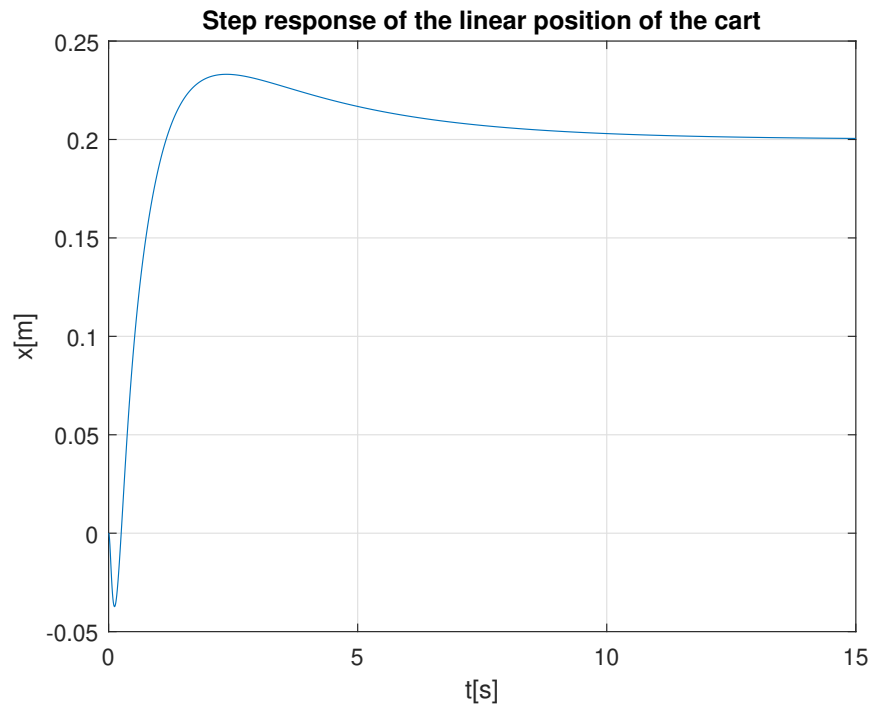


Figure 183: Step response of the linear position of the cart in the parallel architecture and electromechanical Simscape system

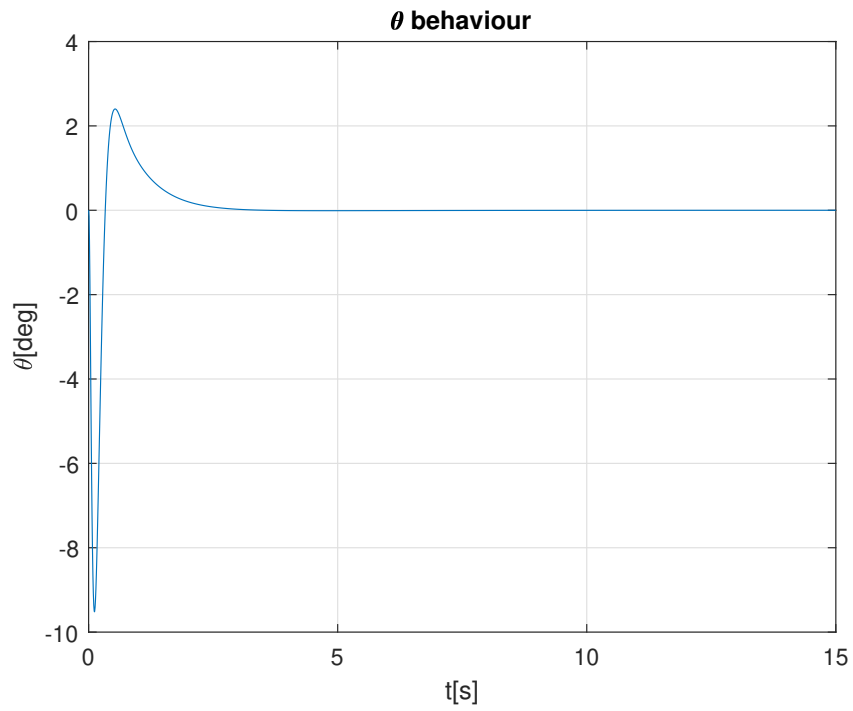


Figure 184: Behaviour of the angle of the pendulum in the parallel and electromechanical Simscape system

The Figure 183 shows that, after a small undershoot, that means the cart is moving backwards, the response presents a rising time of about $1.2s$, an overshoot of about 23.9% and the setpoint can be considered reached in about $8s$.

The Figure 184, instead, allows to visualize the behaviour of the angle of the pendulum. After an undershoot of almost -10° , followed by an overshoot of 2.2° , the angle nullifies in about $3s$.

The pneumatic system is much more difficult to stabilize due to its stronger non-linearities. That is why the autotuning tool is not applicable in this case. The followed approach consists of tuning manually both the inner and the outer PIDs until a good result has been met. By considering the cascade PID control structure, the inner and outer PID are respectively:

$$PID_\theta(s) = \frac{607.12(s + 8.24)(s + 1.647)}{s(s + 748.9)} \quad (111)$$

$$PID_x(s) = \frac{-1.5044(s + 1.07)(s + 0.2568)}{s(s + 4.218)} \quad (112)$$

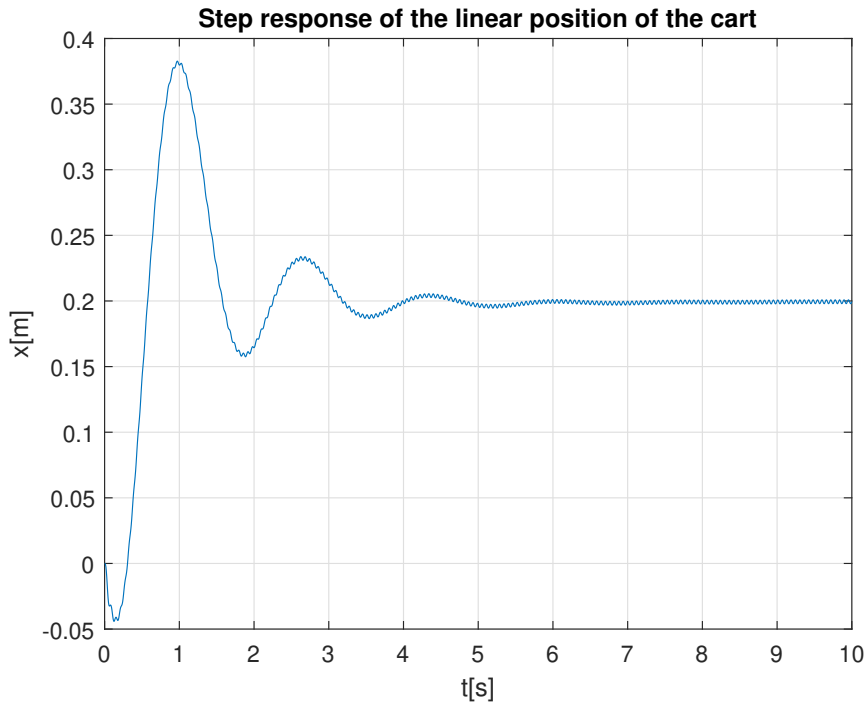


Figure 185: Step response of the linear position of the cart in the cascade architecture and pneumatic Simscape system

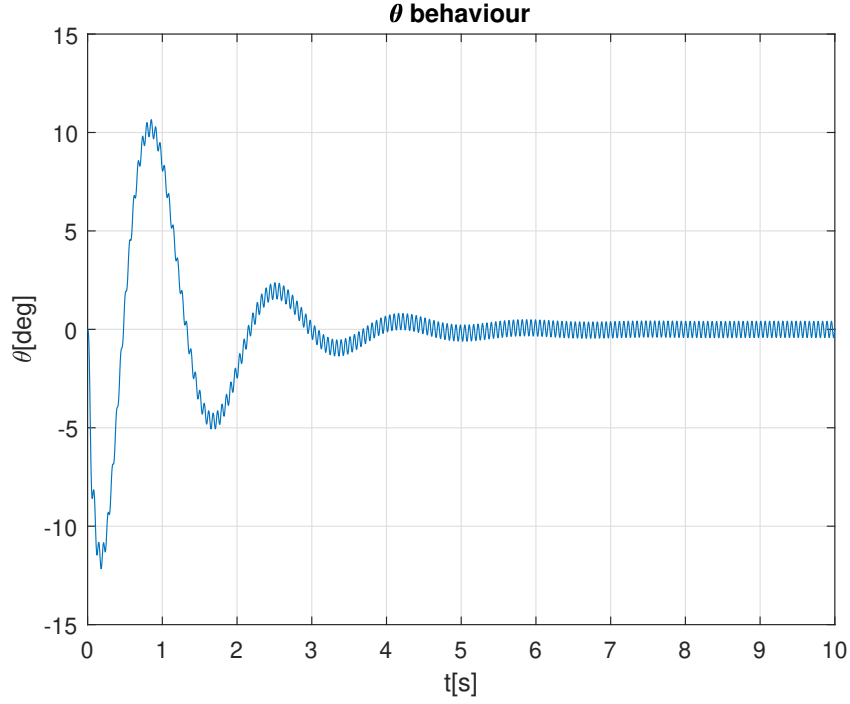


Figure 186: Behaviour of the angle of the pendulum in the cascade and pneumatic Simscape system

The Figure 185 shows a behaviour of the cart that is much nearer to the reality. By considering a null initial condition, after a small undershoot, the response presents a huge overshoot of about 90%, followed by a series of minor undershoots and overshoots. The response presents a rising time of about 0.6s and gets to the setpoint in about 5s. The Figure 186 shows the behaviour of the angle of the pendulum. After an undershoot and a overshoot of about 10°, the pendulum reaches a null angle in about 5s. It is worth noting the oscillating nature of the response, even when the setpoint has been reached. This means that, like in reality, the pendulum will never be stopped in the vertical position but it will keep on oscillating of few degrees around the desired point.

By adopting the same approach as before, it is possible to design the two PIDs in the parallel architecture. The resulting transfer functions of both the inner and the outer PIDs are given by:

$$PID_{\theta}(s) = \frac{335.37(s^2 + 6.508s + 12.4)}{s(s + 472.5)} \quad (113)$$

$$PID_x(s) = \frac{-0.20214(s + 6.038)(s + 0.3123)}{s(s + 2.723)} \quad (114)$$

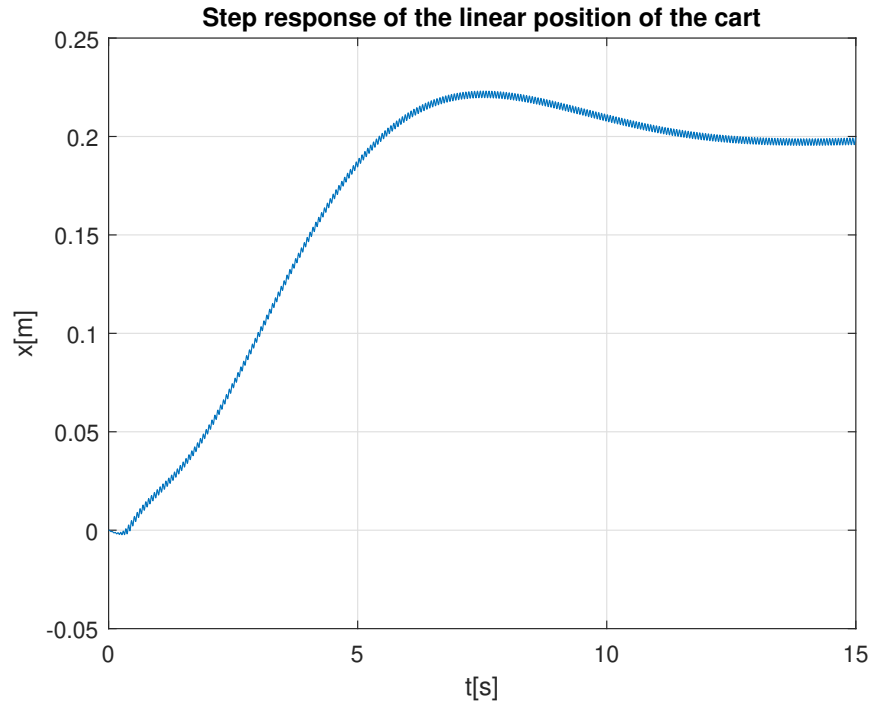


Figure 187: Step response of the linear position of the cart in the parallel architecture and electromechanical Simscape system

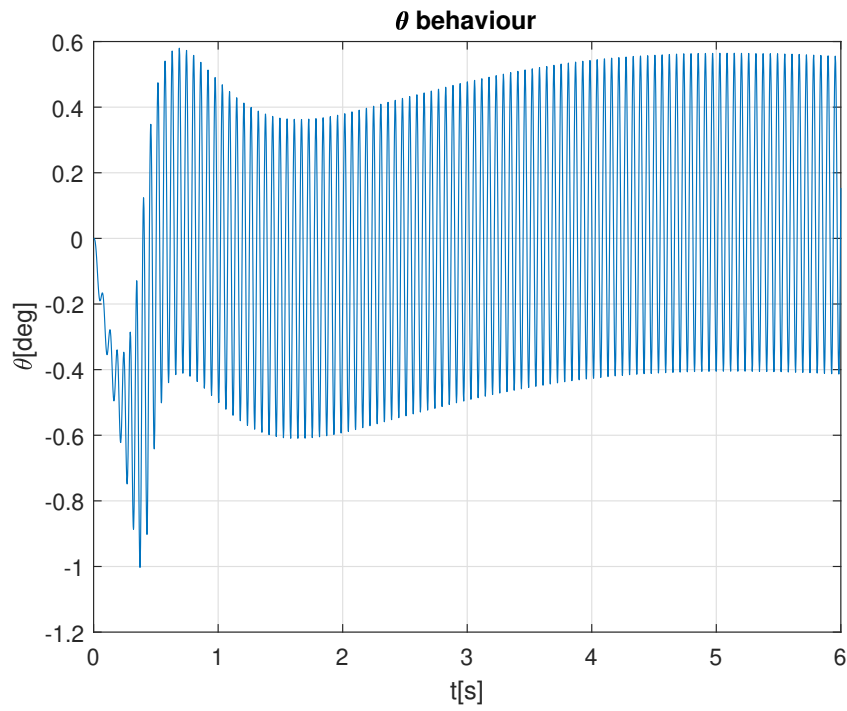


Figure 188: Behaviour of the angle of the pendulum in the parallel and electromechanical Simscape system

The Figure 187 reports the step response of the linear position of the cart, by supposing only a null initial condition. The response presents a rising time of about $5.6s$, an overshoot of about 26% and it reaches the desired setpoint in about $11s$. The response presents some oscillations that witness the model is much nearer to reality than the one studied previously. This is highlighted even more in the Figure 188, representing the angle of the pendulum. After an undershoot of about -1° , followed by an overshoot of about 5.6° , the angle nullifies its value in about $4s$. It can be noticed the presence of oscillations around the established point, of about 0.5° , as the pendulum will never be completely stopped in the vertical position, but it will continue to create small oscillations.

9 Experimental experience

The experimental phase is connected to the control strategies reported in the previous chapters, in particular to the design of cascade PIDs. Unlike what is explained in the chapter 6, it is not possible to perform a control in voltage by using the technological objects in TIA Portal. The applied control is developed by considering as input the acceleration imposed to the cart. A first attempt of control has been implemented in the device PLC s7-1200; the definitive control has then been developed in the s7-1500, that is a more performing device.

9.1 Control strategy in the s7-1200

Once the positioning axis has been defined, according to the instructions reported in the chapter 4, the two PID controllers are inserted in a "Cycle interrupt" block, that interrupts periodically the "Main" block to execute all the commands inside it. Due to the limited performances of this device, the smallest applicable cycle time, without causing overflow, is 8ms. The complete ladder structure of the "Cycle interrupt" block is reported in Appendix C.

The Segment 1 provides the value of the angle the pendulum assumes with respect to the vertical axis, by means of the angular sensor described in the section 2.1.6. The Segments 2 and 3 generate the angular setpoint in input to the inner PID_θ . The output of such a PID is an input of acceleration, but all the technological objects that are usable in this PLC do not allow to act directly on this physical quantity.

It thought to act indirectly on the acceleration through the technological object *MC_Change_Dynamic*. The maximum velocity of the axis is divided by the output of the PID_θ , by obtaining in this way the "rumpup&downtime". The "Rump up time" is the time the axis takes to reach its maximum imposed velocity. The "Rump down time" is the time the axis takes to stop, starting from a maximum velocity. By decreasing the "Ramp up time", it is possible to increase the acceleration, as the system reduces the time it takes to reach the maximum velocity from the rest condition. Therefore, by acting on the "Rump up time" it modifies indirectly the acceleration of the system; the "Ramp down time", instead, acts indirectly on the deceleration.

The technological object *MC_Change_Dynamic* does not update the acceleration in real time; it needs an execution signal for each upgrade. This is performed in the Segments 7 and 9; once the *MC_Change_Dynamic* has changed the dynamic, the "Done" signal passes to the logical level 1, by turning the "*P_trig*" block on, by resetting the "Execute" of the *MC_Change_Dynamic* blocks. To the next cycle, there is the setting of the "Execute" that allows the dynamic to be changed again.

The last Segment contains the technological block *MC_MoveJog*, that moves the axis on the basis of the provided inputs, with the dynamic imposed by the previous blocks.

The limited performances of this PLC have not brought to the desired results, as the pendulum could not be stabilized. The usable technological blocks are, in fact, limited and, moreover, the only "Telegram 3" can be used, that does not permit the IRT (Isochronous Real time) communication between Drive and PLC.

9.2 Control strategy in the s7-1500

Due to all the limits of the PLC s7-1200, the control algorithm has been implemented in a more powerful device, that is the PLC Siemens s7-1512C-1 PN. First of all, it is possible to consider the "Telegram 105", that allows a synchronous communication (IRT) between Drive and PLC. Moreover, the technological objects permit the manipulation of more parameters in input to each block, as acceleration, deceleration and jerk. Unlike the precedent case, it is now possible to act directly on these parameters, to effectuate a real acceleration control.

A further advantage is linked to the reduction of the cycle time from 8ms to 4ms, without provoking overflow.

Its complete ladder structure is reported in the Appendix B, along with its "Main".

The latter contains the *MC_Power* block, mandatory for the activation of the technological axis; an *MC_Reset* block to reactivate the axis if any errors occur and a *MC_MoveAbsolute* block, to take back the cart to the position of 200mm, in case of several errors, such as the overcome of the software end-strokes. Moreover, it contains some "Move" blocks that allows to write the parameters of both the PIDs by means of a data block.

The main of part of the control is contained in the "Cycle interrupt".

The Segment 1 contains the PID_x , whose setpoint is set through a variable that is defined in a data block. The feedback is provided by the real position of the cart, transmitted by the absolute encoder present in the motor. The output of this PID, in a range of $\pm 100\%$, is generated on the basis of the parameters shown in Figure 189:

Parametri PID

☒ Attiva immissione manuale

Guadagno proporzionale: 0.46

Tempo di integrazione: 1.0 s

Tempo derivativo: 1.2 s

Coefficiente ritardo derivativo: 0.155

Ponderazione del componente P: 1.0

Ponderazione del componente D: 1.0

Tempo di campionamento dell'algoritmo PID: 0.004 s

Regola per l'ottimizzazione

Struttura del regolatore: PID

Figure 189: Parameters of PID_x

The Segment 2 allows to scale the percentage output of the PID, by generating an angular setpoint in a range of $\pm 3^\circ$. It can provide an adequate angular setpoint for the stabilization of the overall system. The Segment 3 elaborates and converts the voltage analogical signal coming from the sensor. The Segment 4 has the PID_θ , whose setpoint is coincident with the scaled output of the PID_x and the feedback is given by the real value of the angle, provided by the Segment 3. The output of the PID, in a range of $\pm 100\%$, is generated on the basis of the parameters shown in Figure 190:

Figure 190: Parameters of PID_{θ}

The output, in percentage, is scaled and standardized in the Segment 5, by converting it into an acceleration input in the range $0 \frac{mm}{s^2}$ and $10000 \frac{mm}{s^2}$.

The Segment 6 contains a technological block *MC_MoveJog*, that imposes the motion of the cart. The motion in the positive direction of the x axis happens only when the output of the PID_{θ} is positive; on the contrary, the motion in the negative direction occurs only when the output of the same PID is negative. The "Velocity" input is the maximum velocity that is permitted in the block itself, and it is imposed equal to $1000 \frac{mm}{s}$, through a variable defined in a data block. The motion is realized by means of an acceleration imposed by the scaled values of the PID_{θ} and a jerk that is inserted through a variable in the same data block as before. The last segments of the code are used to monitor all the quantities in interest, like the tracking error, required acceleration and angular input. They were fundamental for the manual calibration of the PIDs.

9.3 PIDs calibration and encountered problems

The design of the PIDs foresees to consider, at first, the only presence of the PID_{θ} . It is calibrated by considering a constant and null angular setpoint. As the system to control is very fast, the implemented controller is a PD. The K_p and the T_d have been calibrated manually until to design a controller able to guarantee a rapid annulment of the tracking error of the angle. By imposing some impulse disturbances to the rod of the pendulum, the final result foresaw the fast compensation of the these variations.

The starting difficulty in the calibration phase has been encountered in the slowness of the reaction of the motor, that could not follow the required acceleration inputs, despite huge values of the PD parameters. The main cause is linked to the default value of the jerk. This caused some very slow variations of the acceleration. This problem has been solved by imposing manually the jerk to its maximum value accepted in the PLC, that guarantees an almost instantaneous variation of the acceleration. The second problem has been found in the default value of the "Coefficiente ritardo derivativo", equal to 1. It influences hugely the derivative component of the PID, as it identifies the passing band of the high-pass filter. Too high values of this parameters slows down excessively the action of the derivative component. As the system to be controlled is very fast, an optimal effect

of the derivative component is reached by considering a "Coefficiente ritardo derivativo" equal to 0.004, corresponding to $250Hz$.

Once the PID_θ has been designed, next step is based on the design of the PID_x . Its purpose is to allow the cart to reach a setpoint of position, by keeping the pendulum in the vertical position.

The sampling times of both the controllers are chosen equal to $4ms$, in such a way they can work synchronously with the "Cycle interrupt". It was necessary a manual calibration of both the PIDs because the theoretical model does not correspond to the real physical system. This deviation is linked to the missing of plenty of information about the Drive and the motor.

9.3.1 Influence of the PID parameters

As specified previously, the calibration of the PID parameters has taken place according to a "trial and error" approach. This section compares the effects of the variations of some of the PID parameters, around the definitive values chosen for the experimental tests. In particular, the effects of the term K_p , related to the PID_x , and the terms K_p and T_d referred to the PID_θ are analyzed.

The purpose of the calibration is to find the PID parameters that minimize the angular oscillations and those of the cart around the setpoint. To analyze the former, it evaluates a dimensionless parameter given by the ratio between the steady-state oscillation range and the maximum angle range. The oscillations of the cart are treated similarly by defining a further dimensionless parameter that relates the oscillation range at steady state and the maximum stroke of the cart.

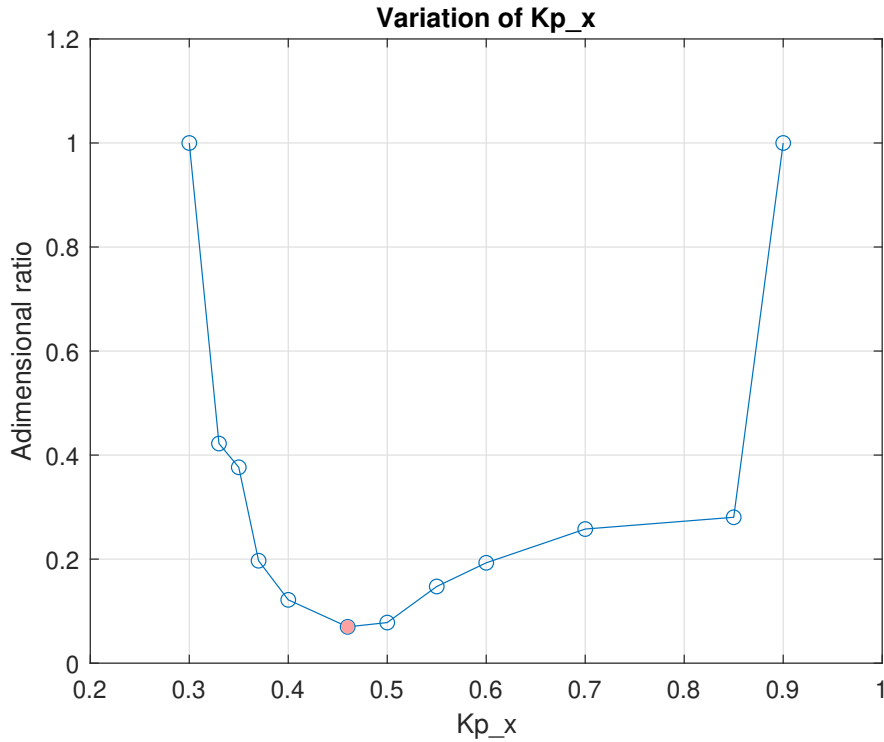


Figure 191: Effect of K_{px} on the steady-state oscillations of the cart

Figure 191 shows the effect of the variation of the proportional coefficient K_{px} on the steady-state oscillations of the cart. The point highlighted in orange coincides with the final value chosen for the experimental tests and is equal to $K_{px} = 0.46$.

Considering a right neighborhood of this point, it can be seen that the oscillations tend to grow slowly up to a value of K_{px} equal to 0.85, and then trigger oscillations such as to reach the limit switches for $K_{px} = 0.9$. A variation around the left instead induces a much faster increase in oscillations, reaching the end stroke for a value of $K_{px} = 0.3$.

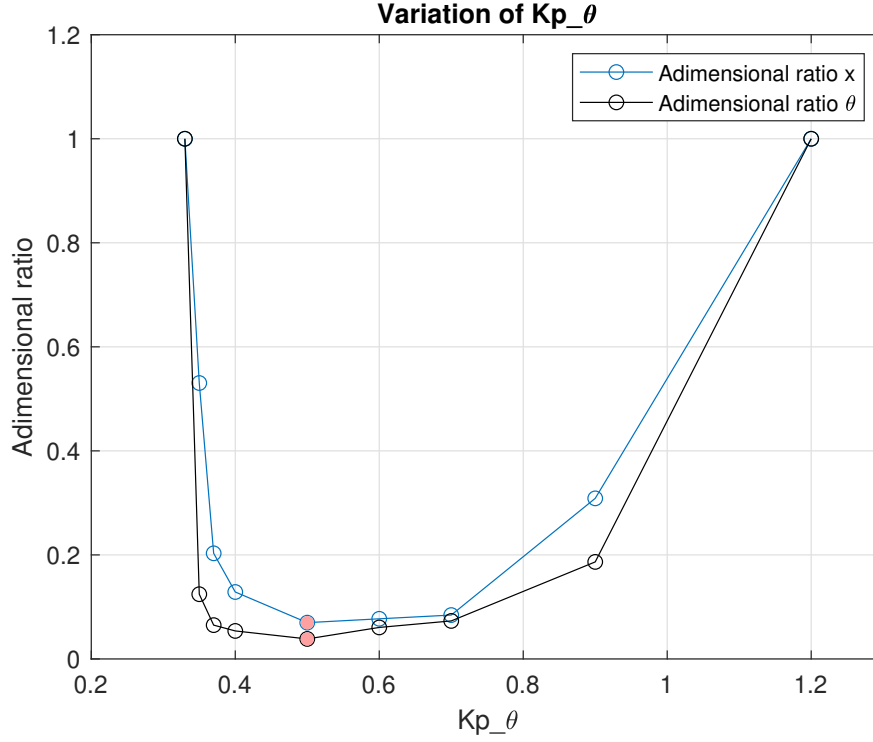


Figure 192: Effect of $K_{p\theta}$ on the steady-state oscillations of the cart

Figure 192 shows the effects of the variation of the proportional coefficient $K_{p\theta}$ on the dimensionless ratios of the cart and angle oscillations.

As in the previous case, the points in orange coincide with the $K_{p\theta}$ chosen for the tests and is equal to $K_{p\theta} = 0.5$. Also in this case the right neighborhood shows a slower increase in oscillations bringing the system to the limit switches for a value of $K_{p\theta} = 1.2$. The left neighborhood shows a more sudden variation, as the end stroke is reached for $K_{p\theta} = 0.33$.

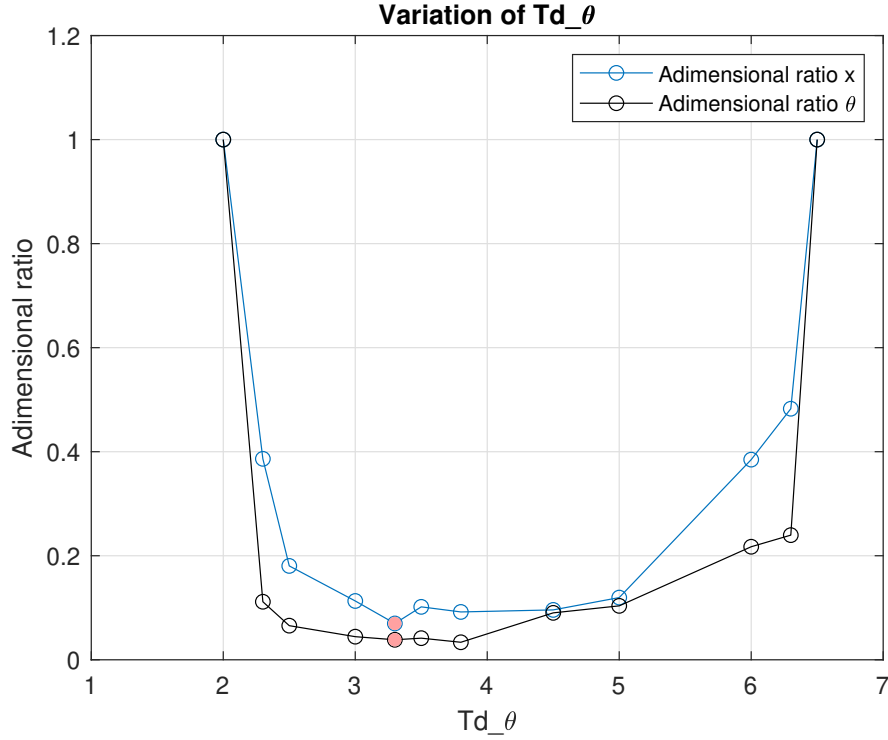


Figure 193: Effect of $T_{d\theta}$ on the steady-state oscillations of the cart and of the angle

Figure 193 shows the influence of $T_{d\theta}$ on the considered dimensionless relations. In this case the orange points, corresponding to a $T_{d\theta} = 3.3$, show that the choice of the definitive $T_{d\theta}$ is not the one that optimizes the angular ratio θ , even if it is little. The optimal value would be for a value of $T_{d\theta} = 3.8$. The choice is made as a compromise, considering that the cart oscillation is minimized. In general, the behavior, both in the right and left surroundings, is similar to that described in the previous graphs.

9.4 Experimental results

The experimental tests are performed by considering four kinds of signals:

- Step signal
- Square signal
- Sinusoidal signal
- Impulsive disturbance

In particular, the first three signals represent the position setpoints that the system must follow, the last is a disturbance applied to the pendulum rod to evaluate the robustness of the designed controllers. The response to a step signal was also analyzed by varying the physical parameters length of the rod and concentrated mass of the pendulum.

9.4.1 Step response and impulsive disturbances

The first test is to apply a step signal to the linear position setpoint. In particular, the tests are carried out with the cart in the initial position of $x = 100mm$ and a step of width $x = 150mm$ is imposed. Initially, the rod has a length of $l = 550mm$ and the concentrated mass of the pendulum is $m = 180g$.

The linear position of the cart is shown in figure 194

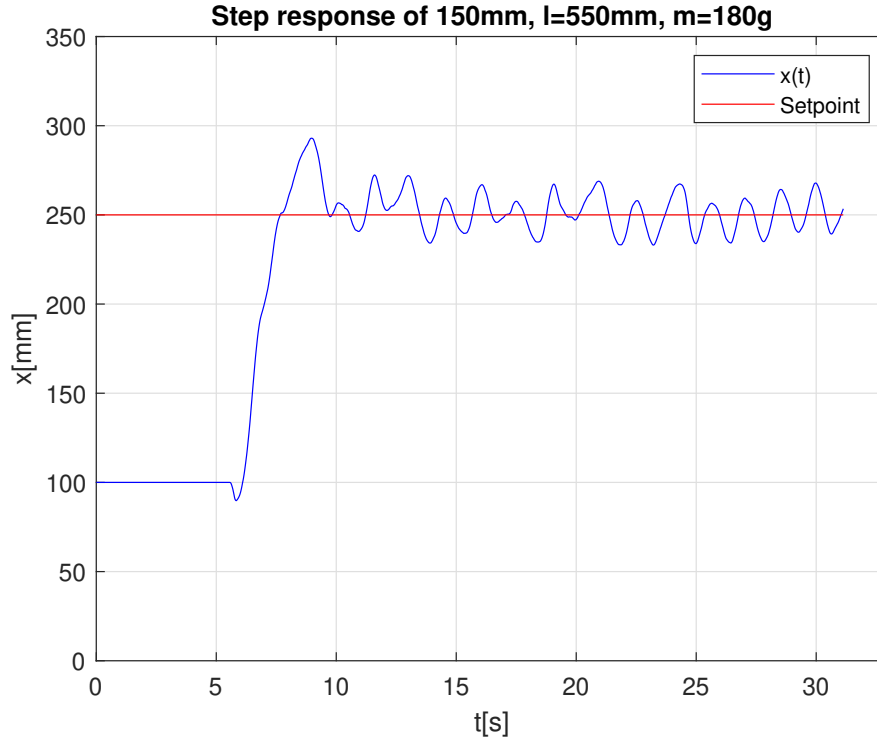


Figure 194: Step response with $l = 550mm$ and $m = 180g$

After a small undershoot, due to the fact that the system is non minimum phase, the cart moves to the required position with a rise time of $2.14s$ and a maximum overshoot of 17% . Once the regime phase has been reached, the cart position remains around the setpoint $x_{SET} \pm 17mm$.

The behaviour of the angle of the pendulum is shown in Figure 195

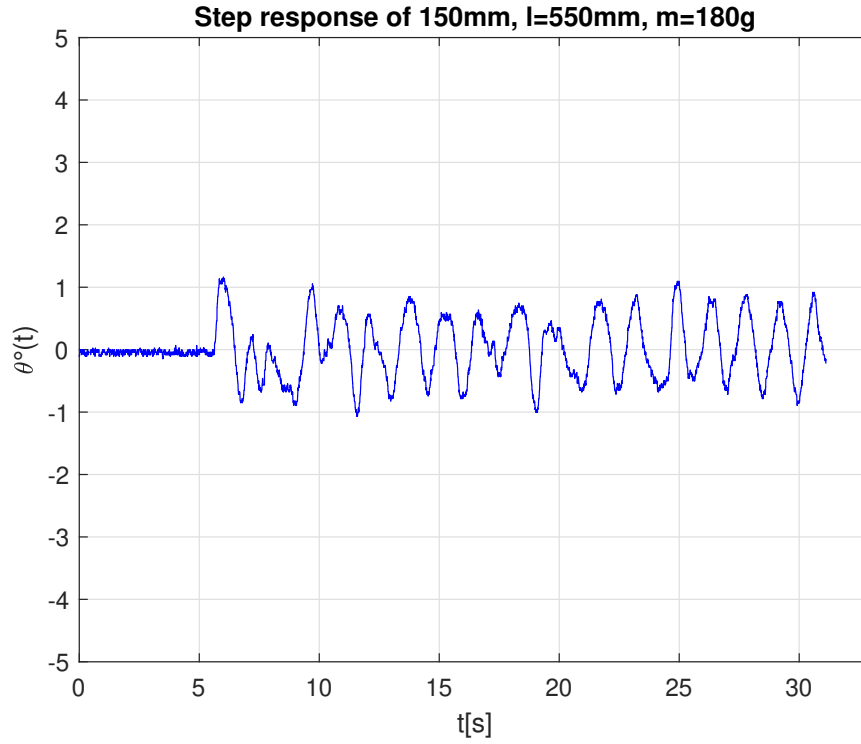


Figure 195: Behaviour of θ to the step response with $l = 550mm$ e $m = 180g$

From the graph it can be seen that the angle θ oscillates between $\pm 1^\circ$, due to the continuous corrections that the system imposes for keeping the pendulum rod in vertical position. On the same configuration, once the regime was reached, the robustness of the system was evaluated by subjecting it to impulsive disturbances, generated by blows inflicted on the concentrated mass. The results are shown in Figure 196 and Figure 197:

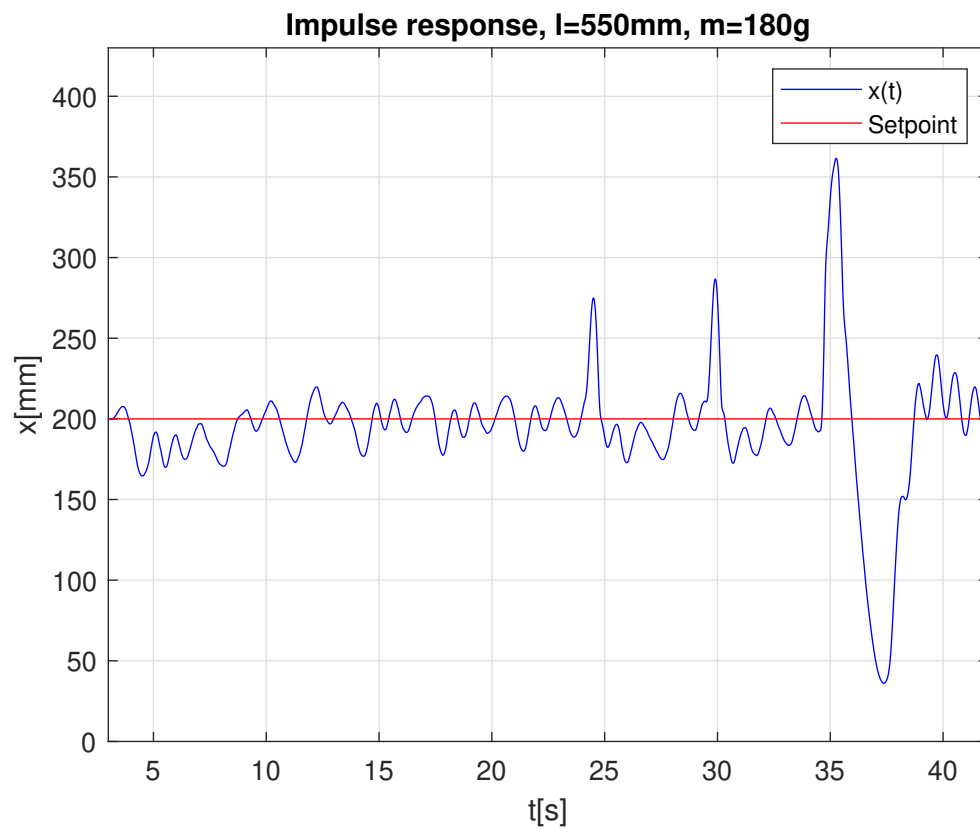


Figure 196: Response to impulsive disturbances with $l = 550\text{mm}$ and $m = 180\text{g}$

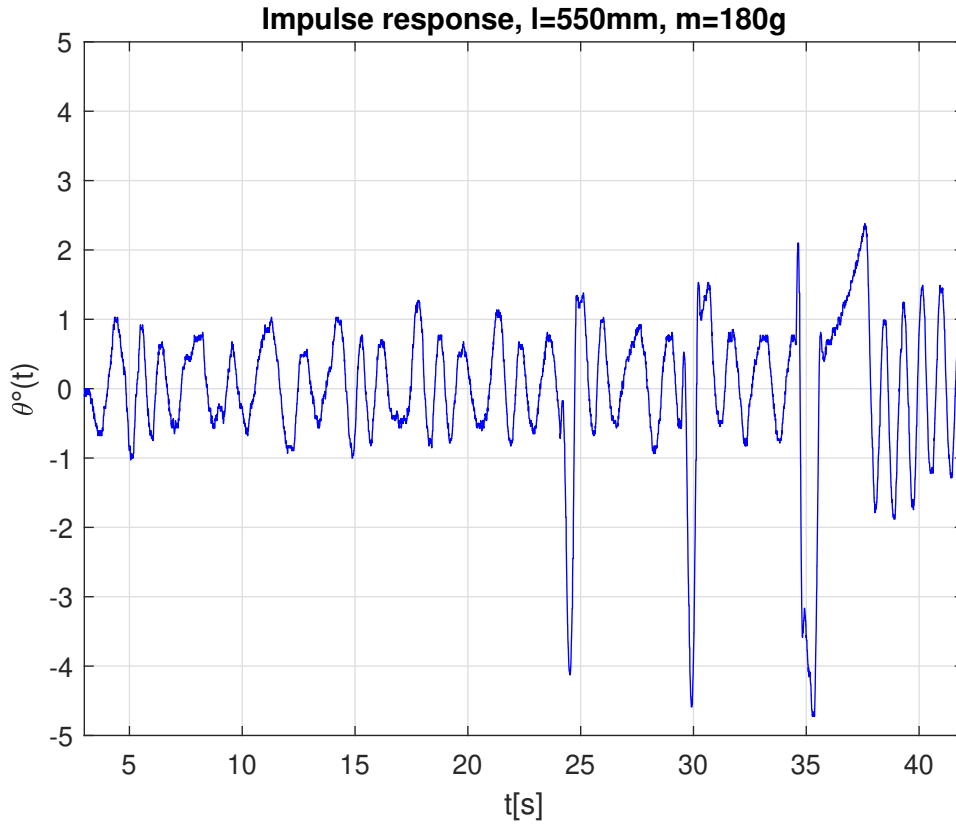


Figure 197: Angular response to the impulsive disturbances with $l = 550mm$ and $m = 180g$

From the graphs shown above, it can be seen that, despite several pulses of different intensity, the system reacts promptly by trying to bring the rod back to a vertical position. To do this, the cart must move in the same direction as the pendulum has moved, and then return to its setpoint. More consistent impulses, which lead the shaft to angles greater than $\pm 6^\circ$, cannot be rejected, given the limited travel.

Subsequently, keeping the length of the rod unchanged and the same step signal, the concentrated mass of the pendulum is changed, taking it first from $m = 180g$ to $m = 560g$ and then from $m = 560g$ to $m = 800g$. In this case, after reaching the regime phase at the step, the response to different impulses is evaluated. The results are shown in the figures below:

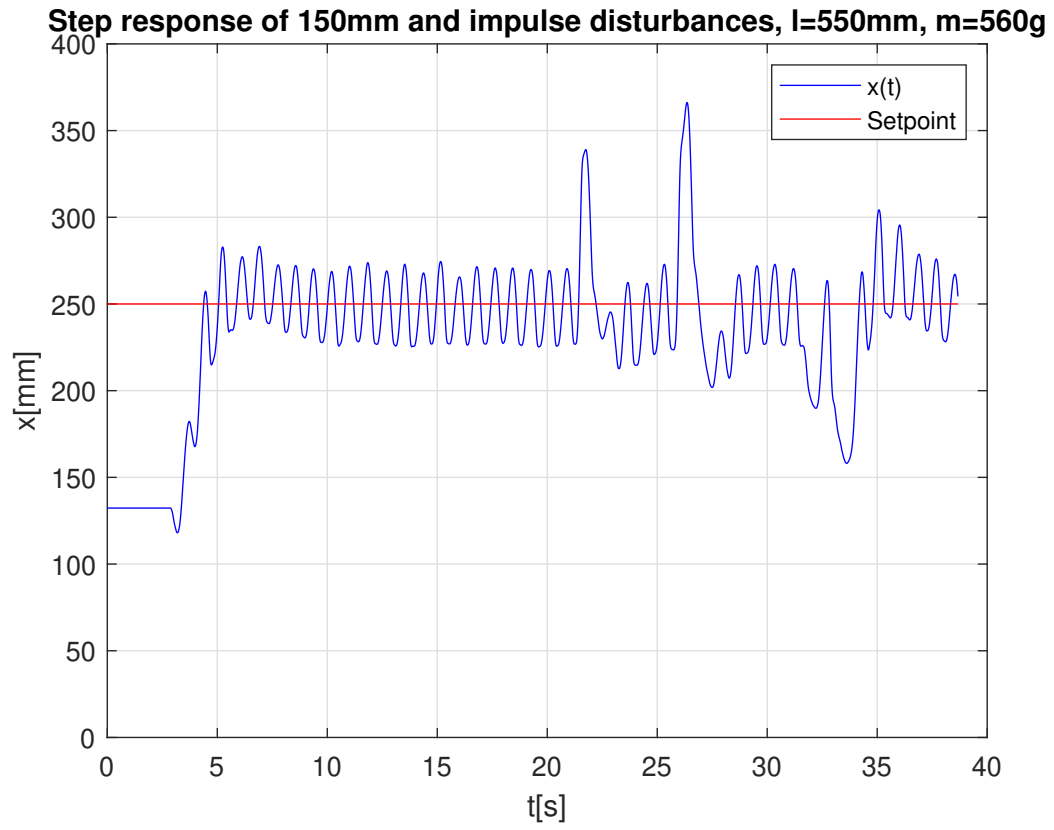


Figure 198: Step response and impulsive disturbances response with $l = 550\text{mm}$ and $m = 560\text{g}$

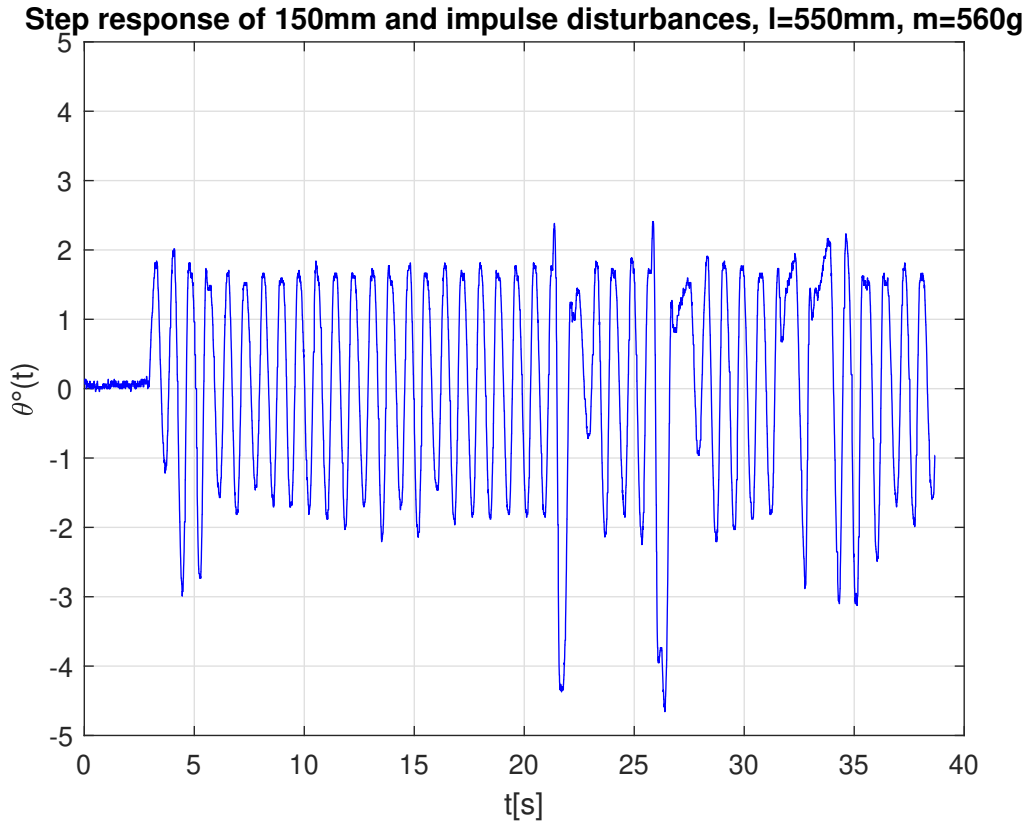


Figure 199: Behaviour of θ to the step response and impulsive disturbances with $l = 550mm$ e $m = 560g$

After a small undershoot, the cart moves to the required position with a rise time of $1,562s$ and a maximum overshoot of 13% . Once the regime phase has been reached, the cart position remains around the setpoint $x_{SET} \pm 21mm$. From the trend it can be seen that the angle θ oscillates between $\pm 2^\circ$.

Also in this case, by subjecting the system to various impulsive disturbances, the robustness of the overall system can be noted.

The last mass variation has the following results:

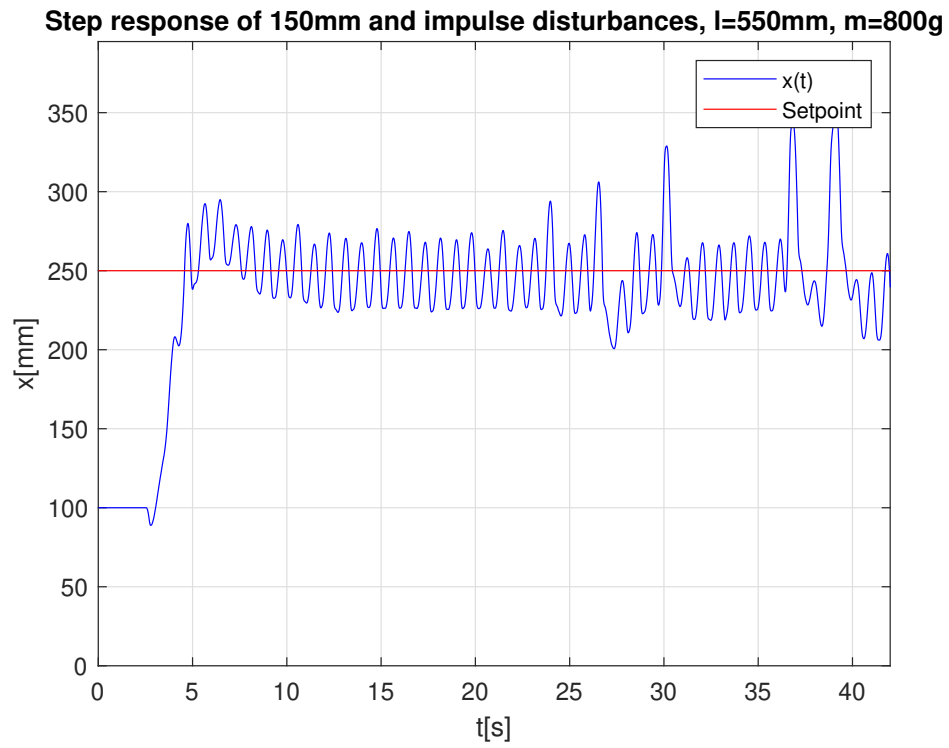


Figure 200: Step response and impulsive disturbances response with $l = 550mm$ and $m = 800g$

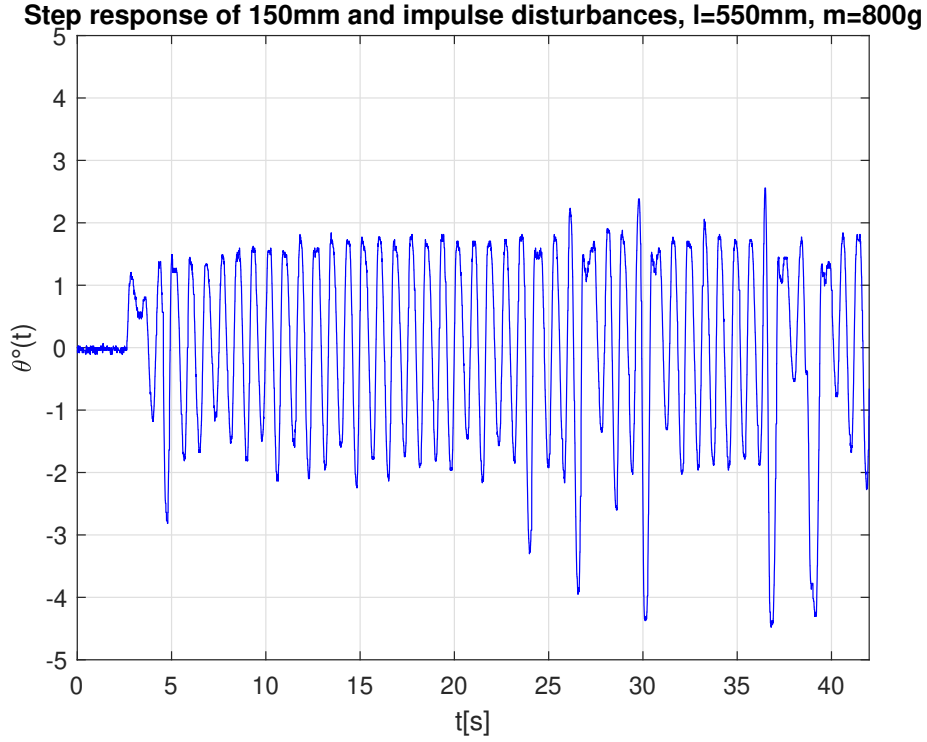


Figure 201: Behaviour of θ to the step response and impulsive disturbances with $l = 550mm$ and $m = 800g$

After the characteristic undershoot, the cart moves to the required position with a rise time of $2,088s$ and a maximum overshoot of 17.6% . Once the regime phase has been reached, the cart position remains around the setpoint $x_{SET} \pm 24mm$. From the trend it can be seen that the angle θ oscillates between $\pm 2^\circ$.

Also in this case, by subjecting the system to various impulsive disturbances, the robustness of the overall system can be seen. Finally, the same test is carried out by shortening the auction to $400mm$ with a mass of $180g$. The results are shown in the figures below:

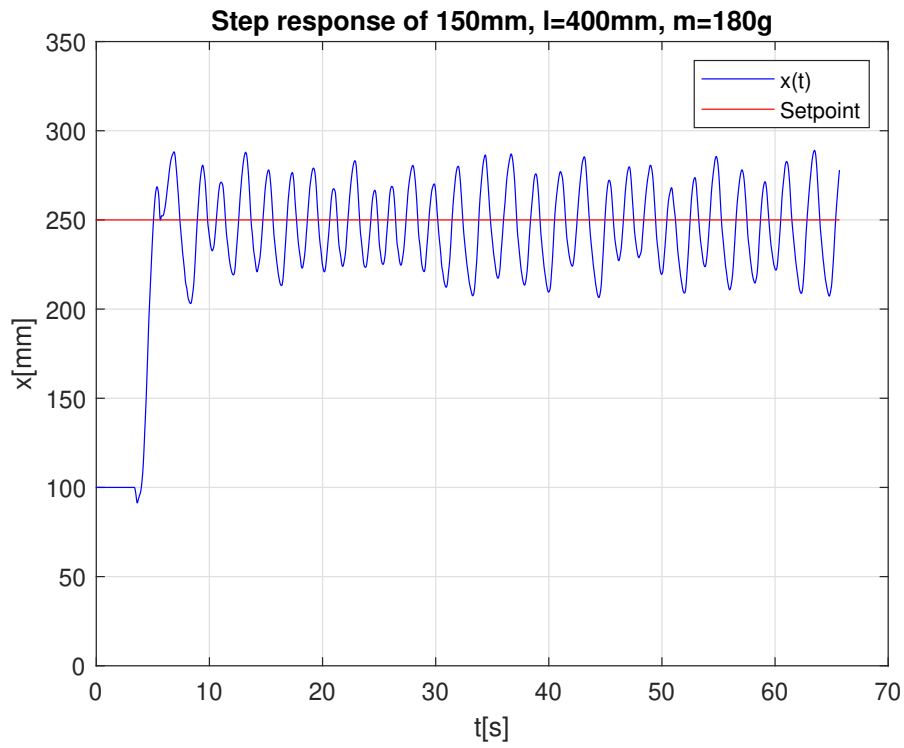


Figure 202: Step response with $l = 400\text{mm}$ and $m = 180\text{g}$

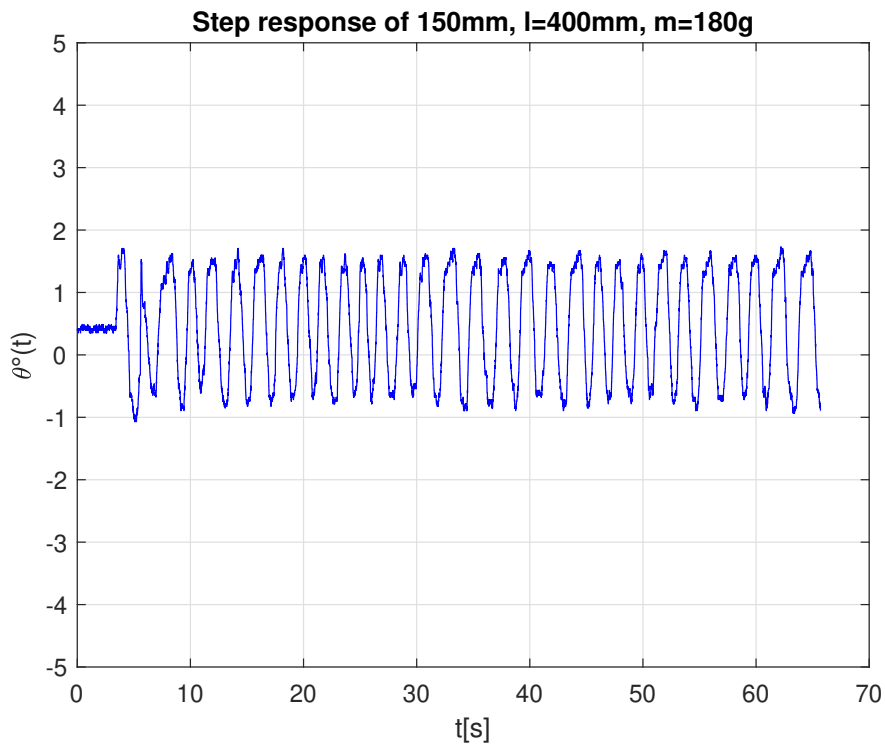


Figure 203: Behaviour of θ to the step response with $l = 400\text{mm}$ e $m = 180\text{g}$

By comparing all the results, it is possible to do some considerations. By increasing the mass of the pendulum, with the same length of the rod, the rise time increases along with the overshoot. This is due to the fact the overall dynamic of the system is slowed down by the concentrated mass that is grown. An isolated case is the first test, with $l = 550mm$ and $m = 180g$. Instead of presenting the faster rise time, as the concentrated mass is the smallest considered, the response is the slowest one, even if the angle oscillates in a minor range of values.

The last test presents the shortest rod of the pendulum and this leads to a slowdown of the response, as the produced torque is now minimized. Generally, by excluding the first test, all the other tests highlight that by increasing the concentrated mass and decreasing the length of the rod, the dynamic of the system is slower and slower.

9.4.2 Square wave signal

Next step is to consider as setpoint imposed to the cart a square wave signal. In particular, the tests have been performed only by taking into account a concentrated mass of the pendulum equal to $180g$ and a length of the rod equal to $550mm$. The amplitude of the signal is fixed to $100mm$, while the period is chosen equal to $10s$ first, then to $8s$ and, finally, to $5s$. The results of the three experiments are reported as follows:

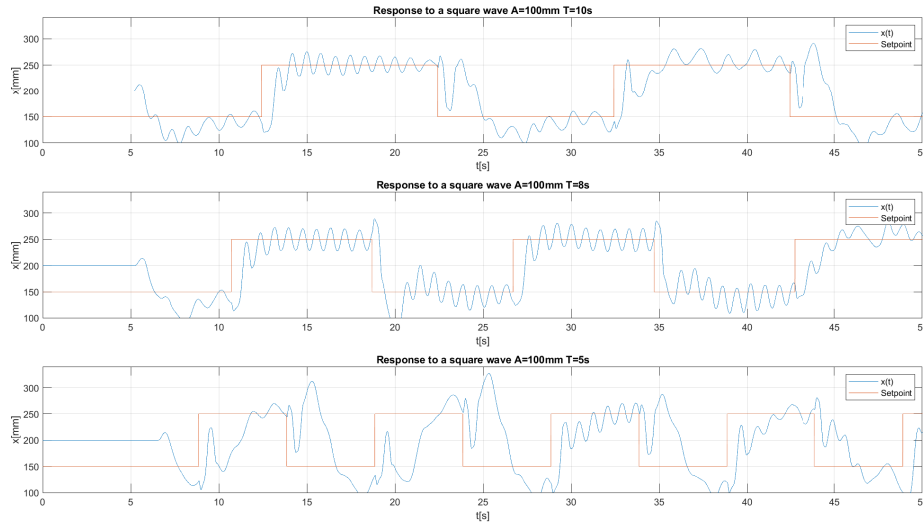


Figure 204: Square wave response

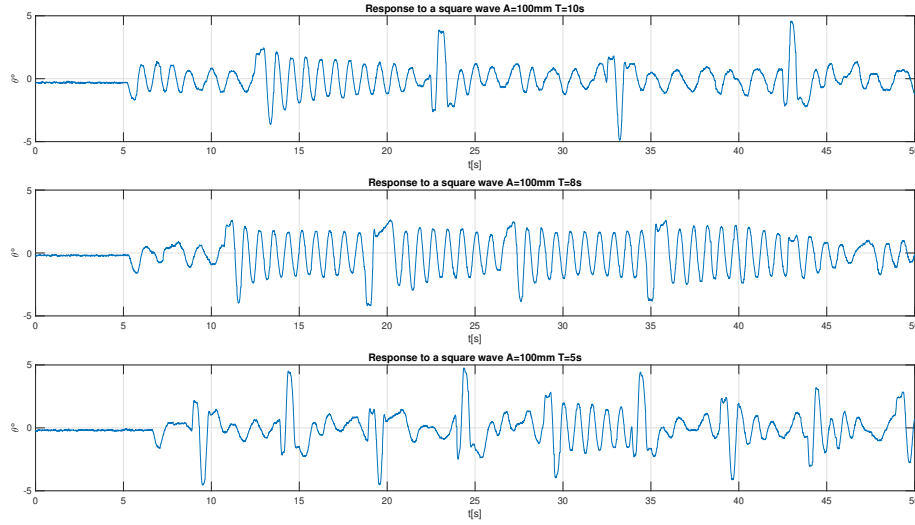


Figure 205: Behaviour of the angle

The Figure 204 shows the behaviour of the cart position for the different considered square waves. It is possible to notice that, by considering the periods of 10s and 8s, the response is quite good as it can follow the continuous changes of the setpoint, imposed by the square wave. The last case, instead, shows a bad tracking capacity of the response as the cart cannot reach the position of the setpoint before it changes. The dynamic of this square wave is too fast.

The Figure 205, instead, reports the behaviour of the angle of the pendulum with these several square waves. The former two cases present a good behaviour of the angle, as it continues to oscillate of few degrees around the null value. There are some peaks corresponding to the change of the square wave. The last case, instead, highlights bigger oscillations, linked to the cart that cannot reach the setpoint completely.

9.4.3 Sinusoidal signal

The last experiment consists of considering the rod of the pendulum equal to 550mm and a concentrated mass of 180g, by imposing as setpoint a sinusoidal wave. In particular, it is taken into account an amplitude of the sine signal equal to 100mm, by imposing a period of the wave of 10s, 7.5s and 6s; the last try considers an amplitude of 50mm and a period equal to 6s.

The first case to analyze is based on a period of 10s, corresponding to a frequency of 0.1Hz, and an amplitude of 100mm. It is reported in Figure 206:

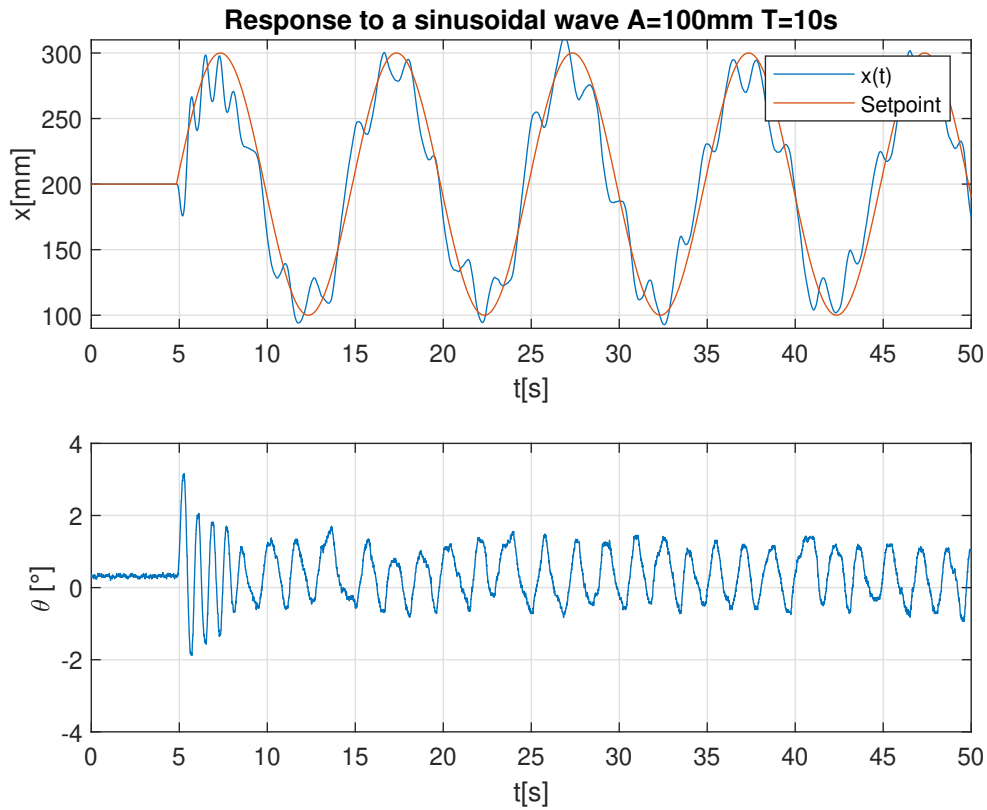


Figure 206: Sinusoidal wave response with $T=10s$ and $A=100mm$

It can be noticed the cart can track the sinusoidal signal, by showing only small oscillations, that witness the good behaviour of the response. The angle does not undergo the effect of the variable setpoint imposed to the cart as, after a small overshoot of about 3° , it keeps on oscillating of about $\pm 1^\circ$ around the zero value.

Next test considers the same amplitude as before but with a period of $7.5s$, corresponding to a frequency of about $0.13Hz$. The result is shown in Figure 207:

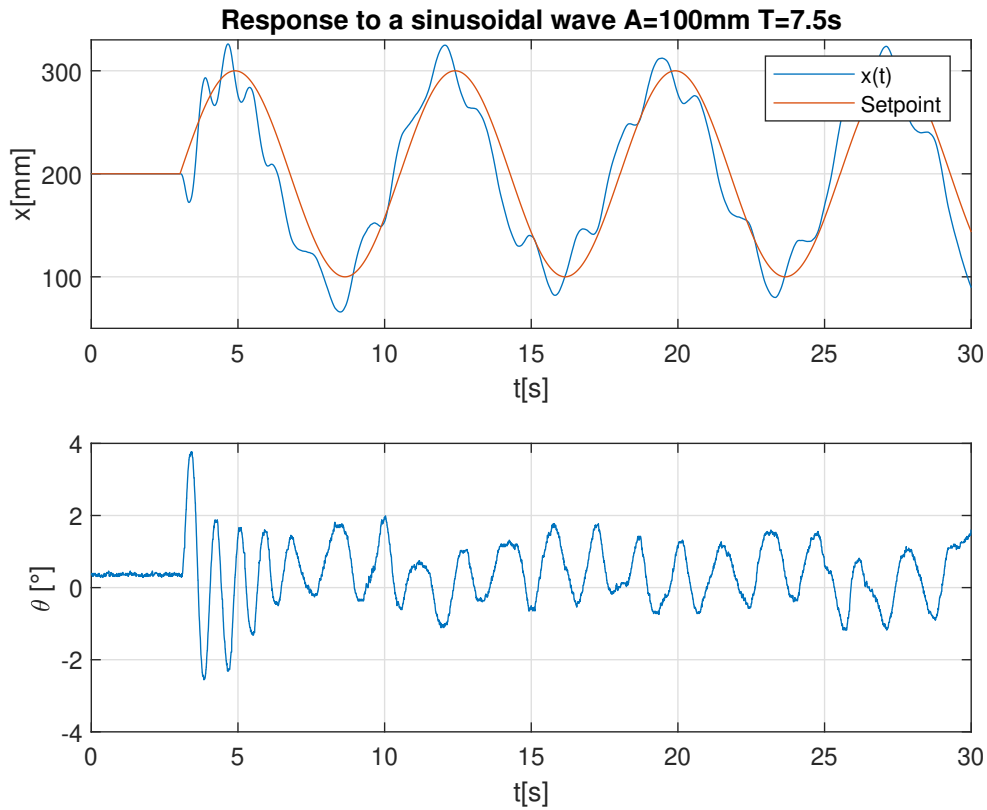


Figure 207: Sinusoidal wave response with $T=7.5s$ and $A=100mm$

It can be noticed now that, with respect to the previous case, the cart cannot follow the sinusoidal setpoint as perfectly as before. In fact, there is the presence of bigger oscillations around the setpoint due to the frequency that is now increased. The angle, instead, presents a similar behaviour as, after a small overshoot of about 4° , it settles around the null value of $\pm 1^\circ$.

Next step consists of considering the same amplitude of the sine wave signal, with a period equal to $6s$, corresponding to a frequency of about $0.17Hz$. The obtained result is reported in Figure 208:

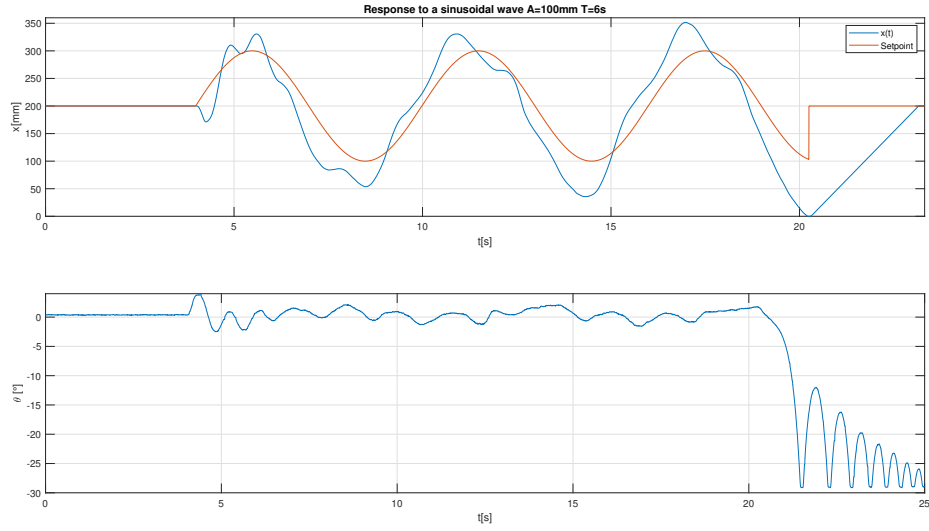


Figure 208: Sinusoidal wave response with $T=6s$ and $A=100mm$

Such a Figure highlights the cart cannot follow the sinusoidal wave in the proper way. In fact, the response presents bigger and bigger oscillations, that are caused by a divergent behaviour of the response itself. After about $20s$, the cart reaches the software limit switch, by leading the system in error. From that moment on the angle, that was initially stabilized, takes back naturally to its negative limit of about -27° .

Last experiment considers the same period as before but a reduced amplitude of the sine wave of $50mm$, to check whether a smaller amplitude allows the response of the cart to track properly the signal with such a frequency. It is reported in Figure 209:

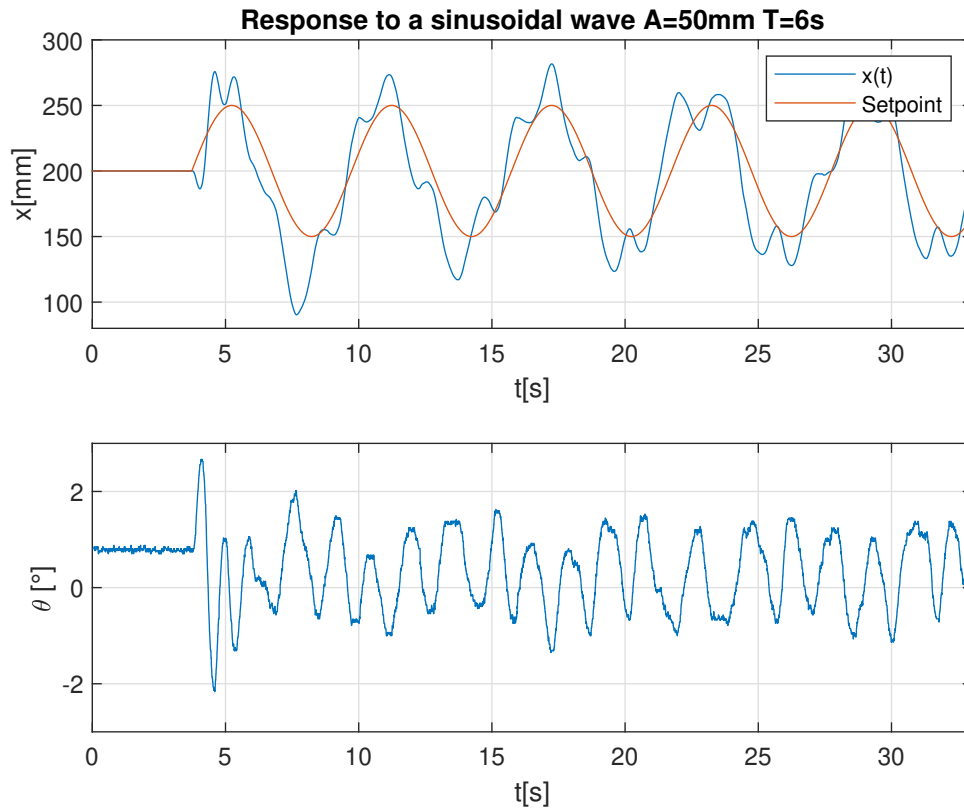


Figure 209: Sinusoidal wave response with $T=6$ s and $A=50$ mm

Even if there is the presence of quite big oscillations, at least the response can track the sinusoidal wave signal without causing a divergent behaviour. The angle, after the usual starting overshoot and undershoot, is then stabilized around the null value. It can conclude that, by increasing the frequency, it becomes harder and harder to obtain a response that can track properly the sine wave setpoint, whether the amplitude is too high. In order to get a good tracking behaviour, the amplitude needs to be chosen smaller and smaller with the increase of the frequency.

10 Future developments

This section provides some ideas about possible future developments of the experimental part.

Firstly, it could try to optimize the obtained PID parameters, to improve the working of the system, and, successively, to try to stabilize the system by using two parallel PIDs. It could also attempt to design a velocity control, instead of acting on the acceleration.

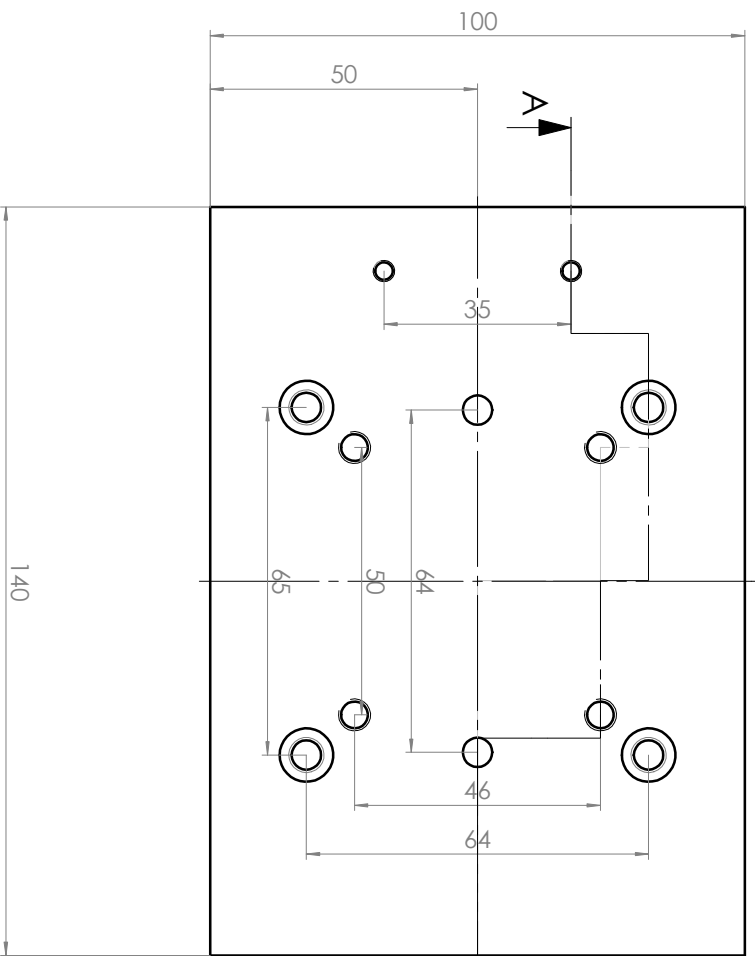
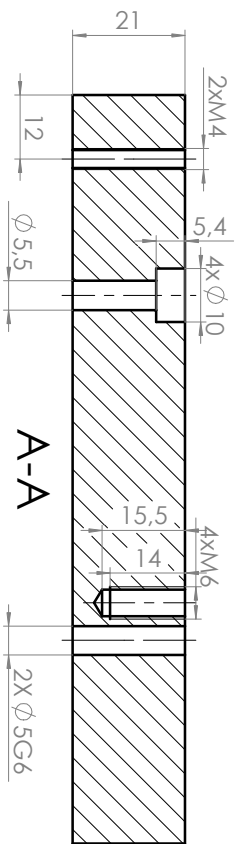
A further aspect is linked to the possibility to search for a model that represents in a more faithful way the real physical system, in particular a best modelling of the actuation system. This would bring to an easier calibration of the PID parameters. It could adopt the identification techniques, even robust ones, to find a transfer function that approximates this system in the best way possible.

Another possibility is given by the connection of the TIA Portal with the Matlab/Simulink environment. This is possible by exploiting the communication protocol OPC. Therefore, it could be possible to implement further control architectures, as MPC, in the Matlab/Simulink environment, and, then, send the control signals to the PLC.

The thesis project has been developed by considering the technological objects. A possible future development is based on the use of the Epos methodology, usable only on a Drive S120. It closes the current loop, the position loop and the velocity loop in the Drive. This would lighten the computational load of the PLC. In this case, new blocks of the TIA Portal need to be adopted like "*Sina_Speed*", "*Sina_Pos*" and "*Sina_Para*".

Finally, it could try, whether possible, a control of voltage or torque by taking advantage of customizable telegrams, whose words can be sorted out through a setting operation in the Starter program.

11 Appendix A: Technical drawings



A

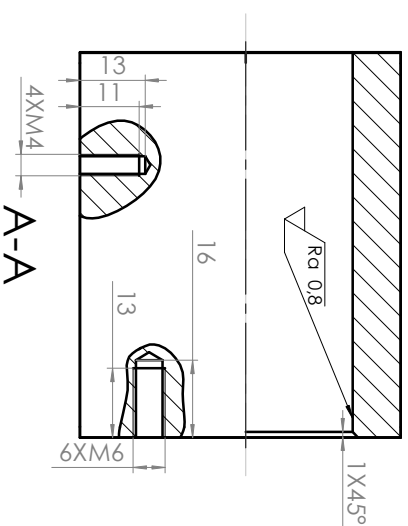
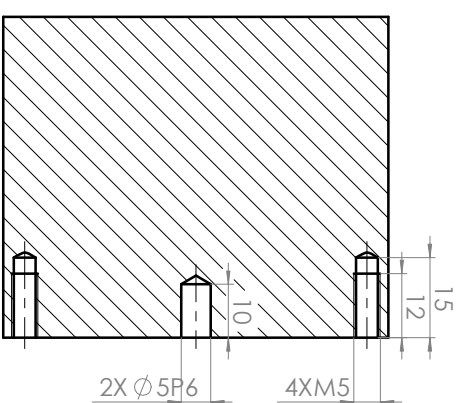
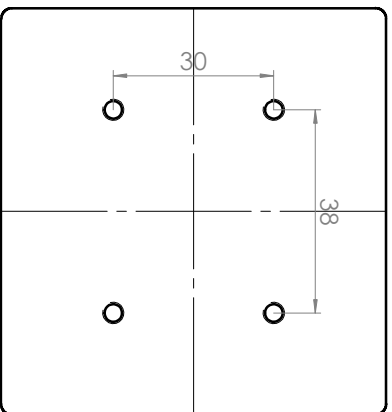
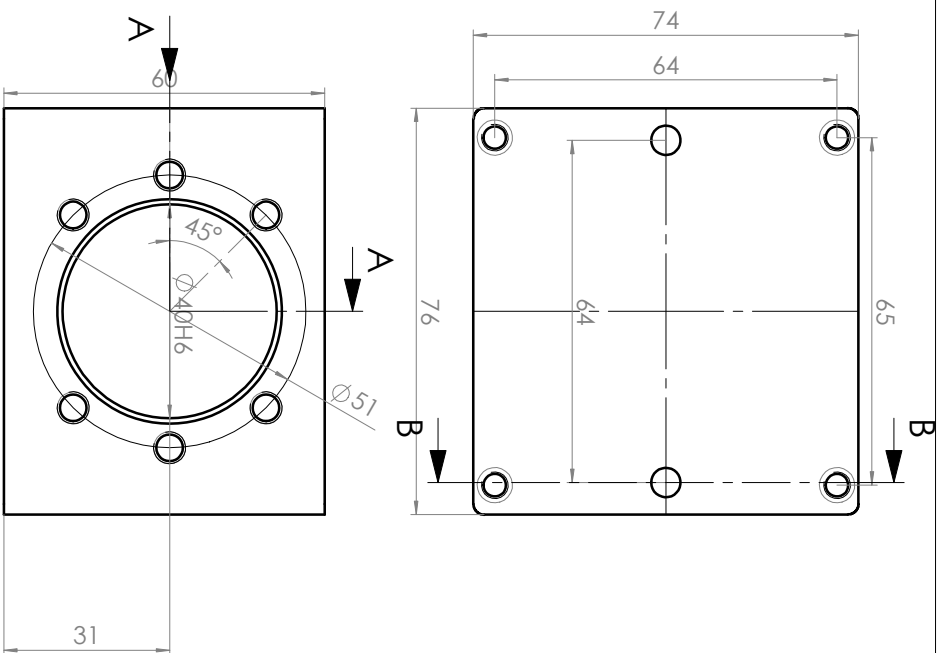
Raccordi non quotati R2
Tolleranze generali UNI EN 2768-mK

Q.TA' _	MATERIALE Alluminio	ALIEVO	Credito
OGGETTO	Piastra superiore		
DESCRIZIONE			
GRADO DI FINITURA		PESO (Kg)	SCALA 1.1
V (V)			
FOGLIO A3 1/1		Disegno N.	



Politecnico di
Torino

Corso Duca degli Abruzzi 24 - 10129 Torino



Raccordi non quotati R2
Tolleranze generali UNI EN 2768-mK

Q.T.A.	MATERIALE	ALIEVO	Credito
-	Alluminio		
OGGETTO	SQUADRA E CORSO		
DESCRIZIONE	Piastre inferiore		

GRADO DI FINITURA

PESO (Kg)

SCALA 1:1

DATA



Politecnico di
Torino

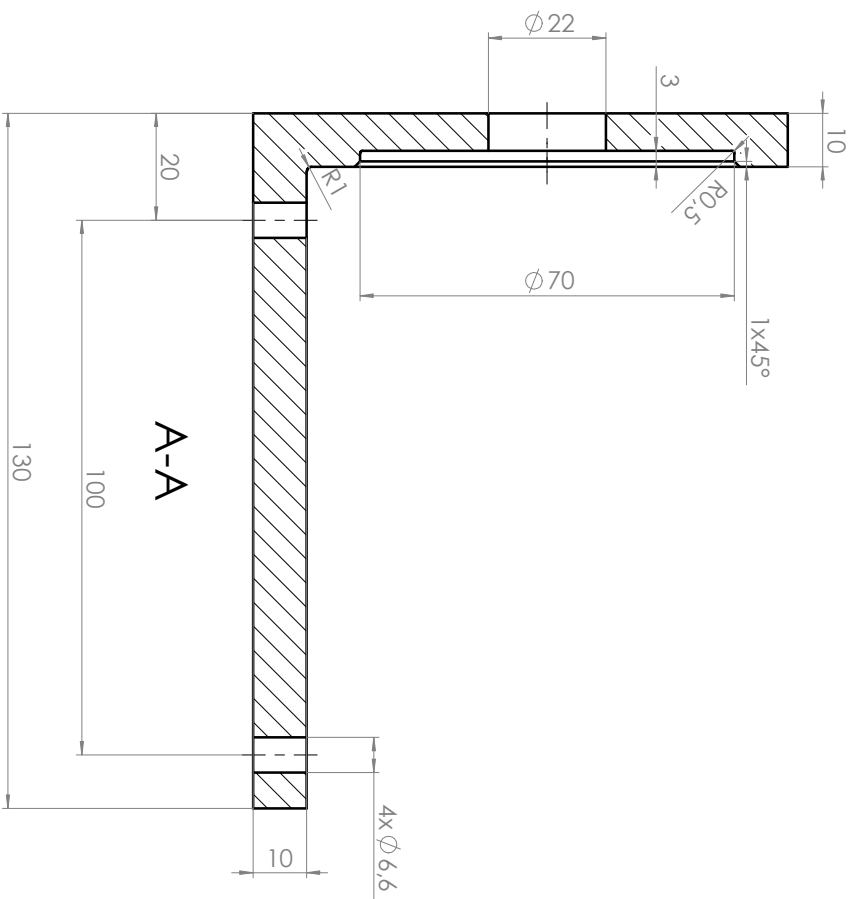
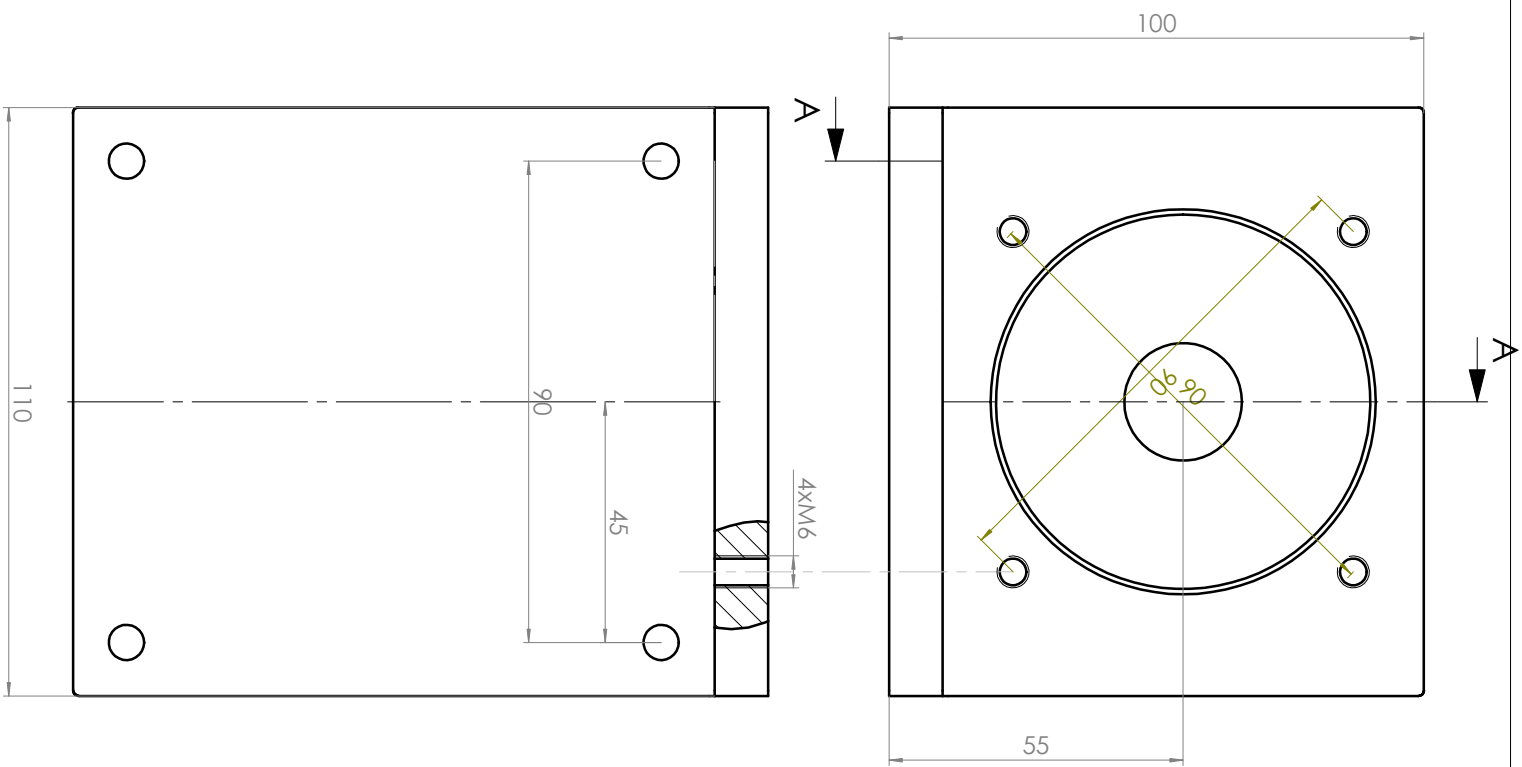
Corso Duca degli Abruzzi 24 - 10129 Torino

✓ (✓)

FOGLIO

Disegno N.





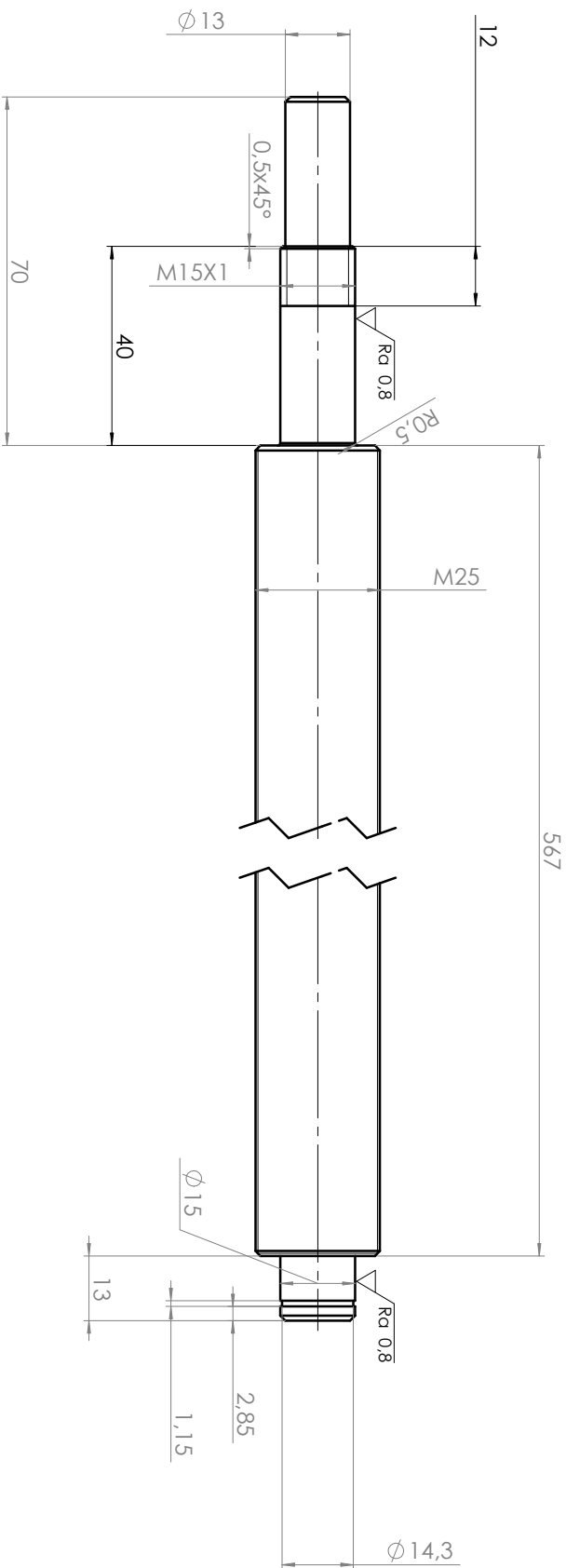
Raccordi non quotati R1
Tolleranze generali UNI EN 2768-mK

Q.TA'	MATERIALE	ALIEVO	Credito
-	Acciaio		
OGGETTO	SQUADRA E CORSO		
DESCRIZIONE	flangia		
GRADO DI FINITURA		PESO (Kg)	SCALA 1:1
✓ (✓)			DATA
Disegno N.			




Politecnico di
Torino

Corso Duca degli Abruzzi 24 - 10129 Torino



Smussi non quotati 1x45°
Tolleranze generali UNI EN 2768-mk

Q.TA'	MATERIALE	ALIEVO	Credito
OGGETTO	SQUADRA E CORSO		
DESCRIZIONE	Vite R25-10-0650-0650		
GRADO DI FINITURA		PESO (Kg)	SCALA 1:2
V (V)			DATA

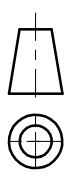


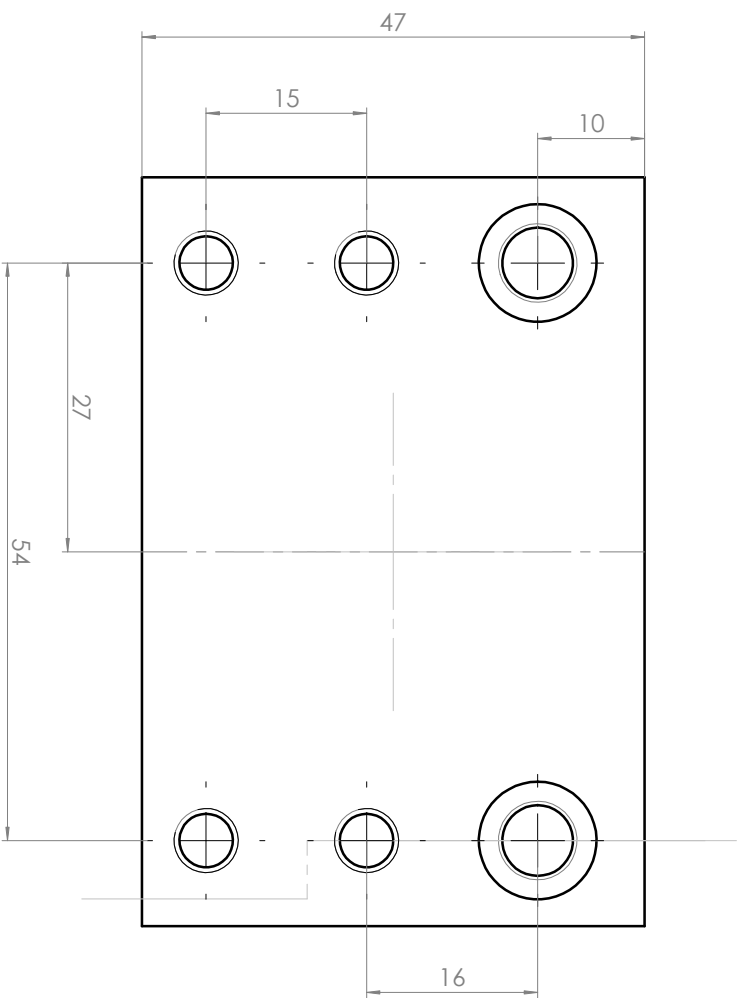
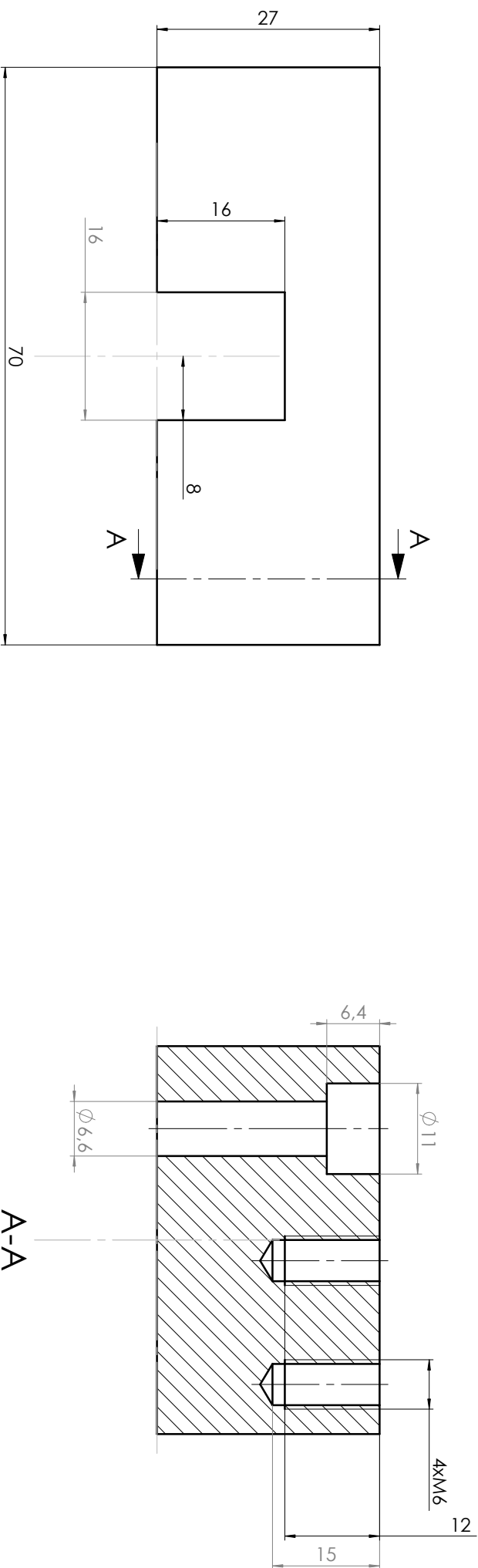
Politecnico di
Torino

Corso Duca degli Abruzzi 24 - 10129 Torino

A3 1/1

Disegno N.





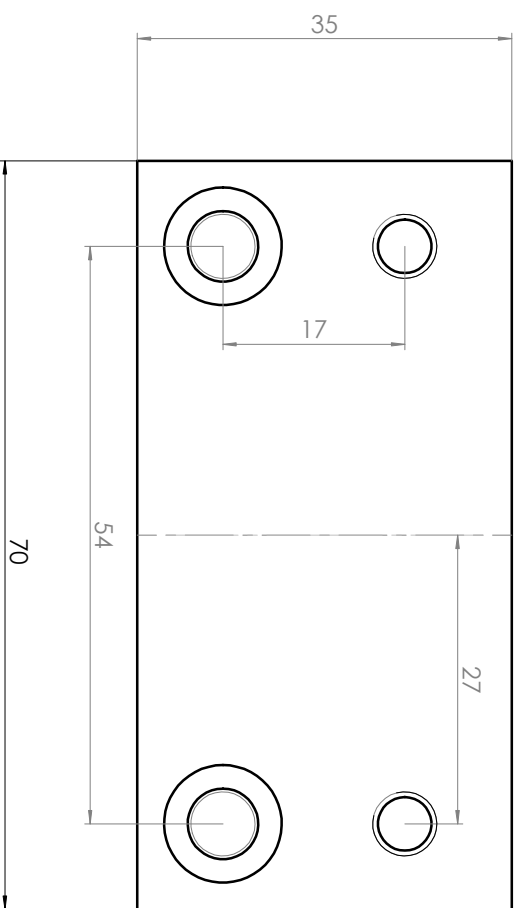
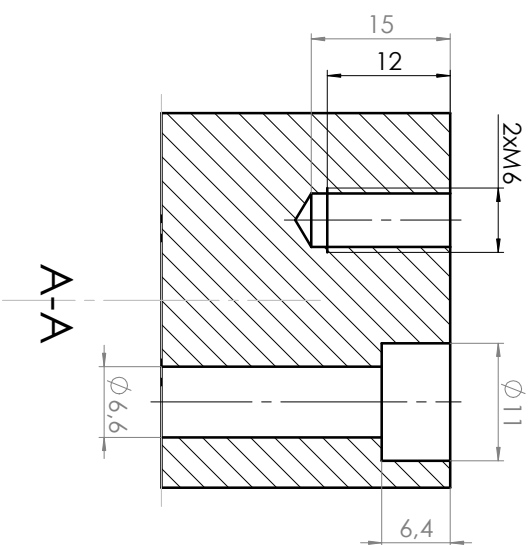
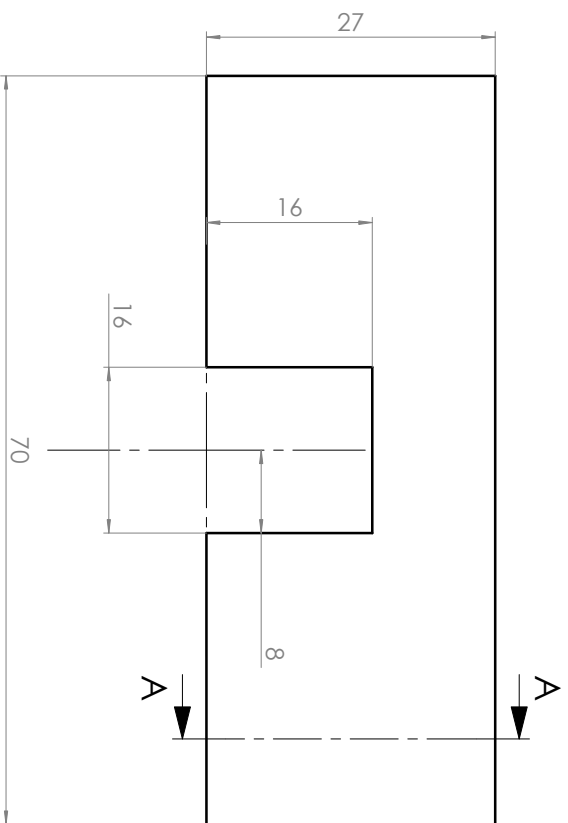
Raccordi non quotati R0,5
Tolleranze generali UNI EN 2768-mK

Q.TA' _	MATERIALE Acciaio	ALLIEVO	Creto
OGGETTO DESCRIZIONE	Base supporto BK		
		SQUADRA E CORSO	SCALA 2:1
		GRADO DI FINITURA ∇ (∇)	PESO (Kg)
		Disegno N.	



Politecnico di
Torino

Corso Duca degli Abruzzi 24 - 10129 Torino



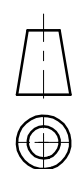
Raccordi non quotati R0,5
Tolleranze generali UNI EN 2768-mK

Q.TA'	MATERIALE	ALIEVO	Credito
-	Acciaio		
OGGETTO	SQUADRA E CORSO		
Base supporto BF15			
DESCRIZIONE	GRADO DI FINITURA		
	V (V)		
		PESO (Kg)	SCALA
			2:1
		DATA	



Politecnico di
Torino

Corso Duca degli Abruzzi 24 - 10129 Torino



Disegno N.

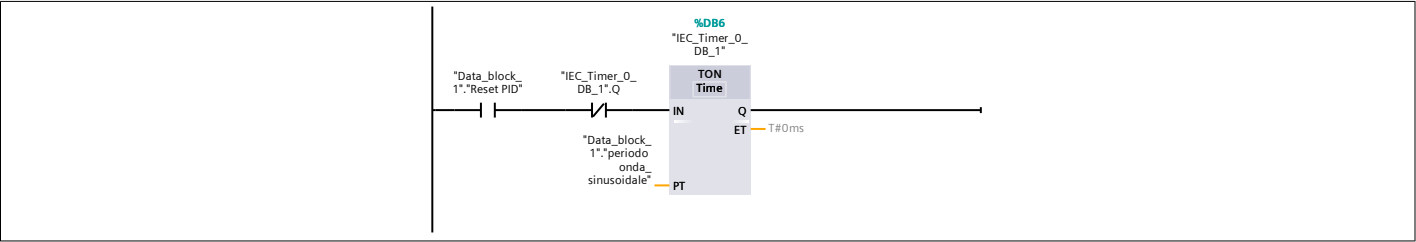
12 Appendix B: s7-1500

Cyclic interrupt_sine [OB31]

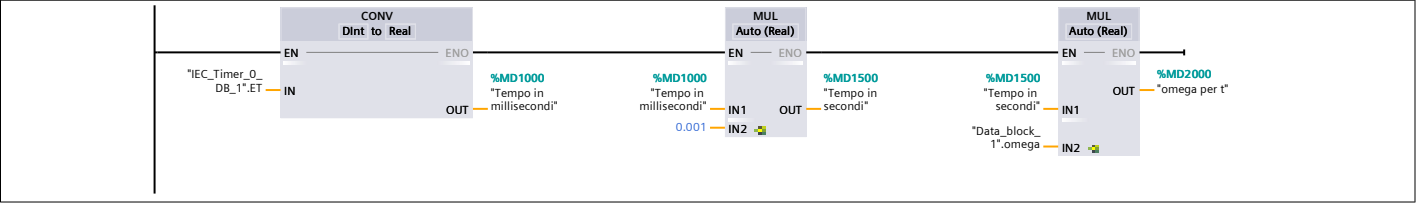
Cyclic interrupt_sine Proprietà							
Generale							
Nome	Cyclic interrupt_sine	Numero	31	Tipo	OB	Linguaggio	KOP
Numerazione	Automatico						
Informazioni							
Titolo	Generazione onda sinusoidale	Autore		Commento		Famiglia	
Versione	0.1	ID definito dall'utente					

Nome	Tipo di dati	Valore di default	Commento
▼ Input			
Initial_Call	Bool		Initial call of this OB
Event_Count	Int		Events discarded
Temp			
Constant			

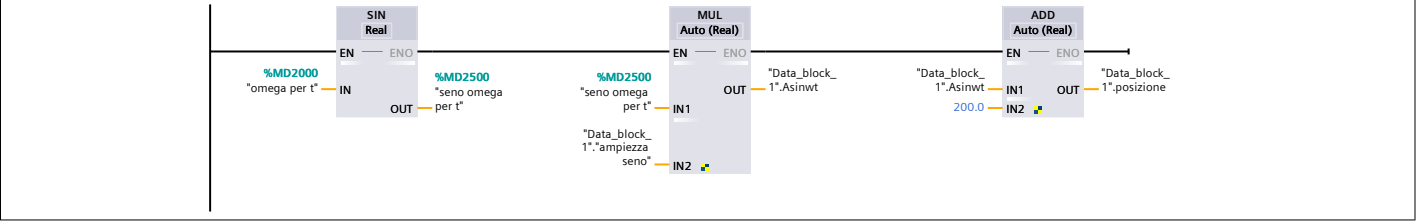
Segmento 1: Attivazione onda sinusoidale ed impostazione del periodo



Segmento 2: Generazione del valore omega*t



Segmento 3: Calcolo di x=A_o+ A*sin(omega*t)

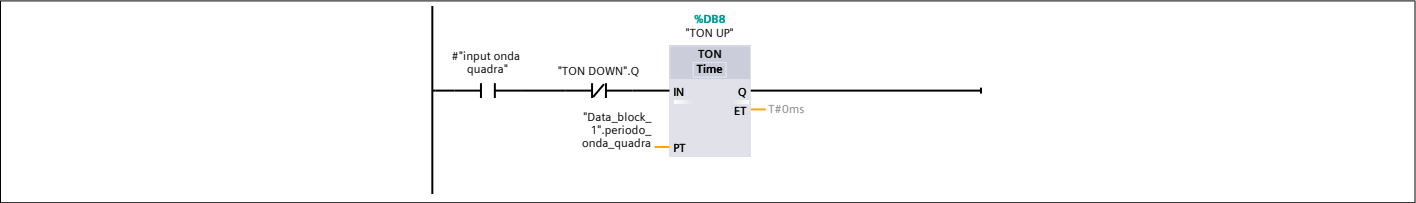


Onda quadra [FB1]

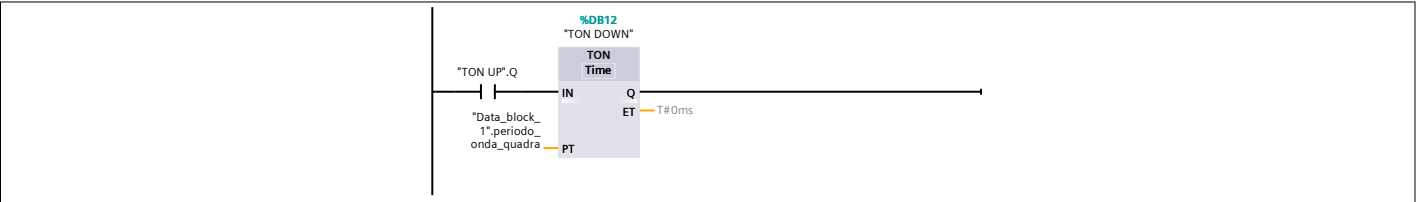
Onda quadra Proprietà							
Generale							
Nome	Onda quadra	Numero	1	Tipo	FB	Linguaggio	KOP
Numerazione	Automatico						
Informazioni							
Titolo		Autore		Commento		Famiglia	
Versione	0.1	ID definito dall'utente					

Nome	Tipo di dati	Valore di default	Ritenzione	Accessibile da HMI/OPC UA/Web API	Scrivibile da HMI/OPC UA/Web API	Visibile in HMI Engineering	Valore di impostazione	Controllo	Commento
▼ Input									
input onda quadra	Bool	false	Non a ritenzione	True	True	True	False		
▼ Output									
setpoint	Real	0.0	Non a ritenzione	True	True	True	False		
InOut									
Static									
Temp									
Constant									

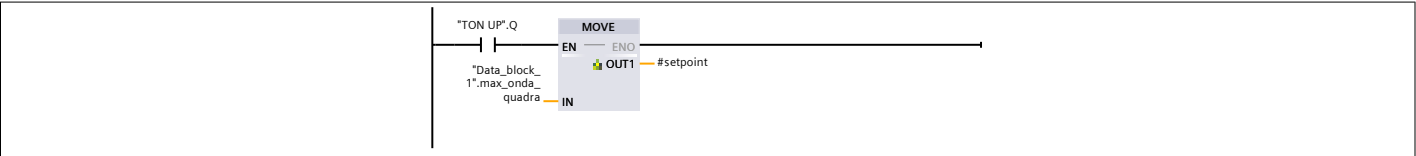
Segmento 1:



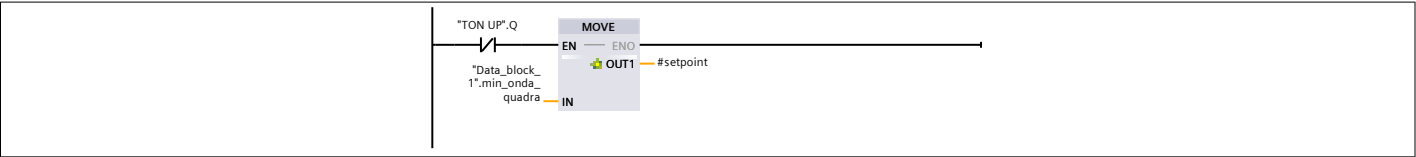
Segmento 2:



Segmento 3:



Segmento 4:



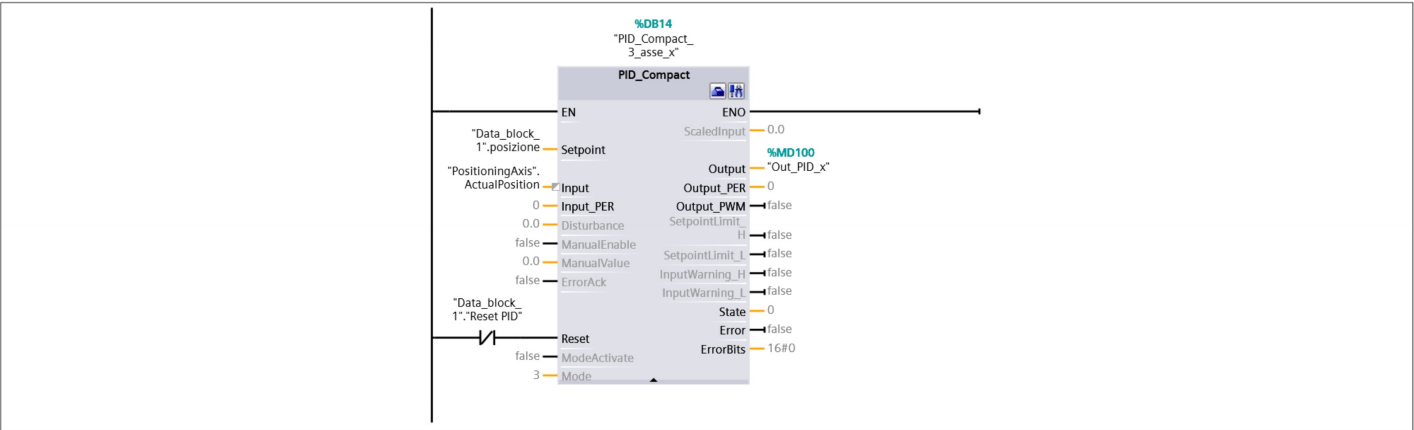
S7-1500 DEFINITIVO

Cyclic interrupt [OB30]

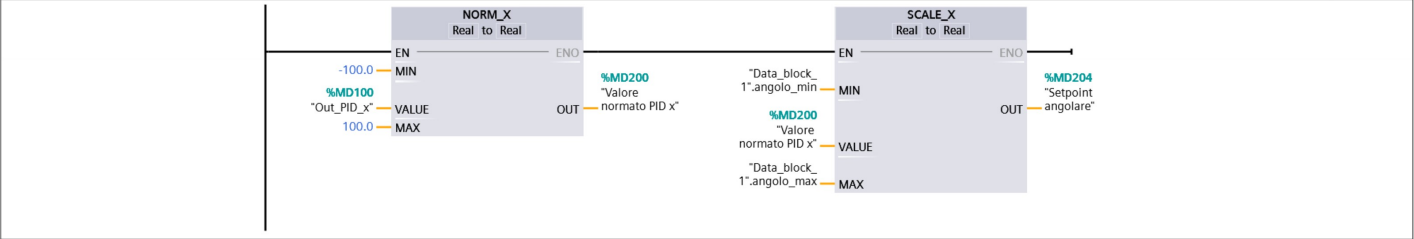
Cyclic interrupt Proprietà							
Generale							
Nome	Cyclic interrupt	Numero	30	Tipo	OB	Linguaggio	KOP
Numerazione	Automatico						
Informazioni							
Titolo		Autore		Commento		Famiglia	
Versione	0.1	ID definito dall'utente					

Cyclic interrupt			
Nome	Tipo di dati	Valore di default	Commento
▼ Input			
Initial_Call	Bool		Initial call of this OB
Event_Count	Int		Events discarded
Temp			
Constant			

Segmento 1: PID X



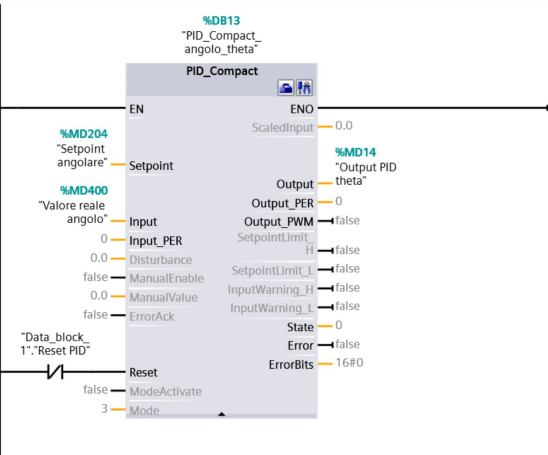
Segmento 2: Creazione del setpoint angolare



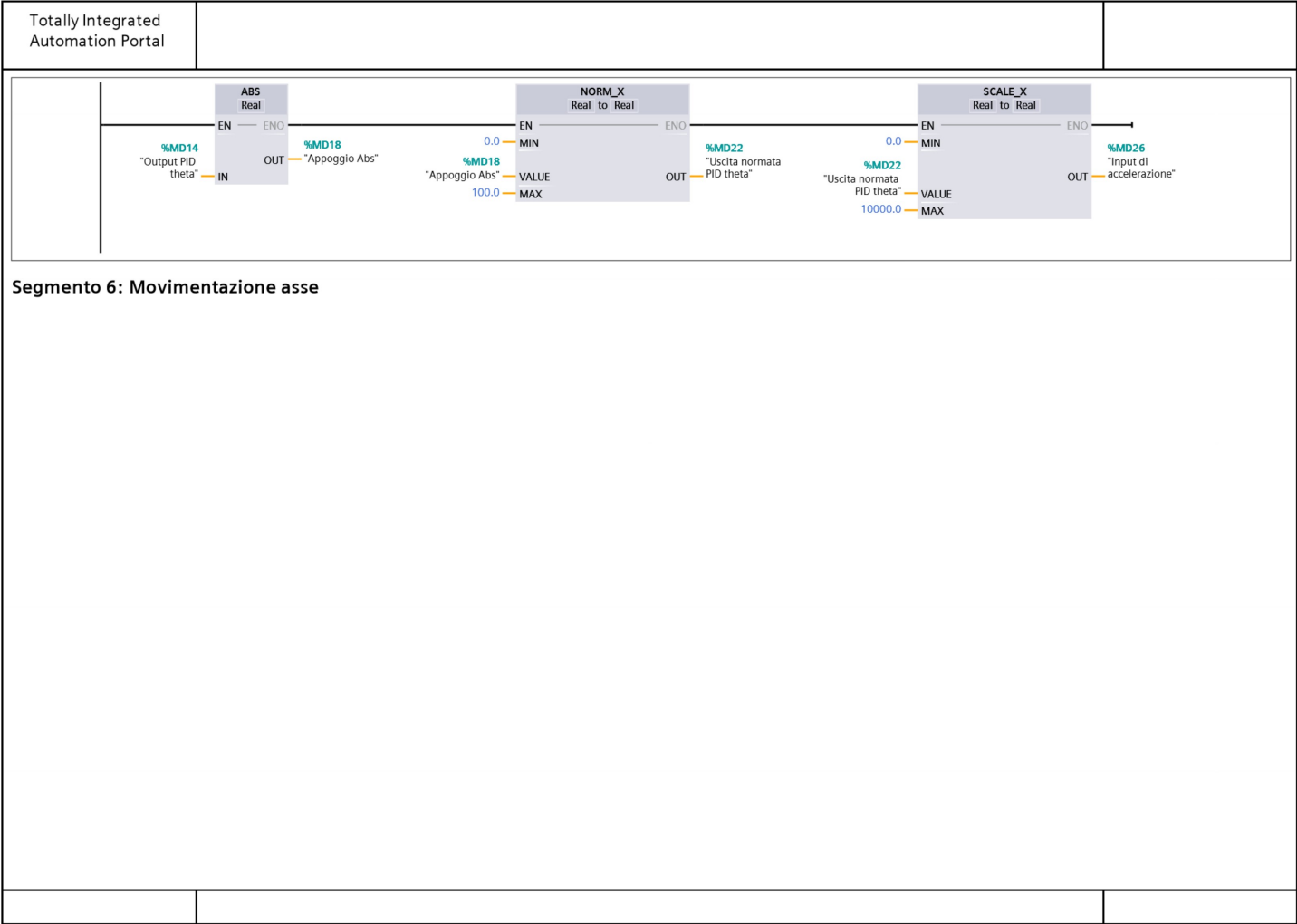
Segmento 3: Lettura angolo reale da sensore angolare

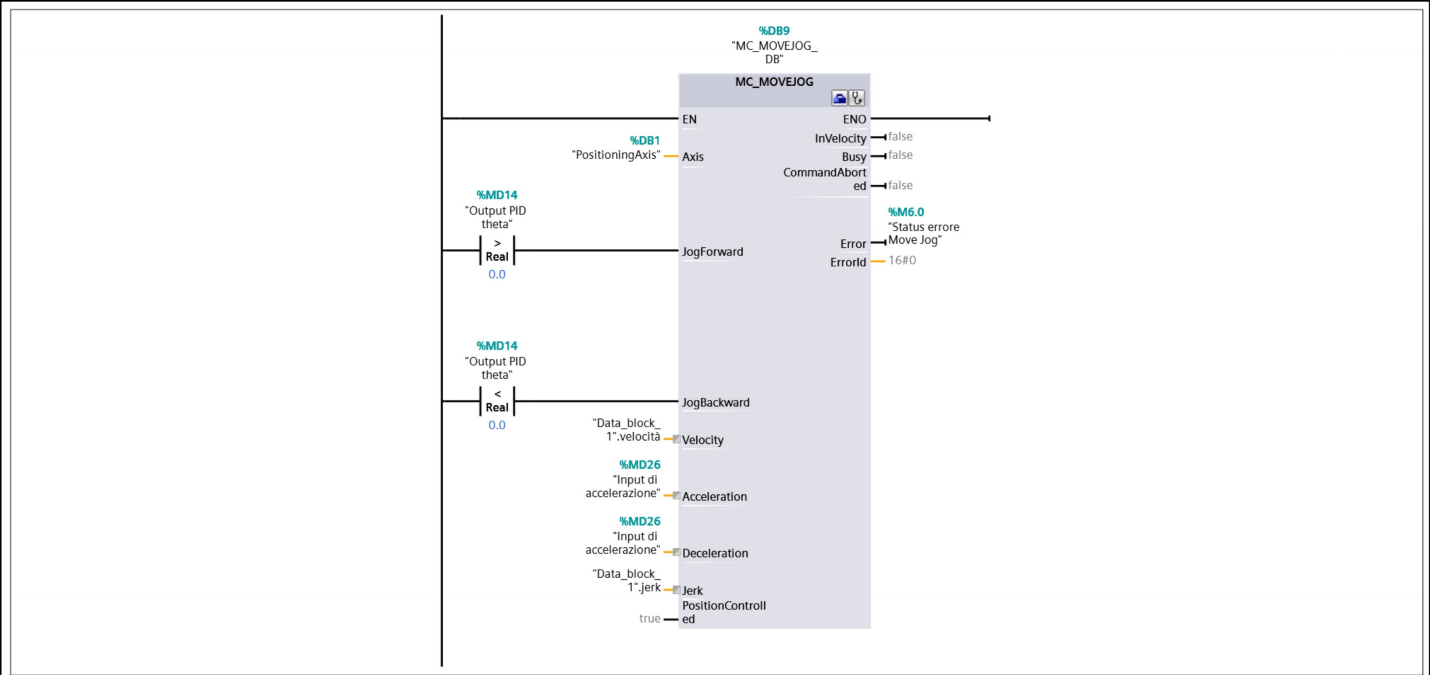


Segmento 4: PID theta

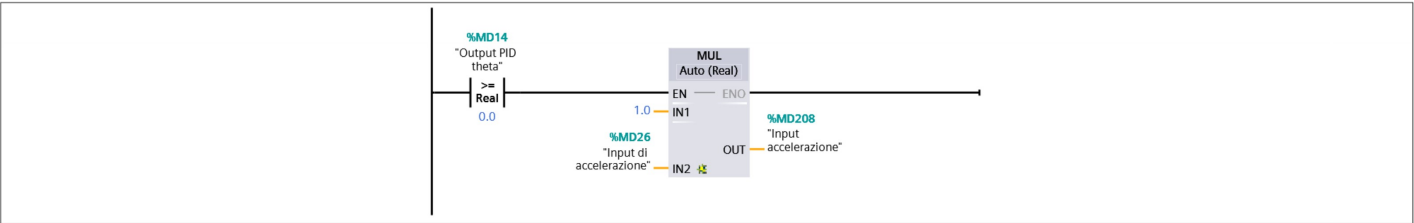


Segmento 5: Generazione input accelerazione

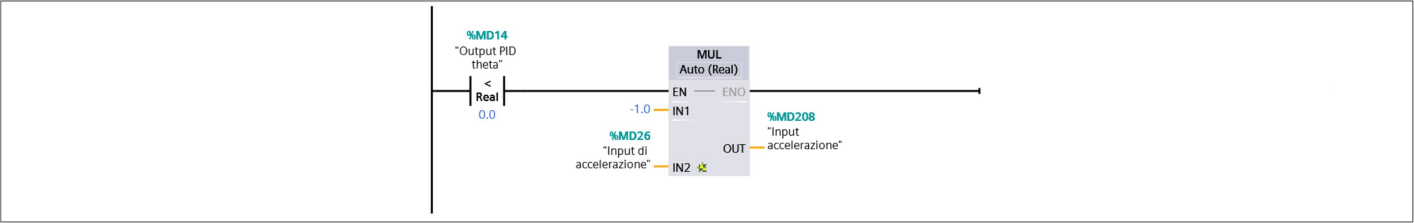




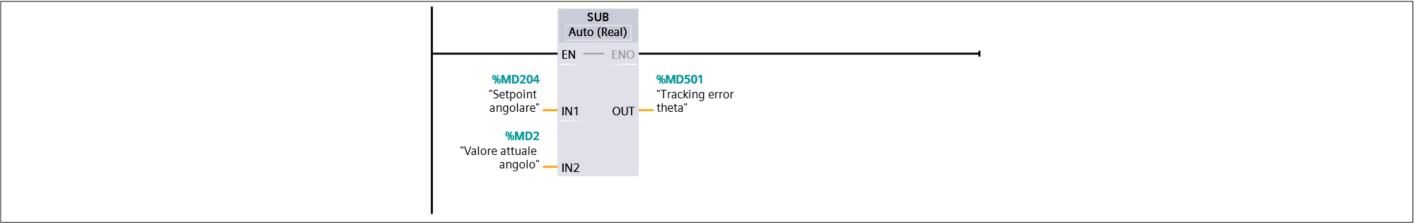
Segmento 7: Elaborazione accelerazione per tracce



Segmento 8: Elaborazione decelerazione per trace



Segmento 9: Tracking error theta



Segmento 10: Tracking error x



13 Appendix C: s7-1200

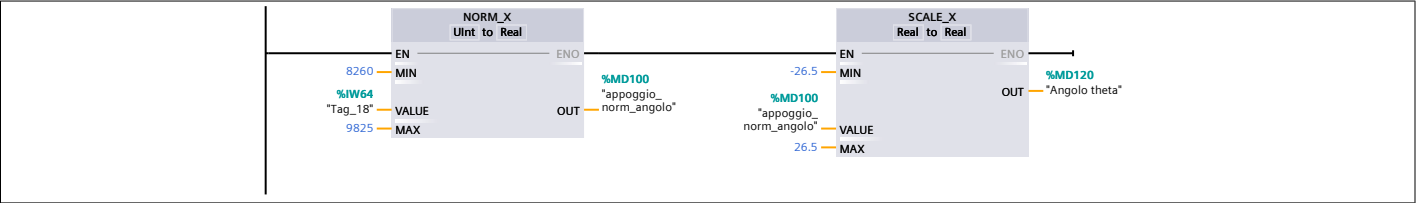
Cyclic interrupt [OB30]

Cyclic interrupt Proprietà							
Generale							
Nome	Cyclic interrupt	Numero	30	Tipo	OB	Linguaggio	KOP
Numerazione	Automatico						
Informazioni							
Titolo		Autore		Commento		Famiglia	
Versione	0.1	ID definito dall'utente					

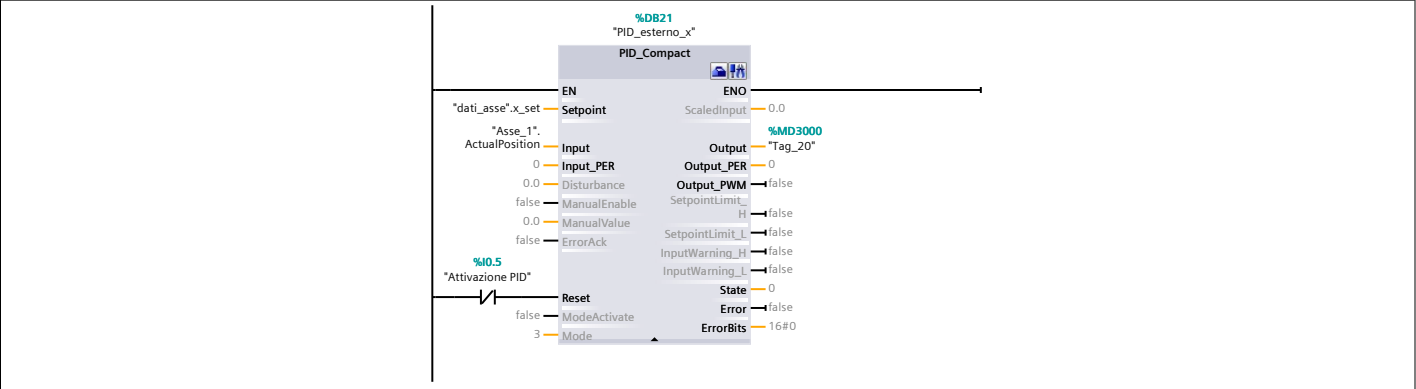
Nome	Tipo di dati	Valore di default	Commento
▼ Input			
Initial_Call	Bool		Initial call of this OB
Event_Count	Int		Events discarded
Temp			
Constant			

Segmento 1: Lettura angolo

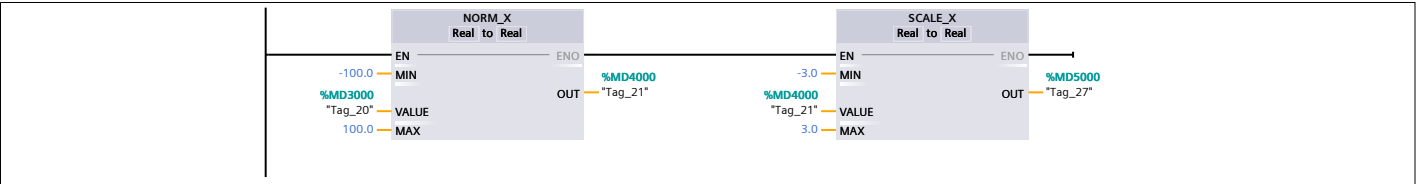
Letture l'input analogico proveniente dal sensore angolare ed operazioni di norma e scala per avere in uscita l'angolo in gradi



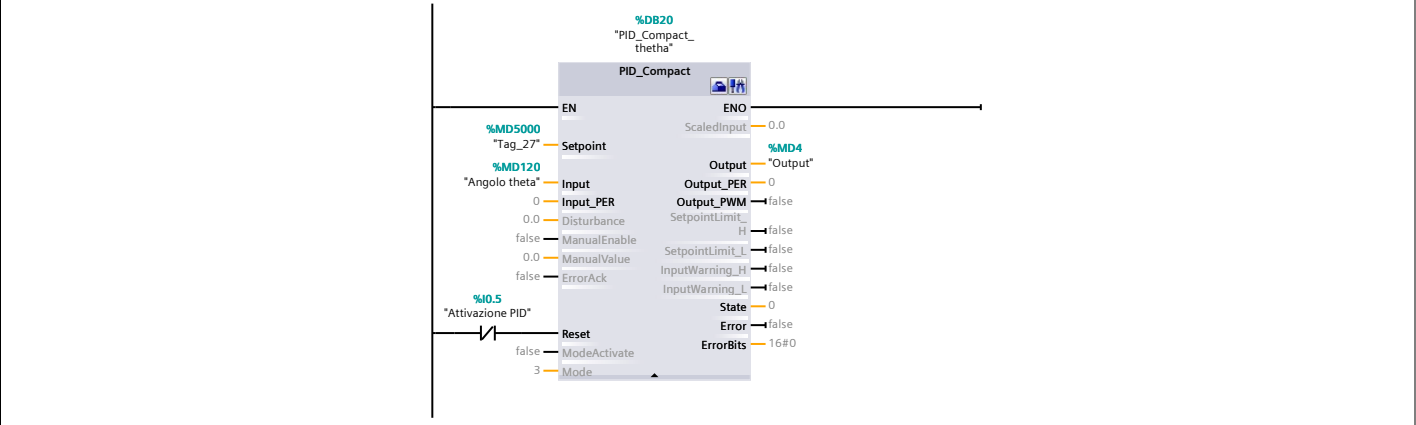
Segmento 2: PID di posizione



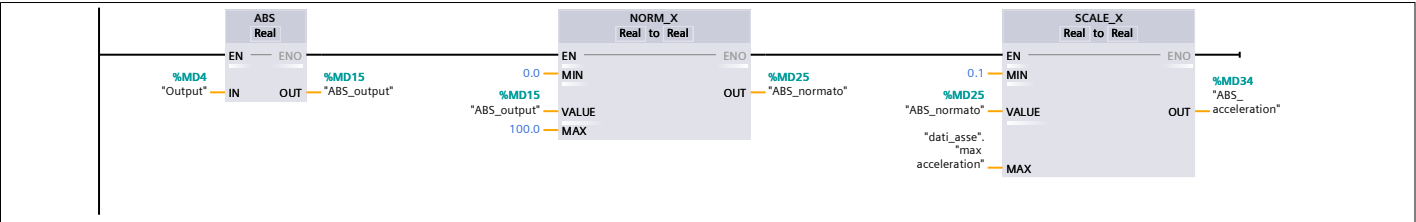
Segmento 3: Creazione setpoint angolare



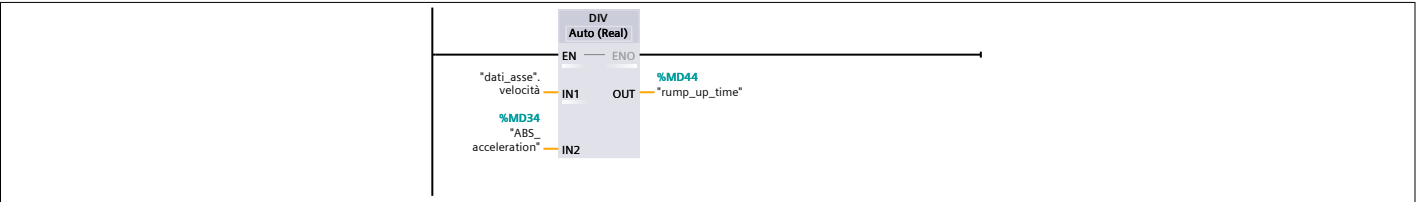
Segmento 4: PID angolare



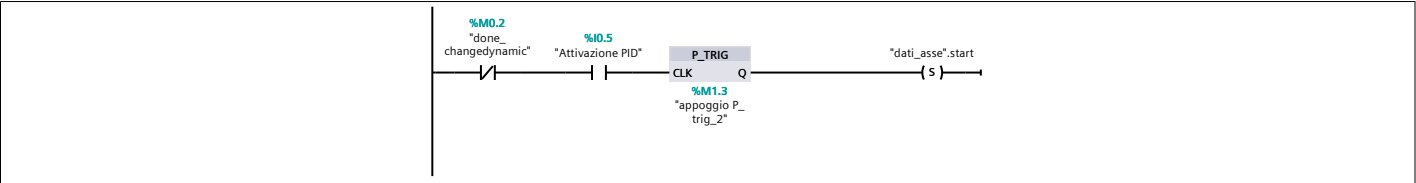
Segmento 5: Input di accelerazione



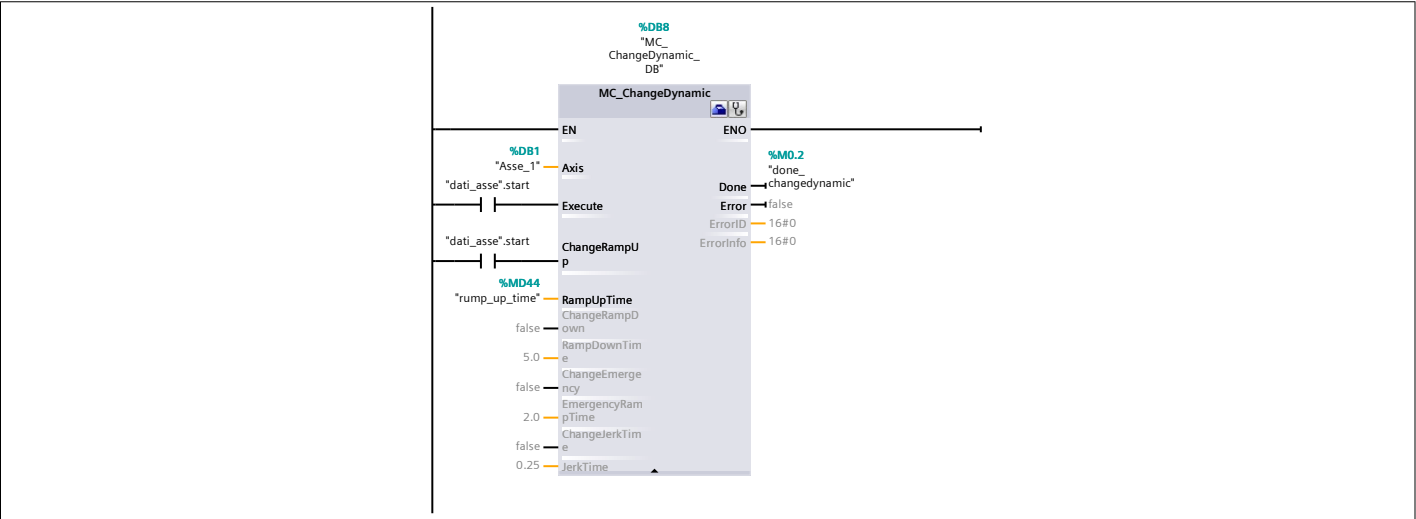
Segmento 6: Rump up time



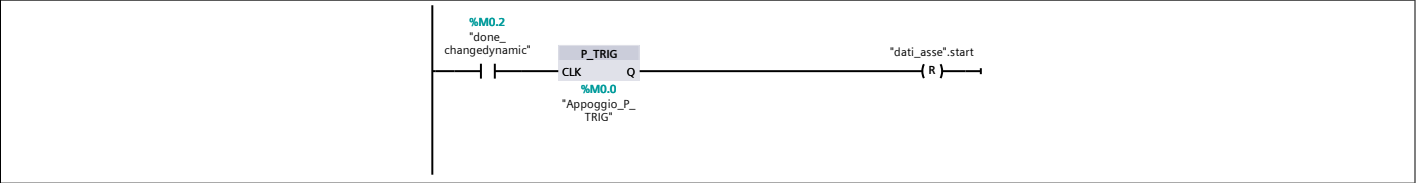
Segmento 7: Attivazione Change_dynamic



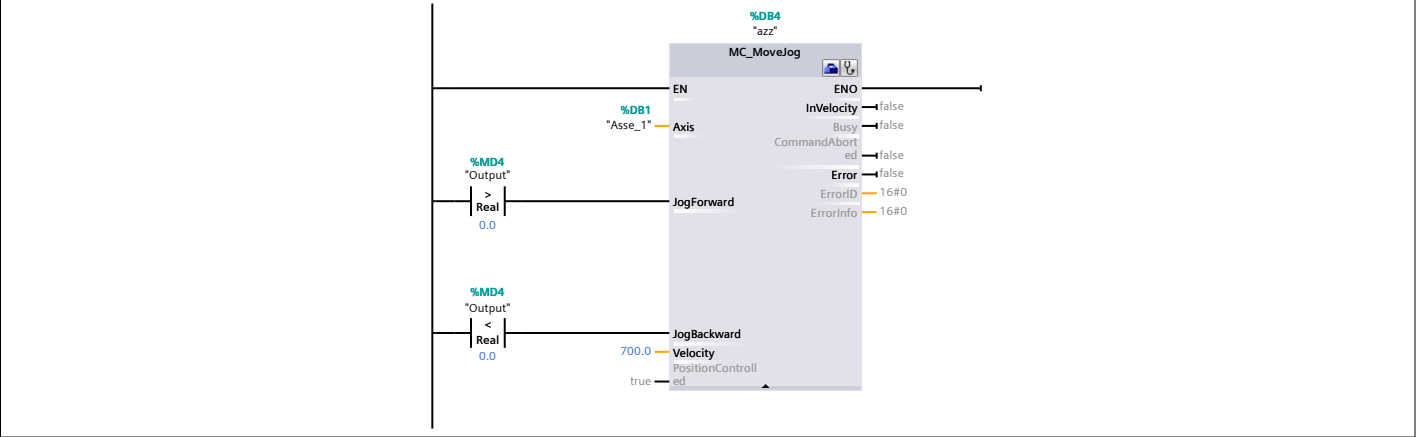
Segmento 8: Blocco per la modifica della dinamica dell'asse



Segmento 9: Reset Change_dynamic



Segmento 10: Movimentazione dell'asse



References

- [1] Olfa Boubaker. The inverted pendulum benchmark in nonlinear control theory: A survey. *International Journal of Advanced Robotic Systems*, 10:233–242, 09 2013.
- [2] Y. Baba, M. Izutsu, Y. Pan, and K. Furuta. Design of control method to rotate pendulum. In *2006 SICE-ICASE International Joint Conference*, pages 2381–2385, 2006.
- [3] Amr Roshdy, Lin Yu zheng, Hany F. Mokbel, and Wang Tongyu. Stabilization of real inverted pendulum using pole separation factor. pages 406–410. Atlantis Press, 2012/12.
- [4] E. Vinodh Kumar and Jovitha Jerome. Robust lqr controller design for stabilizing and trajectory tracking of inverted pendulum. *Procedia Engineering*, 64:169 – 178, 2013. International Conference on Design and Manufacturing (IConDM2013).
- [5] L. B. Prasad, B. Tyagi, and H. O. Gupta. Modelling and simulation for optimal control of nonlinear inverted pendulum dynamical system using pid controller and lqr. In *2012 Sixth Asia Modelling Symposium*, pages 138–143, 2012.
- [6] Z. Shenghao and S. Jinchun. Intelligent predictive fuzzy control for pneumatic inverted pendulum. In *2011 6th IEEE Conference on Industrial Electronics and Applications*, pages 968–972, 2011.
- [7] G. Calafiore. *Appunti di Controlli Automatici*. Edizioni CLUT, Torino, 2006.
- [8] G. Calafiore. *Elementi di Automatica*. Edizioni CLUT, Torino, 2004.
- [9] N. Schiavoni P. Bolzern, R. Scattolini. *Fondamenti di controlli automatici*. McGraw-Hill, Milano, 2008.
- [10] M. Pontin. *Modellazione, realizzazione e controllo mediante PLC di un sistema a pendolo inverso ad attuazione pneumatica*. Politecnico di Torino, Torino, 2018.
- [11] G. Pepe. *Analisi teorico sperimentale di un sistema a pendolo inverso con attuatore pneumatico controllato*. Politecnico di Torino, Torino, 2017.